Università Politecnica delle Marche

PhD course in Life and Environmental Sciences

Marine Biology and Ecology

The evolution of morphology in diatoms

PhD student:

Alessandra Petrucciani

Tutor:

Alessandra Norici

XXXIV cycle

2018/2022

Ad Alessandra, che ha realizzato il suo sogno

A mamma e papa, che l'hanno vista partire troppo presto,

Ad Alessandra, più che semplicemente una guida

INDEX

LIST OF FIGURES

LIST OF TABLES

Abstract

In present oceans, diatoms are abundant and diverse primary producers surrounded by silica shells called frustules; since they account for almost 20% of the total primary production on Earth, diatoms sustain the global food web. Although molecular clocks suggest that diatoms arose as much as 250 million years ago (Ma), the earliest known diatom fossils date from 190 Ma, leading to the suggestion that early diatoms were at best lightly silicified. By the Cretaceous Period, large spherical diatoms with highly silicified frustules thrived in surface oceans, only later to be joined by species with elongated and thinner frustules, with lower SiO_2 content. But how has the synergic action of selective pressure acted on the evolution of morphologically different frustules? The importance of diatoms in Global Carbon and Silicon cycles combined with frustule promising exploitation as emerging biomaterial drives the studies on the topic, in the perspective of future oceanic predictions and research on new bio-based materials. Furthermore, our purpose was to deepen the knowledge on the biological functions of the frustules, often deduced from studies on few centric species, limiting the huge potential of diatoms diversity. To achieve these purposes, two major selective pressures (Si concentration through geologic eras and the interaction with competitors and predators) and their involvement in diatoms radiation were investigated. The physiological response of morphologically distinct diatoms to these selective pressures was evaluated; in particular, cells were acclimated to reconstructed paleoenvironments mimicking Mesozoic/Cenozoic concentration of nutrients (N, Fe, Zn, Mo) in the presence of different Si regimes; the quantity of Si present in the frustule, organic composition, carbon and nitrogen stable isotopic fractionation, photosynthetic performance, frustule structure were assessed. Mono- and mixed cultures of diatoms were exposed to the presence of *Temora longicornis*, a calanoid copepod, to assess if size and shape were primary drivers in avoiding predation. Data confirmed that both selective pressures act on the evolution of different frustule morphologies. Pennate diatoms were favoured as compared to centric species; they showed an acclimatory response to different Si

regimes, modulating Si use efficiency and elongated shape benefited cells in escaping from predators also when facing competition for resources. Evolution led to more competitive shapes. The assessment of the adaptative roles of frustules included defence against predators, competition for resource uptake and sinking. All these roles were related to frustule shape, size and silicification in a role specific manner. Sinking capacity of diatom species was related to frustule density and not to cellular shape and size. A species – specific relation between light and silicification was found, and a direct relation between sinking capacity and growing light intensity was observed, independently from silicification, suggesting an energy dependent buoyancy control at cellular level. Finally, the characterization of frustules to exploit silica biomaterial and the Life Cycle Assessment of the most suitable way to obtain cleaned frustules were carried out. *Chaetoceros muelleri* was found as a promising species for frustule exploitation due to its small size, silicification plasticity in response to light intensity, high surface area and relative high presence of basic sites, important for subsequent functionalization. Furthermore, its fast growth rate is a key feature for frustule productivity on an industrial scale. The acidic removal of the organic matter was a more sustainable option to obtain frustules with 4 kg of equivalent CO_2 released compared to 20 kg released with the oxidation method.

Chapter one: General Introduction

1. General introduction

1.1 Success and diversity of diatoms in modern ocean: an ecophysiological point of view

Diatoms are a greatly diversified group of eukaryotic phytoplankton (Bacillariophyceae) belonging to the supergroup Stramenopiles (Bowler et al., 2010). They were firstly observed in 1703 (Round et al., 1990) and, since then, they have caught the attention of a wide community of scientists, attracting all kind of expertise, from taxonomist, oceanographers, geologists, to more recently engineers and chemists. These photoautotrophic unicellular microorganisms are ubiquitous and can be found not only in aquatic environments, but also in sea ice, soils, lichens, biofilms and airborne, denoting their deep adaptative features (Lohman 1960).

The most fascinating morphological characteristic of diatoms is given by their ability to exploit silicic acid and to build a siliceous shell called frustule. Frustule provides diatoms huge advantages in terms of fitness as compared to other microorganisms (Martin – Jézéquel et al., 2000) since their biological functions are multiple, some of them poorly understood (discussed later). Generally, frustule morphological traits are used with taxonomic value and, since 1990, Round and co-authors have divided the species in two groups based on cellular symmetry: centric diatoms, with a radial symmetry, and pennate diatoms, with an elongated and bilateral symmetry.

Diatoms are thought to be secondary endosymbionts (Gentil et al., 2017, Morozov and Galachyants, 2019), meaning that their precursor was a eukaryote that phagocytized another eukaryote (which became an organelle), resulting in chloroplasts surrounded by 4 membranes. The earliest known fossil of diatoms (**Figure 1.1**) was dated from the Early Jurassic (185 Ma), but molecular clock and sedimentary evidence suggested an earlier origin, when a greater availability of niches occurred during the Permian Mass Extintion (250 Ma). The gap in fossil records during this period has been hypothesized to relate to unsilicified diatoms (Armbrust 2009) or lightly silicified. The radial

centric group of diatoms is the oldest and evolved in different lineages such as bipolar and multipolar centrics, araphid pennates and raphid pennates; the latter are the youngest group and by far the most diversified in terms of species (Armbrust 2009).

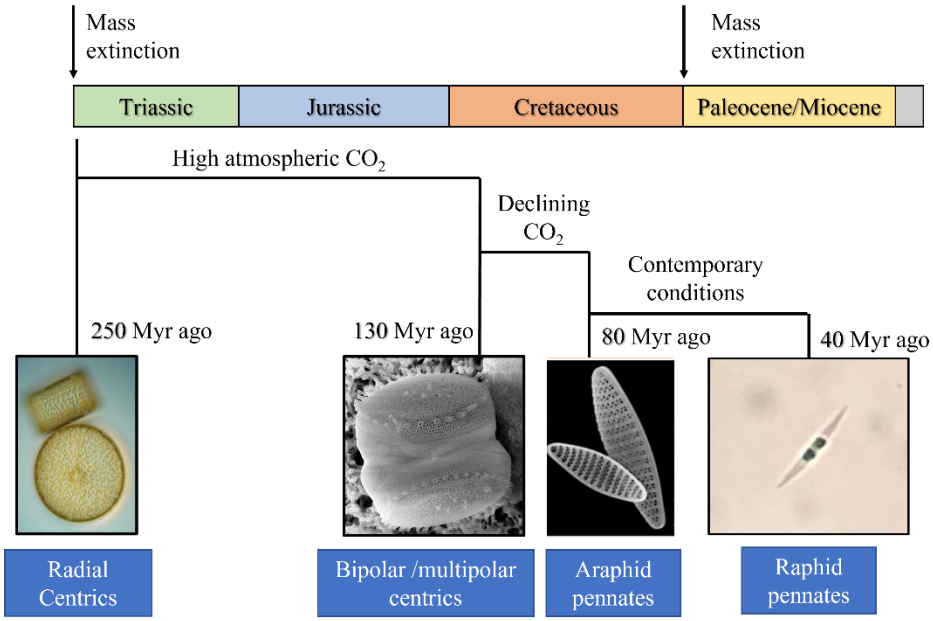

Figure 1.1: Diatom evolution through geologic eras (Modified from Armbrust 2009)

The secrets for diatom success in modern oceans can be listed as follows:

(I) Large central vacuoles to storage nutrients for later use. Thus, diatoms adapt easily to environments where nutrients are available in short pulses (e.g., sea ice) (Hansen et Visser, 2019, Behrenfeld et al., 2021).

(II) Very efficient nutrient acquisition pathways: highly efficient uptake and internal recycle of N and P; a high affinity Fe uptake system and lower trace metal requirements as compared to other algal groups. Recent advances in Si uptake studies showed that diatoms can cope with a very low concentration of external silicic acid (Allen et al., 2011, Hockin et al., 2012, Thamatrakoln, 2021).

(III) Presence of enzymes for a complete urea cycle never found in other photoautotrophs; urea could be exploited as osmolyte, N storage, intermediate molecule for the synthesis of proteins involved in frustule formation, defence against pathogens (Allen et al., 2011).

(IV) Buoyancy control achieved not only thanks to the dense siliceous frustule but also to the formation of spores that can be used to sink out from adverse conditions; some *Thalassiosira* species increase their drag extruding chitin fibers from pores in the frustule (Brunner et al., 2009, Mayzel et al., 2021).

(V) Excretion of exopolysaccharides (EPS) from the raphe of raphid pennates allowing to adhere and move on a mucilaginous surface. Motility gives diatoms the possibility to optimize light conditions, to search for nutrients and therefore to colonize new habitats and niches, also to approach partners for sexual reproduction, to attain vertical migration and escape from predators (Lind et al., 1997, Wang et al., 2013).

(VI) Production of bioactive-unsaturated aldehydes (PUAs) as a good chemical defence against predators (Ianora et al., 2004, Leflaive and Ten-Hage 2009, Ianora and Miralto, 2010, Amato et al., 2018, Barreiro et al., 2011).

(VII) Frustule strength and plasticity as a powerful mechanical protection against predators. It has been observed that silicification is a phenotypically plastic trait modulated by the presence of grazers (Pondaven et al., 2007, Pančić et al., 2019, Petrucciani et al., 2022)

The advances in molecular biology and marine studies are quite recent, therefore the first complete sequenced genome of a diatom was published in 2004 for the centric *Thalassiosira pseudonana* (Armbrust et al., 2004) followed by the genome of *Phaeodactylum tricornutum* (Bowler et al., 2008). From a genetic perspective, there are more differences between these two species than between men and fish, although diatoms diverged more recently, another proof of the extraordinary diversity of diatoms (Montsant et al., 2005). Currently, less than 10 diatom genomes are available.

Broadening knowledge on diatoms is deeply breaking commonly accepted paradigms: many deviations from simplified concepts can occur after field observations.

(I) Diatoms are considered “large species” (>20 µm) and classified in “microphytoplankton” size class together with dinoflagellates (Vidussi et al., 2001). However, from field observations during oceanographic cruises, pico and nanoplanktonic sized diatoms of the genus *Minidiscus* (1 µm diameter) appeared to be the most represented during spring blooms (Leblanc et al., 2018). Furthermore, *Minidiscus* genus is among the top 20 diatoms encountered during Tara – Oceans expedition (Malviya et al., 2016), suggesting how this genus was underestimated in past representations of the group.

(II) The paradigm of Legendre & Lefèvre (1989) clearly separates the function of large phytoplankton, involved in the bloom formation (in energetic and nutrient rich environments) and export of C and Si, and the function of small phytoplankton, involved in the nutrient recycling through microbial loop. After the discovery of *Minidiscus* role, diatoms are also potentially part of the microbial loop. They are also found in nutrient poor – highly stable environments where significantly contribute to C export: even if very small, they can efficiently sink out and bury in less than 14 days (Leblanc et al., 2018).

(III) Margaleff mandala (1978) is a globally accepted succession of coastal oceans which states the success of diatoms in high nutrient and high turbulent environments. Margaleff mandala became an oversimplified rule of diatom distribution. On this basis, it is widely predicted that diatom productivity and efficiency in biological carbon pump (C pump) will decrease with climate change, that is driving towards increased stratification of the oceans. On the contrary, diatom productivity in highly oligotrophic stratified systems is significant (Brun et al., 2015, Kemp et al., 2018).

Trying to describe diatom role in planetary biogeochemical cycles and aquatic food webs it would be misleading considering them as a single, functional group since they are deeply diverse (genetically, in number of species and life strategies, morphologically and so on).

1.2 Role of diatoms in ecosystems

Diatoms are key primary producers in nowadays oceans and their ability to adapt to different even extreme environmental conditions allow them to grow and thrive, overcoming other phytoplanktonic groups during blooms. Their importance could be assessed as 1% of Earth photosynthetic organic biomass, 40% of marine primary production, 20-25% of global Earth primary production (Field et al.,1998, Falkowski et al., 2004).

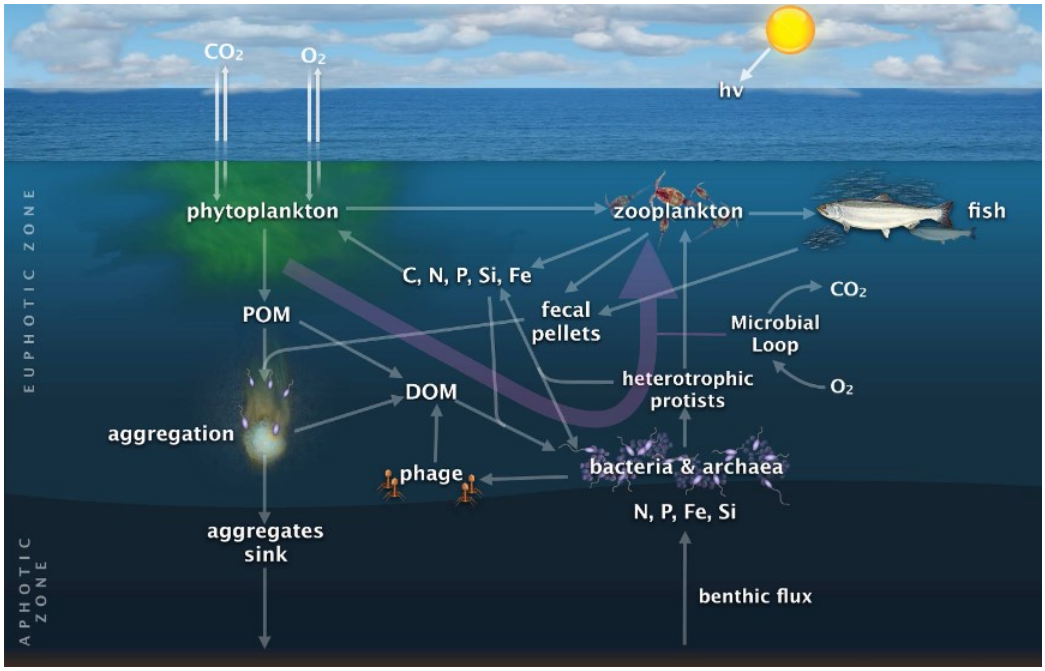

Figure 1.2: A common representation of marine microbial food webs (Worden et al., 2015)

From **Figure 1.2** the different roles of the phytoplanktonic compartment in marine food webs are described. When diatoms bloom:

(I) Diatoms can generate O_2 which is delivered in the atmosphere;

(II) Diatoms are involved in the recycling of nutrients;

(III) Diatoms are key source of food and energy for other organisms in the aquatic environment;

(IV) Diatoms could be involved in controlling global warming reducing the CO_2 content in atmosphere, sequestering it during high-rate photosynthetic process;

(V) Diatoms have a crucial role in the Biological C pump.

The term Biological C Pump means all the processes contributing to the export of C in layers deep enough to be isolated from the atmosphere for a certain amount of time (at least 100 years): this could be achieved if C is transported below 1000 meters (Passow and Carlson 2012).

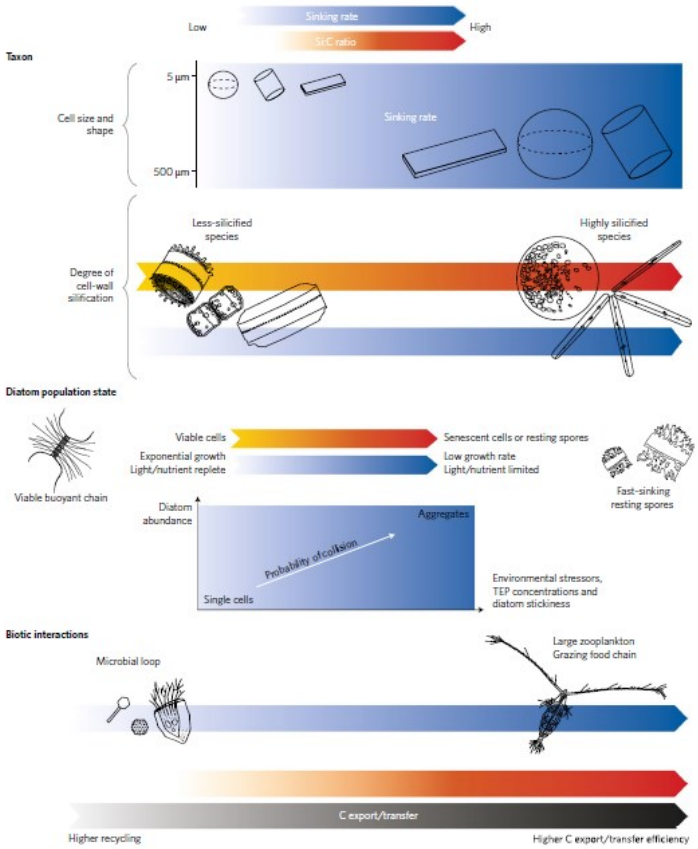

Figure 1.3: Key processes influencing the contribution of diatoms to C export/transfer efficiency potential (Treguér et al., 2018)

Diatoms contribute on average to 20-40% of the C export (Jin et al., 2006): the possibility to form larger particles (aggregates) and the dense frustule improve their sinking capacity. By sinking they rapidly export organic matter to the bottom of the aquatic basin and the organic matter is then sequestered in sedimentary rocks over geological time, constituting fossil fuel deposits. As discussed above, Leblanc and co-authors (2018) found also small diatoms being key players in exporting biomass to the bottom of the sea, therefore it becomes even more crucial to assess how diatom huge diversity and its response to a changing world impact the biological C pump (**Figure**

1.3, Tréguer et al., 2018). As diatoms belong to silicifiers organisms, their metabolism couples C and Si cycles, deeper investigated in the next session.

1.2.1 Global Silicon Cycle

Si is not only a crucial nutrient in diatoms' life cycle but also the second most abundant element in the Earth's crust (Sutton et al., 2018). Therefore, to perceive the global importance of diatoms in our ecosystem it is necessary to understand the role of these organisms in the Global Si Cycle. The latter is deeply studied since its implication in maintaining climatic stability on geological time scale (Siever 1992, Frings et al., 2016, Conley et al., 2017) and in regulating primary productivity in oceans and in continents (Sutton et al., 2018).

In order to study the geochemical cycle of an element, it is necessary to understand:

- The reservoirs (storages of the element),
- Sources, sinks and internal cycles,
- The spatial scale,
- The temporal scale.

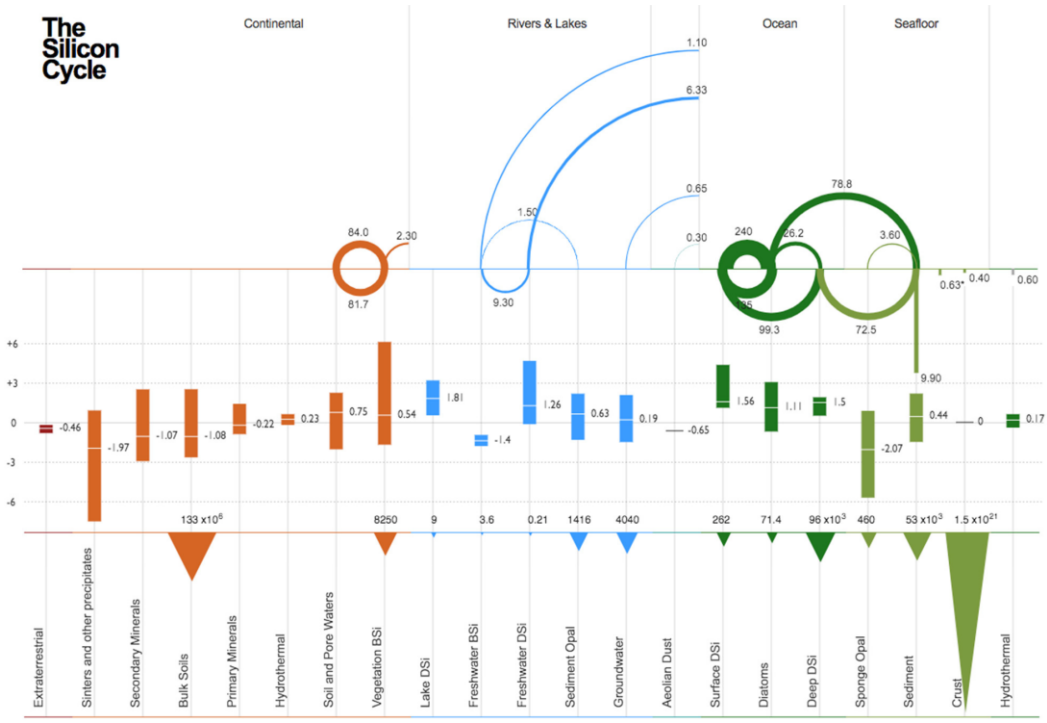

Figure 1.4: Schematic representation of the modern day Global Si Cycle (Sutton et al., 2018). In the upper part of the figure the magnitude of the fluxes (Tmol/yr) is indicated, in the middle their associated δ30 Si values, and in the lower part the size of the reservoirs

Looking at **Figure 1.4**, it is possible to identify four categories of reservoirs: continents, rivers and lakes, oceans and seafloor. Then, according to the Si transfer (flux) source reservoirs are those from which Si is transferred to another reservoir, and sink reservoirs are those that take up Si from another part of the cycle.

Focusing on diatoms, the size of the reservoir is about 71.4 Tmol Si/year, a quite tiny pool if compared to the terrestrial correspondent (Vegetation biogenic Si, 8250 Tmol Si/year, Laruelle et al., 2009). Nevertheless, Si fluxes involving diatoms are impressive, suggesting their struggle role in Si recycling. In particular, they are the sink of 240 Tmol Si/year from surface dissolved Si (DSi), such value overcomes all the other global fluxes (**Figure 1.4**). Furthermore, diatoms are the source of 78.8 Tmol Si/year for the sediment and 26.2 TmolSi/year for deep sea, two of the greatest Si reservoirs.

Since the importance of diatoms in Si recycling, factors controlling their growth (light, temperature, biology, nutrients availability) are also deeply involved in controlling the global spatial distribution of Si (Tréguer et al., 2018). The temporal scale of Global Si Cycle is illustrated in the next session.

1.2.2 Biogeochemical Silicon Cycle in paleo oceans

Given the interconnection between environmental conditions and biota, the reconstruction of paleo-oceanic conditions is crucial to assess evolutive trajectories in organisms and to speculate on their behaviour in future oceans. New powerful tools allow to reconstruct Si cycle through geologic eras (Conley and Carey, 2015, Conley et al., 2017, **Figure 1.5**). In particular, the presence of physical, biological, geochemical proxies (i.e. assemblage analysis, Si stable isotopes) and the development of always more sophisticated models are used to understand Si fluctuation through time, their causes and consequences on living organisms.

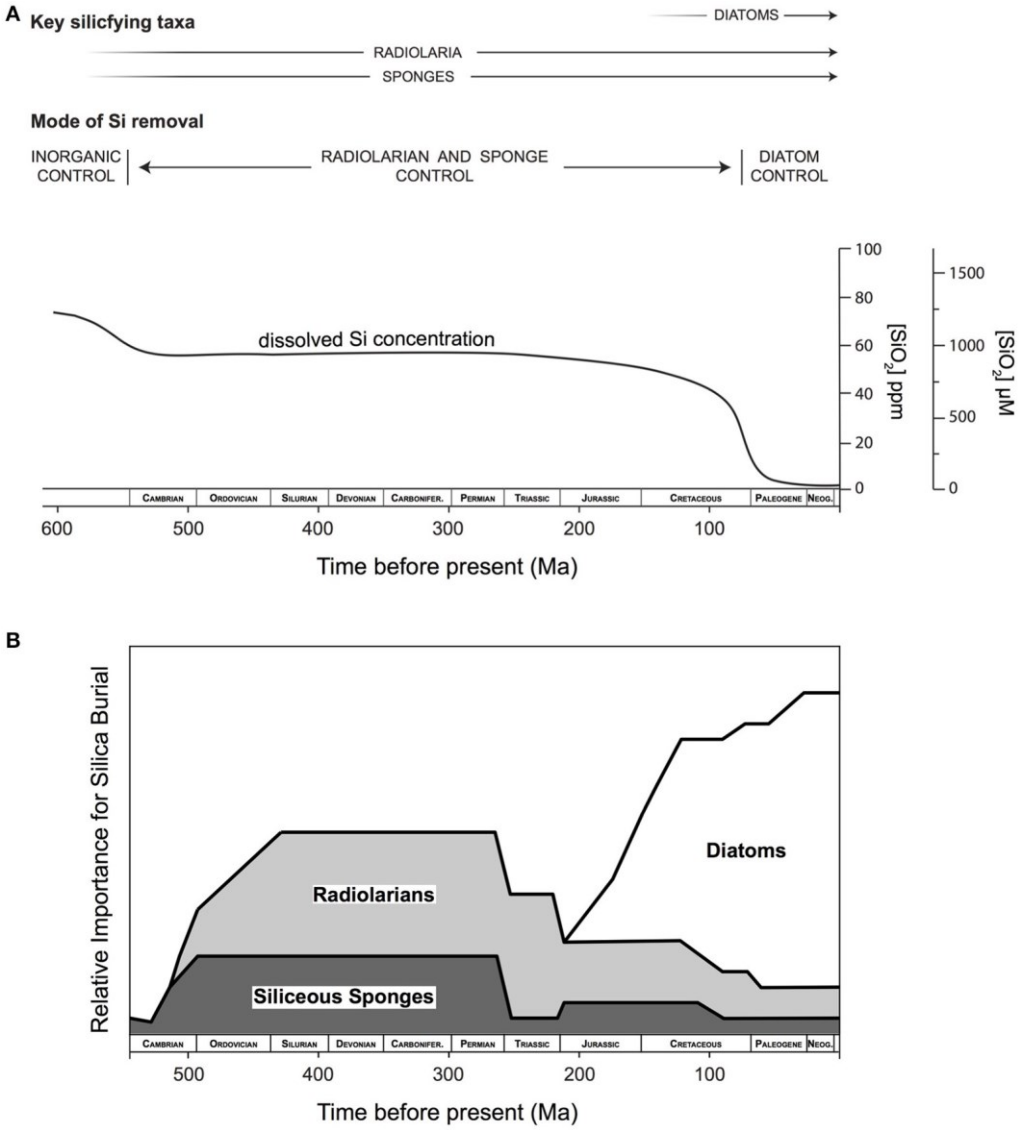

Figure 1.5: Change of the oceanic Si concentration in geologic records (Conley et al., 2017). During the first part of Earth history (Proterozoic), the oceanic Si cycle was controlled by inorganic and abiotic reactions (Siever et al., 1992, Conley et al., 2017), therefore the total DSi input fluxes were not balanced by consistent outputs, leading to a great concentration of seawater DSi (600 µM).

Phanerozoic ecosystems (541 – 66 Ma) were moulded by the appearance of new living groups (Knoll and Follows, 2016) known to have molecular Si transporters and to exploit DSi, such as sponges, radiolarians, dinoflagellates, coccolithophorid, haptophytes, chrysophytes and diatoms (Marron et al., 2016). The radiation of these groups has been considered the main cause of a drawdown of available silicic acid concentration in surface waters which became also less available for organisms (Conley et al., 2017). Conley and co-authors (2017) discussed that DSi decline could

be also associated to periodic changes in hydrothermal fluxes and continental weathering (Frings et al., 2016).

Trying to assess when the drawdown happened in geological history, the appearance of sponges and radiolarians initially lead to a concentration of 500 μM during Palezoic (Conley et al., 2017); later one, it is globally accepted that a second big drawdown strictly correlated to the increased diversity of diatoms, over the last 100 million years, leading to a modern concentration of about 10 μM DSi (Lazarus et al., 2014, Cermeño et al., 2015, Marron et al., 2016, Conley et al., 2017). Consequently, Si use efficiency was a crucial point in species expansion, and it was demonstrated that diatoms diversification of Si specialized transporters (SIT) made them the dominant marine DSi utilizers in Cenozoic Oceans (Durkin et al., 2016; Fontorbe et al., 2017). The geological period called Eocene – Oligocene transition (EOT) was characterized by a long – term cooling, coincident with a drop in atmospheric CO_2 concentration (Zachos et al., 2008) and marks the point of maximum explosion of diatoms. These climate changes altered ocean mixing and likely impacted on diatom growth (Finkel et al., 2005) by stirring up deep waters rich of nutrients and supplying more DSi to surface oceans. Geochemical evidence for a change in DSi circulation at the EOT is also reported: Egan and co-authors (2013) recorded an increase in DSi supply to the surface and an increased uptake or utilisation of DSi, explaining the drawdown of atmospheric CO_2. In addition, a higher supply of DSi from land to ocean (Frings e al., 2016): this could be explained by (i) the expansion of grasslands producing silica phytoliths which are readily soluble, and by (ii) the increase in chemical weathering of silicate rocks due to orogeny or glaciation. Finally, the rising of diatoms could be also favoured by the competition with other silicifying organisms: less efficient competitors for DSi experienced a decline in their diversity and radiation, for example radiolarians and sponges (Harper and Knoll, 1975, Maldonado et al., 1999), enhancing diatoms explosion. Reef building siliceous sponges decreased at Cretaceous-Tertiary boundary; these animals are assumed not to thrive at low silicic acid concentration (Kidder and Tomescu, 2016) and their spicules became progressively less

robust (Maldonado et al 1999). Furthermore, DSi depletion contributed to the radiation of sponges with alternative skeletons which were not dependent on the availability of this nutrient.

From what described diatoms played a key role in ecosystems also in past oceans and moulded species dynamics.

Even though all the evidence and the studies on geochemical archives seemed to tell a clear story about past Si cycle in oceans, new investigations on modern marine biosilicifiers and their Si isotopic fractionation, as well as new mathematical models suggested that what was stated needed to be re-discussed. For example, Alvarez et co-authors in 2017 found massive sponge reefs in areas of modern oceans at relatively low DSi concentration, suggesting these animals are not so susceptible to DSi depletion which is not the only explanation to this shift in sponge lineages. They indeed suggested that the expansion of a less silicified sponge lineage during Cenozoic was more likely a consequence of a greater availability of suitable ecological niches after the collapse of calcareous invertebrates in Cenozoic (Alvarez et al., 2017). Another study published in 2021 by Trower and co-authors shed light on a new hypothesis of a silica depleted Palaeozoic Ocean, before diatoms flourished (Trower et al., 2021). Therefore, much more efforts are needed to achieve a clear knowledge on past Si cycle and on related biota evolution.

1.2.3 Biogeochemical Silicon Cycle in modern oceans

As we learnt how important the Si concentration is to understand the ecological relations among marine organisms in past oceans (Harper and Knoll, 1975, Maldonado et al., 1999, Marron et al., 2016) and the connection of Si cycle with the biological C pump, we shall now focus on Si cycle in modern oceans.

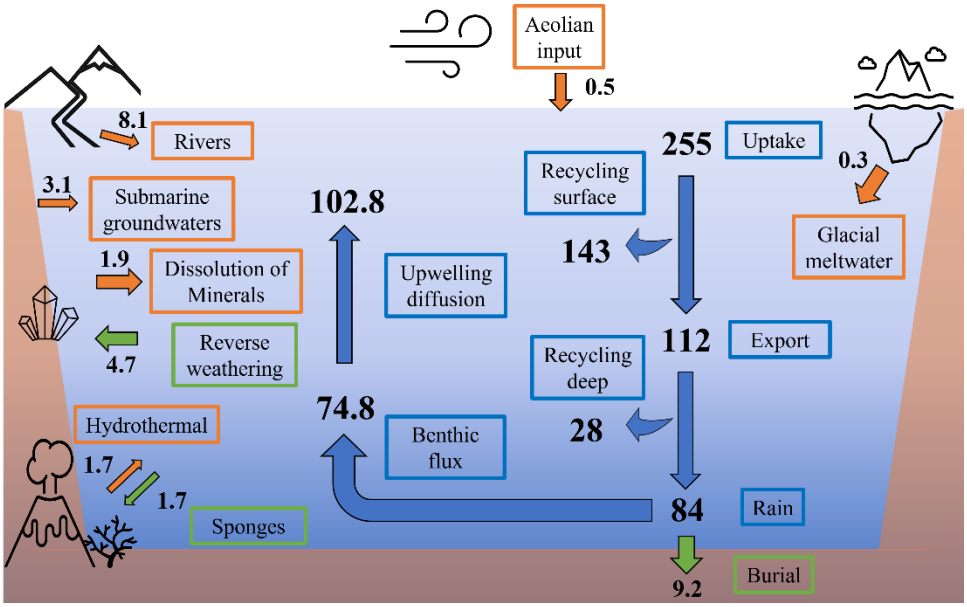

Figure 1.6: Si cycle in the modern ocean at steady state (Modified from Tréguer et al., 2021). All fluxes are in teramoles (10^{12}) of silicon per year ($Tmol_{Si}yr^{-1}$). Green arrows = output flux, orange arrows = input flux, blue arrows = biological flux

In **Figure 1.6** the Tmol of Si transferred every year in global oceans are represented (Tréguer et al., 2021) and, thanks to new research in this filed, values are much higher than previous estimates.

It is hypothesised that modern ocean Si cycle is at steady state with inputs and outputs. The major input is represented by Si particles transferred by rivers, followed by submarine groundwater discharge and the chemical weathering of siliceous material from sediments and subpolar glaciers. Another important continental input is the release of DSi from high and low temperature hydrothermal submarine activity or the particulate lithogenic silica brought by dust and dissolved in oceans at different rates. All these inputs are balanced by the sequestration of DSi from long – lived sponges, formation of new autogenic material (clays, reverse weathering) and long-term burial of planktonic biogenic silica in sediments.

As DSi requirement is crucial for the growth of diatoms, changes in these input and output fluxes need to be considered as potential factors controlling diatoms distribution and abundance. On the other hand, diatoms, as the most efficient DSi users, largely contribute to the 255 Tmol Si year

recycled in the oceans and participate to the 9.2 Tmol Si that are buried every year, so all the other factors affecting these organisms' proliferation would impact oceanic Si cycle.

1.3 Silicification Process in Diatoms

Diatoms are considered the most efficient silicifying organisms, but what does it mean?

Bio-silicification is the process by which living organisms take up DSi from the environment and process it into a solidified form (amorphous silica, randomly arranged atoms of tetrahedra composed by Si binding Oxygen, Grotzinger and Jordan, 2014) for structure formation. According to Marron et al., 2016 this process is widespread even if poorly understood in the major eukaryotic supergroups (Brzezinski et al., 2017, Ikeda 2021) (**Figure 1.7**).

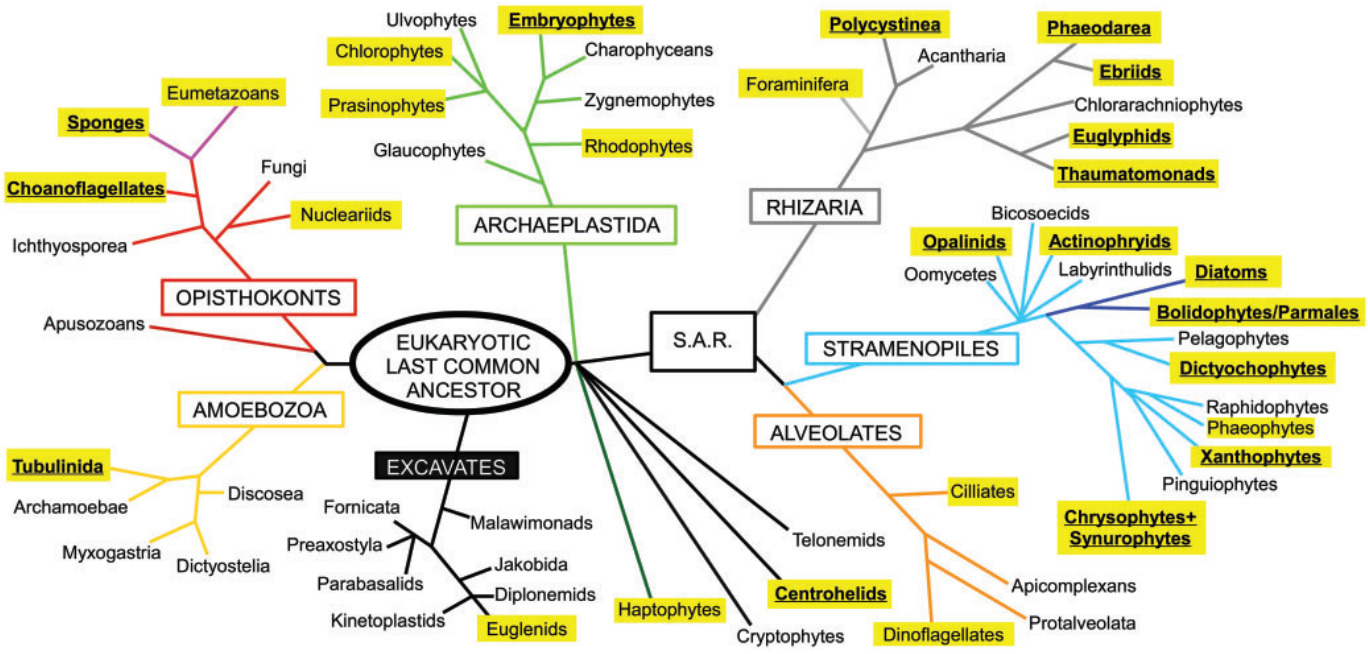

Figure 1.7: Si biomineralization across the Eukaryotes. Taxa highlighted names contain one or more biosilicifying species (Marron et al., 2016).

In humans, Si is essential for proper bone and connective formation, as well as for normal growth and development (Jugdaohsingh, 2007) and collagen synthesis. Si is acquired through various dietary sources (Farooq and Dietz, 2015). Although multiple benefits provided by Si, its requirement and how Si is processed into our bodies are not clearly understood.

Plants take up Si in the form of mono-silicic acid through their roots (abundant in the soil after the weathering of silicate mineral-containing rocks). It precipitates due to supersaturation (> 2mM) of amorphous silica during transpiration process in the aerial part of the plant: the biogenic opal formed is called phytoliths (a mineral form of silicate found in the plants, Opfergelt et al., 2006, Cornelis et al., 2010, Kumar et al., 2021). Si has some positive impacts on plants (resumed in **Figure 1.8**) even though this is not considered as an essential element; not all the plants present phytoliths. Plants have evolved multiple mechanisms for Si uptake: Exley and co-authors (2015) proposed a passive mode of uptake through facilitated or carrier mediated diffusion while Kumar and co-authors (2017) argued for an active mechanism through energy dependent specific transporters. Two kinds of Si transporter are found in rice: LSi1, a passive channel like aquaporins, and LSi2, an active transporter that uses the driving force of a proton gradient to move Si out of the plant cell (Ma et al., 2006).

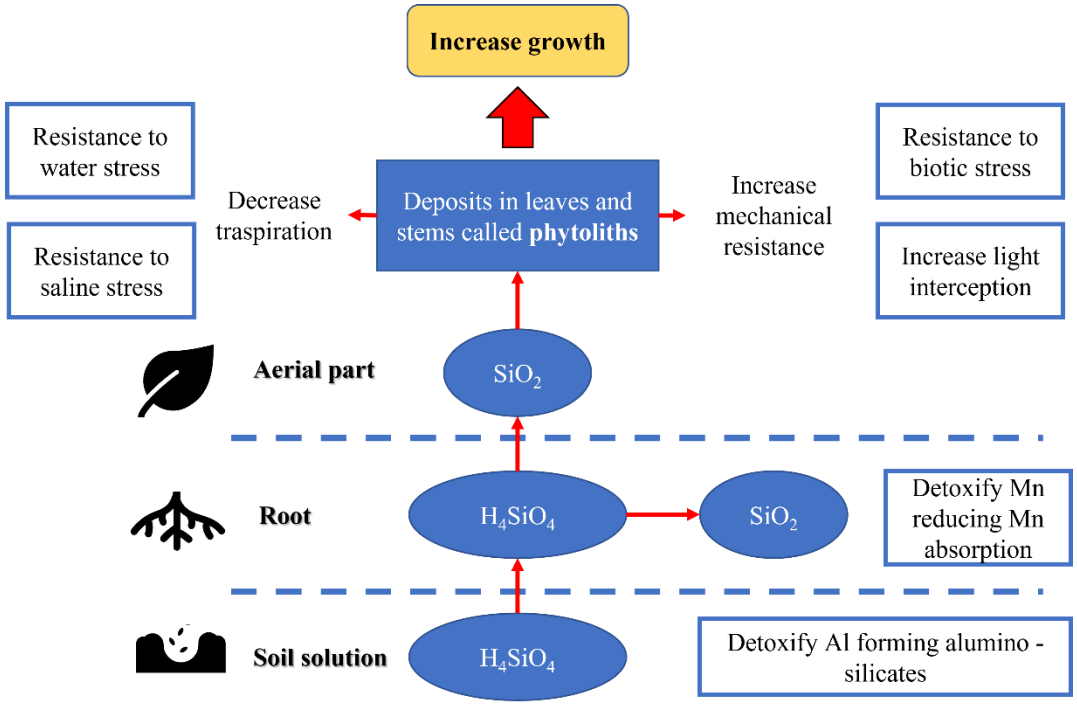

Figure 1.8: Benefits of silicic acid precipitation in plants (Modified from Silica School, S. Opfergelt 2021)

Nevertheless, the most extensive use of Si on the planet occurs in oceans, mostly in diatoms to build their cell wall, but the process it is still poorly understood (**Figure 1.9**).

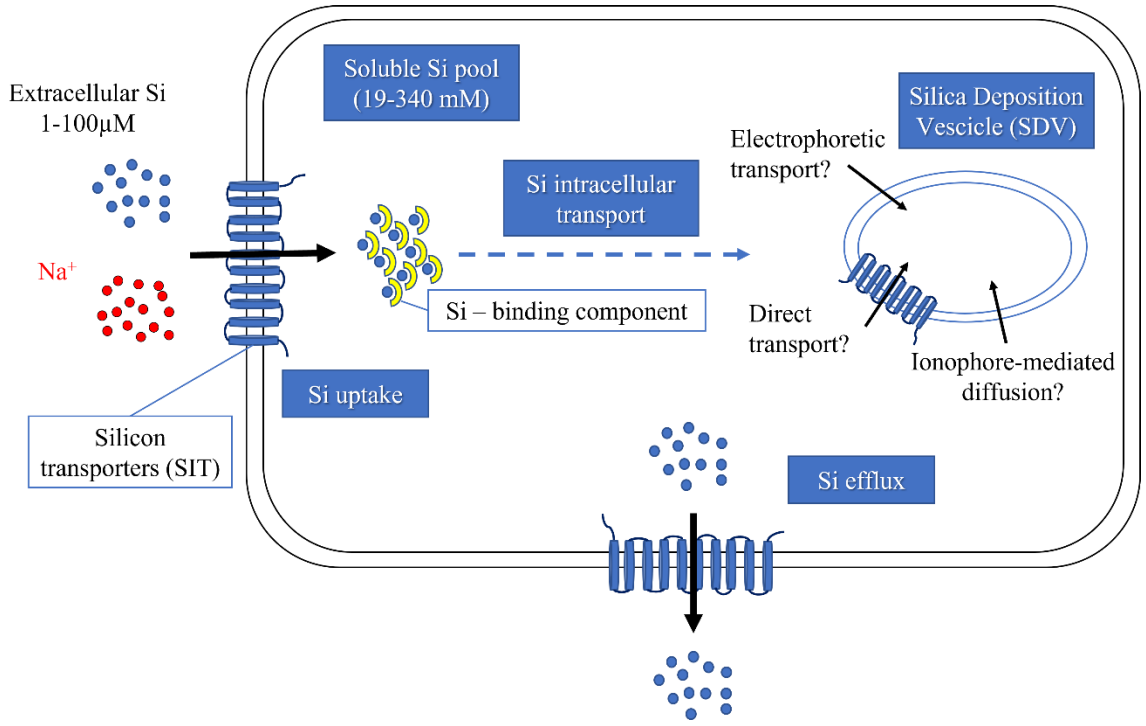

Figure 1.9: Si metabolism in diatoms (Modified from Silica School, Thamatrokoln 2021)

1.3.1 Silicic acid uptake

Extracellular silicic acid is taken up through membrane bound protein transporters called SITs (Hildebrand et al., 1998, Javaheri et al., 2014, Shrestha and Hildebrand, 2015). The average concentration of silicic acid in modern oceans is about 10 µM while a content of soluble Si of 19-340 mM has been measured in diatoms (Kumar et al., 2020), suggesting that the internalization of Si is against the concentration gradient. To achieve it, SITs work as sodium symporters, using the driving force of an inward facing sodium gradient and transporting silicic acid and Na^+ in a 1:1 ratio. However, as silicic acid is a small, uncharged molecule, it has been observed that under environmentally relevant concentrations it can freely diffuse across membranes and diffusion can be the major mode of uptake (Thamatrakoln and Hildebrand, 2008, Hildebrand et al., 2018); while SITs are important at low external Si concentrations (< 30 µM, Thamatrakoln and Hildebrand, 2008, Durkin et al., 2016). SITs consist of 10 transmembrane segments divided into two

symmetrical single 5-TM domains and recently it has been discovered a family of SIT – like transporters consisting of a single 10-TM domain. As in Si saturated oceans the active transport was unnecessary, the ancestral SIT has likely evolved to efflux Si and to prevent toxicity and consisted of a single 5-TM; then, after an internal gene duplication or fusion of two 5-TM domains, a 10-TM domain was formed giving modern diatoms the ability to both uptake and efflux Si (Thamatrakoln and Hildebrand, 2008). The hydroxyl group of silicic acid would bind to the carbonyl group of the glutamine belonging to a conserved "GXQ" motif in the SIT proteins, the bond causes a conformational change that would allow silicic acid to pass through the membrane (Knight et al., 2016). Silicic acid uptake takes place during specific stages of the cell cycle: during G1, to allow cell expansion through new girdle bands and during G2+M, to allow valve formation (Claquin et al. 2002). Most diatoms species are unable to store Si intracellularly and data suggest that the rate of incorporation into the cell wall controls the rate of uptake (Conway et al., 1976; Conway and Harrison, 1977; Hildebrand 2003).

1.3.2 Silica polymerization

Once inside the cell binding components (ligand or proteins, still unidentified) are hypothesized to maintain silicic acid in solution and to prevent autopolymerisation (known to occur at concentration >2 mM) (Martin – Jézéquel et al., 2000). The polymerization process and cell wall synthesis occur within specialized silica deposition vesicles (SDVs), surrounded by a membrane called silicalemma: these vesicles have been visualized using transmission electron microscopy but never biochemically isolated (Hildebrand and Lerch, 2015, Hildebrand et al., 2018). The environment inside the SDVs is slightly acidic in order to promote silicic acid polymerization into silica as a gel network (Iler 1979).

1.3.3 Micromorphogenesis

Valve formation occurs in distinct phases. The base layer on the proximal surface must be formed first and used as a blueprint for structure formation. Deposition of silica follows on the rim of the

valve producing a more rigid structure in this zone and a lack of extensive silicification in the centre. Lastly, the valve gets thicker in the z-axis toward the distal valve surface (Hildebrand et al., 2018).

1.3.4 Organic components involved in silicification

Valve formation in diatoms is mediated by cytoskeleton and other organic components recently identified.

Silaffins: small, lysine and serine reach peptides which catalyse the polymerization of silica. It has been observed that the morphology of the resulting silica depends on the concentration and mixture of silaffins (Kroger et al., 1999, Kroger et al., 2002).

Long-chain polyamines (LCPAs): known to catalyse silica polymerization in presence of polyanions.

Silacidins: proteins rich in serine and acidic amino acids which catalyse silica formation in presence of LCPAs (Wenzl et al., 2008).

If these three groups of proteins have low molecular weight, they catalyse the formation of silica structures lacking higher order structure.

Cingulins: proteins rich in tryptophan and tyrosine; targeted to the girdle bands.

AFIM (ammonium fluoride insoluble proteins): proteins embedded in the silica hypothesized to be the pattern forming base layer (Si Matrix proteins and silaffins).

SAPs (silicalemma associated proteins): proteins which probably serve as an intermediary between cytoskeleton and SDV (Silicanin – 1, Tesson et al., 2017, Kotzsch et al., 2017, Gorlich et al., 2019).

1.3.5 Si efflux

Probably due to the scarce availability of oceanic silicic acid nowadays, Si uptake is considered the crucial part of frustule formation in diatoms. Few authors (Milligan et al. in 2004) focused on an

important but overlooked aspect of Si transport: the efflux of Si from the cell. The importance of efflux in cells' balance is to prevent the over accumulation of intracellular soluble Si that could auto- polymerize and be detrimental to cell function. It has been proposed that efflux may occur through a mechanism similar to that of the influx but working in the opposite way, even if the role of sodium in efflux is unclear (Thamatrakolin et al., 2006). A homolog to a plant Si efflux transport protein, LSi2, has been identified in diatoms, but there is no empirical data to support its role in Si efflux.

1.3.6 Si dissolution

Si dissolution is the process through which silica return in water in the form of silicic acid; it occurs because of concentration gradient (seawater is undersaturated in silicic acid, Tréguer et al., 2021) and basic environmental pH, that is corrosive to the amorphous silica. Si dissolution is not a favourable process for cells because frustules need to be passed to daughter cells, therefore, to prevent Si dissolution frustules are covered by an organic coating (Desikachary and Dweltz, 1961). The rate of dissolution depends on:

(I) Bacterial activity, degrading the organic coating and leading silica accessible to water (Tamburini et al., 2006, Roubeix et al., 2008,),

(II) Environmental temperature, pH, salinity, and silicic acid concentration (Loucaides et al., 2012),

(III) Frustule characteristics (specific surface area, number of active sites, Al content, Van Bennekom et al., 1991, B. Moriceau 2021, silica school),

(IV) Cell aggregation: slower dissolution if diatoms are embedded together (Moriceau et al., 2007).

Recent evidence demonstrate that the dissolution of biogenic silica occurs in two phases: a rapid dissolving phase is followed by a slow dissolving phase (Truesdale et al., 2011).

1.3.7 Factors affecting silicification

Many factors seem to influence the silicification process:

(I) Lower temperature leads to increased silicification (Durbin et al., 1977);

(II) Silicification is inversely correlated to growth rate in nonlimiting Si conditions (Flynn and Martin-Jézéquel 2000). Therefore, all other factors limiting growth control silicification of frustules (levels of $Fe^{2+/3+}$, Zn^{2+}, Martin – Jézéquel et al., 2000 and references therein);

(III) Si deposition depends on Si availability: DSi limiting growth results in reduced levels of silicification (Brzezinski et al., 1990, Shrestha et al., 2012);

(IV) Light alters silicification even though its role is still unclear; increasing silicification is observed at both very low (15µmol photons·m^{-2}·s^{-1}, Xu et al., 2021b) and higher (300 µmol photons·m^{-2}·s^{-1}, Su et al., 2018a) light intensities;

(V) Salinity affects silicification (Vrieling et al., 2007);

(VI) Silicification is affected by pH (Hervé et al., 2012);

(VII) Increased silicification is observed in presence of predators (Pondaven et al., 2007).

1.4 Frustules as potential biomaterials

1.4.1 Silica shell characterization

As discussed above, the most fascinating morphological characteristic of diatoms is their outer silica shell, the frustule. Frustule is a highly intricate ornamented and porous structure, with a species-specific pattern. Beside radial or bilateral symmetry, all frustules present an hypotheca inserted in a bigger epitheca connected with systems of girdle bands, like a Petri-dish, surrounding the living cell; the two valves show differently porous layers.

Frustules are basically composed by hydrated amorphous silica ($SiO_2 \cdot nH_20$) with Si - OH (silanol) and Si - H groups on the surface (Qin et al., 2008, De Tommasi et al., 2017). Thanks to FTIR spectroscopy analysis also organic residual was found in the silica matrix (mainly C - H bounds but also S composites, Kammer et al., 2010, De Tommasi et al., 2016). Frustules are surrounded by extracellular polymers (organic coating mentioned before) involved in sessile adhesion, gliding, formation of biofilm and colonies, protection against drying and silica dissolution (Svetlicic et al., 2013, De Tommasi et al., 2017). Their structural properties can be divided into:

- Mechanical properties: Several studies on the response of frustules after mechanical solicitation were carried out, making use of both Finite Element Method (FEM, numerical simulations performed on rendered frustules) or nanoindentation (direct measurements of frustule breaking point) (Hamm et al., 2003, Moreno et al., 2015, Aitken et al., 2016, Xu et al., 2021). What emerged is that frustules provide great Hardness value, ranging from 0.5 to 36 GPa, combined with Elasticity ranging from 1 to more than 20 GPa (Aitken et al., 2016, De Tommasi et al., 2017, Xu et al., 2021). Values depends not only on different species (Hamm et al., 2003), but also on different silicification degree (Xu et al., 2021) and pore size (Moreno et al., 2015, Lu et al., 2015). This incredible strength (much higher than other natural biomaterial, Aitken et al., 2016) provides frustules the possibility to resist to predator mandibles and to be exploited for multiple purposes (see next paragraph).

- Fluid dynamics properties: the external surface of frustules (consisting in porous layers) interacts with different particles in solution (nutrients, bacteria, viruses); it was demonstrated that surface microtopographies control the diffusion and advection of these particles across the surfaces (Hale and Mitchell 2001, 2002), constituting a way to sort them according to their size (De Tommasi et al., 2017).

  Frustules are certainly also contributing to cell sinking rate (Raven and Waite, 2004, Miklasz and Denny, 2010). As frustules cannot be approximated to spheres, Stoke's law could not accurately describe diatoms sinking capacity, therefore new models describing diatom sinking were formulated, due to the great importance of diatoms in C and Si cycles (Miklasz and Denny, 2010). Even direct measurements of frustule buoyancy control are still limited to few recent studies (Gemmell et al. 2016, Lavoie et al., 2016, Du Clos et al., 2019, Du Clos et al., 2021).
- Optical properties: frustules can be ascribed to photonic crystals, due to their periodic architecture and distribution of refractive index which can block the propagation of light in specific wavelength ranges. The interaction with light consists in three documented phenomena: light confinement (De Stefano et al., 2007), selective transmission (Noyes et al., 2008, Ferrara et al., 2014), photoluminescence (emit blue radiation if irradiated with UVB light, Qin et al., 2008).

Diatoms evolved and have maintained these structures because the mentioned properties have provided them advantages in term of fitness. Advantages are listed as follows:

(I) Protection against predators thanks to high mechanical strength (Hamm et al., 2003),

(II) Enhancement of nutrient uptake and filtration of harmful agents (Hale and Mitchell 2001, 2002),

(III) Controlled movement in water environments (Raven and Waite, 2004),

(IV) Enhancement of the optical scattering properties for light and energy harvesting. In particular, pores can act as light channels and focus, helping to collect and transmit more light in photoreceptors and, therefore, increasing the photosynthetic rate (Medarevic et al., 2016) and simultaneously protecting the nucleus from photodamages,

(V) Proton buffer capacity (Milligan & Morel 2002).

From the huge diversity of frustules, the question rises whether all of them provide the same advantages and if all can guarantee the listed functions, as these are still poorly analysed and understood.

1.4.2 State of art on frustules exploitation

The global demand for smaller and smaller structures in electronic, optical, chemical, and biomedical devices combined with the need to reduce the requirements for high temperatures and aggressive chemicals to manipulate materials pushed the studies to find new suitable biomaterials. Nature has optimized, through frustules, a hard, elastic, highly complex, new material requiring only basic nutrients and sunlight. The cheap cultivation of diatoms (it only requires CO_2, water, salts and light, Lopez et al., 2005) not competing with crops for the arable land (Gordon and Polle, 2007) could be considered as a promising source of biomaterials.

Biomimetic engineering is the global trend to try and get ideas from natural organisms with complex architecture and unique properties. Diatom's frustules in the last 30 years were largely used as nanostructured materials for several applications (Henstock et al., 2015, Maher et al., 2018), due to their (i) hierarchical layers of porous membranes, providing high surface area; (ii) structural architecture for ion transport. Diatom based silica can be obtained also by the exploitation of fossilized diatoms called diatomaceous earth. Possible uses are listed here:

(I) Use of diatomite/diatomaceous earth in toothpaste, facial scrubs, water filtration, thermal insulation, building material, insecticide, soil amendment, abrasive material, food additives.

(II) Functionalized diatom silica for biomedical application:

a. nanoparticles used as vectors in drug delivery,

b. frustules applied in bone repair (Reid et al., 2021).

(III) Exploitation of frustules physical properties:

a. Used as micro lenses,

b. Squeeze light under diffraction limits.

(IV) Frustule efficient interaction with light led to:

a. Bio-inspired solar cells,

b. Bio-based UV filter,

c. Nanostructured substrates in plasmonic,

d. Exploitation of frustules photoluminescence for optical sensors and biosensors.

(V) Exploitation of frustules as scatterers in random lasers.

(VI) Applications after frustule modification. Indeed, the high resistivity of diatoms silica which prevent their use for energy conversion and storage could be overcome transforming silica in other materials while preserving diatom's structure (metabolic insertion of germanium or titania):

a. Nanostructured semiconducting devices for optoelectronics,

b. Light trappers in dye sensitized solar cells,

c. Structured photocatalysts of toxic chemicals.

Given the biotechnological potential, it is crucial to characterize more morphologies of frustules; indeed, most of the studies are focused on few big centric diatoms (*Coscinodiscus sp*. or *Thalassiosira sp.*) missing physical characterization of other species, with other morphologies, even

less silicified frustules but species with higher growth rates and more promising for a future industrial scale up (Vona et al., 2021).

To obtain biosilica from diatoms it is crucial to totally remove the organic matter adhered on their surface, preserving frustule shape, and avoiding its erosion (Sardo et al., 2021). Three ways are mostly used to obtain frustules: (i) oxidative washing protocols using hydrogen peroxide solutions, (the most commonly used) (ii) chemical treatments with acids, and (iii) baking frustules at high temperatures, the simplest and least expensive method but able to alter frustule architecture (Umemura et al., 2010, Sardo et al., 2021 and reference therein). It seems urgent to understand which of them is more affordable in terms of environmental sustainability, with the perspective to exploit this extraordinary natural material.

1.5 Aim of the thesis

Given the impact of diatoms on the global C and Si cycles and the emerging exploitation of frustules as bio-based materials, the general introduction pictured the multidisciplinary state of art about these photosynthetic organisms and highlighted the gaps in knowledge which this thesis shall try to fill. In particular, the main question was how the synergic action of selective pressures has acted on the evolution of morphologically different diatoms. Furthermore, the biological functions of the frustules, often deduced from studies on few centric species, were investigated and shed light on the characterization of biotechnologically suitable silica scaffolds.

This thesis is organized in four different research topics: the first two topics focused on major selective pressures (e.g. Si decline through geologic eras and the interaction of diatoms with competitors and predators) and their involvement in diatom radiation. The physiological response of morphologically different diatoms to these selective pressures was evaluated. A third topic had the scope to investigate sinking behaviour of morphologically different diatoms, trying to understand the adaptative role of frustules in controlling buoyancy. Finally, the last topic addressed in the thesis was a preliminary study on the characterization of frustules with the perspective of a possible exploitation as silica biomaterial; in the view of an industrial scale up, the environmental impact of different cleaning procedures compared by LCA methodology was estimated.

Chapter two: Si decline and diatom evolution - insights from physiological experiments

Alessandra Petrucciani, Andrew H. Knoll, Alessandra Norici

2. Si decline and diatom evolution: insights from physiological experiments

2.1 Introduction

In the modern ocean, diatoms are abundant and diverse primary producers, distinguished by their silica shells, or frustules. Accounting for some 20% of primary production on Earth, diatoms sustain the global food web while being responsible for 240 Tmol of biogenic silica precipitation annually (Loucaides et al., 2012, Vallina et al., 2014, Malviya et al., 2016, Sutton et al., 2018, Vincent and Bowler, 2020, Trèguer et al., 2021). The oldest known diatom fossils occur in Late Jurassic (ca. 165 million years old, Ma) amber (Girard et al., 2020), and since that time, diatoms have diversified to play a crucial role in ocean ecology (Ambrust 2009); indeed, their radiation has moulded marine ecosystems through time (Finkel and Kotrc 2010, Knoll and Kotrc 2015, Cermeño et al., 2015, Medlin 2015, Benoiston et al., 2017, Knoll and Follows 2016,), affecting both the carbon and silica cycles (Siever et al., 1992, Ragueneau et al., 2006, Renaudie 2016, Conley et al., 2017, Trèguer et al., 2018).

In Precambrian oceans, before the evolution of organisms with biomineralized skeletons, the concentration of dissolved silica (DSi) in seawater must have been much higher than today (Siever, 1992; Conley and Carey, 2015, Conley et al., 2017). The Ediacaran/Cambrian radiations of siliceous sponges and radiolarians established biology as a major component of the silica cycle, demonstrably changing the depositional dynamics of silica in the oceans (Maliva et al., 1989, Kidder and Tomescu, 2016) and probably decreasing seawater DSi concentration (Conley et al., 2017). New biological influences emerged during the Mesozoic Era, as multiple clades of silica biomineralizing protists spread through the oceans (Knoll and Kotrc, 2015; Marron et al., 2016). Diatoms, in particular, are thought to have further drawn down DSi in surface seawater, leading to the low concentration (< 30 μM) observed today (Racki and Cordey, 2000, Conley et al., 2017). Changes in hydrothermal fluxes and continental weathering can also have influenced DSi through

time (Frings et al., 2016, Conley et al., 2017), but independent perspectives on orogenesis and seafloor spreading suggest that Mesozoic-Cenozoic DSi decline was largely mediated by biology. Within diatoms, the diversification of specialized transporters (Silicon Transporters, SIT) helped to make them the dominant marine DSi utilizers in Cenozoic oceans (Durkin et al., 2016; Fontorbe et al., 2017), and as a consequence, competitors for this resource, principally radiolarians and sponges, show declines in test mass and/or environmental distribution (Harper and Knoll, 1975, Maldonado et al., 1999, Lazarus et al., 2009; Hendry et al., 2018). Diatoms themselves show a change in skeletal morphology through time, with a trend toward smaller, more elongated and less highly silicified frustules toward the present (Finkel et al, 2005; Armbrust 2009, Finkel and Kotrc 2010). It is worth noting that factors other than DSi availability may have influenced the evolution of silicifiers (e.g., Finkel et al., 2005; Hendry et al., 2018) and that changing selectivity of preservation may also influence the observed record (Westacott et al., 2021). In order to gain further perspective on diatom growth and physiology under changing conditions of DSi availability, four morphologically distinct modern diatoms (*Chaetoceros muelleri*, *Conticribra weissflogii*, *Phaeodactylum tricornutum*, *Cylindrotheca fusiformis*) were acclimated to paleo-reconstructed environments according to Ratti et al. (2011), modified to mimic Mesozoic to modern changes in DSi concentration. As nutrient limitation is known to affect silica deposition and dissolution in diatoms (Takeda 1998, Hutchins and Bruland 1998, Boyle 1998, De la Rocha et al., 2000, Mosseri et al., 2008, Finkel et al., 2010, Bucciarelli et al., 2010, Cohen et al., 2017, Meyerink et al., 2017, Panagiotopoulos et al., 2020), experiments using reconstructed seawater that include interpreted variation in the bioavailability of N, Fe, Zn, and Mo (Ratti et al., 2011, Giordano et al., 2018) better approximate ancient marine environments and their interactions with organisms. Growth, photosynthetic efficiency, organic and inorganic composition, and frustule morphology were assessed.

2.2 Material and Methods

2.2.1 Algal cultures

Two centric diatom species, *Chaetoceros muelleri* (CCAP 1010/3, https://www.ccap.ac.uk/) and *Conticribra weissflogii* (DCG 0320, https://bccm.belspo.be/about-us/bccm-dcg), and two raphid pennate diatoms more recently evolved and characterized by their thin frustules, *Cylindrotheca fusiformis* (NEPCC417) and *Phaeodactylum tricornutum* (DCG 0981), were acclimated for at least ten generations to three newly designed growth media combining the Mesozoic/Cenozoic concentration of nutrients (as already published by Ratti et al., 2011; **Table 2.1**) and the presence of different Si regimes (**Table 2.2**).

There are varying estimates for DSi levels in ancient oceans. Siever (1992) proposed that diatom evolution gradually reduced seawater DSi from some 1000 µM to its present level of < 30 µM in most surface waters. In contrast, Conley et al. (2017) estimated that DSi concentrations of 500 µM in pre-diatom oceans fell rapidly to near-modern levels as diatoms began their radiation. Most recently Trower et al. (2021) used Si isotope ratios to argue that DSi levels could have been as low as 150 µM in Paleozoic oceans. Regardless of starting point, all conclude that diatom radiation reduced DSi concentrations in surface seawater. The DSi values used in our experiments were chosen to explore this range of estimated changes through time.

Table 2.1: Mesozoic/Cenozoic concentration of nutrients. Ratti et al., 2011

Nutrient	Final Concentration
NaNO3	10 µM
$FeCl_3 \cdot 6H_2O$	50 nM
$ZnSO_4 \cdot 7H_2O$	100 nM
$Na_2MoO_4 \cdot 2H_2O$	105 nM

Table 2.2: Silicic acid concentrations added to the Mesozoic/Cenozoic medium and mimicking the progressive DSi depletion through geologic eras

Treatment	Si concentration
Pre- to Early Diatoms	500 µM
Intermediate	205 µM
Modern	25 µM

Cultures were established in 500 mL flasks filled with 200 mL of medium and maintained in a culture chamber at 18 °C, illuminated with cool white fluorescent lamps at 60 µmol m^{-2} s^{-1} and 12:12 h light-dark cycles.

2.*2.2 Specific growth rate and cell volume*

Cell number was measured using a CASY TT cell counter (Innovatis AG, Reutlingen, Germany). Aliquots of 100 µL of culture were diluted in 10 mL of an electrolyte solution (CASY TON; Innovatis AG). Cells were pumped into the cell counter through a 150 µm capillary at a constant flow and the number of cells was determined through the enumeration of events measured as change of conductivity. The electrical current was assessed by two platinum electrodes, between which a pulsed low voltage of 1 MHz was generated. The same instrument was also used to measure the cellular size as the volume of electrolyte solution displaced by the passage of cells through a measuring pore (Palmucci et al., 2011). All determinations were carried out on samples from three distinct cultures. Specific growth rates, µ (2.1), were derived from daily counts of exponentially growing cells, carried out on a minimum of three distinct cultures for each treatment.

$$(2.1)\ \mu = \frac{ln(N_t/N_0)}{t}\ \text{(Monod 1949)}$$

2.2.3 Pigments quantification and photosynthetic efficiency

Algae were centrifuged at 3000 g for 5 min. Then, pigments were extracted from the pellet in 2 mL of 100% (v/v) methanol (Ritchie et al., 2006); the extracts were stored in the dark, at -20°C overnight. Colorless pellet was then separated from the supernatant by centrifugation 13000 g for 5 min. The absorbance of the supernatant was evaluated spectrophotometrically (Beckman DU 640 Spectrophotometer, Beckman Coulter) in a range from 750nm to 350nm (scan speed 0.5nm). Wavelengths of 664, 630 and 470 nm were used for pigment quantification of chlorophyll *a,* chlorophyll c_1 + c_2 and carotenoids, respectively. Methanol absorbance was used as blank and absorbance at 730 nm was subtracted to all measurements.

Chlorophyll concentrations were calculated according to Ritchie 2006 equations:

$$(2.2)\ \text{Chl } a\ (\mu g \cdot mL^{-1}) = 13.2654 \cdot Abs_{664nm} - 2.6839 \cdot Abs_{630nm}$$

$$(2.3)\ \text{Chl } c\ (\mu g \cdot mL^{-1}) = 28.8191 \cdot Abs_{630nm} - 6.0138 \cdot Abs_{630nm}$$

$$(2.4)\ \text{Total Chl}\ (\mu g \cdot mL^{-1}) = \text{Chl } a + \text{Chl } c$$

Carotenoids' concentrations were calculated according to Wellburn 1994 equations:

$$(2.5)\ \text{Total carotenoids}\ (\mu g \cdot mL^{-1}) = (1000 \cdot Abs_{470nm} - 1.63 \cdot \text{Chl}a - 104.96 \cdot \text{Chl}c)/221$$

All results were expressed as pg of pigment per cell.

In vivo variable fluorescence of photosystem II (PSII) chlorophyll *a* (P_{680}) was analyzed by DUAL PAM 100 fluorimeter (Heinz Walz GmbH, Effeltrich, Germany). Samples of 10^7 cells were collected by centrifugation at 3000 g for 5 min, re-suspended in 2 mL of growth medium and dark-adapted for 10 min. Subsequently, samples were transferred into a glass cuvette for the PAM analysis under continuous stirring. The measuring light (40 µmol photons m^{-2} s^{-1}) was turned on to determine the F_0 value, the minimum value for chlorophyll fluorescence. Then, a saturation pulse

(10000 µmol photons m^{-2} s^{-1}, 600 ms) was applied to saturate all centers and allowed to measure the F_m value, the maximum value of fluorescence. Maximum quantum efficiency of PSII, F_v/F_m, was then calculated as follows (2.6):

$$\frac{F_V}{F_m} = \frac{(F_m - F_0)}{F_m} \quad (2.6)$$

F_v/F_m represents a robust indicator of the maximum quantum yield of PSII photochemistry (Misra et al., 2012). All parameters were obtained using the Dual PAM v1.8 software (Walz GmbH, Effeltrich, Germany).

2.*2.4 Elemental composition*

Cellular C and N abundances were determined using an elemental analyser (ECS 4010, Costech Italy) from 0.1 – 1 mg of dry cells washed twice with an ammonium formate solution isosmotic to the culturing media and dried at 80°C. Sulfanilamide (C:N:S = 6:2:1) was used in a standard curve for quantification. Data acquisition and analysis were performed with the software EAS- Clarity (Costech Analytical Technologies Inc., Milano, ItalyOrganic composition). All measurements were carried out on 3 biological replicas.

Similarly prepared samples (0.5 – 1 mg of dry weight) were analysed by an elemental analyser (ECS 4010, Costech Italy) connected to the ID Micro EA isotope ratio mass spectrometer (Compact Science Systems, LymedaleBusiness Centre, Newcastle-Under-Lyme, United Kingdom) to obtain carbon and nitrogen stable isotopes ($\delta^{13}C$ and $\delta^{15}N$) ratios. Urea was the isotopic standard reference showing $\delta^{13}C = -36.6‰$ and $\delta^{15}N = 2.2‰$; its replicates were used to normalize isotopic values of algal biomass. Two blank samples (empty aluminium capsules) were analysed at the start of each analysis to verify CO_2 and N_2 backgrounds were low, and urea standards were also analysed after every 6 samples to monitor instrument performance. Data acquisition and analysis were performed

with the software EA IsoDelta (Compact Science Systems, LymedaleBusiness Centre, Newcastle-Under-Lyme, United Kingdom). All the measurements were carried out on 3 biological replicas.

The absolute abundance of the other elements than C and N and included Silicon was measured using a Total Reflectance X – ray Fluorescence spectrometer (S2 Picofox, Bruker AXS Microanalysis GmbH, Berlin, Germany). Sampled diatoms were washed twice with an ammonium formate solution isosmotic to the culturing media and resuspended in 250 µl of dH_2O. A solution of 0.1 g L^{-1} Ga (Sigma Aldrich, St. Luis, MO, USA) in 5% HNO_3 was added as internal standard to a final concentration of 0.5 $\mu L \cdot L^{-1}$. The suspension was carefully vortexed and an aliquot of 10µl was deposed on a plastic sample holder, dried on a heating plate and measured for 1000 seconds. Spectral deconvolution and quantification of elemental abundances were performed by the SPECTRA 6.1 software (Bruker AXS Microanalysis GmbH, Berlin, Germany).

2.2.5 *Organic composition*

Diatoms collected during exponential phase were washed twice with a 0.5 M solution of ammonium formate and used to prepare samples for analysis of FTIR spectroscopy. Aliquots of 50 µl of cell suspension were transferred to a silicon window and dried at 80°C (Domenighini and Giordano 2009). FTIR spectra were acquired with a Tensor 27 FTIR spectrometer (Bruker Optics, Ettlingen, Germany). Bands were assigned to cellular pools as described by Giordano et al., 2001 and the relative abundances of lipids, carbohydrates, proteins and silica were calculated via band integrals of deconvolved spectra, with OPUS 6.5 software (Bruker Optik GmbH, Ettlingen, Germany). Considering that silica absorbance (~1075 cm^{-1}) masks some of the typical carbohydrate bands in diatoms, only the integrated value at ~1150 cm^{-1} was used as proxy for carbohydrates. Semi-quantification of carbohydrates and lipids was obtained by comparing the total protein content measured by a quantitative method (see below) with the FTIR absorbance ratio between the pool of interest and that of proteins according to Palmucci et al., 2011; the three macromolecular pools expressed in arbitrary units are normalized to the corresponding at 500 µM Si pool.

Protein content was measured according to the Lowry method described by Peterson (1977) on diatoms collected by centrifugation (13000 g for 5 min) during exponential phase. A volume of 500 µl 1% Sodium Dodecyl Sulphate (SDS) and 0.1 $mol \cdot L^{-1}$ of NaOH was added to the pellet to facilitate membrane disruption and solubilization of proteins. The tubes were vortexed and then incubated at room temperature for 10 min. A volume of 500 µl of reagent A (25% H_2O, 25% SDS 10%, 25% NaOH 0.8M, 25% CTC reagent) was added, the samples were vortexed and let sit at room temperature for 10 min. A volume of 250 µl of the reagent B (83.3% H_2O, 16.7 % Folin & Cicalteau's phenol reagent) was then added and samples were immediately vortexed vigorously; finally, they were incubated in the dark for 30 min. Afterwards, the sample absorbance was measured in a Beckman DU 640 Spectrophotometer (Beckamn Coulter) at 750 nm. Protein contents were calculated by interpolating absorbance data in a standard curve constructed with known concentrations of Bovine Serum Albumine (BSA). All the measurements were carried out on 3 biological replicas and results were expressed as pg of proteins per cell.

2.2.6 *Frustules characterization through Scanning Electron Microscopy*

Diatom frustules were obtained through oxidation of the organic material using hydrogen peroxide, H2O2 (modified from BCCM/DCG protocol). The salts of the culture medium were washed out from the cells for 3 times with deionized water, then 30% H2O2 was added to the cell suspension to a final concentration of about 15%. Samples were dried in oven at 60 °C for 1 day (less silicified species, *P. tricornutum* and *C. fusiformis*) or 3 days (more silicified species, *C. muelleri* and *C. weissflogii*). Finally, the material was washed 4 times with deionized water to carefully remove H2O2. Drops of cleaned material were then poured on a cellulose acetate and cellulose nitrate mixture filter (MF-Millipore™, mesh size 0,45 µm) fixed on the conductive carbon adhesive discs pasted on the stub and left to dry completely at 50°C. The stub was then sputter-coated with a thin layer of gold-palladium in a Balzer Union evaporator and analysed by SEM (High Resolution

ZEISS – SUPRA 40). Pictures were taken with different order of magnitude to obtain also morphometrical measurements of frustule details (raphe and fibulae in *C. fusiformis*, Reiman et Lewin 1965; setae and punctae in *C. muelleri*, Reinke 1984).

2.*2.7 Statistical Analysis*

Significant differences among the means of dependent variables in different paleoenvironments (independent variable) were tested with a one – way analysis of variance (ANOVA), followed by Tukey's post-hoc test. Macromolecular pools as dependent variables in response to paleoenvironments and according to diatom species (independent variables) were analysed by two – way ANOVA, followed by Tukey's *post-hoc* test. Comparison of treatment pairs (morphological parameters at 500 and 25 µM Si, Table S2) was achieved with a two-tailed t-test. The level of significance was set at 0.05. GraphPad prism 8.0.2.263 was used to carry out the tests (GraphPad Software, San Diego, CA, USA).

2.3 Results

2.3.1 Growth, cell volume and photosynthetic efficiency

The four diatom populations were acclimated to reconstructed paleoenvironments. Growth of the smaller species *C. muelleri* and *P. tricornutum* was deeply affected by Si availability in the medium (**Figure 2.1**); specifically, the higher the DSi concentration, the lower the growth rate (**Table 2.3**). In fact, *C. muelleri* cells grew very slowly in when DSi was 500 µM. The decrease in growth rate of these species was accompanied by an increase in cell volume (**Table 2.3**). On the other hand, growth rates of the larger species *C. weissflogii* and *C. fusiformis* were similar among the three DSi treatments.

Table 2.3: Average ± SD of specific growth rate (µ) and cell volume in the four diatoms acclimated to different paleoenvironments (n ≥ 3). Different letters indicate significant differences among conditions in the same species ($p > 0.05$).

		500 µM Si	205 µM Si	25 µM Si
Specific Growth Rate (µ, day^{-1})	*C.muelleri*	0.13 ± 0.04^{a}	0.48 ± 0.08^{b}	0.54 ± 0.08^{b}
	C.weissflogii	0.28±0.03	0.28±0.01	0.25±0.03
	P.tricornutum	0.29 ± 0.01^{a}	0.36 ± 0.02^{a}	0.58 ± 0.04^{b}
	C. fusiformis	0.41±0.09	0.52±0.05	0.47±0.15
Cell volume (μm^3)	*C.muelleri*	581 ± 93^{a}	470 ± 55^{ab}	439 ± 56^{b}
	C.weissflogii	1352 ± 229^{a}	1713 ± 209^{b}	1459 ± 160^{ab}
	P.tricornutum	266 ± 50^{a}	143 ± 20^{b}	134 ± 50^{b}
	C. fusiformis	474 ± 64^{a}	363 ± 28^{b}	381 ± 75^{b}

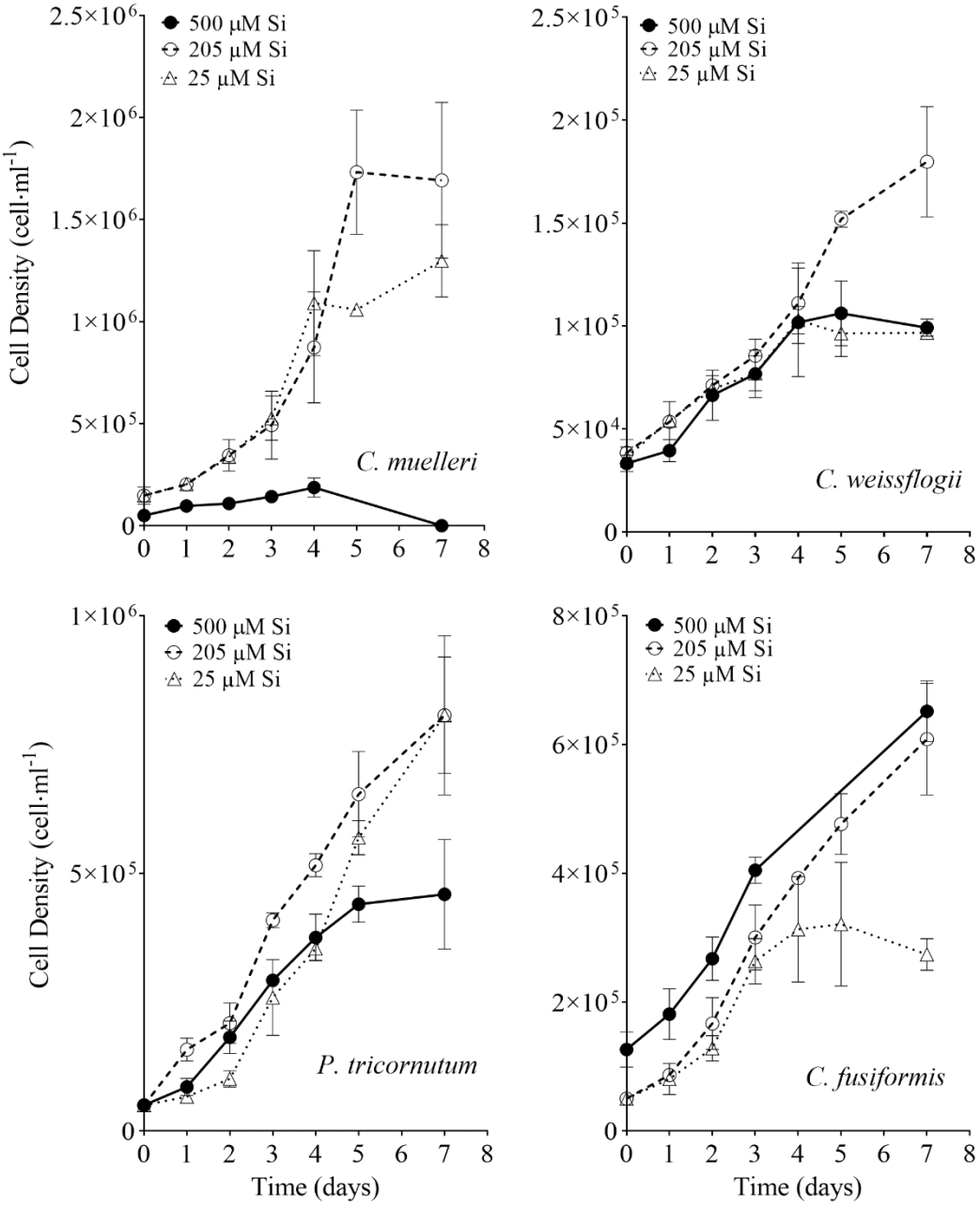

Figure 2.1: Growth curves of the four diatoms acclimated to different paleoenvironments. Data are means of 3 biological replicas. Error bars show SD

2.3.2 Photosynthetic efficiency and pigment quantification

The supply of a high concentration of silicic acid mimicking the Mesozoic regime resulted in a lower maximum PSII Quantum Yield in dark adapted cells, F_v/F_m, of *C. muelleri*, *P. tricornutum* and *C. fusiformis* while *C. weissflogii* did not show any change in the photosynthetic efficiency (**Figure 2.2**).

In the presence of a higher Si availability *C. muelleri* and *C. fusiformis* also showed a lower concentration of pigments (both chlorophylls and carotenoids, **Figure 2.3 A**, **C**). On the other hand, the Chl_a to Chl_{c1+c2} ratio was the same among the conditions in all species except for *P. tricornutum* (**Figure 2.3 B**).

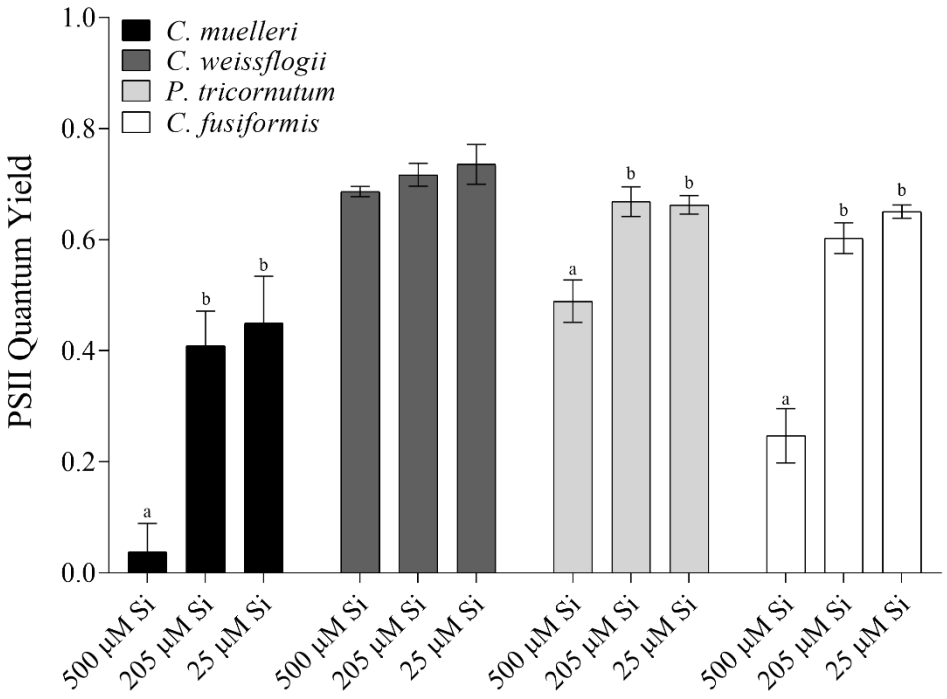

Figure 2.2: PSII Quantum Yield of the four diatoms acclimated to different paleoenvironments. Data are means of 3 biological replicas. Error bars show SD. Asterisks represent significant differences among conditions in the same species (p<0.001).

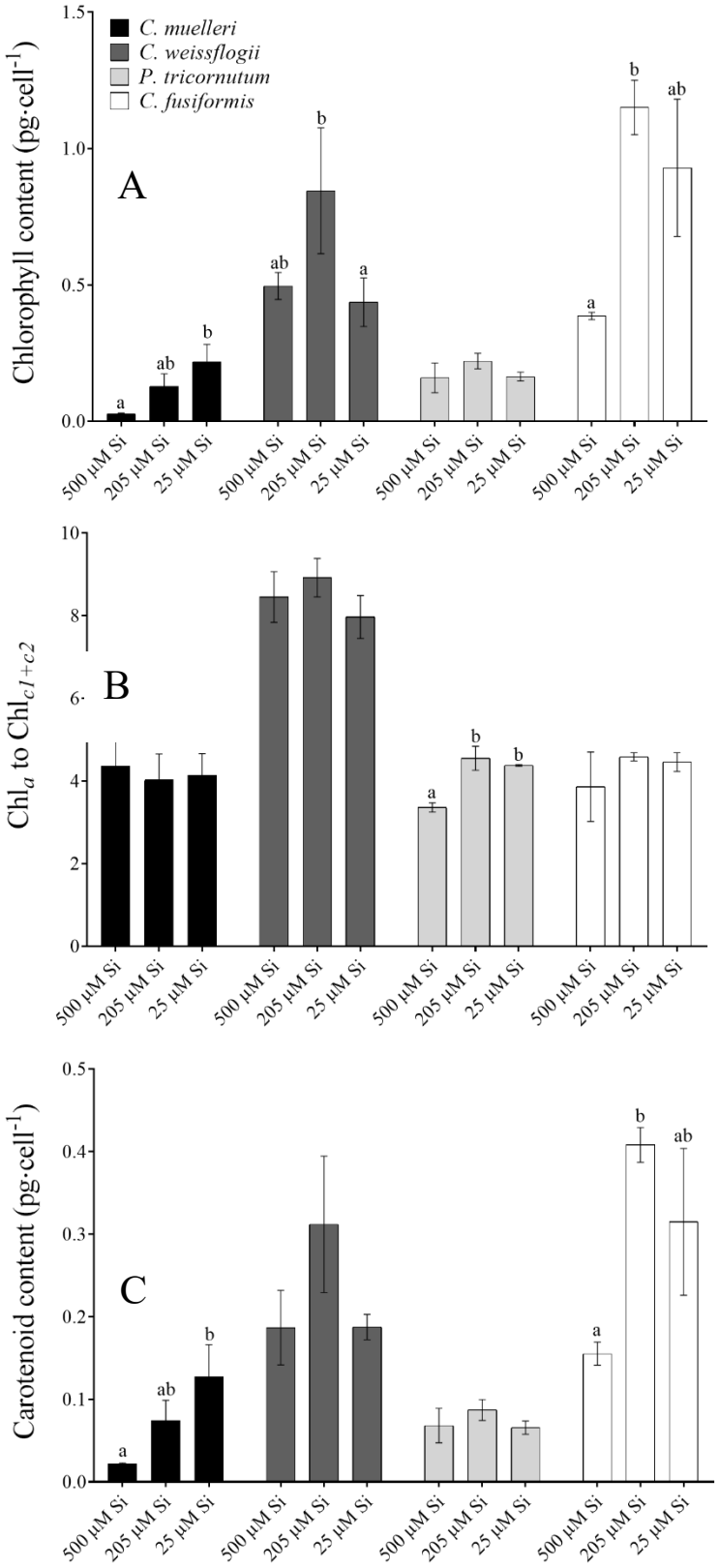

Figure 2.3: Cell contents of pigments in the four diatoms acclimated to different paleoenvironments: (**A**) total chlorophylls, (**B**) Chl *a* to Chl c_1+c_2 ratio (**C**) carotenoids. Data are means of 3 biological replicas. Error bars show SD. Letters represent significant differences among conditions in the same species (p<0.05).

2.3.3 Elemental composition

When cells were subjected to different Si regimes during growth, all diatoms grown in the Mesozoic condition except for *C. weissflogii* accumulated more Silicon per volume unit (**Figure 2.4**). The deepest variation was observed in pennate diatoms, *C. fusiformis* and *P. tricornutum*, showing twice the content when the concentration of external silicic acid reached 500 µM as compared to contents in the other conditions. The same was true when Si content was expressed on a per cell basis (**Table 2.4**).

The P cell quota had a similar trend to that of Si cell quota (**Table 2.4**). Only *P. tricornutum* also showed significantly higher C, N and Fe contents in the highest DSi condition. In particular, when calculating stoichiometry of elements in cells, results highlight a C:N:P:S:Si ratio inversely related to the concentration of silicic acid in the growth medium: lower amounts of assimilated C, N, P and S per unit of cell Si with higher DSi availability (**Table 2.5**). On the other hand, Fe:Si was constant in cells of *P. tricornutum* acclimated to different Si treatments (**Table 2.5**).

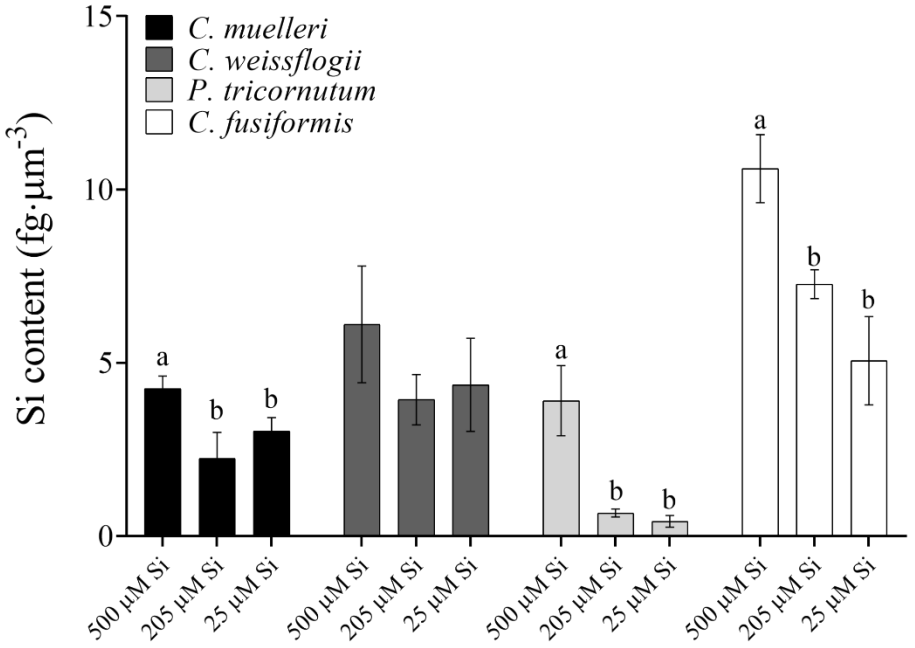

Figure 2.4: Si content per volume (fg·µm^{-3}) in the four diatoms acclimated to different paleoenvironments. Data are means of 3 biological replicas. Error bars show SD. Letters represent significant differences among conditions in the same species (p<0.05).

Table 2.4: Cell quotas of elements (pg·cell^{-1}) in the four diatoms acclimated to different paleoenvironments. Data are means of 3 biological replicas. Error bars show SD. Letters represent significant differences among conditions in the same species (p<0.05)

		500 µM Si	205 µM Si	25 µM Si
Carbon pg·cell^{-1}	*C.muelleri*	33.75±9.08	11.35±2.38	21.41±7.05
	C. weissflogii	16.85±13.00	7.79±3.03	7.79±4.08
	P. tricornutum	20.27±5.69^{a}	7.41±0.97^{b}	6.00±0.27^{b}
	C. fusiformis	17.52±3.23	22.83±0.89	10.61±3.08
Nitrogen pg·cell^{-1}	*C.muelleri*	6.52±2.07	2.48±0.58	4.37±1.66
	C. weissflogii	3.89±3.34	1.21±0.58	0.92±0.46
	P. tricornutum	4.27±0.6^{a}	1.14±0.08^{b}	0.83±0.04^{b}
	C. fusiformis	3.34±0.58	4.35±0.22	1.33±0.32
Silicon pg·cell^{-1}	*C.muelleri*	2.51 ± 0.66^{a}	1.02 ± 0.25^{b}	1.35 ± 0.1^{b}
	C. weissflogii	5.33±2.04	6.28±0.43	8.16±2.55
	P. tricornutum	0.98 ± 0.14^{a}	0.10 ± 0.03^{b}	0.06 ± 0.008^{b}
	C. fusiformis	5.27±1.29^{a}	2.53±0.33^{b}	2.02±0.25^{b}
Phosporous pg·cell^{-1}	*C.muelleri*	1.45±0.34^{a}	0.46±0.009^{b}	0.37±0.2^{b}
	C. weissflogii	0.09±0.04	0.13±0.001	0.06±0.02
	P. tricornutum	0.49±0.005^{a}	0.26±0.04^{b}	0.22±0.03^{b}
	C. fusiformis	0.83±0.1^{a}	0.38±0.05^{b}	0.29±0.03^{b}
Sulfur pg·cell^{-1}	*C.muelleri*	0.64±0.16^{a}	0.33±0.04^{b}	0.25±0.07^{b}
	C. weissflogii	0.31±0.21	0.38±0.08	0.40±0.21
	P. tricornutum	0.41±0.03	0.31±0.08	0.27±0.01
	C. fusiformis	0.56±0.1	0.28±0.03	0.67±0.5
Potassium pg·cell^{-1}	*C.muelleri*	0.02±0.004	0.03±0.02	0.013±0.004
	C. weissflogii	0.008±0.002	0.08±0.02	0.009±0.01
	P. tricornutum	0.01±.0.006	0.007±0.003	0.003±0.0003
	C. fusiformis	0.02±0.002	0.01±0.002	0.015±0.004
Calcium pg·cell^{-1}	*C.muelleri*	0.15±0.1	0.08±0.01	0.05±0.02
	C. weissflogii	0.03±0.008	0.18±0.07	0.03±0.01
	P. tricornutum	0.05±0.01	0.10±0.07	0.09±0.1
	C. fusiformis	0.1±0.02	0.05±0.03	6.14±5.03
Iron pg·cell^{-1}	*C.muelleri*	0.06±0.02	0.14±0.1	0.02±0.008
	C. weissflogii	0.01±0.008	0.03±0.01	0.02±0.01
	P. tricornutum	0.07±0.008^{a}	0.008±0.002^{b}	0.005±0.0003^{b}
	C. fusiformis	0.093±0.09	0.01±0.001	0.067±0.01

Table 2.5: Cell stoichiometry in relation to Si content (pg·cell^{-1}) of the four diatoms acclimated to different paleoenvironments. Data are means of 3 replicates ± SD. Different letters indicate significant differences among conditions in the same species ($p > 0.05$, One – way ANOVA followed by Tukey's *post hoc* test)

		C:Si	N:Si	P:Si	S:Si	Fe:Si
C. muelleri	500 µM Si	13.56 ± 3.14	2.66 ± 0.97	0.58 ± 0.03	0.18 ± 0.07	0.02 ± 0.007
	205 µM Si	11.23 ± 1.90	2.44 ± 0.39	0.47 ± 0.13	0.33 ± 0.09	0.14 ± 0.09
	25 µM Si	16.13 ± 6.65	3.30 ± 1.52	0.28 ± 0.17	0.26 ± 0.07	0.02 ± 0.003
C. weissflogii	500 µM Si	2.38 ± 1.90	0.58 ± 0.57	0.01 ± 0.002	0.035 ± 0.01	0.001 ± 0.001
	205 µM Si	1.22 ± 0.38	0.19 ± 0.08	0.02 ± 0.001	0.062 ± 0.02	0.006 ± 0.002
	25 µM Si	1.60 ± 0.84	0.19 ± 0.09	0.01 ± 0.007	0.096 ± 0.09	0.004 ± 0.001
P. tricornutum	500 µM Si	20.90 ± 7.26^{a}	4.34 ± 0.54^{a}	0.50 ± 0.07^{a}	0.42 ± 0.06^{a}	0.08 ± 0.006
	205 µM Si	78.01 ± 31.42^{b}	11.94 ± 4.36^{b}	2.67 ± 0.53^{b}	3.01 ± 0.42^{b}	0.07 ± 0.01
	25 µM Si	93.7 ± 14^{b}	12.93 ± 2.19^{b}	3.47 ± 0.62^{b}	4.27 ± 0.73^{c}	0.08 ± 0.01
C. fusiformis	500 µM Si	3.57 ± 1.60^{a}	0.68 ± 0.29^{a}	0.16 ± 0.02	0.11 ± 0.08	0.02 ± 0.01^{a}
	205 µM Si	9.13 ± 1.09^{b}	1.74 ± 0.23^{b}	0.15 ± 0.006	0.11 ± 0.004	0.005 ± 0.0009^{ab}
	25 µM Si	5.29 ± 1.66^{ab}	0.66 ± 0.16^{ab}	0.15 ± 0.03	0.35 ± 0.29	0.03 ± 0.009^{a}

Interestingly, our centric and pennate diatoms show divergent trends in carbon isotopic fractionation across treatments (**Figure 2.5**). Centric diatoms significantly increased observed fractionation (more negative $\delta^{13}C$) as DSi decreased, just the opposite of observed trends in our pennate species. Also, a strong correlation (Pearson r = -0.99 in *P. tricornutum* and -0.96 in *C. fusiformis*, **Figure 2.6**) between the $\delta^{13}C$ and intracellular Si content was observed in pennate cells, but in our centric species.

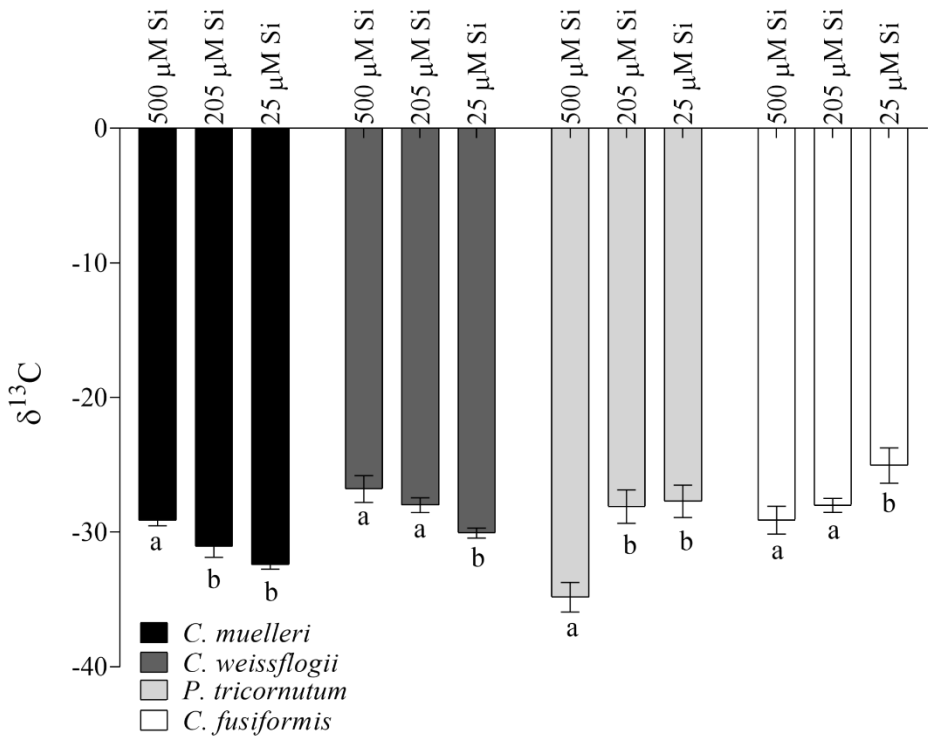

Figure 2.5: $\delta^{13}C$ values in the four diatoms acclimated to different paleoenvironments. Data are means of 3 biological replicas. Error bars show SD. Letters represent significant differences among conditions in the same species ($p<0.05$).

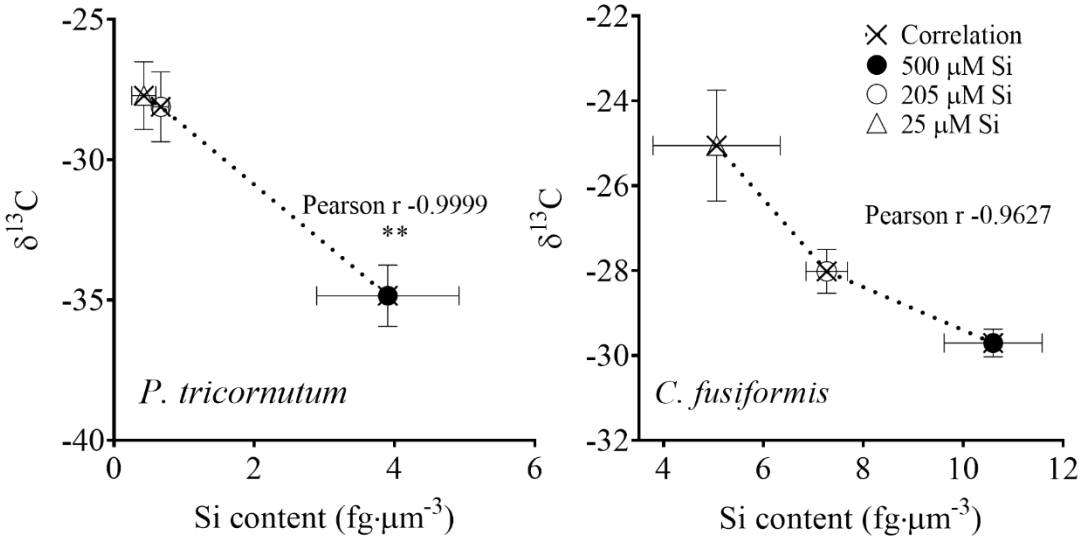

Figure 2.6: Correlation between Si content ($fg \cdot \mu m^{-3}$) and $\delta^{13}C$ in the two pennate diatoms acclimated to different paleoenvironments. Data are means of 3 biological replicas. Error bars show SD. Asterisks indicate significant difference ($p<0.01$).

2.3.4 Organic composition

In cells of *C. muelleri, C. fusiformis* and *P. tricornutum* proteins were more abundant in response to a higher silicic acid concentration in the growth medium (**Figure 2.7**). In pennate diatoms the same trend was observed for the carbohydrate pool. Save for *C. weissflogii*, all diatoms did not significantly change the lipid pool in response to DSi treatment. Regarding macromolecular ratios the cellular carbohydrate/lipid ratio showed C reallocation in all species (**Table 2.6**). In centric diatoms the protein to carbohydrate ratio was not affected while the protein to lipid ratio was significantly higher in response to higher DSi availability (**Table 2.6**).

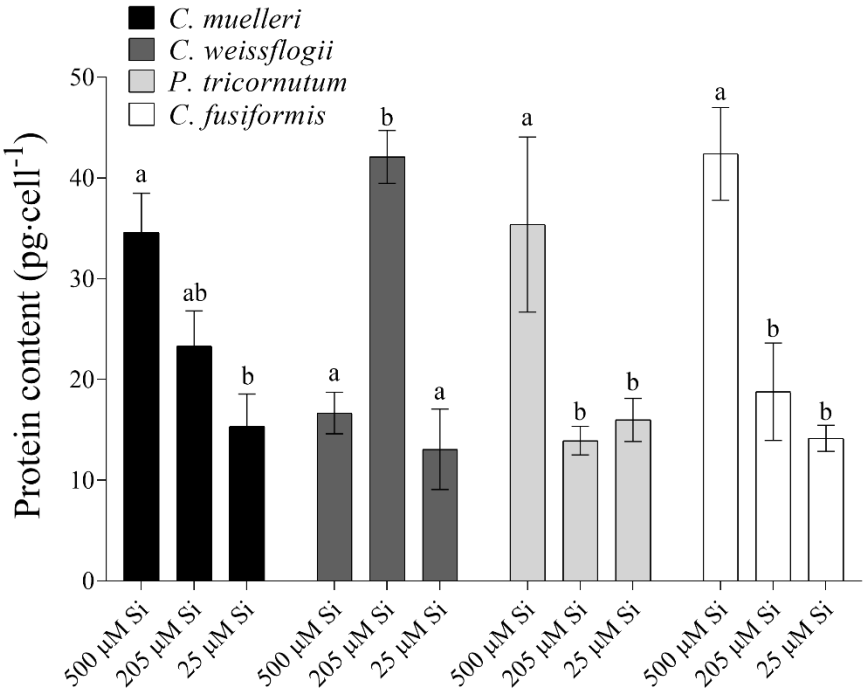

Figure 2.7: Protein content in the four diatoms acclimated to different paleoenvironments. Data are means of 3 biological replicas. Error bars show SD. Different letters represent significant differences among conditions in the same species (p<0.05)

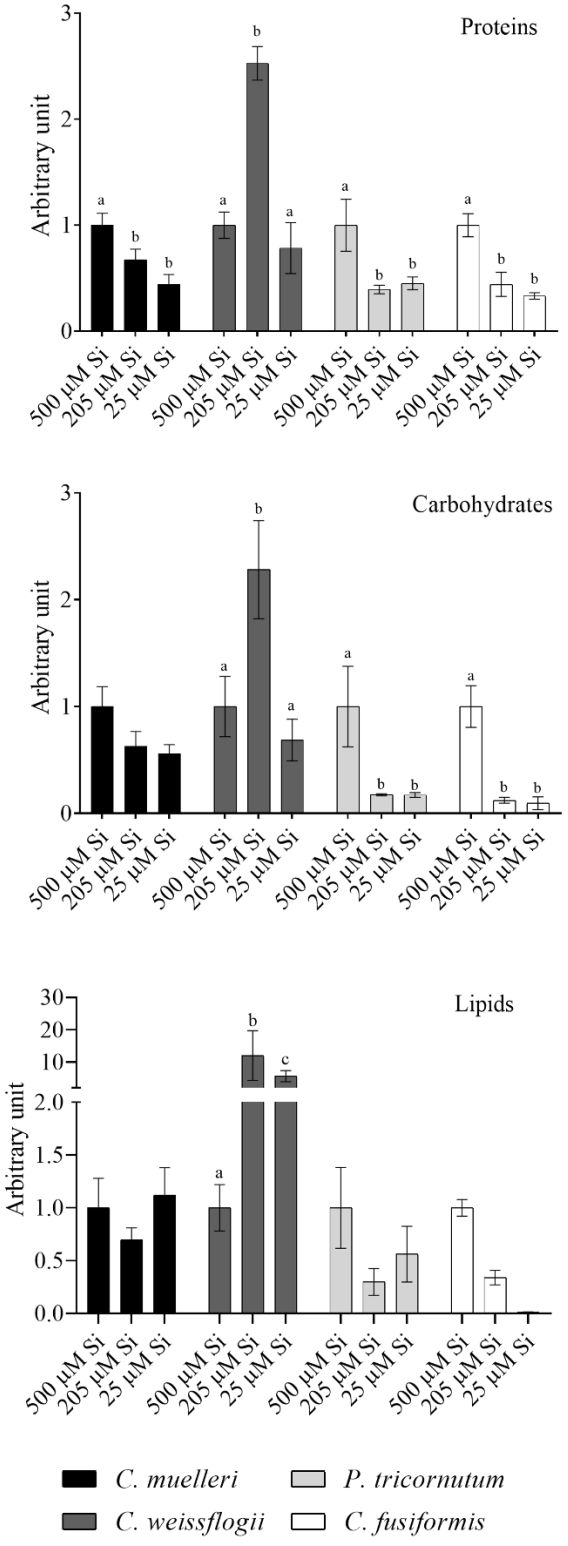

Figure 2.8: Protein, Carbohydrates and Lipid pools in the four diatoms acclimated to different paleoenvironments. Data are means of 3 replicates. Error bars show SD. Different letters represent significant differences among conditions in the same species ($p<0.05$, Two – way ANOVA followed by Tukey's *post hoc* test)

Table 2.6: Macromolecular pool ratios (arbitrary unit) for the four diatoms acclimated to different paleoenvironments. Data are means of 3 replicates±SD. Letters represent significant differences among conditions in the same species ($p<0.05$, One – way ANOVA followed by Tukey's *post hoc* test)

		500 µM Si	205 µM Si	25 µM Si
Proteins/Carbohydrates	*C. muelleri*	0.9±0.1	0.98±0.22	0.72±0.24
	C.weissflogii	0.31 ± 0.03	0.34 ± 0.08	0.34 ± 0.02
	P. tricornutum	0.79±0.14^{a}	1.84±0.66^{ab}	2.18±0.65^{b}
	C. fusiformis	0.51±0.11^{a}	1.79±0.07^{ab}	2.24±1.18^{b}
Proteins/Lipids	*C. muelleri*	13.4±2.46^{a}	12.57±1.61^{a}	5.50±2.60^{b}
	C.weissflogii	51.17 ± 11.46^{a}	6.80 ± 0.44^{b}	6.09 ± 0.26^{b}
	P. tricornutum	9.37±1.7	12.83±3.83	7.88±2.25
	C. fusiformis	6.63±0.61^{a}	8.73±1.81^{a}	231±72^{b}
Carbohydrates/Lipids	*C. muelleri*	14.96±3^{a}	13.21±1.36^{a}	7.45±0.96^{b}
	C.weissflogii	169 ± 57	36.77±23.97	18.04±1.47
	P. tricornutum	11.92±0.13^{a}	7.79±3.67^{ab}	3.63±0.05^{b}
	C. fusiformis	13.26±1.72^{a}	5.01±0.99^{a}	57.12±47^{b}

2.3.5 Frustules evaluation through Scanning Electron Microscopy

No evident change in the frustule structure of *C. muelleri* could be visible except for an increased width of the setae (**Figure 2.9 C, D, Table 2.7**) even if not statistically significant. *C. weissflogii* did not show a different arrangement of silica deposition in frustules (**Figure 2.9 B**). On the other hand, pennate diatoms appeared the most variable in terms of frustule morphology in response to environmental silicic acid concentration (**Figure 2.10**, **Table 2.7**). *P. tricornutum* highlighted a significant major width of the frustule combined with a greater thickness of the raphe in Mesozoic condition (**Figure 2.10 A, C, D** and **Table 2.7**) meanwhile *C. fusiformis* showed a larger width of the raphe (**Figure 2.10 B, E, F** and **Table 2.7**).

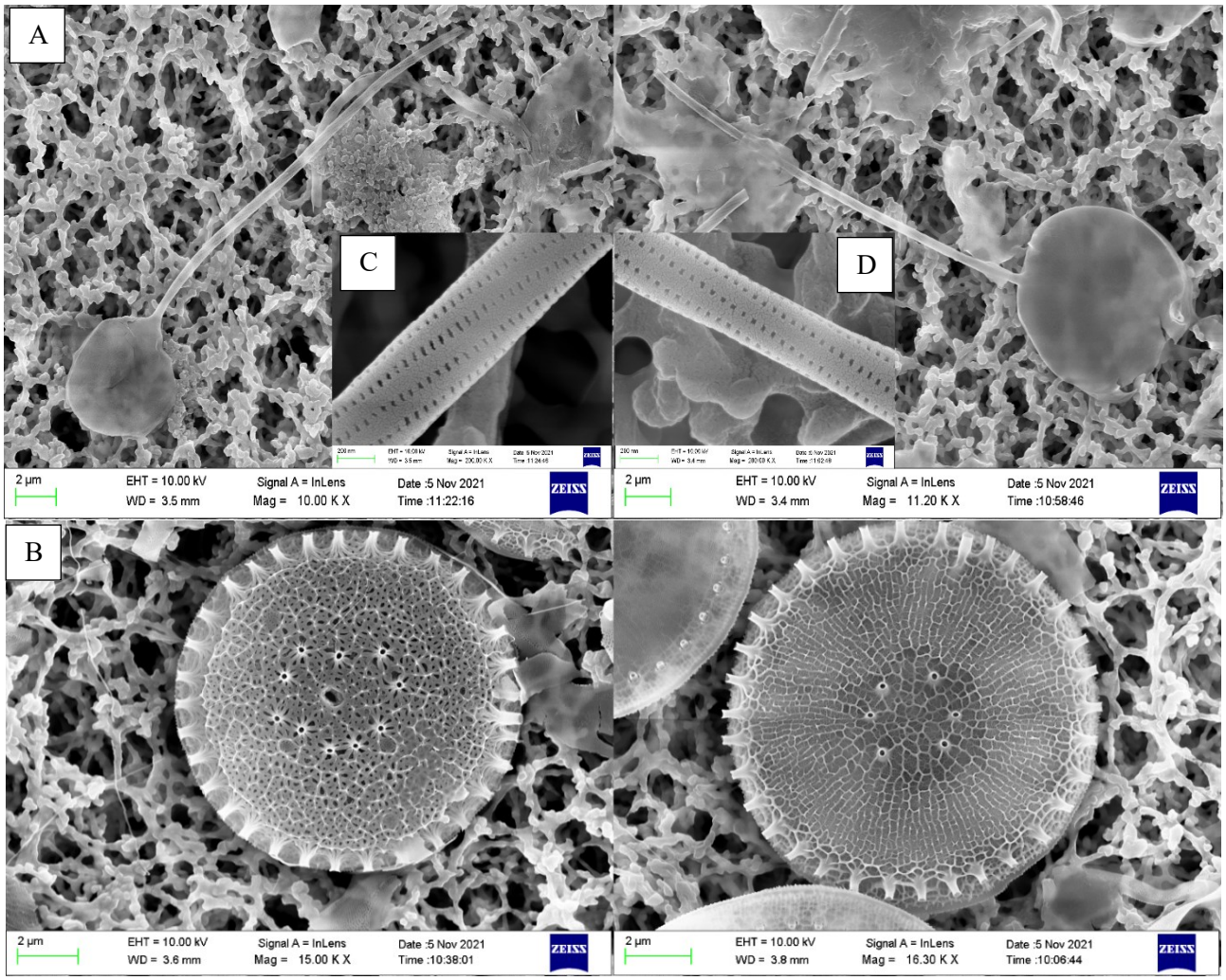

Figure 2.9: SEM images of centric diatoms (*C. muelleri* **A**, *C. weissflogii* **B**) frustules acclimated to 500 µM Si (left images) and Present (right images) conditions. Details of *C. muelleri* setae in Mesozoic condition (**C**) and Present condition (**D**) are shown.

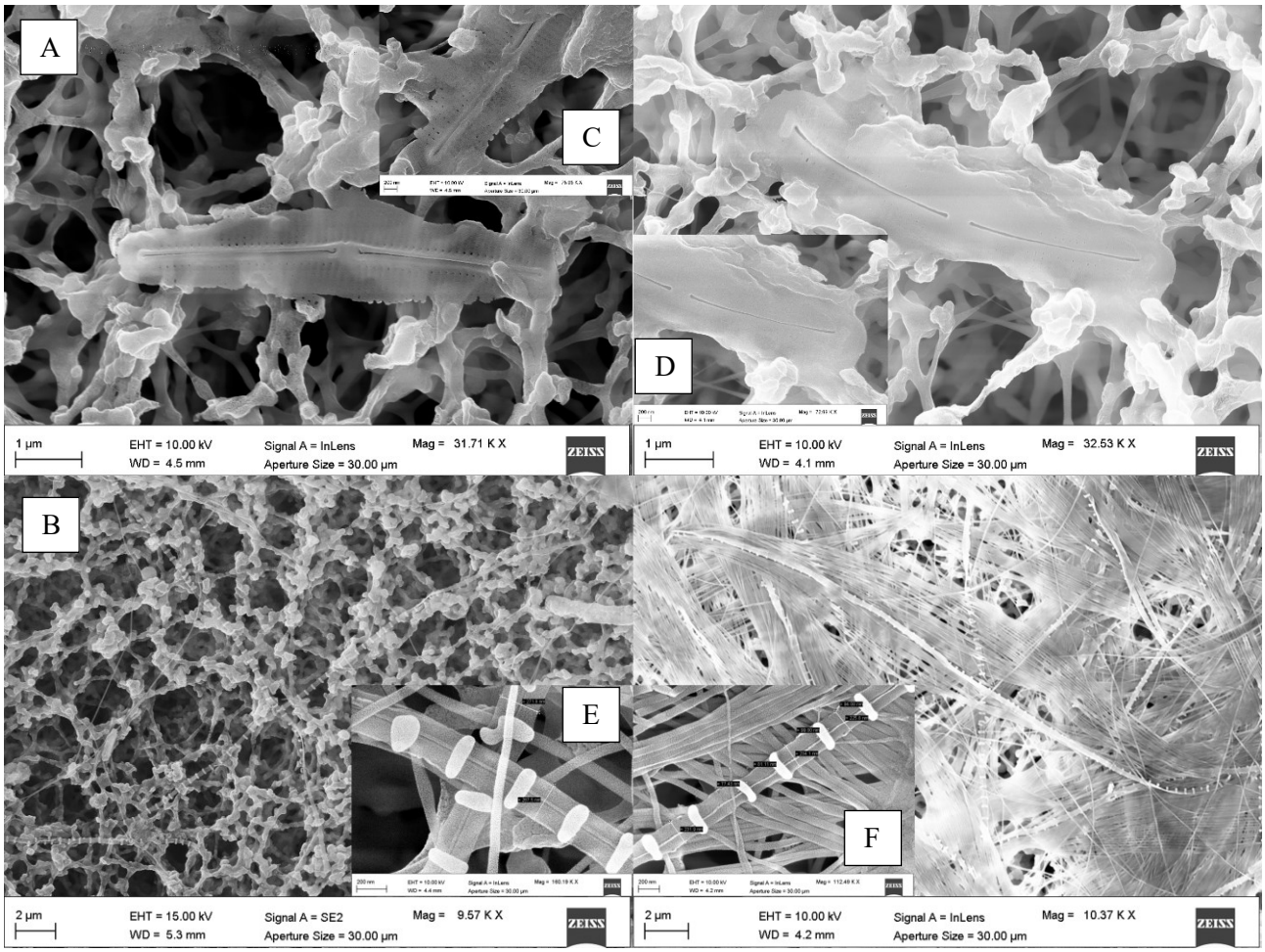

Figure 2.9: SEM images of frustules belonging to the pennate diatoms P. tricornutum (**A**) and C. fusiformis (**B**) acclimated to 500 µM Si (left images) and 25 µM Si (right images) conditions. Details of *P. tricornutum* and *C. fusiformis* raphae at 500 µM Si (**C** and **E** respectively) and 25 µM Si (**D** and **F** respectively) are shown

Table 2.7: Frustule morphological characterization of *C. muelleri*, *P. tricornutum* and *C. fusiformis* acclimated to different paleoenvironments. Data are means of 10 measures ± SD on frustules from 3 biological replicas. Asterisks represent significant differences between condition in the same species (* $p<0.05$; **** $p<0.0001$)

		500 µM Si	25 µM
C. muelleri	Width of setae (nm)	427.7±57.9	388.6±57.8
	Width of puntae (nm)	41.9±7.8	36.4±9.7
P. tricornutum	Lenght of frustule (µm)	6.48±0.06	6.15±0.55
	Width of frustule (µm)	1.59±0.12*	1.12±0.20
C. fusiformis	Lenght of raphe (µm)	29.3±1.1	29.3±1.5
	Width of raphe (nm)	248.9±21.3****	215.3±10.9
	Thickness of fibulae (nm)	87.1±9.9	86.1±12.1

2.4 Discussion

Paleontological and geochemical data support the hypothesis that diatom radiation drove a decline in the DSi of surface seawater, with consequences for both diatoms and other organisms that form skeletons of silica (Finkel et al., 2005, Rabosky and Sorhannus 2009, Conley et al., 2017, Hendry et al., 2018). At the same time, other factors, including climate change, orogenesis, and predation pressure may have influenced both observed paleontological patterns and inferred temporal variation in seawater composition (Falkowski et al., 2004, Zachos et al., 2008, Ratti et al., 2013, Lazarus et al., 2014, Conley et al., 2017, Giordano et al., 2018, Petrucciani et al., 2022). The experiments reported here confirm that whatever other factors inform our understanding of Mesozoic-Cenozoic diatom evolution, declining DSi had a direct influence on diatom growth, physiology, and morphogenesis. Even with our small sample size, it becomes clear that diatom responses to changing silica bioavailability are commonly individualistic; that is, there may be few parameters for which diatoms universally respond in the same way. At the same time, the centric and pennate species in our experiments commonly responded in different ways or to different degrees, suggesting that centrics and pennates may show broad and consistent differences in their physiological responses to changing DSi levels.

Growth in reconstructed paleoenvironments: facing high [DSi] - Perhaps counterintuitively, our experimental species did not grow better at high DSi concentrations; indeed, just the opposite occurred. All the diatoms in our experiments thrived at the low concentrations of N, Fe, Zn, Mo and Si characteristic of modern oceans (**Table 2.3**, **Figure 2.1**). In modern oceans, regional and seasonal Si limitation (i.e., in the Southern Ocean) is known to downregulate Si uptake and silicification in DSi users, including diatoms (Pinkerton et al. 2021). Nevertheless, diatoms maintain nearly maximal division rates (Olsen and Paasche 1986). Our data underscore that different species show distinct responses to Si availability. On the other hand, growth of the two smaller species, *C. muelleri* and *P. tricornutum*, was significantly lower at high DSi concentration

(500 µM) (**Figure 2.1**, **Table 2.3**). The drastic reduction in photosynthetic efficiency was consistent with growth limitation (**Figure 2.2**). Indeed, acclimation to 500 µM DSi concentration of the small species *C. muelleri* was strongly hampered (**Figure 2.1**, **2.2**, **Table 2.3**). It has been suggested that a high silicic acid concentration in the external medium can lead to cytotoxic effects (Marron et al., 2016) through auto-polymerization of intracellular soluble Si which then over- accumulates (Milligan et al., 2004).

Why a high external concentration of DSi should result in higher intracellular Si concentration is unclear. It is known that Si influx makes use of i) energy dependent transporters for Si uptake (SIT), which have acquired the influx function in response to the scarce availability of Si in oceans, and ii) diffusion (Thamatrakoln et al., 2006, Thamatrakoln and Hildebrand, 2008, Hildebrand et al., 2018). On the other hand, Si efflux is an overlooked and poorly understood process in diatom metabolism. It has been hypothesised this originally utilized ancestral SITs, requiring energy, as do currently utilized SITs (Martin-Jezequel et al., 2000, Milligan et al., 2004, Thamatrakoln and Hildebrand, 2008, Shrestha and Hildebrand, 2015, Hildebrand et al., 2018). Our data likely indicate that efficient DSi uptake was not turned off by algal cells and/or was counterbalanced by an efficient efflux mechanism. The effect could be observed in less silicified and smaller species characterized by a higher S/V ratio and thus incurring more cost for energy dependent transport (**Figure 2.1**, **Table 2.3**). It is worth noting that in *P. tricornutum* cells acclimated to different DSi the Fe:Si ratio is the only one unaffected by growth treatment (**Table 2.5**); this result is consistent with the hypothesis that Fe is directly required for Si transport, with Fe serving as a CO-factor for silicic acid transport molecules, postulated by De la Rocha and co-authors in 2000.

The densely silicified and larger (hence, lower S/V ratio, **Table 2.3**, **Figure 2.4**) cells of *C. weissflogii* had a different fate when grown under high DSi conditions (**Figure 2.1**, **Table 2.3**). In the presence of higher environmental DSi concentration, diffusion of silicic acid across membranes is supposed to make a bigger contribution to the Si uptake than it does in lower DSi growth

conditions. This could explain why energy is saved and reallocated into *C. weissflogii* growth, assuming DSi influx trough SITs is less relevant can be downregulated and the efflux is not needed due to the high Si requirement for thicker *C. weissflogii* frustules. Only in this species did the photosynthetic efficiency remain unchanged by varying DSi level (**Figure 2.2**).

Cell composition in reconstructed paleoenvironments: facing high [DSi] – Cell composition in terms of macromolecular pools varied among treatments and in a shape dependent manner. At high [DSi], cells of pennate diatoms were most costly (in terms of energy investment associated to the observed organic composition; Gerotto et al. 2020) and palatable (Palmucci et al., 2011, Ratti et al., 2013), preferentially allocating fixed C into carbohydrates and proteins ((**Figure 2.7**, **Figure 2.8, Table 2.6**).

Data suggest that over geologic times DSi availability has affected the overall C allocation pattern of diatoms (in particular pennates) and, therefore, predation pressure via its influence on palatability for predators. Lastly, DSi decline has favoured the evolution of energy-saving, less palatable cells, which are more competitive in intraspecific and interspecific interactions (Petrucciani et al., 2022).

Interestingly, Si availability also affected C isotopic fractionation: when DSi concentration was higher, pennate diatoms increased C fractionation (more negative $\delta^{13}C$) (**Figure 2.5**). This could be explained by a change in availability of intracellular inorganic carbon among growth regimes: in fact, a lower contribution of inorganic C mobilized from HCO_3^- to the fixed C in pennates grown in high Dsi conditions results in increased discrimination against $^{13}CO_2$ (Korb et al., 1996, Keller and Morel, 1999, Vuorio et al., 2006). This may well reflect to a downregulation in pennates of CCM (Riebesell et al., 2000) in favour of other mandatory energy dependent mechanisms such as Si deposition or Si efflux under high DSi conditions (Giordano et al., 2005, Giordano et al., 2017). Therefore, lower photosynthetic efficiencies were reported (**Figure 2.2**). In any event the correlation between silicon content and C fractionation observed in these species underscores the

deep interaction between the two elements as well as between biomineralization and C fixation (**Figure 2.6**). This is somewhat unexpected since in centric diatoms the uncoupling of silicon compared with carbon and nitrogen metabolisms was reported (Claquin et al., 2002, Suroy et al., 2015). The observed variations in isotopic fractionation also add further nuance to physiological and paleoenvironmental interpretation of organic carbon isotopes in Mesozoic and Cenozoic marine sediments (Hayes et al., 1999).

Greater availability of DSi was associated, as well, with a greater accumulation of Si in both cells (**Table 2.3**) and frustules (**Figures 2.9** and **2.10**) as also evident in the literature compilation of Finkel and coauthors (2010). The high Si content was not simply a function of greater cell volume since Si content expressed on a per volume basis was also higher in the 500 µM Si treatment (**Figure 2.4**). In addition, a higher Si quota per cell in diatoms is known to be induced by a slower growth rate (Brzezinski et al., 1990, Friedrichs et al., 2013). Both factors (high DSi and low growth rate) were present when *C. muelleri* and *P. tricornutum* showed the highest Si content (**Figure 2.1**, **Table 2.3**). The change in Si quota was striking in pennate diatoms (**Figure 2.4**, **Table 2.4**) as shown by raphe thickening in *P. tricornutum* frustules (**Figure 2.9 A**, **B**). The entire cellular stoichiometry was overturned (**Table 2.5**). *C. fusiformis* showed a similar trend, suggesting that the pennate diatoms acclimated to changing growth conditions by modulating Si use efficiency: the higher the available DSi in the environment and lower the efficiency in its use (**Table 2.5**). In contrast, centric diatoms had a homeostatic behaviour regarding their elemental stoichiometry: such strategy did not allow growth in *C. muelleri* and limited maximal cell density in *C. weissflogii* (**Table 2.5, Figure 2.1**).

While we cannot discount climate change and changing preservational selectivity as influences on the observed fossil record of diatoms, the experiments reported here bolster the case that decreasing [DSi] played an important role in shaping diatom morphology through time. In particular, the

observed physiological responses of pennate species may have helped to drive their differential diversification, governing reduced size and silica usage in diatoms as a group.

Chapter three: Interaction of diatoms with competitors and predators

Alessandra Petrucciani, Peter Chaerle, Alessandra Norici

3. Interaction of diatoms with competitors and predators

3.1 Introduction

Diatoms are important oceans' primary producers, which strongly affect global food webs. From a biological perspective, the world of diatoms has been moulded by the competitive interactions with other phytoplankton groups, resulting in the spatial patterns of marine primary production observed today (Armbrust 2009, Vallina et al., 2014, Burson et al., 2018, Vincent & Bowler 2020), and by the co-evolution with copepods and other micro-predators that have influenced radiation trajectories from higher levels of food webs (Turner 2004, Hamm and Smetacek, 2007; Giordano et al., 2018, Lürling 2021). Evolution led to an explosion of morphological varieties of diatom cells, from a radial to an elongated geometry, with a significant change in the frustule silicification (Finkel & Kotrc 2010, Kotrc & Knoll 2015). This change in silicification is consistent with a decreasing availability of silicic acid in oceans through geologic eras (Maliva et al., 1989, Lazarus et al., 2009, Finkel et al., 2010, Finkel & Kotrc 2010, Lazarus et al., 2014, Conley et al., 2017), so the more recently evolved pennate diatoms developed thinner, thus less silicified frustules. The morphological shift is still in progress and probably linked to a continuous balance between an effective response to different selective pressures including predation and the cost of shell thickening (Martin – Jézéquel et al., 2000, Hildebrand et al., 2018, Gronning & Kiørboe 2020). Phytoplankton has evolved multiple strategies to avoid predation (Pančić & Kiørboe 2018, Lürling 2020), those may involve not only morphological defences (e.g. colony formation, thick silica shell) but also behavioural defences (e.g. motility) or physiological defences (e.g. toxicity). In particular, pennate diatoms with a thinner frustule have adopted new chemical ways to avoid predation as compared to centric diatoms, i.e. they may produce apo-fucoxanthinoids or domoic acid, known to be toxic for predators (Shaw et al., 1994, Shaw et al., 1995a, Shaw et al., 1995b, Shaw et al., 1997, Tammilehto et al., 2014). Beside the macroevolutionary morphological changes, increasing

silicification of diatoms has also been observed as a rapid response to a sudden exposure to predators (Pondaven et al., 2007; Pančić et al., 2019). In fact, as already reported (Friedrichs et al., 2013, Liu et al., 2016, Zhang et al., 2017, Xu et al., 2021), silicon deposition in the diatom cell wall is adopted as selective criterion by predators to choose suitable preys since higher silicification provides a stronger armour against predation, decreasing diatoms palatability. However, cited studies only report exposure to predators of a single algal species at the time. So, for a deeper comprehension of the frustule role in shaping evolution, our purpose was to verify if lower silicified pennate diatoms were selected by copepods when strongly shielded centric diatoms where in the same culture. Furthermore, the role of diatom morphology in predator-prey relation is not independent from the role played in the competition for resources: both cell size and shape are crucial in phytoplankton light harvesting, nutrient uptake, and buoyancy (Pahlow et al., 1997, Key et al., 2010, Naselli – Flores & Barone, 2011, Naselli-Flores et al., 2021). Culturing differently sized and shaped diatoms allowed us to introduce interspecies competition for growth-related resources next to the predation pressure, mimicking more natural dynamics. Therefore, two centric diatoms *Thalassiosira pseudonana* and *Conticribra weissflogii*, and two pennate diatoms *Cylindrotheca closterium* and *Phaeodactylum tricornutum* were exposed to *Temora longicornis* for up to 7 days. Analysis of cellular morphology, Si content and elemental composition were carried out at different timepoints during the exposure to grazers and compared to the corresponding values obtained in cultures without grazing pressure. Finally, it was possible to accurately study predator-prey interactions as well as interspecies competition on cultures of diatom species mixed together due to the single cell approach of Imaging Flow Cytometry, which allowed to analyse in detail cell populations of different diatom species in a mix (**Figure 3.1**)

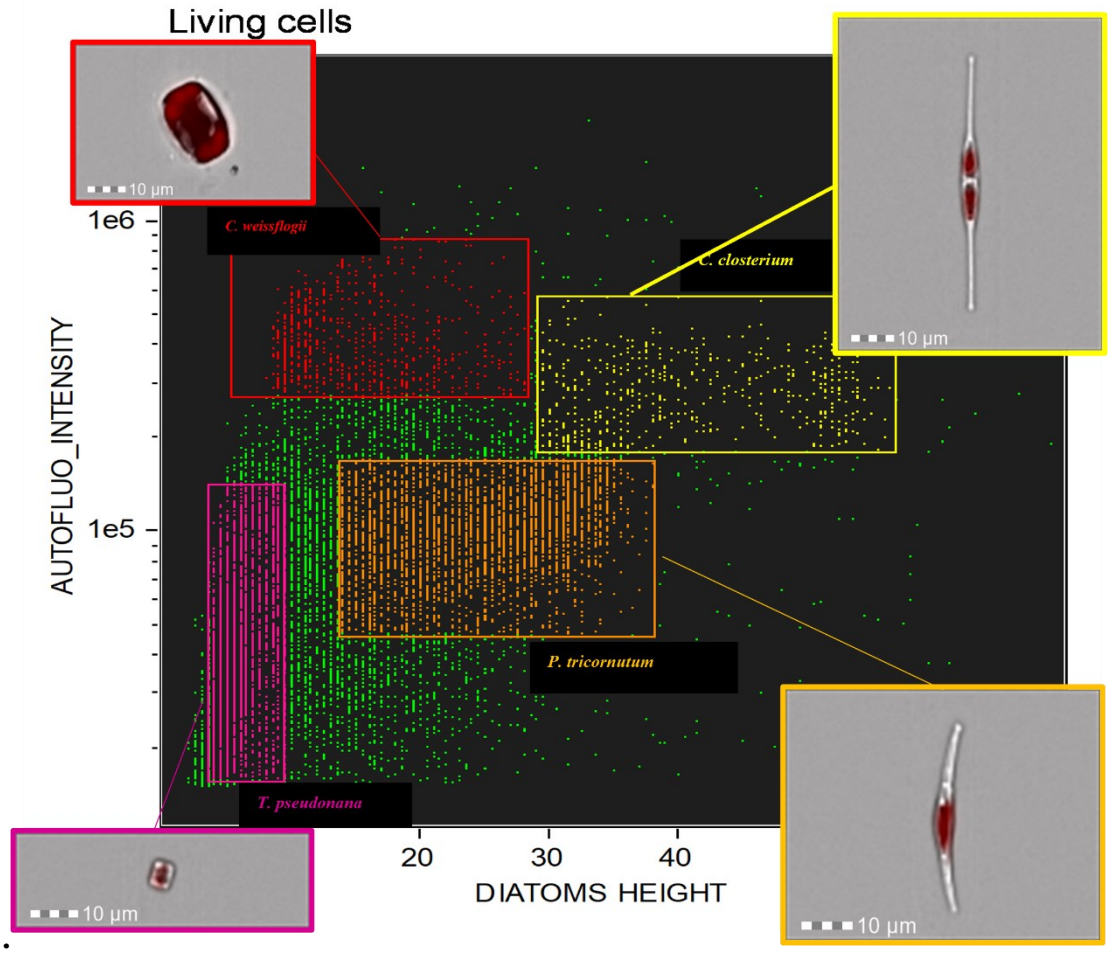

Figure 3.1: Samples of mixed diatoms analysed through Imaging Flow Cytometer

3.2 Material and Methods

3.2.1 Cultures

Two centric diatom species, *Thalassiosira pseudonana* (CCAP 1085/12, https://www.ccap.ac.uk/) and *Conticribra weissflogii* (DCG 0320), and two raphid pennate diatoms characterized by their pronounced elongated shape and thin frustules, *Cylindrotheca closterium* (DCG 0685) and *Phaeodactylum tricornutum* (DCG 0981) (**Figure 3.2**), were cultured using f/2 medium (Guillard 1975) in a controlled-environment room at 18 °C, illuminated with cool white fluorescent lamps at 60 µmol photons·m^{-2}·s^{-1} and 12:12 h light-dark cycles. These species were selected because of their contrasting shapes and difference in cell size, ranging from 2 µm to 45 µm. The DCG strains were acquired from the BCCM/DCG Diatoms Collection (https://bccm.belspo.be/about-us/bccm-dcg).

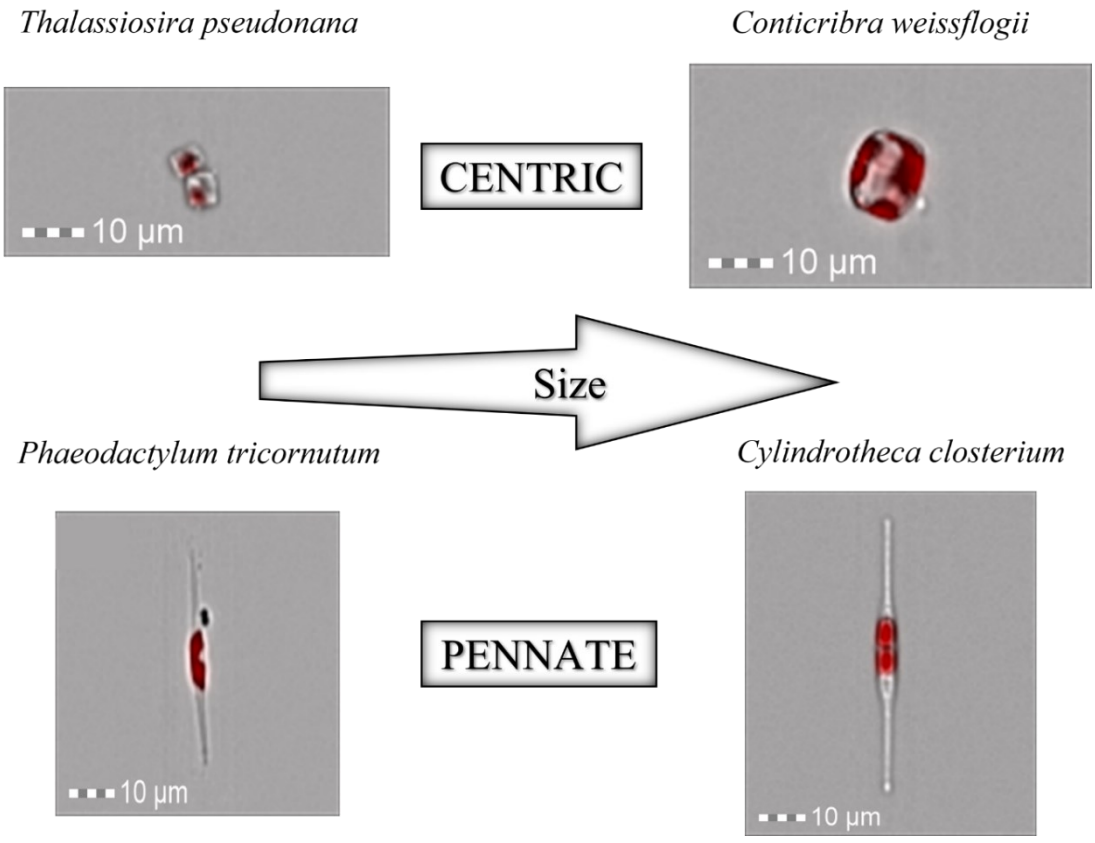

Figure 3.2: Images of the four morphologically different diatoms (*Thalassiosira pseudonana, Conticribra weissflogii, Phaeodactylum tricornutum, Cylindrotheca closterium*) chosen for the experiments. Images were obtained by ImageStream®X Mark II, (Amnis Corp., Seattle, WA), merging the bright field, collected in channel 1, and red chloroplast autofluorescence in channel 5 (Details in the section Morphological features by IFC analysis of material and methods)

Predators were caught offshore in the Belgian North Sea (51°18.088 Lat., 2°39.667 Long., **Figure 3.3**) while on board of the Flanders Marine Institute vessel RV Simon Stevin. Sampling was performed using a WP2 vertical planktonic net (total length: 2,6 m, mesh width: 200 µm).

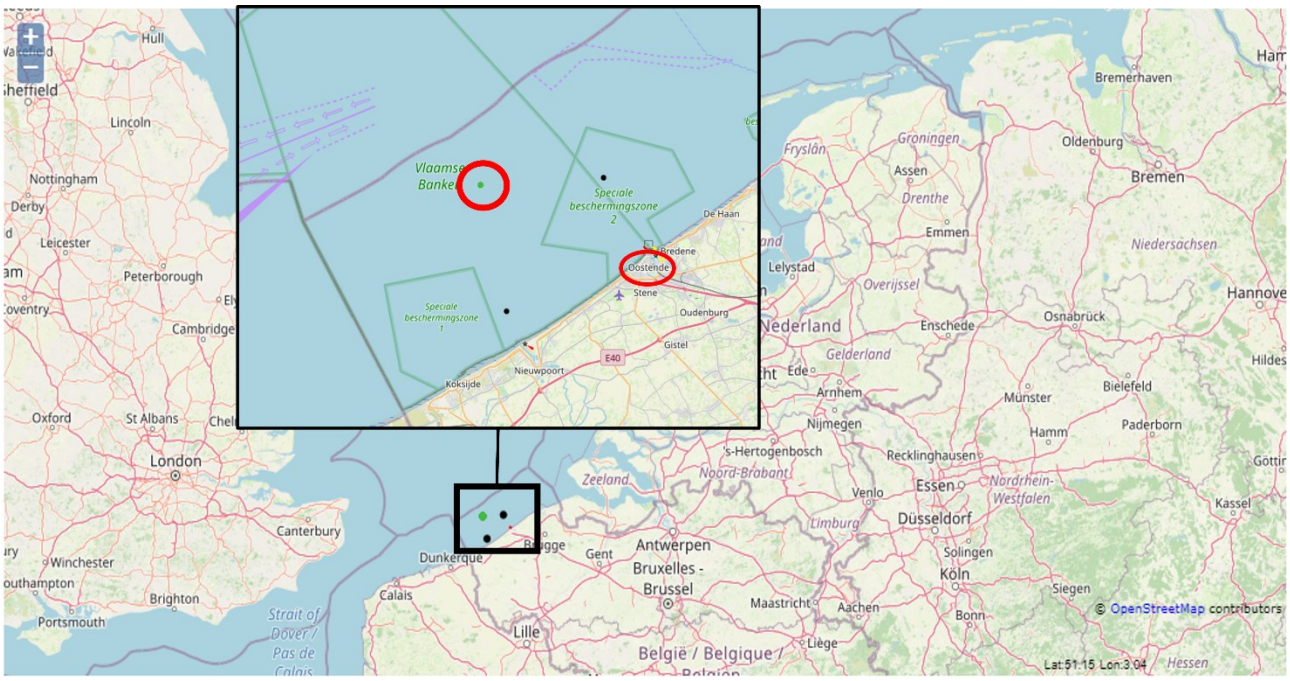

Trip 03 Sep 2019

Figure 3.3: Sampling map of calanoid copepods in the Belgian North Sea

Zooplankton was collected through light attraction and the copepod species *Temora longicornis* was isolated and identified using a stereomicroscope and subsequently caught with a pipette and put in a separate tank (**Figure 3.4**). This species was chosen as diatoms feeder due to its known capacity to break differently sized frustules (Miller et al., 1990, Jansen 2008, Pančić et al., 2019). The copepods were maintained in natural seawater in climate chambers with aerators, illuminated with cool white fluorescent lamps at 60 µmol photons·m^{-2}·$s^{-1}$and 12:12 h light-dark cycles.

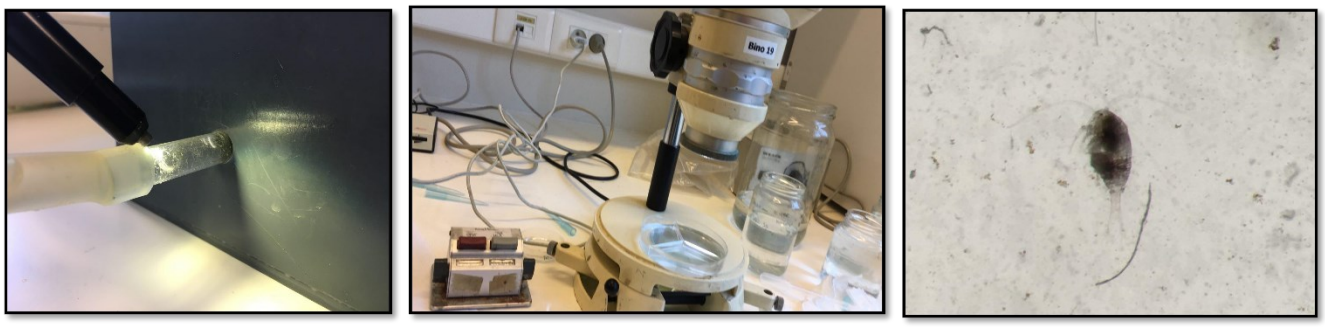

Figure 3.4: (1) Zooplankton sorting through light attraction (2) isolation of the calanoid copepod *T. longicornis* using a stereomicroscope (3) light microscope image of *T. longicornis*

Monospecific diatom cultures were established in 175 mL plastic flasks (VWR Tissue Culture Flask, treated, vented cap, sterile. Manufactured for VWR International, LLC Radnor Corporate Center, 100 Matsonford Rd. Radnor, PA USA 19087) filled with 50 mL of f/2 medium. The density of the inoculated diatom cells was determined to obtain a ratio of 1 copepod to 0,2-0,7 mg algal C (Ratti et al., 2013): $8*10^5$ cells/ml of *T. pseudonana* and *P. tricornutum* were exposed to 2 copepods, $4*10^5$ cells/ml of *C. closterium* to 1 copepod and $8*10^4$ cells/ml of *C. weissflogii* to 2 copepods. Copepods were washed and kept for 3 hours in f/2 medium in a controlled-environment room at 18 °C, illuminated with cool white fluorescent lamps at 60 µmol photons$\cdot m^{-2}\cdot s^{-1}$and 12:12 h light-dark cycles before being transferred to the diatom cultures. Cultures in three replicas were checked daily and each dead copepod was replaced with a new living individual; diatom cultures without copepods were maintained as controls under the same growth conditions. Diatoms were sampled and analysed before (day 0 in tables, T0 in text and graphs) and after 1, 3, and 7 days (day 1, 3, 7 in tables, T1, T3, T7 in text and graphs) of copepods exposure. Copepods and fecal pellets were removed with a 0.45 mm filter prior to each analysis.

Next to the monospecific tests, three mixed diatom cultures were established (**Table 3.1**, **Figure 3.5**), with and without copepods to evaluate grazing pressure during interspecies diatom competition, each of them in three replicas. The initial inoculum was calculated considering the C

ratio of algae to copepods as described before but applying a dilution factor of 10 (1 Copepod – 0,02-0,07 algal C) to avoid dense algal cultures and hence to limit possible self-shading, transient O_2 inhibition and nutrient shortage. The experimental sampling was conducted as described above for monospecific culture tests.

Table 3.1: Composition of the 3 mixed diatom cultures: algal species, number of algal cells and copepods added to 50 ml of cultures

	Diatoms	Initial inoculum (total amount of cells)	Copepods (n)
Centric mix	*C. weissflogii*	$1.86*10^5$	**3**
	T. pseudonana	$1.51*10^6$	
Mix without *P. tricornutum*	*T. pseudonana*	$1.0*10^6$	**3**
	C. weissflogii	$1.24*10^5$	
	C. closterium,	$1.26*10^6$	
Mix	*T. pseudonana*	$7.55*10^5$	**3**
	C. weissflogii	$9.32*10^4$	
	C. closterium	$9.44*10^5$	
	P. tricornutum	$6.82*10^5$	

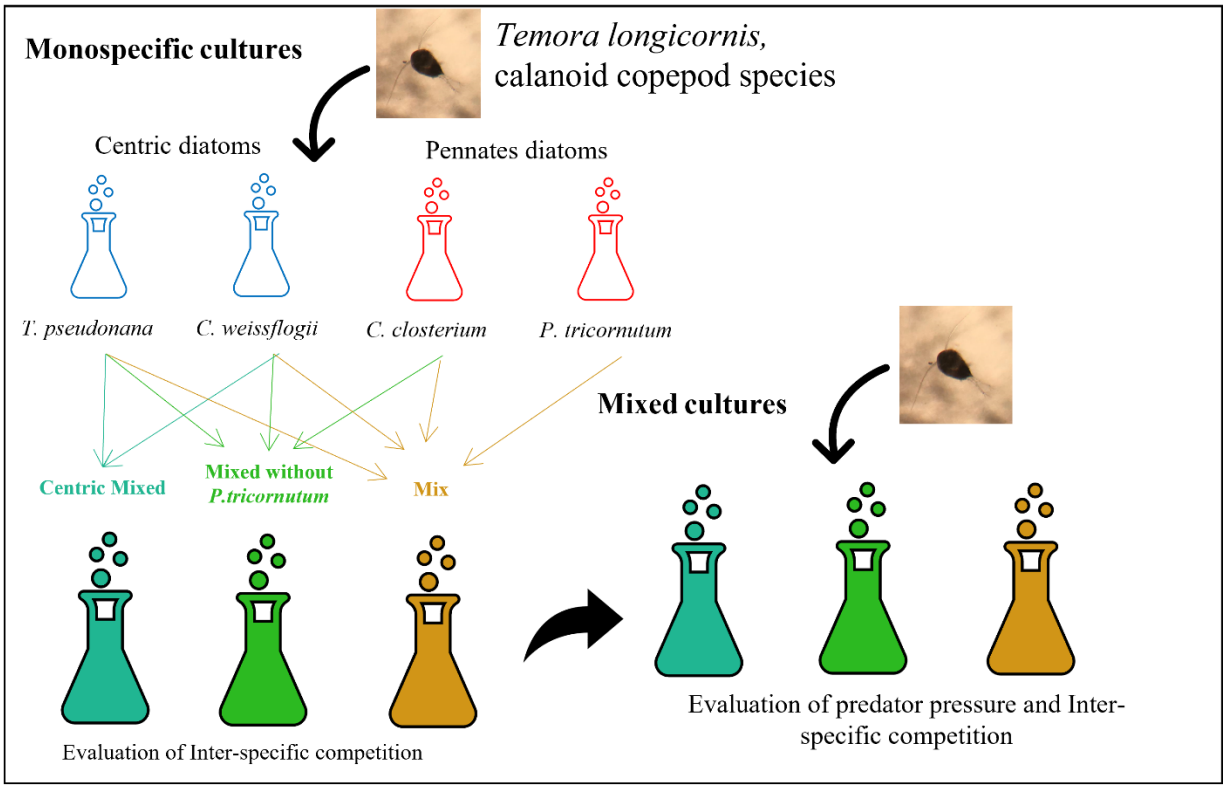

Figure 3.5: Experimental design of monospecific and mixed cultures

3.2.2 Morphological features by IFC analysis

Diatoms were analysed using the Imaging Flow Cytometer (IFC) ImageStream®X Mark II, (Amnis Corp., Seattle, WA) using the INSPIRE software package (Amnis Corp.) to determine cell density and morphometric characteristics. For each analysis, a volume of 2,5 mL diatom culture was sampled and centrifuged (Centrifuge Sigma 4K15) for 5 minutes at 3500 rpm. The supernatant fluid was removed, the cell pellet resuspended in 30 µl of f/2 medium and subsequently stored at 4°C. All IFC samples were analysed within 24 hours after sampling. IFC data of all objects present in the 30 µl were saved. Details and settings of the IFC technique were as follows: 10 µm core size diameter, 66 mm/s speed, 40x magnification; bright field data were collected in channel 1 (LED intensity 34.63 mW) and chloroplast autofluorescence in channel 5 (642 nm, laser 0.5 mW). Post – acquisition data analysis was performed using the IDEAS software package. Specific masks, separating the pixels occupied by the diatoms from the background, for both brightfield and autofluorescence images were created for each diatom species (**Figure 3.6**). All objects lacking chloroplast autofluorescence, as determined by the Intensity feature of the IDEAS software, were considered debris or dead diatoms and, consequently, excluded from cell counting and all other metrics. Among the living cells, only single and well-focused diatoms were gated to obtain morphological parameters.

Figure 3.6: Example of masks creation on *C. weissflogii* cells by IDEAS software for Imaging Flow Cytometer

The morphological features considered for the analysis were Height, Width, Length, Elongatedness (height/width), Thickness max, Area, Circularity (IDEAS User Manual, version 6.0, March 2013). Given numbers refer to at least 1000 cells for each biological replica.

Height and Width were used to calculate the biovolume of cells using the equation [$V= \pi/4 \cdot d^2 \cdot h$] for *C. weissflogii* and *T. pseudonana* (cylinder, Hillebrand et al., 1999) and [$V= \pi/6 \cdot d^2 \cdot h$] for *C. closterium* and *P. tricornutum* (prolate spheroid, Hillebrand et al.,1999).

3.2.3 Algal growth

Cell density was determined as described before by IFC analysis or by Burker hemocytometer counts (depth 0.1 mm, MARIENFELD Superior, Germany) for the monospecific control cultures. Diatom growth rates, μ (3.1), were derived from cell samples taken at the abovementioned 4 time points (day 0, 1, 3, 7). To estimate grazer feeding rate for the monospecific culture tests, the rate of growth of the different diatom species cultured with and without copepods was compared. In mixed cultures plus copepods, the growth rate of each species was compared to the ones of other diatoms in the mix and to the one of the same species in the mix without copepods.

$$(3.1)\ \mu = \frac{ln(N_t/N_0)}{t}\ \text{(Monod 1949)}$$

3.2.4 Elemental composition

Cellular C and N quotas were determined by elemental analyser (ECS 4010, Costech Italy) on 0.1 – 1 mg DW of cells which were previously washed twice in ammonium formate solution isosmotic to the culturing media (0.5 M) and dried at 80°C (Ratti et al.,2011). Elemental quantification used sulfanilamide (C:N:S = 6:2:1) for the standard curve. Data acquisition and analysis were performed using the software EAS- Clarity (Costech Analytical Technologies Inc., Milano, ItalyOrganic composition). All measurements were performed on 3 biological replicas of samples collected on day 0 and day 7 of monospecific cultures.

The amount of P, S, K, Ca, Fe, Si per cell was measured by Total Reflectance X – ray Fluorescence spectrometer (S2 Picofox, Bruker AXS Microanalysis GmbH, Berlin, Germany). Sampled diatoms were washed twice with an ammonium formate solution isosmotic to the culture media and resuspended in 250 μl of dH_2O. A solution of 0.1 g L^{-1} Ga (Sigma Aldrich, St. Luis, MO, USA) in

5% HNO3 was added as an internal standard to a final concentration of 0.5 µL L^{-1}. The suspension was carefully vortexed and an aliquot of 10 µl was deposed on a plastic sample holder, dried on a heating plate and measured for 1000 seconds (Ratti et al., 2013). Spectral deconvolution and quantification of elemental abundances were performed by the SPECTRA 6.1 software (Bruker AXS Microanalysis GmbH, Berlin, Germany). All measurements were performed in both monospecific and mixed cultures on day 0, 1, 3 and 7.

3.2.5 Statistical analysis

Significant differences among the means of Si content per volume (dependent variable) over time (independent variable) were tested with a one-way analysis of variance (ANOVA), followed by Tukey's *post-hoc* test. Comparison of growth dependent variables (growth rate and maximum cell density) between cells exposed or not to copepods (independent variable) was carried out with a two-tailed t-test. Significant differences among the means of growth dependent variables (cell density and growth rate) in different species (independent variable) growing in the presence or in the absence of copepods (independent variable) were tested with a two-way analysis of variance (ANOVA), followed by Tukey's *post-hoc* test. The level of significance was set at 0.05. GraphPad prism 8.0.2.263 was used to perform the aforementioned tests (GraphPad Software, San Diego, CA, USA).

Principal Component Analysis (PCA) was done using PAST 4.03 (Hammer et al., 2001. PAST: Paleontological statistics software package for education and data analysis). PCA was performed on different morphological features (e.g. Height, Width, Length, Elongatedness (height/width), Thickness max, Area, Circularity) obtained through Imaging Flow Cytometer analysis as dependent variables along the time course of the experiment (independent variable) and in different species (independent variable) exposed or not to copepods (independent variable). Data were normalized using z-values ((n-mean)/SD).

3.3 Results

3.3.1 Monospecific cultures

The presence of copepods strongly affected the growth rate of both centric diatoms (**Figure 3.7 D**). In particular, *T. pseudonana* showed a negative growth rate as well as a maximum cell density that was half when grazers were present. In *C. weissflogii* growth rate was significantly lower when cells were exposed to copepods (p = 0.04, supplemental material), but no difference in maximum cell density was observed. A statistically significant increase in Si content per cell volume was observed on day 1 compared to days 0, 3 and 7 in *C. weissflogii* ($F(3, 7) = 40.59$, $p<0.0001$, **Figure 3.7 B**). Moreover, on day 1, *C. weissflogii* was the only species showing a decrease in cell density. In *T. pseudonana,* the highest Si concentration per volume on day 7 occurred when the cell number was lowest ($F(3, 7) = 8.806$, $p = 0.0090$). It is worth mentioning that the peak in Si concentration was always present together with a higher concentration of C, N, P, S, K, Ca, Fe elemental quotas per volume (**Table S1**).

Morphological observations of centric diatoms (Circularity, Thickness, Width, Height, **Figure 3.7 C**) were presented through PCA. PC1 and PC2 explained 97.94% of the total variation present in the data matrix with PC1 accounting for 65.06% and PC2 for 32.88%. Loading values (eigenvalues in **Table S3**, means values **Table S4**,) differentiated days 0 and 7 of copepod exposure from days 1 and 3 according to PC2, indicating an increase in circularity when the stress was present. Furthermore, there is a separation between *T. pseudonana* T0 and T7 according to PC1, recording the reduction in size after grazing pressure.

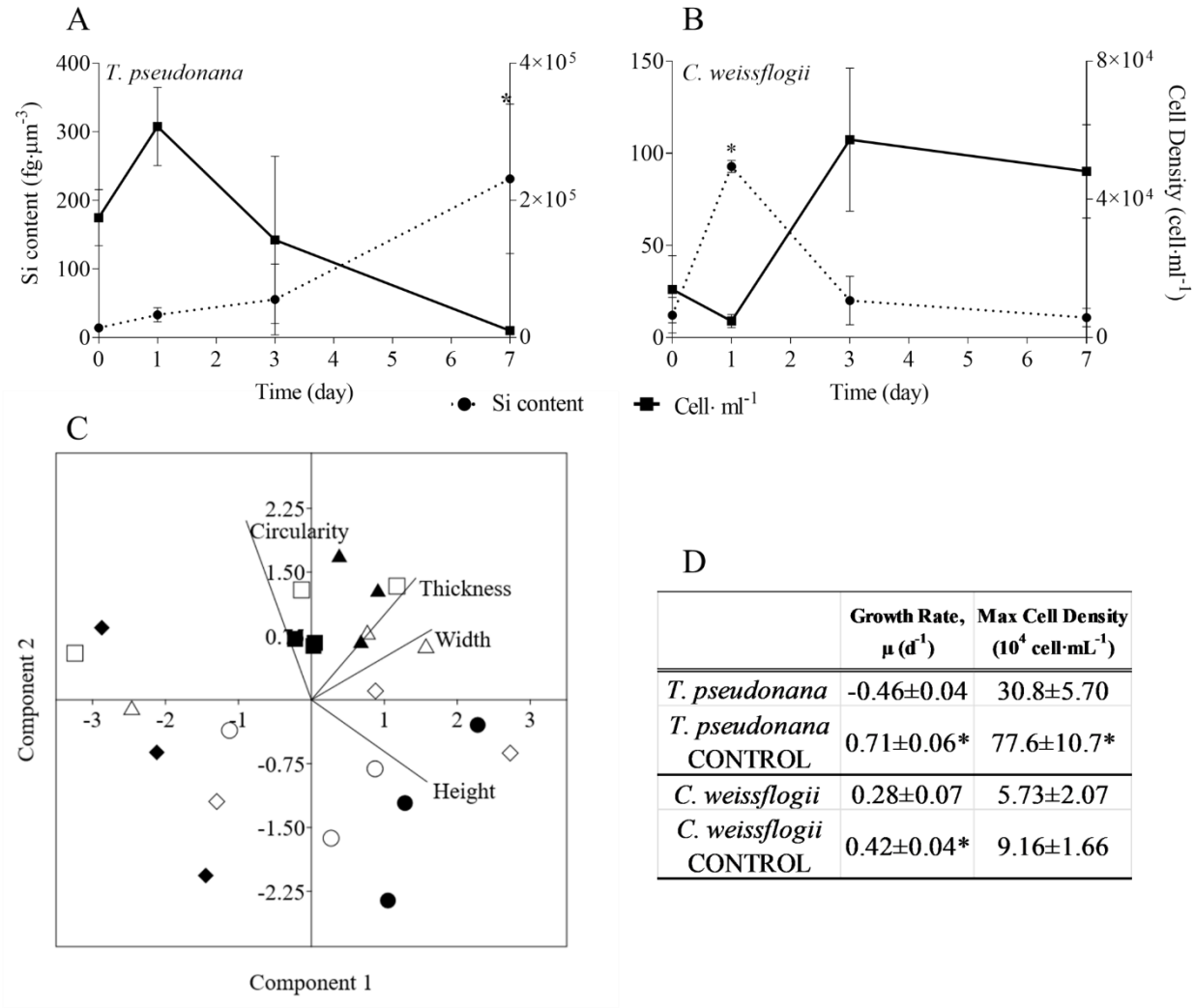

	Growth Rate, µ (d^{-1})	Max Cell Density (10^4 cell·mL^{-1})
T. pseudonana	-0.46±0.04	30.8±5.70
T. pseudonana CONTROL	0.71±0.06*	77.6±10.7*
C. weissflogii	0.28±0.07	5.73±2.07
C. weissflogii CONTROL	0.42±0.04*	9.16±1.66

Figure 3.7: (**A**, **B**) Si content (fg·µm^{-3}; dashed line) and cell density (cell ml^{-1}; solid line) in the two centric diatom species under copepods exposure. Data are means of 3 biological replicas. Error bars show SD while asterisks indicate significant differences in Si content of each species among days (One - way ANOVA with Tukey's *post hoc* test, p<0,05). (**C**) PCA analysis on morphological characteristics of centric diatoms (*T. pseudonana* and *C. weissflogii*) in monospecifc cultures. Different symbols indicate different time points during the experiment: T0 ○●; T1 □■, T3Δ▲, T7 ◊♦, while different colours indicate different species: black for *T. pseudonana* white for *C. weissflogii*. (**D**) . Comparison of growth rates (d^{-1}) and maximum cell densities (cells·mL^{-1}) for each of the two diatom species between cultures with and without (CONTROL) copepods. The values are means of 3 biological replicas ± SD. For each species, asterisks indicate when growth rate or max cell density were statistically different between diatoms exposed or not (CONTROL) to copepods (unpaired t test, p<0,05).

Regarding the pennate species, neither growth rate nor maximum number of cells were significantly affected by the presence of copepods (**Figure 3.8 D**). Except for the higher Si content per cell volume of *C. closterium* at day 1 as compared to the other time points (F (3, 8) 11.73, p = 0.0027),

also observed in the response of *C. weissflogii*, in both the pennate diatoms there was not a statistically significant change in Si content (**Figure 3.8 A, B**). The morphological characterization of pennate diatoms through PCA (Elongatedness, Length, Thickness, Width, **Figure 3.8 C**) explained 94.68% of the total variance (PC1 plus PC2), where the weight of PC1 was 60.36% while PC2 34.32%. It showed a net division between T0 and T7 according to PC2, but the two species on day 7 were separated according to PC1. Indeed, both underwent a reduction in width after 7 days of copepods pressure, but *P. tricornutum* increased the elongatdness while *C. closterium* reduced its length.

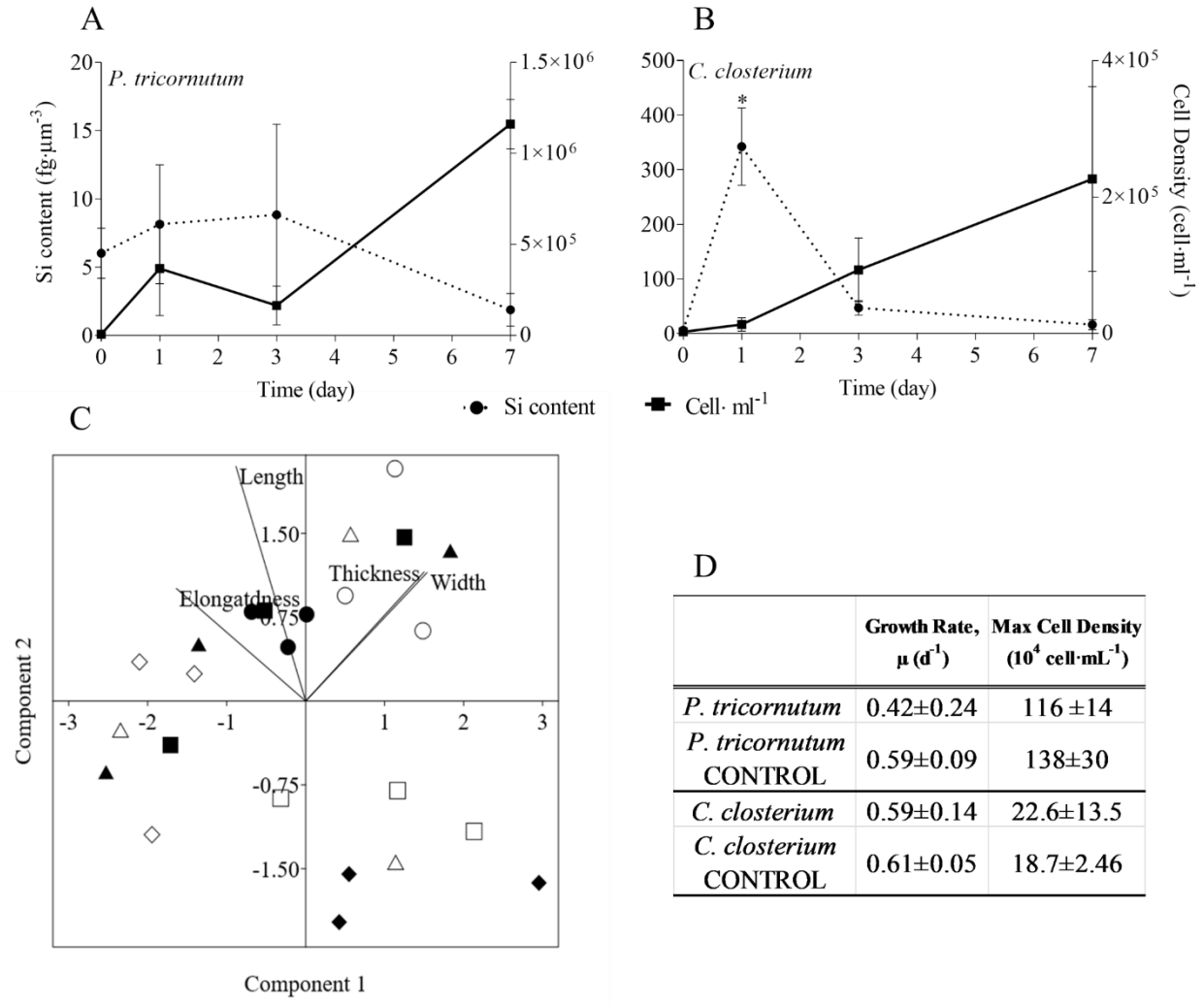

	Growth Rate, µ (d^{-1})	Max Cell Density (10^4 cell·mL^{-1})
P. tricornutum	0.42±0.24	116 ±14
P. tricornutum CONTROL	0.59±0.09	138±30
C. closterium	0.59±0.14	22.6±13.5
C. closterium CONTROL	0.61±0.05	18.7±2.46

Figure 3.8. (**A**, **B**) Si content (fg·µm^{-3}; dashed line) and cell density (cell ml^{-1}; solid line) in the two pennate diatom species under copepods exposure. Data are means of 3 biological replicas. Error bars show SD while asterisks indicate significant differences in Si content of each species among days (One-way ANOVA with Tukey's *post hoc* test, p<0,05). (**C**) PCA analysis on morphological characteristics of pennate diatoms (*C. closterium* and *P.tricornutum*) in monospecifc cultures. Different symbols indicate different time points during the experiment: T0 ○●; T1 □■, T3Δ▲, T7 ◊♦, while different colours indicate different species: black for *P. tricornutum*, white for *C. closterium*. (**D**) Comparison of growth rates (d^{-1}) and maximum cell densities (cells·mL^{-1}) for each of the two diatom species between cultures with and without (CONTROL) copepods. The values are means of 3 biological replicas ± SD. For each species, asterisks indicate when growth rate or max cell density were statistically different between diatoms exposed or not (CONTROL) to copepods (unpaired t test, p<0,05).

3.3.2 Mixed cultures

For the centric mix, according to the growth curves (**Figure 3.9**) and the growth rate values (**Figure S1**), *T. pseudonana* was growing significantly faster than *C. weissflogii* in both the presence (F =

27.04, $p < 0.0001$) and the absence of copepods (F = 89.36, $p < 0.0001$,. Whereas *C. weissflogii* was negatively affected by grazers only on day 7 (**Figure 3.9 A**).

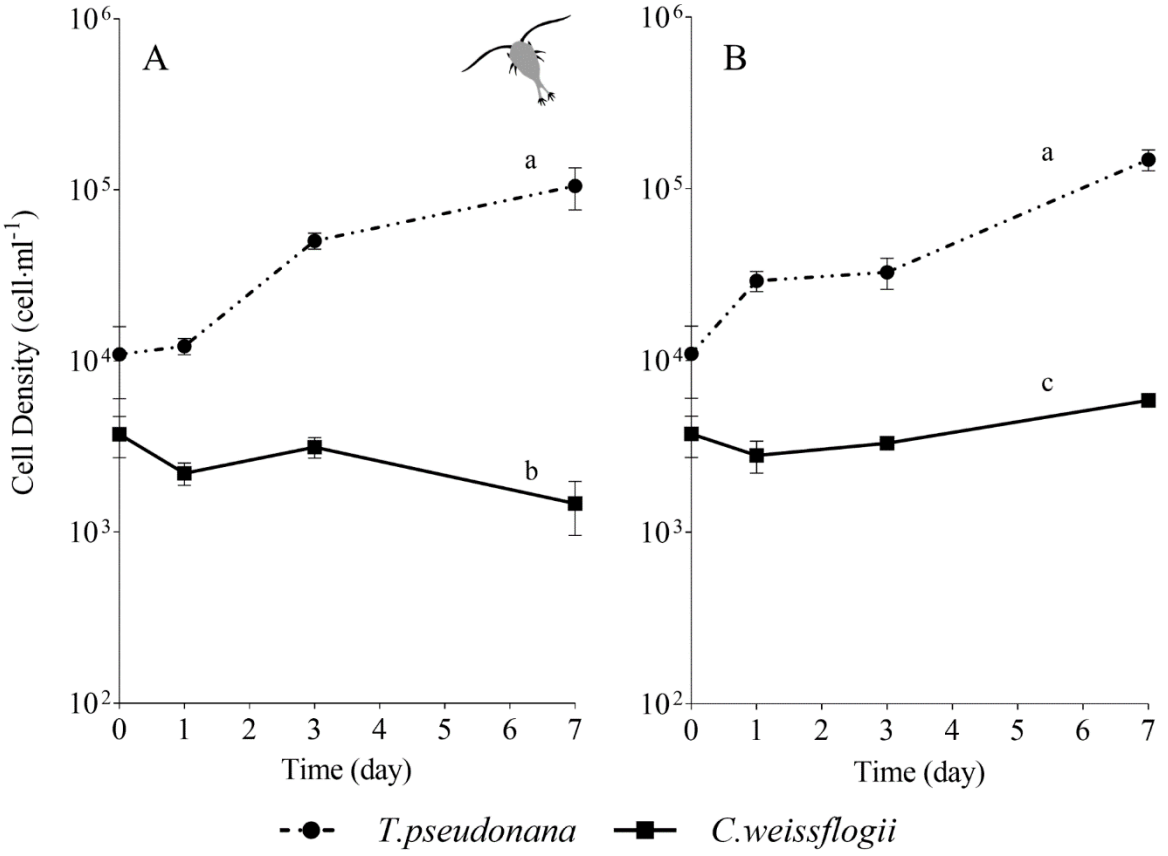

Figure 3.9: Comparison between growth curves of the centric diatom mix exposed (**A**) or not (**B**) to copepods. The data are means of 3 biological replicas. Error bars show SD while letters indicate significant difference (Two – way ANOVA and Tukey's *post hoc* test, p<0,05)

Morphological features for centric mixed diatoms (Circularity, Area, Width, Height) were represented with PCA in **Figure 3.10**. PC1 + PC2 accounted for 99.9% (91.3% + 8.6%) and 98.3% (60.3% + 38.0%) of the total variation present in *T. pseudonana* and *C. weissflogii*, respectively (**Figure 3.10 A** and **B**, eigenvalues in **Table S5**, means values **Table S6**). In both centic diatoms, PCA differentiated day 0 from day 7 according to PC1, recording a change in cells' circularity, in *T. pseudonana* also for PC2 adding a decrease in size during the experiment. Interestingly, *C.*

weissflogii showed separation according to PC2 in the different condition analysed (exposure or not to copepods) at day 7, highlighting an increase in Area only when copepods were absent.

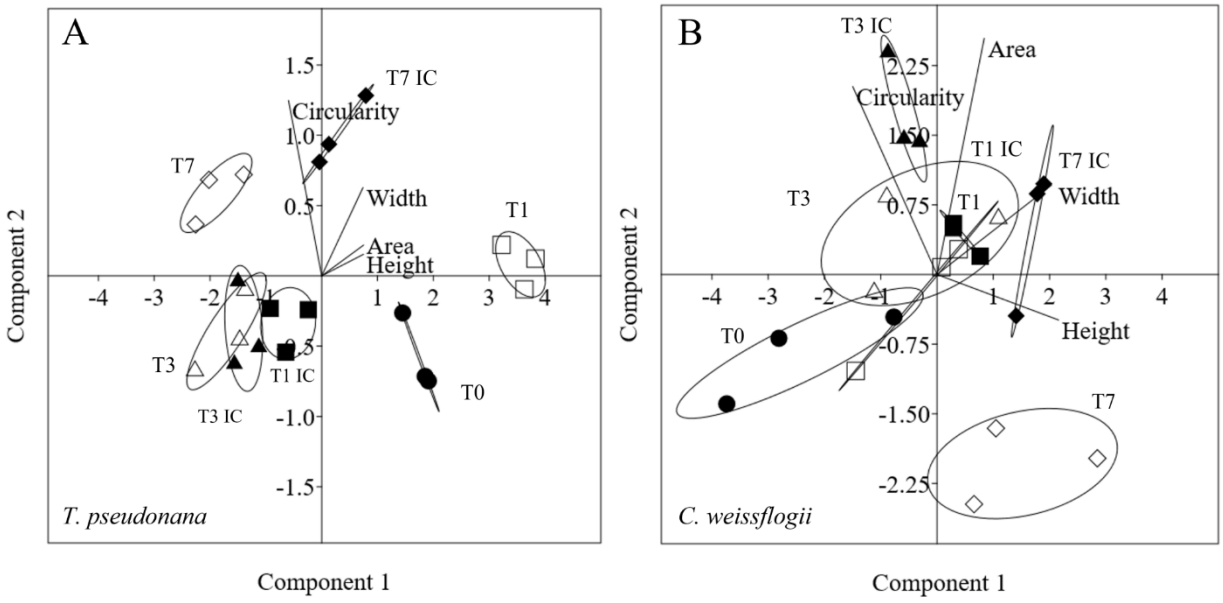

Figure 3.10: PCA analysis on morphological characteristics in *T. pseudonana* (**A**) and *C. weissflogii* (**B**) when mixed together. Different symbols indicate different time during the experiment: T0 ○●; T1 □■, T3Δ▲, T7 ◊♦; white symbols indicate copepods exposure while black symbols indicate absence of copepods and interspecies competition (IC) only

In the mix with the two centric diatoms and the pennate *C. closterium,* growth of *T. pseudonana* had a positive trend under grazing pressure (**Figure 3.11 A**) while in the absence of copepods cell density declined after reaching the maximum value on day 1, without further recovery (**Figure 3.11 B**). Cell density of *C. weissflogii* showed a peak on day 1 and then decreased until day 7, independently from copepods pressure (**Figure 3.11 A, B**). After initial cell decline (days 1 and 3), *C. closterium* grew on day 7, reaching a similar cell density of *T. pseudonana* (**Figure 3.11 A**) when exposed to copepods. In the absence of grazers, *C. closterium* had the highest cell density among the species after 7 days (**Figure 3.11 B**). Overall, data resumed in **Figure 3.11** showed that in the presence of copepods *T. pseudonana* and *C. closterium* managed to grow even if not from the

first day; in both cases, species grew better than in the absence of copepods (see also **Figure S1B**). Conversely, *C. weissflogii* growth had the same negative behaviour in both the analysed conditions.

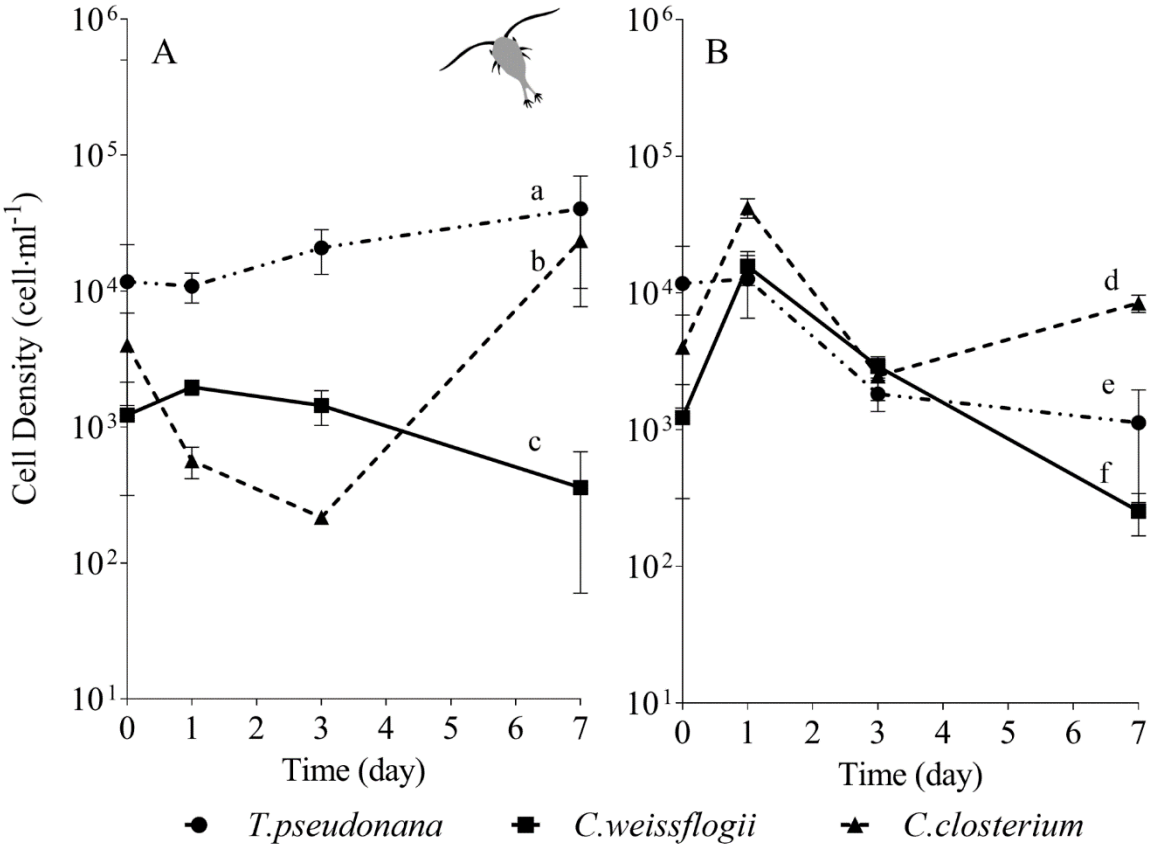

Figure 3.11: Comparison between growth curves of the diatom mix without *P. tricornutum* exposed (**A**) or not (**B**) to copepods. The data are means of 3 biological replicas. Error bars show SD while letters indicate significant difference (Two – way ANOVA and Tukey's *post hoc* test, p<0,05)

Morphological features for centric diatoms (Circularity, Area, Width, Height) and pennate diatoms (Elongatedness, Length, Height, Width) were represented with PCA in **Figure 3.12**. Considering the mixed culture of the two centric diatoms and *C. closterium*, in **Figure 3.12 A** and **B**, PC1 + PC2 accounted for respectively 98.8% (86.2% + 12.6%) and 78.7% (48.6% + 31.1%), of the total variation in *T. pseudonana* and *C. weissflogii.* Day 0 and 7 were again separated according to PC1 and PC2 (eigenvalues in **Table S7**, means values **Table S8**). *T. pseudonana* showed, independently from copepods pressure, a reduced area combined with an increased circularity. *C. weissflogii* had a

different morphological behaviour depending on the presence of grazers: they reduced area and circularity when copepods were in the culture, contrarily they increased area and circularity when copepods were absent. PCA in *C. closterium* (**Figure 3.12 C**, eigenvalues in **Table S7**, means values **Table S8**) explained 99.7% of the total variance (PC1 and PC2 being 53.4% and 46.3%). Here, PC1 differentiated all the experimental days, recording a significant fluctuation in cell length and height during the experiment in both conditions (copepods exposure and interspecies competition). Furthermore, in days 1 and 3, interspecies competition and grazing pressure data were separated according to PC2, indicating that copepods presence increased diatoms width (**Table S8**).

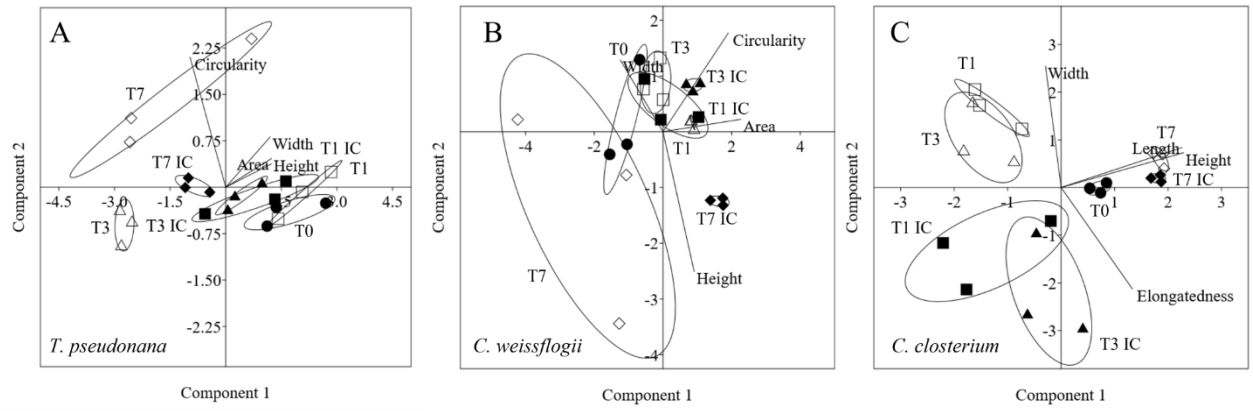

Figure 3.12: PCA analysis on morphological characteristics in *T. pseudonana* (**A**), *C. weissflogii* (**B**) and *C. closterium* (**C**) when mixed together. Different symbols indicate different time during the experiment: T0 ○●; T1 □■, T3Δ▲, T7 ◊♦; white symbols indicate copepods exposure while black symbols indicate absence of copepods and interspecies competition (IC) only

In the mixed culture of the four diatom species exposed to copepods (**Figure 3.13 A**), after initial growth, *T. pseudonana* showed no further variation in the next days, whereas in the absence of grazers (**Figure 3.13 B**) showed a decline at day 7. *C. weissflogii* in both the situations (**Figure 3.13 A**, **B**), never succeeded in growing at day 7, as occurred in the previously described mix (i.e., two centric diatoms and *C. closterium*, see also **Figure 3.11**). In the presence of grazers (**Figure 3.13 A**), both pennate diatoms had a decline in growth at day 3, but they succeeded in increasing cell density at day 7, while in the absence of copepods (**Figure 3.13 B**) *C. closterium* was the only one

which managed to grow at day 7. In conclusion, *C. closterium* was the only diatom showing a positive trend of growth independently of the presence of grazers (**Figure S1B** and **S2C**).

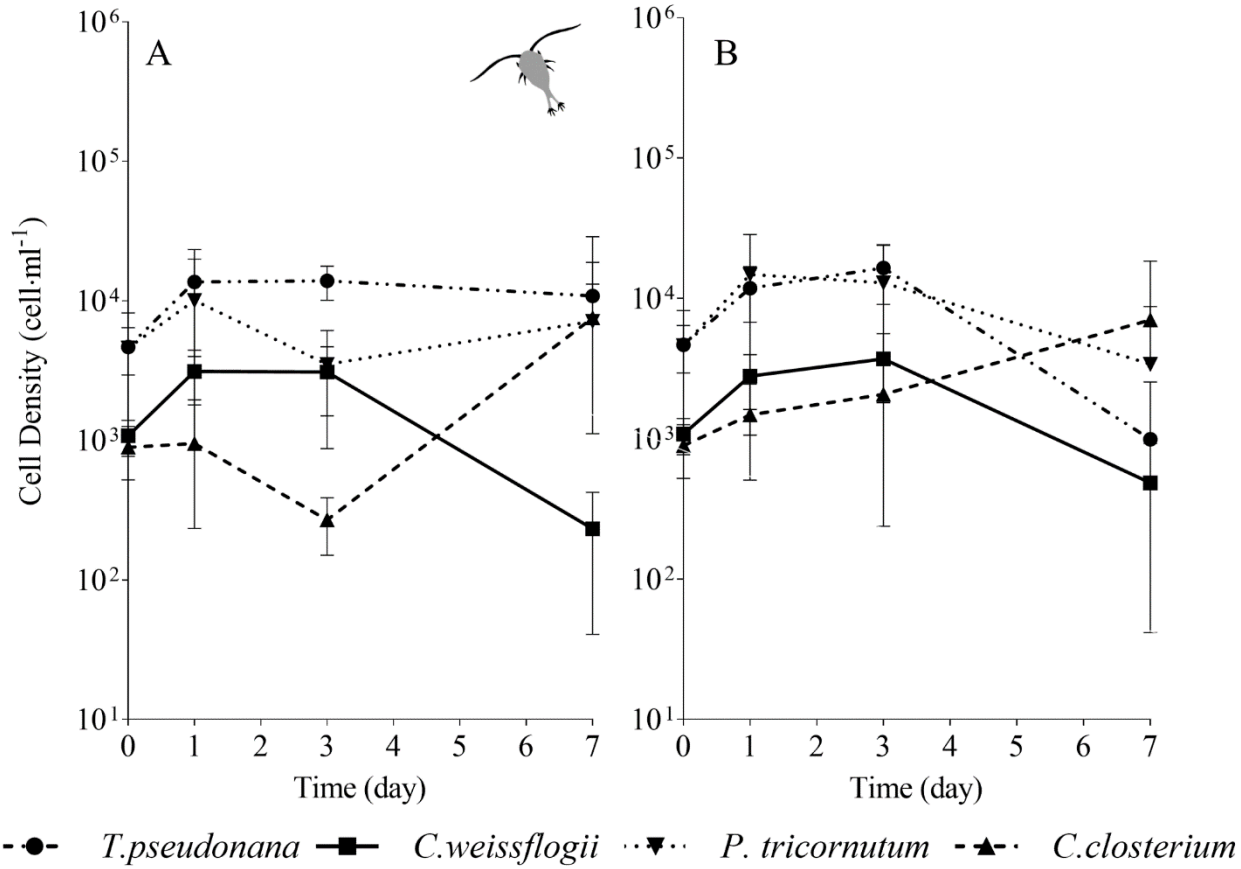

Figure 3.13: Comparison between growth curves of the diatom mix containing all the species exposed (**A**) or not (**B**) to copepods. The data are means of 3 biological replicas. Error bars show SD; no significant difference is observed (p<0,05)

In **Figure 3.14**, the PCA pictured increasing complexity due to 4 mixed diatom species in a single culture; it accounted for 99.5% (PC1 + PC2 being 78.8% + 20.7%, **Figure 3.14 A**), 93.4% (PC1 + PC2 being 59.7% + 33.9%, **Figure 3.14 B**), 97% (PC1 + PC2 being 92.1% + 4.9%. **Figure 3.14 C**) and 99.4% (PC1 + PC2 being 86.4% + 13.0%, **Figure 3.14 D**) of the overall variation in *T. pseudonana*, *C. weissflogii*, *P. tricornutum*, and *C. closterium* respectively (eigenvalues in **Table S9**, means values **Table S10**). Conversely from what observed in the other mixes (**Figure 3.10** and **3.12**), the two centric diatoms *T. pseudonana* (**Figure 3.14 A**) and *C. weissflogii* (**Figure 3.14 B**)

did not show a regular trend in morphological changes during the experiment. In *C. closterium* (**Figure 3.14 D**), different days of exposure were separated according to PC1; as occurred in the previous mix (see also **Figure 3.12 C**), length and height fluctuations during the experiment were recorded. *P. tricornutum* (**Figure 3.14 C**) was not characterized by consistent shape evolution during the experiment.

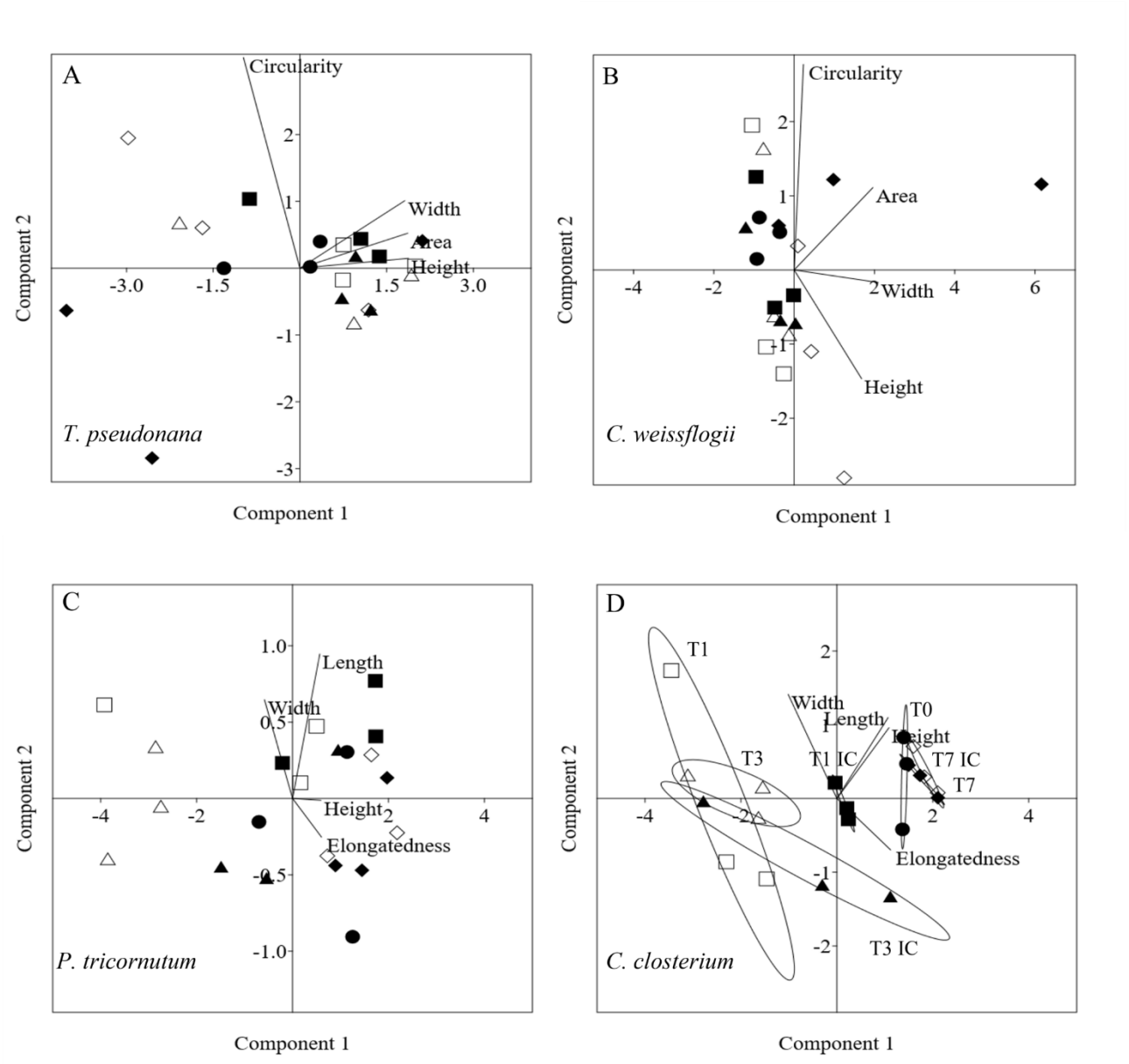

Figure 3.14: PCA analysis on morphological characteristics in *T. pseudonana* (**A**), *C. weissflogii* (**B**) *P. tricornutum* (**C**) and *C. closterium* (**D**) when mixed together. Different symbols indicate different time during the experiment: T0 ○●; T1 □■, T3Δ▲, T7 ◊♦; white symbols indicate copepods exposure while black symbols indicate absence of copepods and interspecies competition (IC) only

3.4 Discussion

Monospecific cultures

Of the four monospecific cultured diatoms, *T. pseudonana* was the most affected by predation and showed a population decline when grown together with copepods compared to cultures maintained without these predators (**Figure 3.7 A**). The initial size (161±3 μm^3, **Table S2**) and the shape characteristics of *T. pseudonana* were clearly fit to feed the adult copepods. Although cells of *T. pseudonana* exposed to copepods changed in morphology and elemental composition (**Figure 3.7 A**, **C**, **Table S1**, **S2**, **S4**), these alterations were insufficient to counter the decrease of the predated populations. In diatoms, increasing Si content is a known strategy to rise mechanical strength and to reduce predation pressure (Pančić et al., 2019, Gronning & Kiørboe 2020). However, a higher Si deposition corresponds to a higher cost of shell thickening (Friedrichs et al., 2013, Pančić et al., 2019, Gronning & Kiørboe 2020) and thus, this extra cost may also have contributed to the lower growth rate shown in **Figure 3.7 A**, **D** for *T. pseudonana*.

Unlike *T. pseudonana*, Si shell thickening occurred in *C. weissflogii* already after 24 hours of exposure to the predators (**Figure 3.7 B**), confirming a similar trend described in the literature (Pondaven et al., 2007, Pančić et al., 2019). A temporary growth decline was observed while this extra Si accumulation happened (**Figure 3.7 B**), this could be explained by the extra cost associated with the shell thickening process as discussed above.

Considering the observed maximum cell density (**Figure 3.7 B**, **D**), a higher mechanical resilience successfully acted as feeding deterrent against predators in *C. weissflogii* but not in *T. pseudonana*. Our data suggested size may play a major role, as the studied *C. weissflogii* is c. 30 times bigger than the examined *T. pseudonana* (**Table S2**). Moreover, bigger size and higher silicification play an important role in sinking, driving vertical movements in the water column, steering prey away from certain predators (Raven & Waite, 2004, Gemmell et al., 2016). The response of *C. weissflogii*

to the studied predators allowed to overcome predation by copepods as it represented the best compromise between minimizing the cost of adjusting to the new condition and growth rate maximization (Giordano 2013).

Copepods also fed on cultured pennate diatoms (as proved by the presence of fecal pellets, data not shown) but algal growth rates and maximum cell densities were unaltered compared to the values in unexposed cells (**Figure 3.8 D**). Such response was already observed in *Synechococcus sp.* cultures under similar predation pressure and discussed in Ratti et al. (2011), where these authors stipulated that microalgal growth is being stimulated in presence of predators.

The *P. tricornutum* we studied did not present any change in Si content per biovolume (**Figure 3.8 A**) suggesting that these small, spindle shaped, and very poorly silicified cells do not rely on Si shell thickness for their defence against predators. On the other hand, becoming more elongated in shape (**Figure 3.12 C**, **Table S4**) likely provided a better buoyancy (Durante et al., 2019). Shape dependent predator-prey interaction likely caused the evolution of new defence strategies (i.e. vertical movements) in these elongated organisms (Pančić & Kiørboe, 2018). Among possible strategies *P. tricornutum* is known to produce apo-fucoxanthinoids as feeding deterrents (Shaw et al., 1995a, Shaw et al., 1995b, Shaw et al., 1997, Tammilehto et al., 2014). The production of an anti-predation substance could be a valid explanation for the high number of dead copepods (and needed to be replaced) in cultures of *P. tricornutum* (**Figure S2 A**).

Mixed cultures

When growing populations of different diatom species in one culture, the study of predator-prey interactions from an ecophysiological point of view also involves interspecies competition (e.g., for resources, algal interactions) (Armbrust 2009, Vallina et al., 2014, Vincent & Bowler 2020) and to the best of our knowledge there are no detailed studies available combining predation pressure and interspecies competition involving several species of diatoms exposed to copepods. For instance,

competition among species was observed in our mixed cultures where diatoms showed lower growth rates (**Figure S1 A**) compared to their control ones (**Figure 3.7 D**, **Figure 3.8 D**).

Moreover, the small diatom *T. pseudonana* had higher growth rates than the bigger *C. weissflogii* (**Figure 3.9**, **Figure S1 A**), this most probably due to a larger surface-to-volume (S/V) ratio in *T. pseudonana*, which allowed a more efficient resource uptake, especially when algal growth reduced the availability of nutrients and light in the mixed culture (Reynolds 2006, Ryabov et al., 2021).

The interspecies competition brought out a striking difference between the growth rates of the *C. weissflogii* populations in the co-cultured centrics with and without copepods (**Figure 3.9**, **Figure S1 A**) suggesting that copepods preferred bigger diatoms.

Although this behaviour did not support the selection of smaller preys to prevent C loss according to the 'sloppy feeding' theory (Roy et al. 1989, Moller and Nielsen 2001, Moller 2004), it has already been observed that *T. longicornis* came up with extraordinary ways to avoid inefficient nutrient uptake (Jansen 2008) optimizing feeding tools (e.g. mouth appendages) to capture and break even large diatom frustules without losing cell organic matter (Smetacek 2001). The energetic convenience of feeding on larger cells is likely due to the lower number of bites performed to acquire a higher amount of nutrients per cell (Friedrichs et al., 2013) as shown by our results (**Table S1** and **S2**).

When culturing *C. weissflogii* and *T. pseudonana* populations together, from our findings morphological changes in the latter did not depend on predation pressure but rather on competition for resources since reducing surface area (**Figure 3.10**, **Table S6**) improves the S/V ratio. Contrary, cells of *C. weissflogii* increased their area and reduced circularity (**Figure 3.10**, **Table S6**) becoming bigger due to the growth limitation independently from predation pressure. This can be explained by the general trend in diatoms to accumulate fixed C in macromolecular storage pools (i.e. lipids, carbohydrates) and thus enlarging their cell volume (Palmucci et al., 2011, Giordano et

al., 2017) when resource availability decreases. Thus, according to our data, interspecies competition disadvantaged bigger species (cells) when co-cultured with a smaller species (cells), even more so when copepods are added to the mix because the increasing size, due to resource limitation, made the larger diatoms even more susceptible to predation. When the pennate diatom *C. closterium* was co-cultured with the centric diatoms, in our setup including copepods, *T. pseudonana* growth was still favoured (**Figure 3.11**, **Figure 3.13**, **Figure S1 B, C**) compared to the two bigger species (**Table S2**), at least for the first 3 days (when resources were likely still plentiful), again proving the size dependent prey selection by predators. Conversely, in the setup without copepods, where big cells were not selectively eaten, cells of *T. pseudonana* stopped growing after the first day while the pennate diatom species showed the highest cell density after day 3 (**Figure 3.13 B**). Overall, *C. closterium* seemed to be the best performing in terms of growth with or without copepods (**Figure 3.11**, **Figure 3.13**, **Figure S1 B, C**). A similar trend was observed when the 2 centric diatoms were cultured together with both pennate species (**Figure 3.11 A**, **Figure 3.13 A**). The morphological response followed growth behaviour, this is particularly visible in cells of *C. closterium* where the elongated shape which characterized this diatom at the start (day 0) was attenuated at time 1 and 3, when a reduction in length and an increase in width were observed (**Table S8** and **S10**). Remarkably, the elongated shape observed on day 0 was then restored on day 7 (**Figure 3.12 C, Figure 3.14 D**). In general, our data show that, in the presence of copepods, small diatoms increase growth performance compared to the bigger diatoms in the same culture, but when predation is absent and interspecies competition acts as the only stress factor, an elongated shaped diatom is more efficient in resource acquisition than a radial shaped one (Pahlow et al., 1997, Key et al., 2010, Naselli – Flores & Barone, 2011, Naselli-Flores et al., 2020, Ryabov et al., 2021). Under predation pressure, although frustules of pennate diatoms are in general less thick (silicified) compared to centric ones (Finkel & Kotrc 2010, Kotrc & Knoll 2015) and copepods may theoretically spend less energy by processing them, the pennate shape *per se* benefits cells in escaping from predators. Indeed, elongated diatoms have lower sinking rates (Durante et al.,

2019), therefore better buoyancy and stability in the water column allowing active substrate adhesion and gliding motion thanks to raphe (Cohn and Disparti, 1994) as a response to many external factors such as light (Cohn et al., 2015), monosaccharides (Cooksey & Cooksey, 1988), dissolved silicate (Bondoc et al., 2016a) and pheromone (Bondoc et al., 2016b, Bondoc et al., 2019a, Bondoc et al., 2019b). Since the pennate diatoms used in this study were raphid, we could not rule out that adhesion and gliding motion were involved to actively migrate away from microcurrents generated by copepods appendix to convey algae near to their mouth (Sengupta et al., 2017). Moreover, as already discussed for monospecific cultures, the higher number of dead copepods replaced in mixed cultures where *P. tricornutum* was present (**Figure S2 B**) could mark the presence of toxic metabolites (Pančić & Kiørboe 2018) which were most likely produced by *P. tricornutum* as a response to the predation pressure (Shaw et al., 1995a, Shaw et al., 1995b, Shaw et al., 1997, Tammilehto et al., 2014). Cell size, robustness, shape and behaviour are therefore crucial in moulding phytoplanktonic communities, as the aforementioned characteristics are not only involved in actively or passively avoiding predators, but also in nutrient uptake, photosynthetic efficiency and buoyancy.

3.5 Supplemental Material

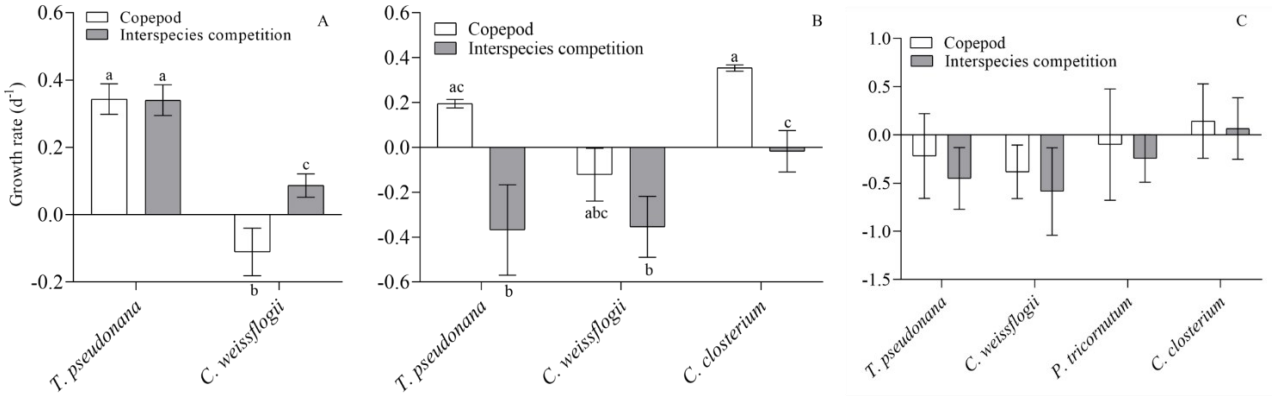

Figure S1: Growth rate of mixed diatom species exposed or not to copepods: (**A**) mix of centric diatoms, **(B**) diatom mix without *P. tricornutum*, (**C**) diatom mix containing all the species. The data are means of 3 biological replicas. Error bars show SD and letters indicate significant difference (Two-way ANOVA followed by Tukey's *post - hoc* test, $p<0.05$)

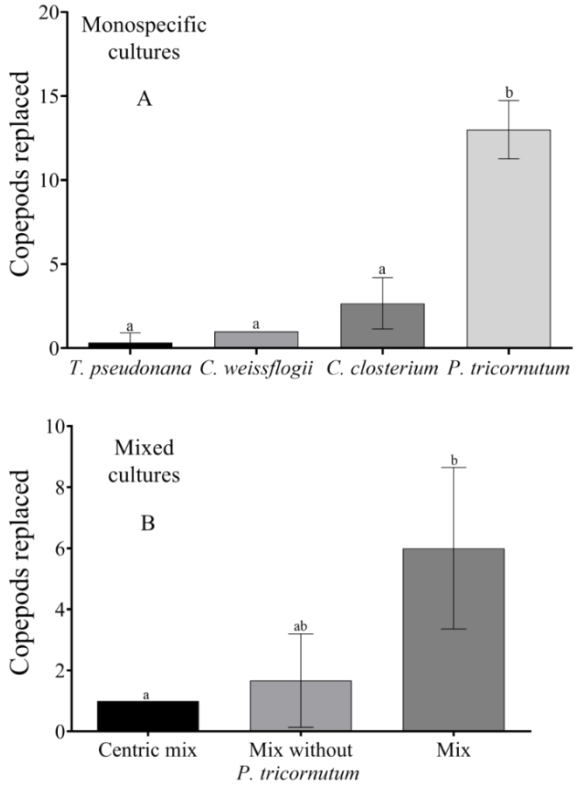

Figure S2: Number of dead copepods replaced with new living individuals during the 7 days grazing trial: (**A**) Monospecific cultures of the four diatoms; (**B**) Mixed cultures. Letters indicate significant differences ($p<0.05$)

Table S1: Elemental composition of the four diatom species studied in monospecific cultures during the exposure to copepods. The values ($pg \cdot \mu m^{-3}$) are means of 3 biological replicas ± SD. Letters indicate significant differences (p<0,05) among days in each species

		C	N	P	S	K	Ca	Fe
T. pseudonana	Day 0	15.65±4.24 [a]	2.83±0.68 [a]	1.25±0.79[a]	3.78±2.13[a]	0.82±0.69[a]	0.39±0.30[a]	1.81±0.65[a]
	Day 1			2.60±2.26[a]	10.64±3.42[a]	1.43±1.63[a]	1.66±0.24[a]	1.46±0.32[a]
	Day 3			11.69±7.04[a]	71.29±9.33[a]	4.25±2.99[a]	6.84±4.96[a]	4.20±3.37[a]
	Day 7	431.77±127.80 [b]	53.39±6.54 [b]	45.42±14.78[b]	258.37±109.89[b]	31.88±12.39[b]	46.60±14.25[b]	32.41±16.08[b]
C. weissflogii	Day 0	6.82±1.41 [a]	1.26±0.23 [a]	1.19±0.85[a]	0.78±0.56	0.76±0.67[a]	0.23±0.21[a]	0.14±0.10[a]
	Day 1			17.31±6.22[b]	48.09±32.59	25.19±1.68[b]	5.14±0.24[b]	2.42±0.14[b]
	Day 3			1.65±0.59[a]	2.74±1.37	1.35±0.71[a]	0.86±0.49[a]	0.39±0.25[a]
	Day 7	22.40±8.05 [b]	3.89±1.51 [b]	0.44±0.23[a]	3.14±12.41	0.17±0.09[a]	0.39±0.26[a]	0.15±0.07[a]
C. closterium	Day 0	5.38±1.66 [a]	1.51±0.99 [a]	0.69±0.51[a]	0.89±0.81[a]	0.09±0.07[a]	0.15±0.07[a]	1.12±1.34[a]
	Day 1			42.92±16.86[b]	95.71±14.20[b]	4.56±2.87[b]	9.21±5.08[b]	25.92±0.13[b]
	Day 3			6.21±1.48[a]	7.67±0.91[a]	1.14±0.51[a]	1.58±0.59[a]	3.64±1.22[a]
	Day 7	32.01±5.77 [b]	5.01±0.49 [b]	2.03±1.77[a]	2.98±1.53[a]	0.25±0.24[a]	0.41±0.32[a]	1.47±1.02[a]
P. tricornutum	Day 0	29.39±11.68	5.37±2.08	0.43±0.29[a]	0.85±0.11[a]	0.03±0.04	0.04±0.04[a]	0.24±0.06[a]
	Day 1			1.83±0.72[ab]	2.59±0.64[ab]	0.28±0.16	0.22±0.02[a]	1.09±0.33[ab]
	Day 3			12.19±5.94[b]	26.07±14.61[b]	3.28±1.72	2.33±1.09[b]	3.37±1.41[b]
	Day 7	5.38±5.18	0.84±0.83	0.67±0.33[a]	3.83±1.92[ab]	0.24±0.15	0.40±0.17[ab]	0.55±0.10[a]

Table S2: Volume (in μm^3) of the four diatom species examined in monospecific cultures during the exposure to copepods. The values are means of 3 biological replicas ± SD. Letters indicate significant differences ($p<0.05$) among days in each species

	T. pseudonana	*C. weissflogii*	*P. tricornutum*	*C. closterium*
Day 0	161±3	4322±488	722±123	1278±35
Day 1	152±1[c]	4173±1089	471±17	1253±250
Day 3	155±2[ac]	4442±1073	540±165	1208±273
Day 7	143±4[b]	4760±1079	493±76	897±43

Table S3: PCA eigenvalues of the morphological features studied for the monospecific centric and pennate diatom cultures exposed to copepods

Centric diatoms		Pennate diatoms	
PC	Eigenvalue	PC	Eigenvalue
1	2.49	1	2.31
2	1.26	2	1.31
3	0.07	3	0.17
4	0.01	4	0.03

Table S4: Values (mean±SD) of the morphological characteristics (in µm) used in the PCA analysis for the four monospecific diatom species exposed to copepods

		Height	Thickness	Width	Circularity	Length	Elongatedness
T. pseudonana	Day 0	6.80±0.03	5.85±0.09	5.48±0.05	8.10±0.28		
	Day 1	6.51±0.01	5.89±0.007	5.45±0.01	9.02±0.05		
	Day 3	6.53±0.06	5.95±0.005	5.50±0.03	9.09±0.22		
	Day 7	6.42±0.21	5.70±0.04	5.32±0.01	8.97±0.57		
C. weissflogii	Day 0	19.94±0.98	16.11±0.47	16.59±0.57	12.37±1.30		
	Day 1	19.01±1.89	16.66±1.46	16.58±1.45	15.90±0.56		
	Day 3	19.65±1.82	16.78±1.38	16.85±1.37	14.52±0.46		
	Day 7	20.65±1.61	16.76±1.29	17.03±1.31	12.60±1.13		
C. closterium	Day 0		6.84±0.08	7.33±0.07		45.45±1.31	6.56±0.25
	Day 1		6.87±0.38	7.25±0.67		45.20±1.45	6.56±0.47
	Day 3		6.75±0.52	7.12±0.91		45.17±2.10	6.63±0.85
	Day 7		6.62±0.34	7.51±0.35		30.54±3.70	4.42±0.70
P. tricornutum	Day 0		6.20±0.19	6.89±0.32		28.85±2.24	4.28±0.10
	Day 1		6.09±0.21	6.24±0.29		23.18±1.45	4.09±0.35
	Day 3		5.91±0.33	6.18±0.61		26.61±3.91	4.49±0.61
	Day 7		5.57±0.11	5.82±0.29		27.68±1.80	4.92±0.18

Table S5: PCA eigenvalues of the morphological features studied for the mixed culture of both centric diatoms, *T. pseudonana* and *C. weissflogii*, which were grown with (interspecies competition and copepod predation) and without (interspecies competition only) copepods

T. pseudonana		*C. weissflogii*	
PC	Eigenvalue	PC	Eigenvalue
1	3.78	1	2.41
2	0.36	2	1.52
3	0.002	3	0.05
4	0.0007	4	0.01

Table S6: Values (mean±SD) of the morphological characteristics (in µm) for the mixed culture of both centric diatoms, *T. pseudonana* and *C. weissflogii*, which were grown with (interspecies competition and copepod predation) and without (interspecies competition only) copepods

		Copepods				**Interspecies Competition**			
		Height	Area	Circularity	Width	Height	Area	Circularity	Width
T. pseudonana	Day 0	8.70±0.08	51.27±0.20	7.20±0.19	7.36±0.004	8.70±0.08	51.27±0.20	7.20±0.19	7.36±0.004
	Day 1	9.15±0.08	56.12±0.60	7.10±0.12	7.68±0.04	8.17±0.07	45.98±0.94	7.86±0.10	7.07±0.05
	Day 3	7.89±0.12	43.42±1.30	8.08±0.07	6.92±0.10	7.97±0.06	44.25±0.42	8.03±0.17	6.95±0.05
	Day 7	7.89±0.12	43.70±1.02	8.61±0.06	7.007±0.08	8.45±0.11	48.95±1.22	8.31±0.02	7.34±0.09
C. weissflogii	Day 0	18.73±0.44	224.36±5.19	10.55±0.69	15.86±0.24	18.73±0.44	224.36±5.19	10.55±0.69	15.86±0.24
	Day 1	19.39±0.27	233.77±5.70	9.37±0.04	16.11±0.17	19.52±0.12	237.26±0.04	9.59±0.43	16.33±0.01
	Day 3	19.30±0.40	237.10±3.95	9.99±0.75	16.19±0.18	19.15±0.13	243.21±1.44	11.72±0.89	16.26±0.06
	Day 7	20.01±0.33	225.77±2.41	6.40±0.68	16.31±0.22	19.85±0.05	239.97±4.41	8.63±0.60	16.51±0.11

Table S7: PCA eigenvalues of the morphological features studied for the mixed culture of both centric diatoms (*T. pseudonana* and *C. weissflogii*) and *C. closterium*, which were grown with (interspecies competition and copepod predation) and without (interspecies competition only) copepods

T. pseudonana		*C. weissflogii*		*C. closterium*	
PC	Eigenvalue	PC	Eigenvalue	PC	Eigenvalue
1	3.45	1	1.94	1	2.13
2	0.51	2	1.25	2	1.85
3	0.03	3	0.77	3	0.001
4	0.01	4	0.04	4	0.0002

Table S8: Values (mean±SD) of the morphological characteristics (in µm) for the mixed culture of both centric diatoms (*T. pseudonana* and *C. weissflogii*) and *C. closterium*, which were grown with (interspecies competition and copepod predation) and without (interspecies competition only) copepods

		Copepods				**Interspecies Competition**			
		Height	Area	Circularity	Width	Height	Area	Circularity	Width
T. pseudonana	Day 0	8.73±0.20	51.31±1.44	7.26±0.15	5.22±0.10	8.73±0.20	51.31±1.44	7.26±0.15	5.22±0.10
	Day 1	8.79±0.13	52.64±1.81	7.32±0.03	5.27±0.10	8.47±0.25	49.38±2.53	7.58±0.17	5.19±0.14
	Day 3	7.73±0.05	41.95±0.60	8.21±0.15	4.81±0.03	8.44±0.10	49.46±1.44	7.72±0.03	5.11±0.05
	Day 7	8.17±0.49	46.07±3.88	8.98±0.09	5.04±0.24	8.26±0.08	46.67±0.21	8.12±0.14	4.97±0.04
C. weissflogii	Day 0	19.01±0.31	226.03±1.61	9.37±1.18	6.50±0.13	19.01±0.31	226.03±1.61	9.37±1.18	6.50±0.13
	Day 1	19.04±0.20	232.43±3.51	10.92±0.58	6.55±0.13	19.14±0.22	237.30±6.61	10.68±0.51	6.46±0.17
	Day 3	18.96±0.02	234.49±0.52	11.13±0.07	5.99±0.05	19.05±0.11	241.47±3.96	11.64±0.14	6.34±0.07
	Day 7	19.26±0.76	208.00±13.74	7.65±0.93	6.29±0.32	19.82±0.10	250.65±2.75	10.51±0.21	6.21±0.06
		Height	Length	Elongatedness	Width	Height	Length	Elongatedness	Width
C closterium	Day 0	49.87±0.32	48.44±0.41	7.41±0.07	7.52±0.10	49.87±0.32	48.44±0.41	7.41±0.07	7.52±0.10
	Day 1	46.58±0.83	45.77±0.62	5.35±0.53	9.46±0.45	44.67±2.55	43.24±2.52	6.43±0.54	7.37±0.54
	Day 3	45.99±0.81	44.88±0.95	5.69±0.60	8.84±0.72	46.30±1.04	44.99±1.00	5.67±0.89	8.70±1.12
	Day 7	52.48±0.18	51.31±0.22	7.54±0.17	8.03±0.18	52.21±0.2	50.80±0.22	7.65±0.06	7.83±0.09

Table S9: PCA eigenvalues of the morphological features studied for the mixed culture of both centric diatoms (*T. pseudonana* and *C. weissflogii*) and both pennate diatoms (*P. tricornutum* and *C. closterium*), which were grown with (interspecies competition and copepod predation) and without (interspecies competition only) copepods

T. pseudonana		*C. weissflogii*		*P. tricornutum*		*C. closterium*	
PC	Eigenvalue	PC	Eigenvalue	PC	Eigenvalue	PC	Eigenvalue
1	3.15	1	2.38	1	3.69	1	3.46
2	0.83	2	1.35	2	0.2	2	0.52
3	0.01	3	0.24	3	0.09	3	0.02
4	0.003	4	0.02	4	0.02	4	0.004

Table S10: Values (mean±SD) of the morphological characteristics (in µm) for the mixed culture of both centric diatoms (*T. pseudonana* and *C. weissflogii*) and both pennate diatoms (*P. tricornutum* and *C. closterium*), which were grown with (interspecies competition and copepod predation) and without (interspecies competition only) copepods

		Copepods				**Interspecies Competition**			
		Height	Area	Circularity	Width	Height	Area	Circularity	Width
T. pseudonana	Day 0	8.71± 0.38	51.16±4.09	7.32±0.14	7.39±0.30	8.71± 0.40	51.16±4.09	7.32±0.14	7.40±0.30
	Day 1	9.31± 0.28	57.31±3.22	7.01±0.22	7.78±0.22	9.04±0.47	55.26±4.52	7.42±0.50	7.68±0.31
	Day 3	8.88± 0.86	53.65±7.56	7.08±0.78	7.50±0.50	9.18±0.09	56.27±1.32	6.82±0.27	7.67±0.08
	Day 7	8.47± 0.83	47.76±8.10	7.81±1.16	7.15±0.42	8.17±1.41	44.78±14.74	6.85±0.82	6.82±1.11
C. weissflogii	Day 0	19.55± 0.18	236.04±4.82	9.36±0.43	16.36±0.11	19.55± 0.18	236.04±4.82	9.36±0.43	16.36±0.11
	Day 1	19.81±0.79	232.06±5.32	8.46±2.94	16.41±0.17	19.87±0.54	236.80±3.43	9.01±1.44	16.39±0.21
	Day 3	19.79±0.53	237.72±2.98	8.69±2.32	16.44±0.17	19.89±0.51	235.28±2.53	8.18±1.09	16.43±0.29
	Day 7	20.81±1.09	238.78±8.79	7.18±1.89	16.90±0.29	20.86±1.12	270.08±41.45	10.98±1.29	17.42±1.66
		Height	Length	Elongatedness	Width	Height	Length	Elongatedness	Width
C closterium	Day 0	54.51±0.45	53.33±0.65	7.91±0.22	8.07±0.41	54.51±0.45	53.33±0.65	7.91±0.22	8.07±0.41
	Day 1	51.59±0.42	49.30±0.74	6.02±0.98	9.65±1.55	53.38±0.12	51.79±0.05	7.31±0.15	8.39±0.25
	Day 3	51.89±0.35	49.71±0.92	6.19±0.44	9.64±0.66	52.14±1.32	50.43±0.86	7.25±1.18	8.32±1.46
	Day 7	54.95±0.14	53.71±0.05	8.11±0.30	7.90±0.29	54.77±0.03	53.65±0.13	8.11±0.25	7.85±0.29
P.tricornutum	Day 0	28.44±1.10	25.19±1.29	4.59±0.57	9.64±0.65	28.44±1.10	25.19±1.29	4.59±0.57	7.89±0.29
	Day 1	25.80±4.66	24.77±1.65	3.70±1.22	8.32±1.46	29.39±1.26	26.75±1.46	4.69±0.51	7.85±0.29
	Day 3	24.28±1.27	21.72±1.02	2.90±0.18	9.85±0.21	27.28±1.72	24.33±1.83	4.17±0.49	6.75±0.41
	Day 7	29.88±0.42	26.35±1.09	4.90±0.48	7.88±0.45	30.40±1.05	25.92±0.94	4.77±0.22	6.74±0.23

Chapter four: Light and silicification- implications on diatom vertical movements

In collaboration with Dr. P. Moretti, Prof. M. G. Ortore

4. Light and Silicification – implications on diatom vertical movements

4.1 Introduction

The ability to incorporate Si in frustules is a dominant feature in diatoms; its original role is still controversial, but a frustule more than a cellulosic or carbonate cell wall increases cell density and, therefore, it is known to contribute to diatom faster sinking as compared to that of other phytoplanktonic groups (Raven and Waite, 2004). Consequently, diatoms become good players not only in Si precipitation to the bottom of the ocean (Moriceau et al., 2007) but also in the biological C pump (Tréguer et al., 2018). In nature, frustules are diverse in terms of morphology and silicification; therefore, frustule traits indirectly control sinking capacity by changing cell density. In particular, Si deposition showed a phenotypical response to different external factors (i.e. grazers, nutrient availability and light intensity) (Pondaven et al., 2007, Su et al., 2018, Xu et al., 2021, Petrucciani et al., 2022). Among them, light is a crucial driver on the distribution of phytoplankton through the water column not only affecting their photosynthetic performance but also influencing the silicification process. Nevertheless, direct findings assessing the light role on diatom Si deposition are still controversial: according to some authors light deficiency enhanced Si deposition in frustules (Xu et al., 2021) while other authors suggested the latter was directly related to the increase in light intensity (Su et al., 2018).

New insights into the fascinating diversity of diatoms confirmed that also very small and scarcely silicified diatoms (*Minidiscus sp.*, Leblanc et al., 2018) are able to rapidly sink out: their impact on Si and C exports to the bottom of the oceans is significant even though their small size and biomineralization do not classify them as good sinkers. These new observations open a lot of questions on the relation between the huge diatom diversity in size and silicification and their contribution to the C and Si cycles (Tréguer et al., 2018).

Sinking is an important determinant of diatom spatial distribution, enhancing their access to light and nutrients (Smayda 1970, Margalef 1978). Numerous findings verified the presence of cellular mechanisms to control buoyancy in diatoms (Waite et al., 1992, Lavoie et al., 2016, Lavoie and Raven, 2020) but new insights revealed also the existence of an unsteady sinking behaviour in which cells vary the sinking speed over more than an order of magnitude repeatedly within tens of seconds in response to physiological and environmental conditions (Gemmell et al. 2016, Du Clos et al., 2019, Du Clos et al., 2021). Controlling buoyancy over short time scales may allow diatoms to take advantage of patchy distributions of nutrients or to escape from predators (Raven and Waite 2004, Du Clos et al., 2021).

The aim of this work was to investigate diatom sinking capacity and the implication of silicification processes on such frustule adaptative role. To achieve this purpose four different diatoms in terms of size, shape and silicification (*Chaetoceros muelleri*, *Conticribra weissflogii*, *Pheodactylum tricornutum*, *Cylindrotheca fusiformis*) were acclimated to different light conditions (15, 60, 180 µmol photons·$m^{-2}s^{-1}$) in order to manipulate their Si deposition. Dynamic Light Scattering (DLS), a physical technique used to determine the size distribution profile of nanoparticles in solution, was here applied as an innovative tool in ecophysiological studies to directly assess the sinking capacity of diatoms. Lastly diatoms physiological performance in terms of growth, change in morphology, photosynthetic efficiency, inorganic composition was investigated.

It was hypothesized that the sinking capacity was dependent on cell morphology and silicification and it was asked whether light and silicification influence each other in ways that govern growth and buoyancy, addressing the integrative effects of factors commonly treated in isolation.

Resulting considerations will help to elucidate also the crucial role of diatoms in ocean ecosystems, biological C pump and Si cycle.

4.2 Material and Methods

4.2.1 Algal cultures

Two centric species of diatom, *Chaetoceros muelleri* (CCAP 1010/3, https://www.ccap.ac.uk/) and *Conticribra weissflogii* (DCG 0320, https://bccm.belspo.be/about-us/bccm-dcg), and two raphid pennate diatoms, *Cylindrotheca fusiformis* (NEPCC417) and *Phaeodactylum tricornutum* (DCG 0981), were acclimated for at least four generations to three different light intensities (15, 60, 180 µmol photons·$m^{-2}s^{-1}$). Cultures were established in 250 mL flasks filled with 100 mL of AMCONA medium (Fanesi et al., 2014) and maintained in a culture chamber at 18 °C, illuminated with cool white fluorescent lamps at 12:12 h light-dark cycles.

4.2.2 Specific growth rate, cell volume and dry weight

Cell number was measured using a CASY TT cell counter (Innovatis AG, Reutlingen, Germany). Aliquots of 100 µL culture were diluted in 10 mL of an electrolyte solution (CASY TON; Innovatis AG). In the cell counter, cells were pumped into a 150 µm capillary at a constant flow and the number of cells was determined through the enumeration of events measured as change of conductivity. The electrical current was assessed by two platinum electrodes, between which a pulsed low voltage of 1 MHz was generated. Specific growth rates, µ (**Eq. 4.1**), were derived from daily counts of exponentially growing cells, carried out on a minimum of three distinct cultures for each treatment.

$$(\mathbf{4.1})\ \mu = \frac{ln(N_t/N_0)}{t}\ \text{(Monod 1949)}$$

The same instrument was also used to measure the cellular size as the volume of electrolyte solution displaced by the passage of cells through a measuring pore (Palmucci et al., 2011). Diatoms collected during exponential phase were put in pre-weighted tubes and dried at 80°C till obtaining the cellular dry weight. All measurements were carried out on samples from three distinct cultures.

4.2.3 Quantification of Silicon

The abundance of elements, included Si, was measured using a Total Reflectance X – ray Fluorescence spectrometer (S2 Picofox, Bruker AXS Microanalysis GmbH, Berlin, Germany). Sampled diatoms were washed twice with an ammonium formate solution isosmotic to the culturing media and resuspended in 250 µl of dH_2O. A solution of 0.1 g L^{-1} Ga (Sigma Aldrich, St. Luis, MO, USA) in 5% HNO_3 was added as internal standard to a final concentration of 0.5 µL L^{-1}. The suspension was carefully vortexed and an aliquot of 10 µl was deposed on a plastic sample holder, dried on a heating plate and measured for 1000 seconds. Spectral deconvolution and quantification of elemental abundances were performed by the SPECTRA 6.1 software (Bruker AXS Microanalysis GmbH, Berlin, Germany).

4.2.4 Sinking Capacity

Dynamic Light Scattering measurements were carried out using a Malvern Zetasizer PRO system, at room temperature, with a fixed angle of 173° and with fixed attenuator in order to fulfil the desired measurement. For all measured samples, data represented the average of at least five different autocorrelation functions.

Cells were sampled during the exponential phase, diluted to obtain $5 \cdot 10^5$ cells in 1 ml of culturing medium and loaded into the system.

The data relating to the photon counts on the detector (**Figure 4.1**), obtained as a function of time, were averaged, and reported in graphs as exponential function describing diatoms sedimentation (**Eq. 4.2**). The obtained τ values indicated diatom sedimentation rates, obtained for 3 biological replicas.

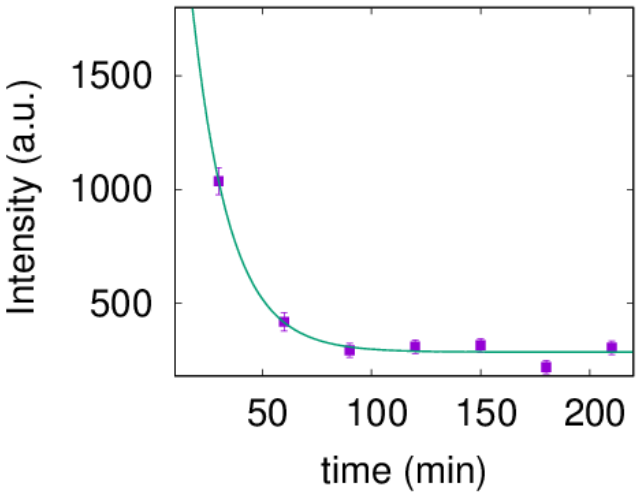

Figure 4.1: Example of DLS analysis on diatoms: photons count as function of time of living cells in their growth medium

$$(\mathbf{4.2})\ I_{(t)} = I_{(0)}e^{\left(-\frac{t}{\tau}\right)} + b$$

The τ value indicates diatom sedimentation rates and were obtained from 3 biological replicas.

4.2.5 Pigments quantification and photosynthetic efficiency

Algae were centrifuged at 3000 x g for 5 min, then, pigments were extracted from the pellet in 2 mL of 100% (v/v) methanol (Ritchie et al., 2006); the extracts were stored in the dark, at -20°C overnight. A colorless pellet was then separated from the supernatant by centrifugation at 13000 x g for 5 min. The absorbance of the supernatant was evaluated spectrophotometrically (Beckman DU 640 Spectrophotometer, Beckman Coulter) in a range from 750nm to 350nm (scan speed 0.5nm). Chlorophyll concentrations were calculated according to equations by Ritchie 2006 (**Eqs. 4.3-4.5**):

$$(\mathbf{4.3})\ \text{Chl } a\ (\mu g \cdot mL^{-1}) = 13.2654 \cdot Abs_{664nm} - 2.6839 \cdot Abs_{630nm}$$

$$(\mathbf{4.4})\ \text{Chl } c\ (\mu g \cdot mL^{-1}) = 28.8191 \cdot Abs_{630nm} - 6.0138 \cdot Abs_{630nm}$$

(**4.5**) Total Chl ($\mu g \cdot mL^{-1}$) = Chl *a* + Chl *c*

Carotenoid concentrations were calculated according to Wellburn (1994) following the equation (**Eq. 4.6**):

(**4.6**) Total carotenoids ($\mu g \cdot mL^{-1}$) = $(1000 \cdot Abs_{470nm} - 1.63 \cdot Chl a - 104.96 \cdot Chl c)/221$

Methanol absorbance was used as blank and absorbance at 730 nm was subtracted from all measurements to avoid background noise. All results were expressed as pg of pigment per cell.

In vivo variable fluorescence of photosystem II (PSII) chlorophyll *a* (P_{680}) was analyzed with DUAL PAM 100 fluorimeter (Heinz Walz GmbH, Effeltrich, Germany). A sample of 10^7 cells was collected by centrifugation at 3000 x g for 5 min, re-suspended in 2 mL of growth medium, and dark-adapted for 10 min. Subsequently, samples were transferred into a glass cuvette for the PAM analysis under continuous stirring. The measuring light (40 µmol photons m^{-2} s^{-1}) was turned on to determine F_0, the minimum value for chlorophyll fluorescence. Then, a saturation pulse (10000 µmol photons m^{-2} s^{-1}, 600 ms) was applied to saturate all reaction centers and allow to obtain F_m (the maximum value of fluorescence). From F_m and F_0, the maximum quantum efficiency of PSII, F_v/F_m, was calculated as follows (**Eq. 4.7**):

$$(\mathbf{4.7}) \quad \frac{F_V}{F_m} = \frac{(F_m - F_0)}{F_m}$$

F_v/F_m represents a robust indicator of the maximum quantum yield of PSII photochemistry (Misra et al., 2012). All parameters were obtained through the Dual PAM v1.8 software (Walz GmbH, Effeltrich, Germany).

4.2.6 Morphological characterization

Diatoms collected during exponential phase were analysed with the Imaging Flow Cytometer (IFC) FlowSight® (Amnis Corp., Seattle, WA) using the INSPIRE software package (Amnis Corp.) to determine morphometric characteristics. For each analysis, a volume of 10 mL was analysed within 24 hours after sampling. IFC data of more than 50000 objects present in the samples were saved. Details and settings of the IFC technique were as follows: 10 μm core size diameter, 132 mm/s speed, 20x magnification; bright field data were collected in channel 1 (LED intensity 35.46 mW) and chloroplast autofluorescence in channel (642 nm, laser 2 mW). Post – acquisition data analysis was performed using the IDEAS software package. For each diatom species - specific masks, separating the pixels occupied by the diatoms from the background, were created for both brightfield and autofluorescence images. All objects lacking chloroplast autofluorescence, as determined by the Intensity feature of the IDEAS software, were considered debris or dead diatoms and, consequently, excluded from metrics. Among the living cells, only single and well-focused diatoms were gated to obtain morphological parameters. The morphological features considered for the analysis were Height, Width, Length, Elongatedness (height/width), Perimeter, Diameter, Compactness, Area, Circularity (IDEAS User Manual, version 6.0, March 2013). Given numbers refer to at least 1000 cells for each biological replica.

4.2.7 Frustules characterization

Diatom's frustules of the centric diatoms (*C. muelleri* and *C. weissflogii*) were obtained through oxidation of the organic material using HCl-$KMnO_4$ (modified from Friedrichs et al., 2012). The salts of the culture medium were washed 4 times with deionized water, then 1.5 ml of a supersaturated solution of $KMnO_4$ was added to the cell suspension and let overnight at room temperature. A volume of 3 ml of HCl was added slowly to the suspension, then samples were moved to a warming bath at 100 °C for 40 minutes. Finally, the material was washed 4 times with

deionized water to carefully remove the acidic solution. Drops of cleaned material were then poured on a MF-Millipore™ mixtures of cellulose acetate and cellulose nitrate filter (mesh size 0,45 μm) fixed on the conductive carbon adhesive discs pasted on the stub and left to dry completely at 50 °C. The stub was then sputter-coated with a thin layer of gold-palladium in a Balzer Union evaporator and analysed by SEM (High Resolution ZEISS – SUPRA 40). Pictures were taken with different order of magnitude in order to obtain also morphometrical measurements of frustule details (setae and punctae in *C. muelleri*, Reinke 1984).

4.2.8 C and N analysis

Cellular C and N content were determined using an elemental analyser (ECS 4010, Costech Italy) connected to the ID Micro EA isotope ratio mass spectrometer (Compact Science Systems, LymedaleBusiness Centre, Newcastle-Under-Lyme, United Kingdom) to obtain C and N stable isotopes ($\delta^{13}C$ and $\delta^{15}N$) ratios. A dry weight of 0.5 – 1 mg of cells previously washed twice with an ammonium formate solution and dried at 80°C, was analysed. Replicate analyses of isotopic standard reference materials Urea ($\delta^{13}C = -36.6‰$; $\delta^{15}N = 2.2‰$) were performed and used to normalize isotopic values of algal biomass. Two blank samples were analysed before each sample run to verify backgrounds and urea standards were also analysed after every 6 samples to monitor instrument performance. Data acquisition and analysis were performed with the software EA IsoDelta (Compact Science Systems, LymedaleBusiness Centre, Newcastle-Under-Lyme, United Kingdom). All the measurements were carried out on 3 biological replicas.

4.2.9 Statistical analysis

Data were expressed as mean ± standard deviation (SD). Significant differences among the means were tested with a one – way analysis of variance (ANOVA), followed by Tukey's *post-hoc* test.

When there were more than one variable, Two-way ANOVA followed by Tukey's *post-hoc* test was performed. Comparison of treatment pairs was achieved with a two-tailed *t*-test. The level of significance was set at 0.05. GraphPad prism 8.0.2.263 was used to carry out the tests (GraphPad Software, San Diego, CA, USA).

Principal Component Analysis (PCA) was done using PAST 4.03 (Hammer et al.,2001. PAST: Paleontological statistics software package for education and data analysis). PCA was performed on different morphological features (e.g., Height, Width, Length, Elongatedness (height/width), Perimeter, Diameter, Compactness, Area, Circularity) obtained through Imaging Flow Cytometer analysis as dependent variables in different species (independent variable) acclimated to different light intensities (independent variable). Data were normalized using z-values ((n-mean)/SD).

4.3 Results

4.3.1 Growth analysis

Figure 4.2 and **Table 4.1** represent growth of the four diatoms acclimated to increasing light intensities (15, 60, 180 µmol photons·m^{-2}·s^{-1}). Growth of *C. muelleri* and *P. tricornutum* was significantly limited by the lowest light intensity (15 µmol photons·m^{-2}·s^{-1}, **Table 4.1**). On the other hand, growth rate of *C. weissflogii* and *C. fusiformis* was stable among the conditions, even though the number of cells reached by *C. fusiformis* grown at 15 µmol photons·m^{-2}·s^{-1} was half the density in the other two conditions (**Figure 4.2**).

Table 4.1: Mean ± SD of specific growth rate (µ) in the four diatoms acclimated to different light intensities (n ≥ 3). Letters indicate significant difference among conditions in the same species (p > 0.05)

		15 µmol photons·m^{-2}·s^{-1}	60 µmol photons·m^{-2}·s^{-1}	180 µmol photons·m^{-2}·s^{-1}
Specific Growth rate (µ, day^{-1})	*C.muelleri*	0.43±0.01^{a}	0.50±0.01^{b}	0.51±0.03^{b}
	C.weissflogii	0.29±0.04	0.21±0.01	0.33±0.07
	P.tricornutum	0.30±0.01^{a}	0.46±0.02^{b}	0.42±0.03^{b}
	C. fusiformis	0.26±0.05^{a}	0.23±0.02^{ab}	0.16±0.01^{b}

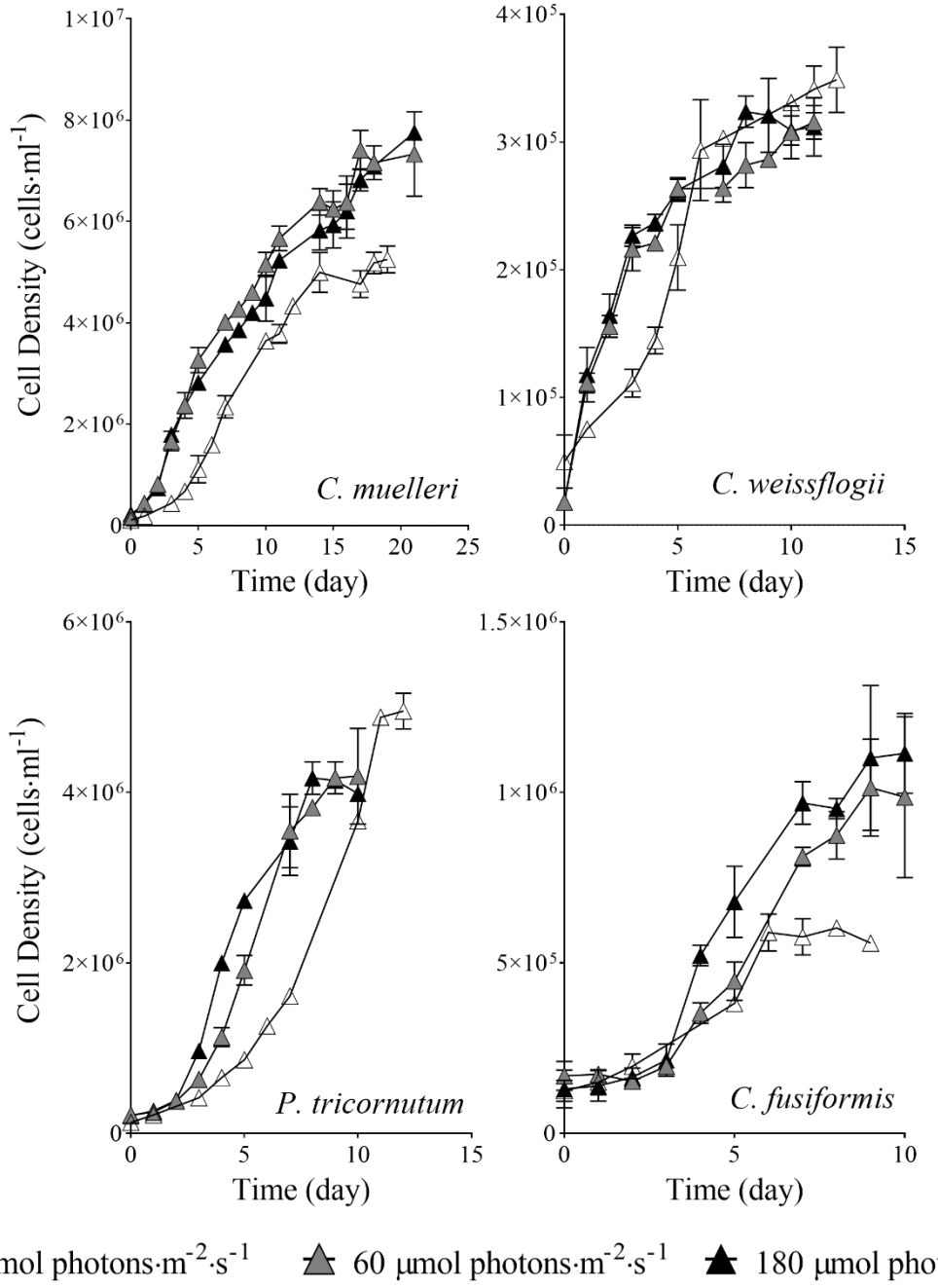

Figure 4.2: Growth curves of the four diatoms acclimated to different light intensities. Data are means of 3 biological replicas. Error bars show SD.

4.3.2 Silicon quantification

Si content per biovolume in the four morphologically different diatoms acclimated to different light intensities is pictured in **Figure 4.3**: in pennate diatoms (*P. tricornutum* and *C. fusiformis*) Si quota was significantly lower when the availability of light was scarce. On the other hand, centric diatoms showed a deeply different behaviour: in *C. muelleri* the Si content was lowest at 60 µmol photons·m^{-2}·s^{-1} while in C. *weissflogii* it did not change.

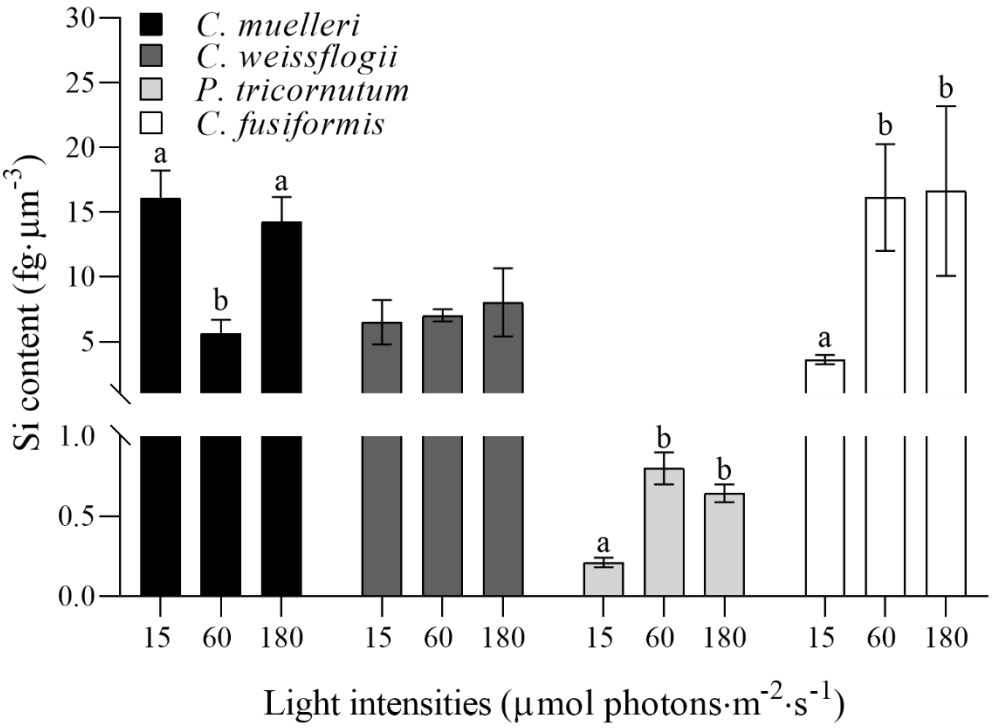

Figure 4.3: Si content per volume unit (fg·µm^{-3}) in the four diatoms acclimated to different light intensities. Data are means of at least 3 biological replicas. Error bars show SD. Letters represent significant differences among conditions in the same species (p<0.05)

4.3.3 Sinking capacity

Sinking behaviour was assessed in diatoms through DLS technique highlighting a direct relation between the light intensity used to grow diatoms and buoyancy: in particular, the sedimentation rate (τ) was significantly higher when the light was lower in all the species, the difference was more evident in centric ones (**Figure 4.4**).

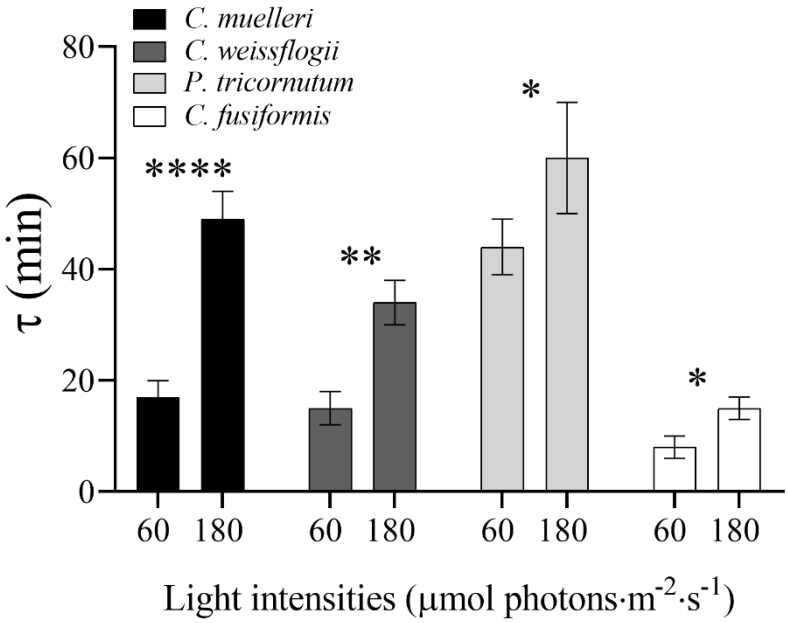

Figure 4.4: τ values representing sedimentation rate (min) in the four diatoms acclimated to different light intensities. Data are means of at least 3 biological replicas. Error bars show SD. Asterisks represent significant differences between conditions in the same species (* p<0.05, ** p<0.001, **** p<0.00001)

4.3.4 Pigments quantification and photosynthetic efficiency

A statistically significant decrease in photosynthetic efficiency was recorded only in *C. weissflogii* cells acclimated to higher light intensity (**Figure 4.5**), while other species did not show changes in the photosynthetic apparatus. A higher accumulation of chlorophylls was observed in diatoms acclimated to a lower light intensity (**Figure 4.6**). *C. fusiformis* underwent the greatest change in pigmental pattern, also showing a change in chlorophylls ratio and in carotenoid content.

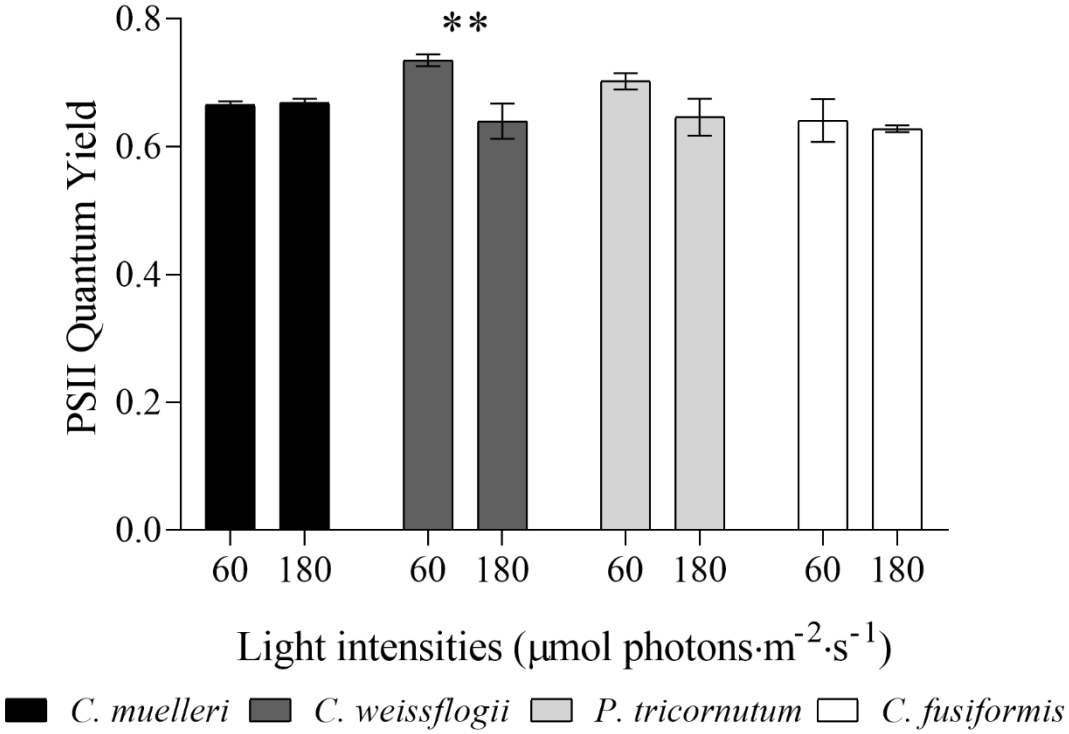

Figure 4.5: PSII Quantum Yield of the four diatoms acclimated to different light intensities. Data are means of 3 biological replicas. Error bars show SD. Asterisks represent significant differences among conditions in the same species (* $p<0.05$, ** $p< 0.001$).

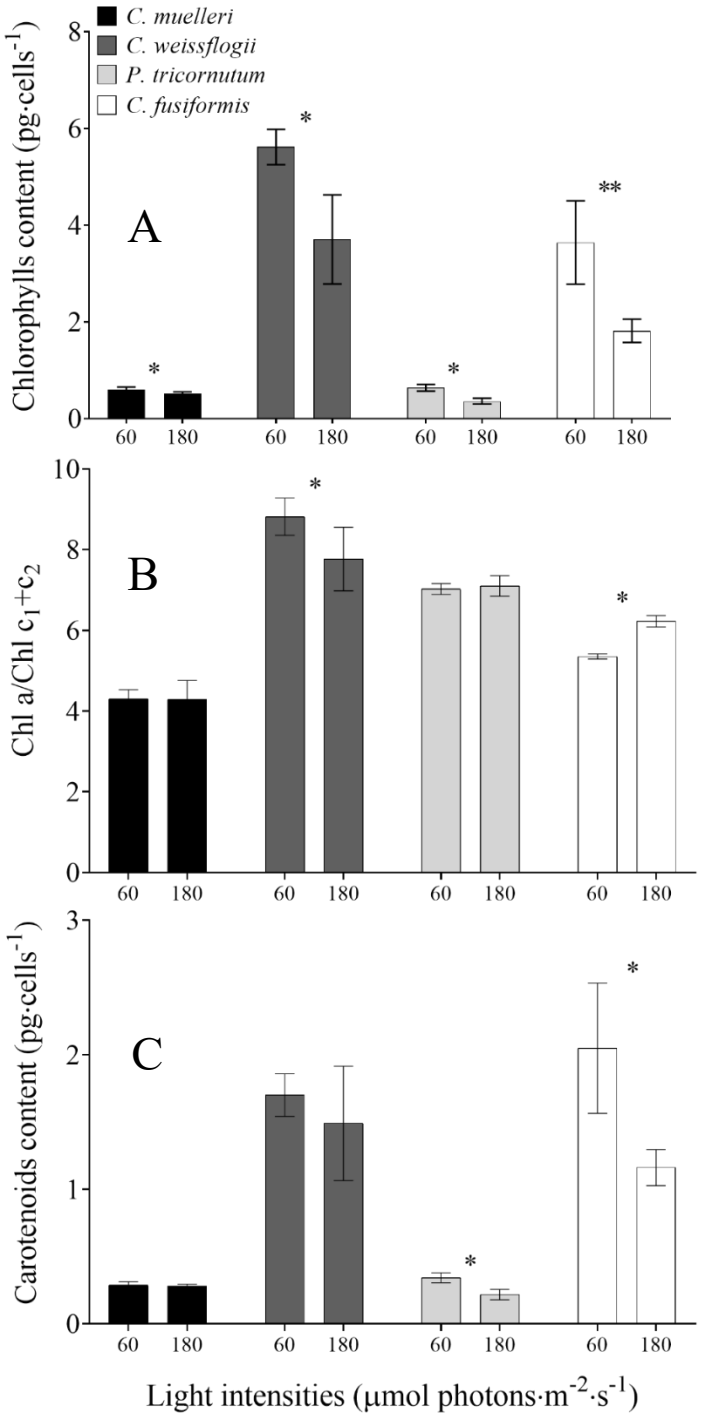

Figure 4.6: Pigments analysis of the four diatoms acclimated to different light intensities: (**A**) chlorophylls quantification, (**B**) Chl_a/Chl_{c1+c2} ratio and (**C**) carotenoids quantification. Data are means of 3 biological replicas. Error bars show SD. Asterisks represent significant differences among conditions in the same species (* p<0.05, ** p< 0.001).

4.3.5 Morphological characterization

Morphological features of centric diatoms (Circularity, Area, Width, Height, Perimeter, Diameter, Compactness) were presented through PCA (**Figure 4.7**). In *C. muelleri*, PC1 + PC2 explained 91.96% of the total variation contained in the data matrix with PC1 accounting for 66.57% and PC2 for 25.38%. Cells acclimated to different light intensities were differentiated according to PC1, indicating a change in width and perimeter. In *C. weissflogii,* PCA explained 88.99% of the total variation (65.04% + 23.94%, PC1 + PC2) and highlighted a slight change in height according to PC1 in cells acclimated to different light intensities.

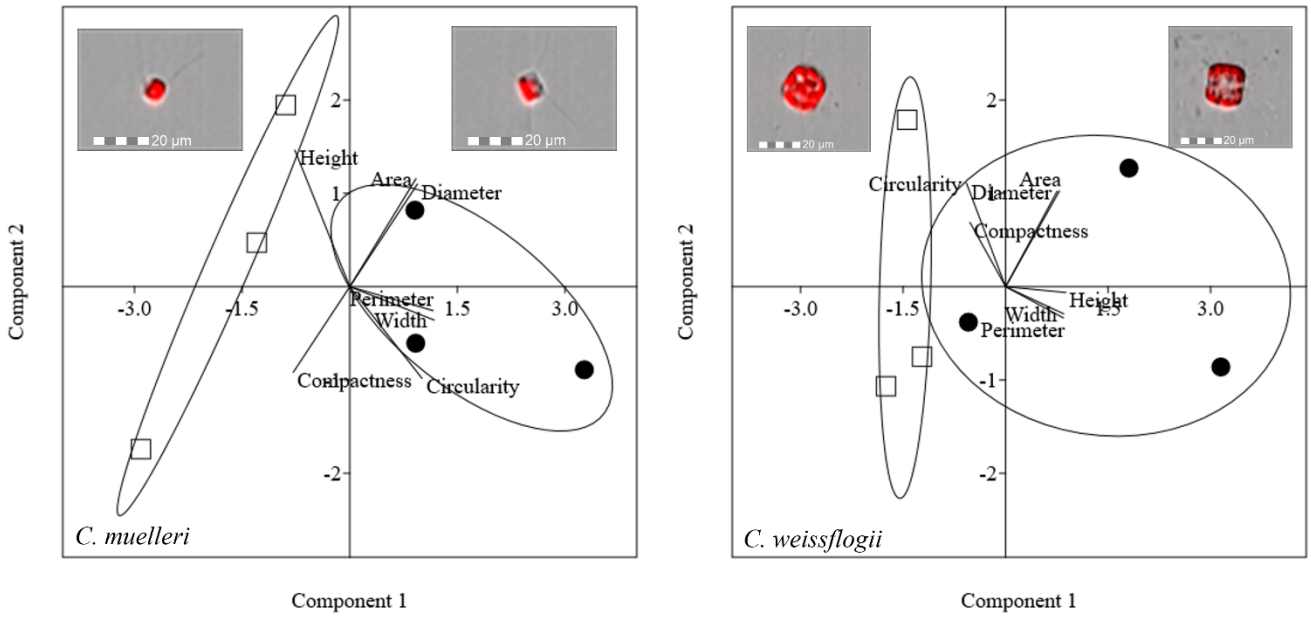

Figure 4.7: PCA analysis on morphological characteristics of centric diatoms (*C. muelleri* and *C. weissflogii*). Different symbols indicate different growth lights: □ 60 µmol photons·m^{-2}·s^{-1} ● 180 µmol photons·m^{-2}·s^{-1}. Images representing cells acclimated to different light intensities were obtained by FlowSight® (Amnis Corp., Seattle, WA), merging the bright field, collected in channel 1, and red chloroplast autofluorescence in channel 5 (Details in the section Morphological characterization by IFC analysis of material and methods).

Frustules of centric diatoms were also characterized by Scanning Electron Microscopy. No significant changes were observed in frustules acclimated to different light intensities (**Figure 4.8**).

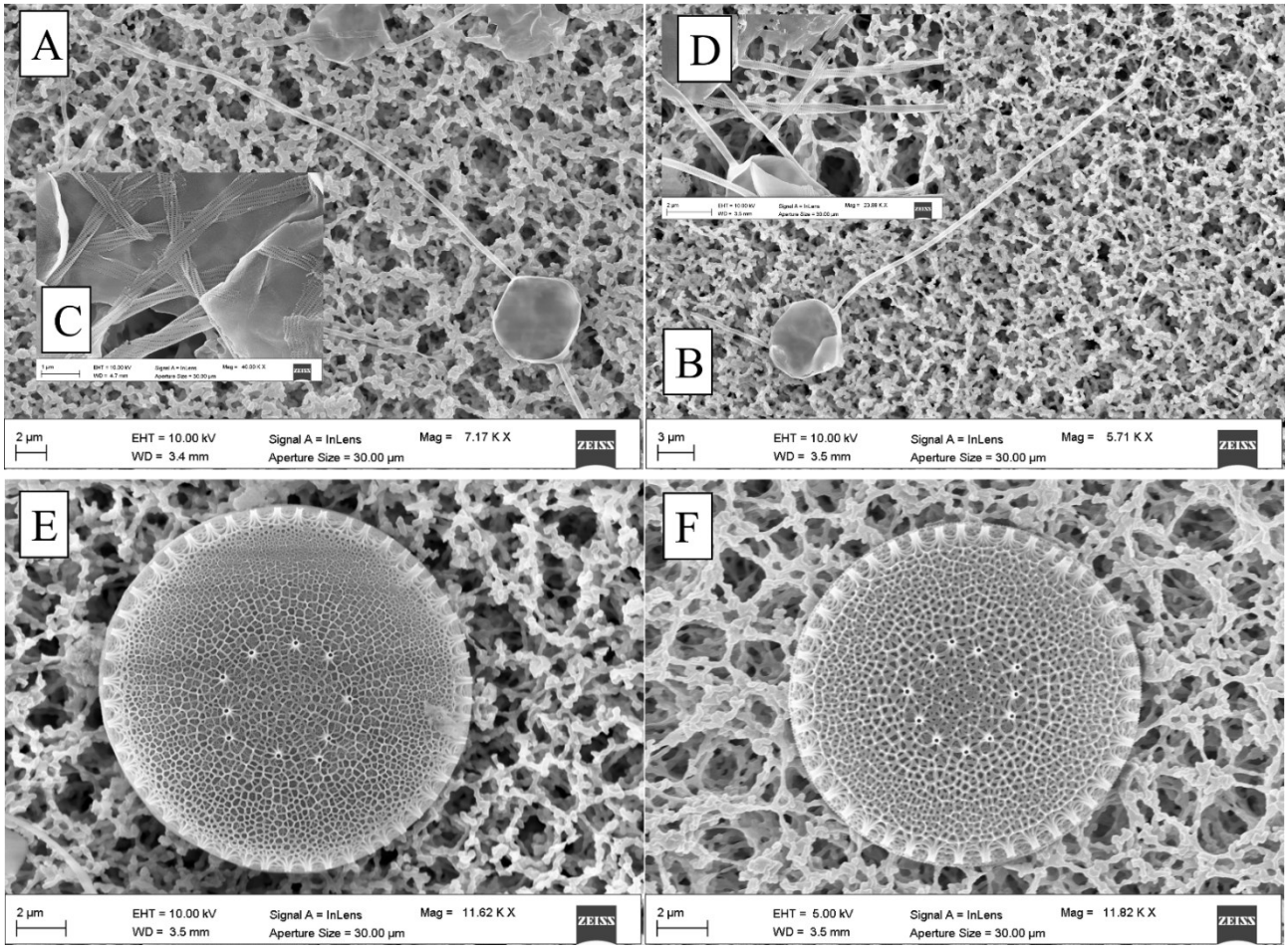

G	60 µmol photons·m^{-2}·s^{-1}	180 µmol photons·m^{-2}·s^{-1}
Lenght of setae (µm)	38.10 ± 11.02	36.17 ± 7.10
Dimension of puntae (nm)	47.07 ± 7.08	46.70 ± 6.91

Figure 4.8: SEM images of centric diatoms (*C. muelleri* **A**, **B**; *C. weissflogii* **E**, **F**) frustules acclimated to 60 µmol photons·m^{-2}·s^{-1} (left images) and 180 µmol photons·m^{-2}·s^{-1} (right images) conditions. Details of *C. muelleri* setae at 60 µmol photons·m^{-2}·s^{-1} (**C**) and 180 µmol photons·m^{-2}·s^{-1} (**D**) are shown and mean values ± SD (n>10) are presented in the Table **G**.

Morphological characterization of pennate diatoms through PCA (Elongatedness, Area, Width, Height, Perimeter, Length, Compactness) is pictured in **Figure 4.9**. In *P. tricornutum* 95.43% of the total variance was explained by PC1 + PC2; the weight of PC1 was 64.72% while PC2 30.71%. PCA did not show a net division between cells acclimated to different lights. In *C. fusiformis* PCA explained 92.17% of the total variance, being PC1 74.65% and PC2 17.52%. Cells acclimated to

different light intensities were separeted according to both PC1 and PC2, indicating a change in width and area.

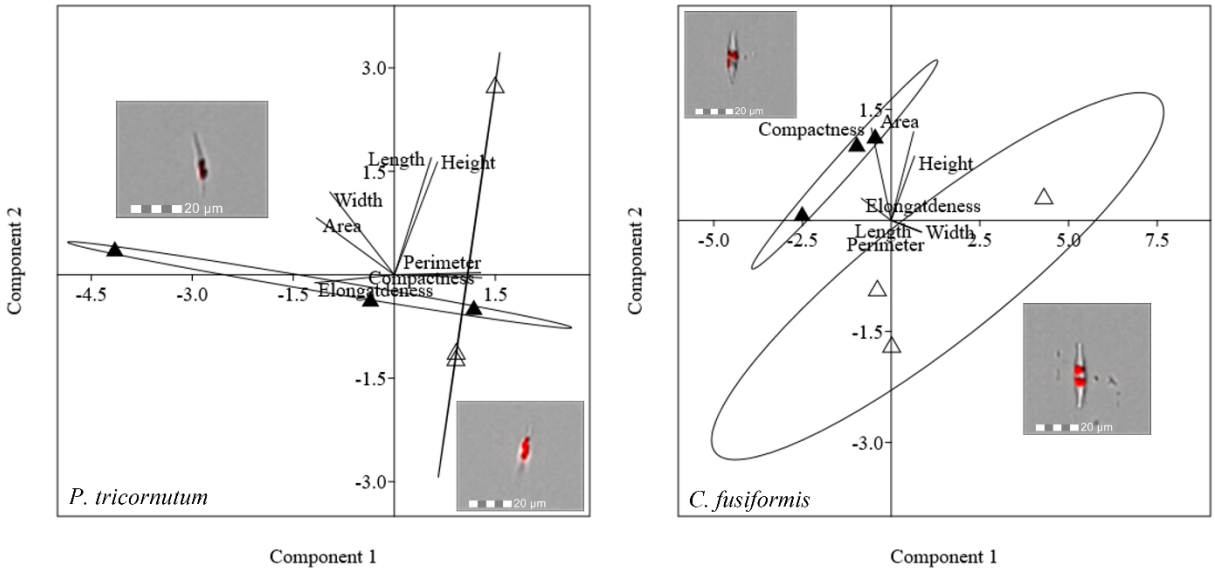

Figure 4.9: PCA analysis on morphological characteristics of pennate diatoms (*P. tricornutum* and *C. fusiformis*). Different symbols indicate different growing light: Δ 60 µmol photons·m^{-2}·s^{-1} ▲ 180 µmol photons·m^{-2}·s^{-1}. Images representing cells acclimated to different light intensities were obtained by FlowSight® (Amnis Corp., Seattle, WA), merging the bright field, collected in channel 1, and red chloroplast autofluorescence in channel 5 (Details in the section Morphological characterization by IFC analysis of material and methods).

Cellular volume and dry weight of the four diatoms indicated that no significant changes were observed in response to different light intensities (**Table 4.2**).

Table 4.2: Mean ± SD of Cell volume (μm^3) and Dry weight (pg) in the four diatoms acclimated to different light intensities (n ≥ 3). Asterisks indicate significant difference between conditions in the same species ($p > 0.05$)

		60 µmol photons·m^{-2}·s^{-1}	180 µmol photons·m^{-2}·s^{-1}
Cell volume (μm^3)	*C. muelleri*	262 ± 11	244 ± 23
	C. weissflogii	2418 ± 290	2384 ± 158
	P. tricornutum	60.67 ± 5.87	72.33 ± 10.97
	C. fusiformis	464 ± 26	428 ± 43
Dry weight (pg)	*C. muelleri*	8.77 ± 0.88	10.63 ± 1.64
	C. weissflogii	281 ± 15	269 ± 21
	*P. tricornutum**	5.49 ± 0.92	1.14 ± 1.08
	C. fusiformis	98 ± 7	118 ± 49

4.3.6 C and N

The analysis of the elemental composition in the four diatoms acclimated to different light intensities (**Table 4.3**) revealed that no significant changes were observed in terms of %C and %N, while *C. weissflogii* highlighted a decreased C/N ratio when grown at lower light intensity. Despite no changes in % of the two elements were recorded, significant differences were observed in N and C Stable Isotopic fractionation (**Figure 4.10**); centric diatoms showed an increased $\delta^{13}C$ and $\delta^{15}N$ when acclimated to higher light intensity and in *C. muelleri* this difference is greater. Nevertheless, in pennate diatoms this increase was observed only in $\delta^{15}N$ of *C. fusiformis*.

Table 4.3: Elemental composition (% of C and N on dry weight, and C/N) of the four diatoms acclimated to different light intensities. Data are means of 3 biological replicas ± SD. Asterisks represent significant differences between conditions in the same species (p<0.05).

		60 µmol photons·m^{-2}·s^{-1}	180 µmol photons·m^{-2}·s^{-1}
% Carbon	*C. muelleri*	37.55 ± 0.84	36.46 ± 2.47
	C. weissflogii	46.47 ± 1.11	42.98 ± 3.72
	P. tricornutum	54.27 ± 1.76	54.88 ± 0.57
	C. fusiformis	51.88 ± 2.06	52.58 ± 1.94
% Nitrogen	*C. muelleri*	5.05 ± 0.61	5.84 ± 0.41
	C. weissflogii	6.39 ± 0.49	6.80 ± 0.30
	P. tricornutum	6.94 ± 0.22	6.85 ± 0.09
	C. fusiformis	7.47 ± 0.23	7.21 ± 0.39
C/N	*C. muelleri*	6.44 ± 0.33	7.26 ± 0.64
	*C. weissflogii**	6.32 ± 0.30	7.29 ± 0.37
	P. tricornutum	7.82 ± 0.14	8.01 ± 0.12
	C. fusiformis	6.94 ± 0.18	7.29 ± 0.24

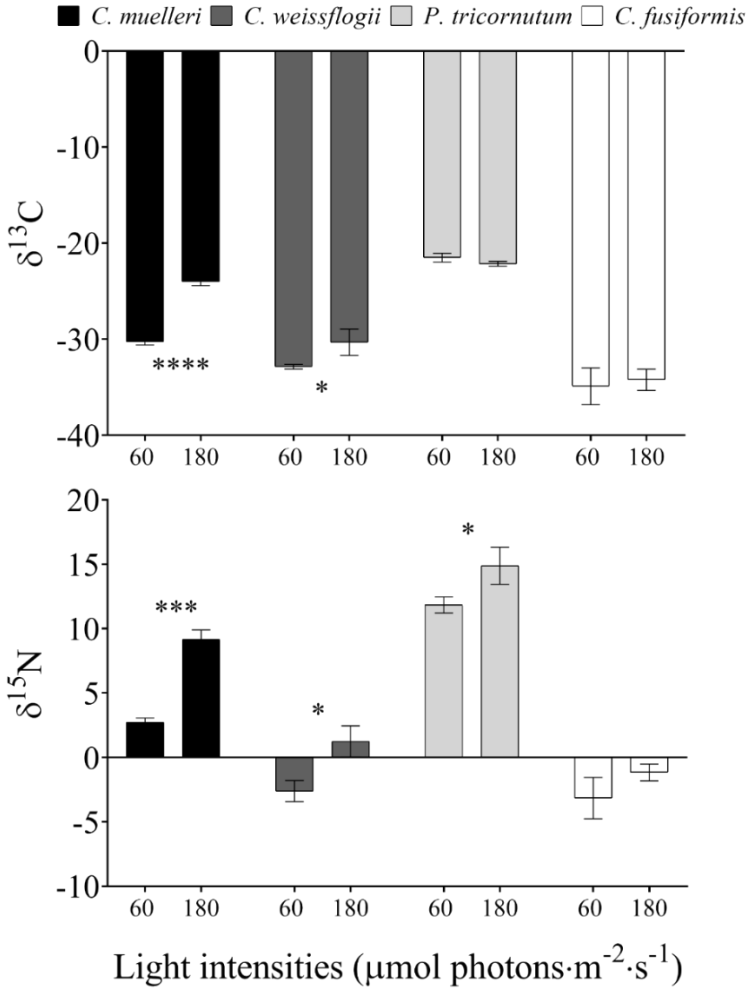

Figure 4.10: $\delta^{13}C$ and $\delta^{15}N$ values in the four diatoms acclimated to different light intensities. Data are means of 3 biological replicas. Error bars show SD. Asterisks represent significant differences between conditions in the same species (* $p<0.05$, *** $p<0.0001$, **** $p<0.00001$)

4.4 Discussion

Considering the tremendous biodiversity of diatoms and their key role in aquatic environments, considering silica shell is able to modify diatom density, a question arose whether the adaptative role of frustule on buoyancy is dependent on diatom morphology and silicification. Buoyancy and buoyancy control are indeed crucial to vertical movements not only allowing a rapid escape from predators, but also providing a way to retrieval essential resources such as light and nutrients (Raven and Waite 2004, Gemmel et al., 2016, Raven and Levoie, 2020, Du Clos et al., 2021, Petrucciani et al., 2022).

Morphology and Silicification affecting sinking capacity

According to results, silicification was the major driver affecting buoyancy as compared to size, shape and weight: indeed, frustule density expressed as silicification per volume was inversely related to the capacity of sinking out in the water column expressed as sedimentation rate (**Figure 4.11**). *C. fusiformis* was the most silicified species per unit volume (**Figure 4.3**) among the experimental ones, and it was the fastest to sink out even though not the biggest or the heaviest. Moreover, this species is known to secrete extracellular polymeric substances (EPS) to assist in surface attachment, providing adhesion and aggregation among cells (Tong and Derek 2021). Lavoie and co-authors also highlight that enhanced polysaccharide synthesis results in increased density favouring rapid sinking rate as observed here (Lavoie et al., 2016).

Conversely from what proposed by Durante and co-authors in 2019, no shape dependent pattern was observed in sedimentation rate. Pennate cells showed different sinking capacity even if similar in shape. On the other hand, morphologically different centric diatoms (i.e. presence/absence of setae, hierarchical porous ultrastructure) showed a similar sedimentation rate. Data confirmed that there is no obligate correlation between cell morphology and sinking rate for metabolically active cells (Waite et al., 1997, Gemmel et al., 2016).

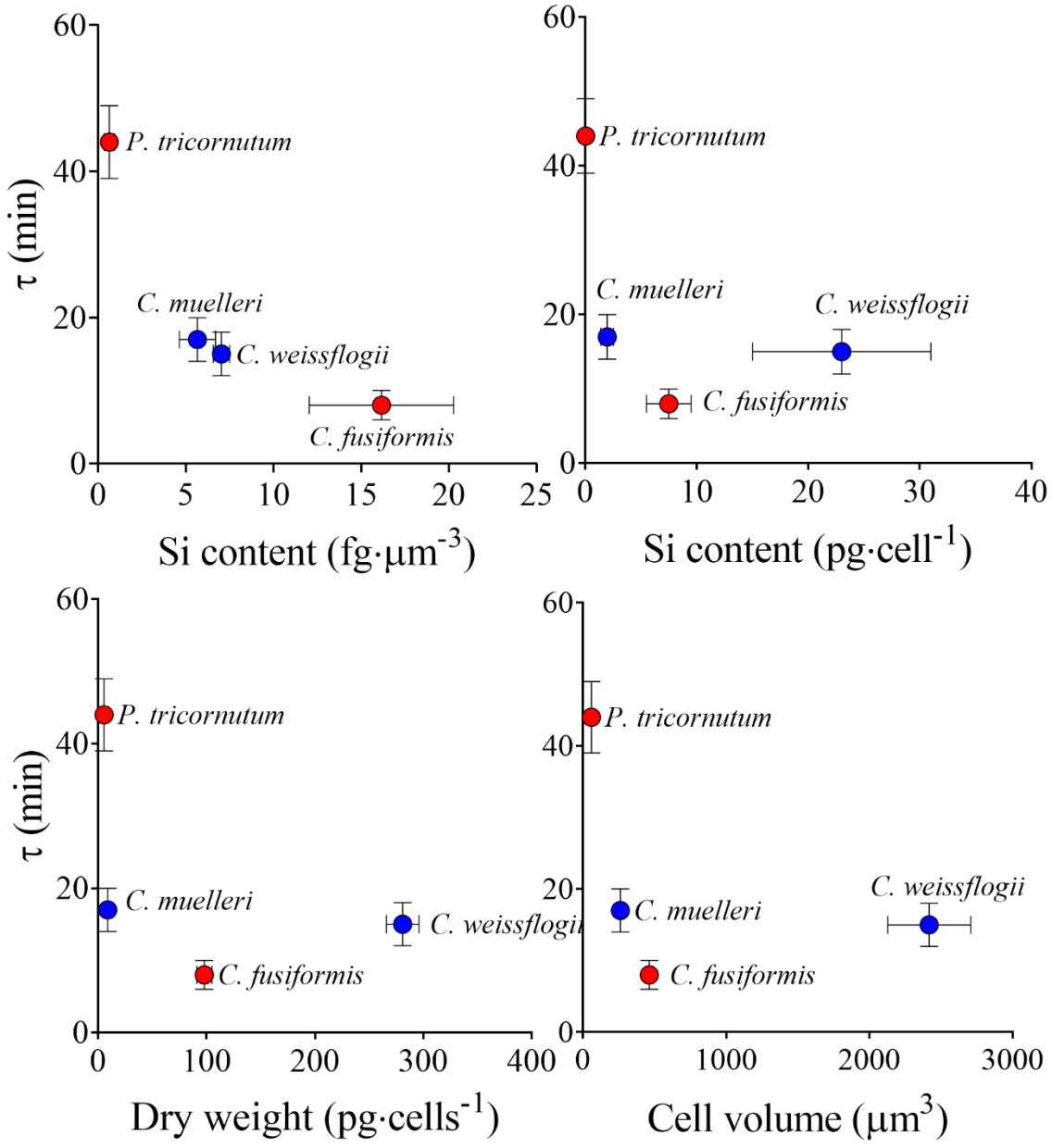

Figure 4.11: Sedimentation rates of the four diatoms related to their shape, size and silicification.

Direct observation of sinking capacity in diatoms was carried out for the first time through DLS analysis, allowing a continuous record of cells disappearance from the top section without perturbing the water column. Given the importance to direct assess sinking capacity in phytoplankton, numerous efforts were made to figure out a suitable method (Holland and Walsby

2005 and reference therein, Gemmel et al., 2016, Bannonn and Campbell 2017, Hamano et al., 2021); this study confirms the feasibility of using DLS physical technique to achieve this purpose.

Light and Si deposition

Light is an abiotic factor known to affect silicification (Su et al., 2018, Xu et al., 2021, Ryderheim et al., 2022). In this study a variation in light intensity not always led to a change in Si content (**Figure 4.3)** as opposed to previous literature. Data suggested that there is a species – specific relation between light intensity and Si deposition. Furthermore, even different strains could show a different response to light in terms of silicification: in fact, Xu and co-authors (2021) as well as Ryderheim and co-authors (2022) reported a higher Si content in cells of *C. weissflogii* grown at the lower light of 15 μmol photons·$m^{-2}s^{-1}$ which was not confirmed by this study where the strain DCG 0320 showed a homeostatic behaviour (**Figure 4.3**). Moreover, a lower growth limiting light did not always correspond to a higher frustule thickness (expressed as Si content per volume) since *P. tricornutum* showed less Si content per volume when grown at 15 μmol photons·$m^{-2}s^{-1}$ (**Figure 4.3**).

Better understanding the silicification process will help to predict the effect of external factors on frustule dynamics, thus facilitating frustule manipulation in a view of biotechnological applications (Sardo et al., 2021).

Light dependent buoyancy control

Light was chosen as a tool to investigate diatom strategy in controlling buoyancy by manipulating Si content in the experimental diatoms (**Figure 4.3**).

For each species the different sinking rates were not consistent with a change in silicification due to light exposure, suggesting that buoyancy control was not regulated by the frustule density at a cellular level (**Figure 4.3** and **4.4**). In *C. muelleri* a lower sinking rate was observed despite a higher

frustule thickness. Indeed, a significant increase of the sedimentation rate (slower sinking) was observed any time diatoms were acclimated to a higher light intensity independently from their Si content (**Figure 4.4**). Among the factors regulating cell density light availability could either increase or decrease diatom sinking rate (Bienfang 1981, Bienfang et al., 1983, Gemmel et al., 2016). In this study, the two light conditions applied in the sinking experiments (60 and 180 μmol photons·$m^{-2}s^{-1}$) were not limiting growth (**Figure 4.2, Table 4.1**): in fact, growth was limited at 15 μmol photons $m^{-2}s^{-1}$. In addition, the highest experimental light was not photo – damaging diatoms since growth rate and photosynthetic efficiency of cells acclimated to 180 μmol·photons $m^{-2}s^{-1}$ were similar to those of cells acclimated to 60 μmol·photons $m^{-2}s^{-1}$ (Conn et al., 2004, **Figure 4.5** and **4.6**). Therefore, sinking as a way to escape from excess irradiance which damages the photosynthetic apparatus as a first target (Raven and Waite, 2004), was not adopted by diatoms in this experimental set up.

A higher light availability enhancing diatom floating (**Figure 4.4**) means a higher energy availability to cells which can be converted into metabolic energy and activate energy dependent mechanisms (Waite et al., 1997, Raven and Lavoie, 2020, Du Clos et al., 2021).

Cell growth, C and N quotas, cellular volume of all the species were not affected by the light variation (**Table 4.3**). Overall, it was not recorded a drastic morphological change that could explain a change in sedimentation rate (**Figure 4.7** and **4.9**). Also, frustules did not show significant changes in ultrastructure (**Figure 4.8**). None of these parameters would thus help in elucidating which mechanisms could be involved in buoyancy control except for isotopic fractionation in centric diatoms. In fact, $\delta^{13}C$ (and $\delta^{15}N$) values were affected by light in centric diatoms which showed a higher difference in τ values in response to light intensities (**Figure 4.10**). A change in C fractionation could be due to a shift in inorganic C source (Vuorio et al., 2006); in particular higher light intensity led to decreased fractionation and therefore an increased use of HCO_3^- during

photosynthesis, suggesting the possible activation of energy dependent mechanisms such as CO_2 concentrating mechanisms when more energy was available (Riebesell et al., 2000). The presence of an active CCM enhances photosynthesis and reduces photorespiration in algae (Giordano et al., 2005), thus providing more metabolic energy to reduce sinking rate (Waite et al., 1992).

What energy dependent mechanisms are active in pennate diatoms to control buoyancy were not evident from the data set, but both in pennate and centric diatoms they were possibly including modulation of vacuolar solution density and the fraction of cell volume occupied by the vacuole (Lavoie and Raven 2020 and references therein). The density of the frustules in diatoms is indeed countered by the presence of vacuoles, whose density is supposed to be rapidly modulated in three ways: (i) high-frequency modulation of Na^+ and K^+ permeability by selective ion transport, as occurs in action potentials with transmembrane ion exchange; (ii) metabolism interconverting low-density organic cations and higher density cations; and (iii) fast cyclical changes in the cell expansion rate (i.e. active water transport, cytoskeletal motors). The last one is the most energetically convenient (Lavoie and Raven, 2020), as confirmed by our data which did not record a change in K^+ cell content between cells acclimated to low and high intensities (**Table 4.4**).

Table 4.4: K content ($pg \cdot cell^{-1}$) in the four diatoms acclimated to different light intensities. Data are means of 3 biological replicas ± SD.

	60 µmol photons·m^{-2}·s^{-1}	180 µmol photons·m^{-2}·s^{-1}
C. muelleri	0.12 ± 0.02	0.21 ± 0.11
C. weissflogii	0.14 ± 0.04	0.17 ± 0.04
P. tricornutum	0.002 ± 0.00001	0.002 ± 0.001
C. fusiformis	0.03 ± 0.01	0.03 ± 0.006

Chapter five: Frustule potential exploitation of a Silica bearing biomaterial

In collaboration with Mr D. Linsalata, Prof. A. Dibenedetto, Prof. M. Aresta, Dr. A. Amato

5. Frustule: potential exploitation of a Silica bearing biomaterial

5.1 Frustule structural characterization of morphologically different diatoms

5.1.1 Introduction

The most fascinating morphological characteristic of diatoms is their outer silica shell called frustule. Frustule is a highly intricate ornamented and porous scaffold which can show greatly different micro and nanoscale structures (i.e. holes, setae, elevations) and presents different shapes and sizes grounding to the overall extraordinary diatom diversity.

In nature frustules have been selected to provide different adaptative functions: (i) frustules are strong armour against predators (Hamm et al., 2003), (ii) they enhance the acquisition of growth-limiting resources (i.e. light, nutrients and CO_2, Finkel and Kotrc 2010), (iii) they can control buoyancy by changing cell density (Raven and Waite, 2004), (iv) they can act as proton buffer (Milligan and Morel 2002), (v) they can modulate light within the cells, both screening out UV radiation (Aguirre et al., 2018, Ellegaard et al., 2018, De Tommasi et al., 2018) and focusing incident light inside the cell (De Stefano et al., 2007, Toster et al., 2013, Romann et al., 2015).

Moreover, human society has been more and more demanding new materials for micro-scale technological purposes and pushing more studies on diatom frustules which are cheap promising ultrastructures suitable for multiple applications (i.e. biomedical, chemical, physical) (Sardo et al., 2021). These materials can indeed exhibit different physicochemical properties than their analogues on a normal scale, for example greater chemical reactivity due to a larger surface area.

Therefore, a structural, chemical and mechanical characterization of frustules shall allow not only a better comprehension of the relationship between diatom morphology and its selective radiation but also unravel new bio-based scaffolds (De Tommasi et al., 2017). Among frustule properties surface

area and presence of basic sites are crucial for subsequent functionalization (De Tommasi et al., 2017, Terracciano et al., 2018, Rogato and De Tommasi, 2020, Sardo et al., 2021).

The characterization of structurally different centric frustules was carried out; in particular, *Chaetoceros muelleri*, with four long and porous silica spines called setae, and *Conticribra weissflogii*, with hierarchical layers of porous membranes. The acclimation of cells to different light intensity was used as a tool to manipulate chemical and structural characteristics of frustules.

5.1.2 Material and Methods

5.1.2.1 Algal growth and frustule preparation

Two centric diatoms, *Chaetoceros muelleri* (CCAP 1010/3, https://www.ccap.ac.uk/) and *Conticribra weissflogii* (DCG 0320, https://bccm.belspo.be/about-us/bccm-dcg), were acclimated for at least four generation to two different light intensities (60 and 180 µmol photons·$m^{-2}s^{-1}$). Cultures were established in 250 mL flasks filled with 100 mL of AMCONA medium (Fanesi et al., 2014) and maintained in a culture chamber at 18 °C, illuminated with cool white fluorescent lamps at 12:12 h light-dark cycles.

For BET analysis 3L flasks filled with 2L of AMCONA medium were established. Frustules were achieved after chemical removal of the organic matter (modified from Friedrichs et al., 2012) from cells collected during exponential phase. Cells were washed in deionized water 3 times (centrifuge set at 3000 rpm for 10 minutes), then the pellet was resuspended in 1.5 mL deionized water, charged with 1.5 mL of a saturated solution of $KMnO_4$ and left at ambient temperature for 24 h. Subsequently, 3mL of HCl (37%) was added and heated in boiling water until the solution became colourless (1 hour approximately). Finally, cleaned frustules were washed 4 times with deionized water and stored at 4°C until further processing.

5.1.2.2 Elemental composition of frustules

The abundance of elements, included Si, was measured using a Total Reflectance X – ray Fluorescence spectrometer (S2 Picofox, Bruker AXS Microanalysis GmbH, Berlin, Germany) and expressed as pg per frustule calculated on the base of the corresponding number of cells. Frustules obtained as described before were resuspended in 250 µl of dH_2O. A solution of 0.1 g L^{-1} Ga (Sigma Aldrich, St. Luis, MO, USA) in 5% HNO_3 was added as internal standard to a final concentration of 0.5 µL L^{-1}. The suspension was carefully vortexed and an aliquot of 10 µl was deposed on a plastic sample holder, dried on a heating plate and measured for 1000 seconds.

Spectral deconvolution and quantification of elemental abundances were performed by the SPECTRA 6.1 software (Bruker AXS Microanalysis GmbH, Berlin, Germany).

5.1.2.3 Inorganic stoichiometry of frustules

Frustules obtained as described before were used to prepare samples for FTIR analysis. A volume of 50 µl of frustules suspension was transferred to a silicon window and dried in oven at 80°C overnight (Domenighini and Giordano 2009). FTIR spectra were acquired with a Tensor 27 FTIR spectrometer (Bruker Optics, Ettlingen, Germany). Bands were attributed to silicon species as described by Artega - Larios and co-authors (2014) and the ratio of SiO/SiOH was calculated through band integrals at 800 and 950 cm^{-1} respectively, with OPUS 6.5 software (Bruker Optik GmbH, Ettlingen, Germany).

5.1.2.4 UV absorption

Frustules obtained as described before were used for spectrophotometric assessment of UV absorption. The absorbance of the suspension of frustules in dH_2O was evaluated with a spectrophotometer in a range from 200 nm to 400 nm (scan speed 0.5nm). dH_2O absorbance was used as blank and was subtracted to all measurements. Data were normalized on the frustule number within each species and not among species ($5 \cdot 10^5$ cell ml^{-1} were used in *C. weissflogii* samples and $3 \cdot 10^6$ cell ml^{-1} in *C. muelleri* samples).

5.1.2.5 Proton buffer capacity of frustules

According to Milligan and Morel, 2002, exponentially growing cells of *C. muelleri* and *C. weissflogii* acclimated to 60 and 180 µmol photons$\cdot m^{-2} \cdot s^{-1}$ were put in 8 ml of buffer-free AMCONA growth medium (Fanesi et al., 2014). A final Si concentration of 3 mM in each sample

was used for the measurements and cell number varied accordingly to the Si cell content. Titration curves were obtained adding 0.1M NaOH to the cell suspension starting from a pH of 7 and reaching a pH of 9. The same was done using cleaned frustules instead of cells in the same conditions; cleaning procedure was described in 5.1.2.1.

5.1.2.6 Frustule surface characterization

A quantity of 30 mg of cleaned and dried frustules derived from *C. muelleri* cells (as described above) was used to characterize silica surface. All the analysis were performed using a Micromeritics ChemiSorb 2750. Surface area was determined using a single point Brunauer, Emmett and Teller (BET) method with a 30 % N_2/70 % He gas mixture. CO_2 chemisorption tests were carried out using Rivoira 99,9999 % CO_2 and a loop with nominal volume equal to 0,1 µL (calibrated). The flow was set to 20 mL/min during the chemisorption process and increased up to 25 mL/min for TPD analysis. TPD profiles were recorded using a 15°C/min ramp. All the samples were dried in oven at 80 °C for 24 hours before the analysis. Both BET and chemisorption analysis required pre-treatment of the sample at temperatures up to 500°C. In order to prevent irreversible modification of the frustules structure samples were analysed with pre-treatment at 2 different temperatures, 350 and 500°C. By increasing the temperature organic matter was removed from the frustules and a carbonization process was observed in absence of oxygen (He flow). Samples turned brownish at 350°C and black at 500°C.

5.1.2.7 Statistical analysis

Data were expressed as mean ± SD. Significant differences among the means were tested with a one – way analysis of variance (ANOVA), followed by Tukey's *post-hoc* test. When there were more than one variable, Two-way ANOVA followed by Tukey's *post-hoc* test was performed. Comparison of treatment pairs was achieved with a two-tailed *t*-test. The level of significance was

set at 0.05. GraphPad prism 8.0.2.263 was used to carry out the tests (GraphPad Software, San Diego, CA, USA).

5.1.3 Results

5.1.3.1 Elemental composition of frustules

Larger cells of *C. weissflogii* showed higher content of Si in frustules as compared to *C. muelleri* (**Figure 5.1**); on the other hand, less silicified frustules of *C. muelleri* significantly increased their Si content in response to a higher energy availability (180 µmol photons $m^{-2} \cdot s^{-1}$), while *C. weissflogii* did not modulate Si content when acclimated to different light intensities. According to **Table 5.1**, no significant change in elemental quotas was observed in response to different light intensities in both the analysed species; interestingly, the content of Zn, Br and Sr was the same in both the species despite their difference in size.

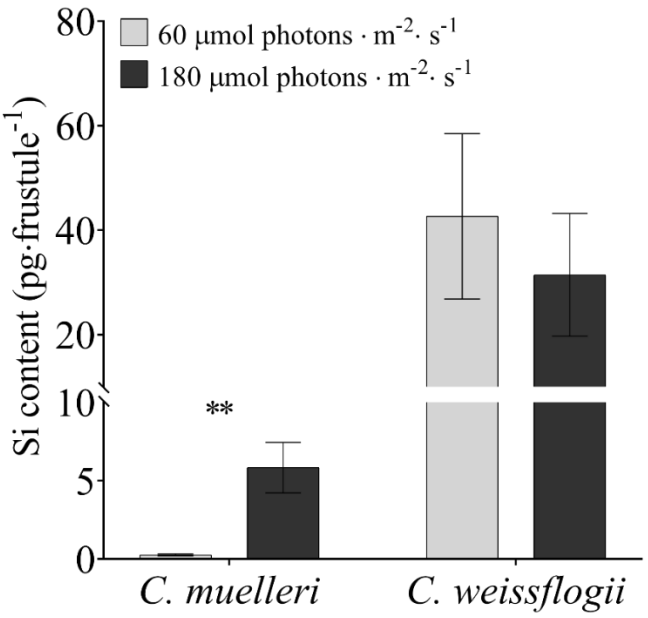

Figure 5.1: Si content per cleaned frustule ($pg \cdot frustule^{-1}$) in the two diatoms acclimated to different light intensities. Data are means of 3 biological replicas. Error bars show SD. Asterisks represent significant differences between conditions in the same species (* p<0.05, ** p<0.001, **** p<0.00001)

Table 5.1: Quotas of elements per cleaned frustule (pg·frustule^{-1}) in the two diatoms acclimated to different light intensities. Data are means of 3 biological replicas. Error bars show SD. Asterisks represent significant differences between conditions in the same species (* p<0.05, ** p<0.001, **** p<0.00001)

		60 µmol photons·m^{-2}·s^{-1}	180 µmol photons·m^{-2}·s^{-1}
Sulfur	*C. muelleri*	0.07 ± 0.05	0.09 ± 0.03
	C. weissflogii	0.93 ± 0.82	1.70 ± 0.80
Zinc	*C. muelleri*	0.001 ± 0.0009	0.002 ± 0.001
	C. weissflogii	0.007 ± 0.0007	0.006 ± 0.001
Bromine	*C. muelleri*	0.002 ± 0.0009	0.003 ± 0.0007
	C. weissflogii	0.04 ± 0.009	0.04 ± 0.008
Strontium	*C. muelleri*	0.0005 ± 0.0004	0.0004 ± 0.0001
	C. weissflogii	0.009 ± 0.004	0.01 ± 0.005

5.1.3.2 Inorganic stoichiometry of frustules

All FTIR spectra (**Figure 5.2** and **5.3**) showed the characteristic Si species stretching mode band (i) Si – O – Si at 1095 cm^{-1} (ii) Si – O at 460 – 470 and 789 – 802 cm^{-1} (iii) Si – OH (silanol group) at 950 cm^{-1}. Considering *C. muelleri* frustules (**Figure 5.2** and **Figure 5.4**), different light intensities influence the Si receptor sites available for trapping O_2 at the surface, i.e. Si atoms ready to react with adsorbing O atoms or OH radicals; indeed significant change were observed in SiO/SiOH ratio when cells were acclimated at lower light intensity (**Figure 5.3**). On the other hand, *C. weissflogii* frustules did not show any significant changes SiO/SiOH (**Figure 5.3** and **Figure 5.4)**.

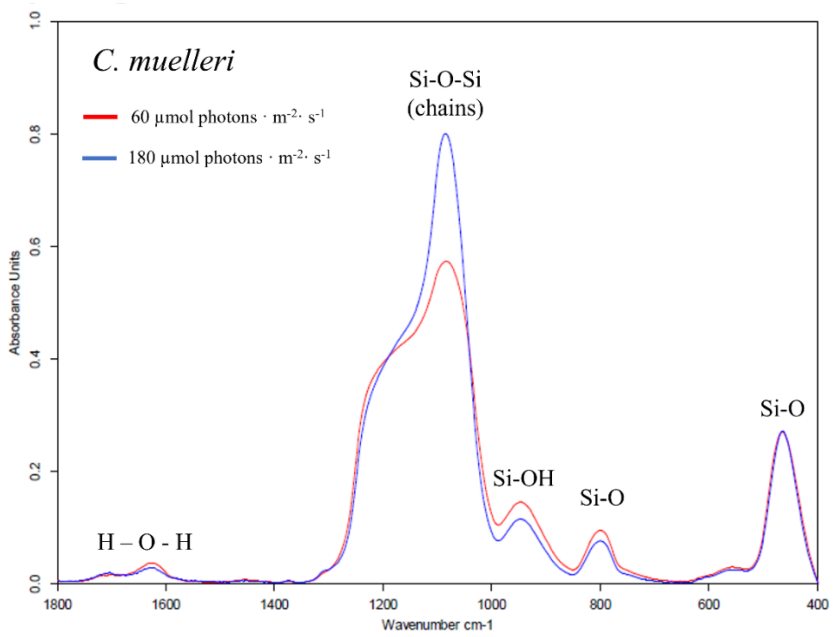

Figure 5.2: FT IR spectra (400 – 1800 nm) of *C. muelleri* frustules derived from cells acclimated to different light intensities. Spectra are average of three distinct biological replicas.

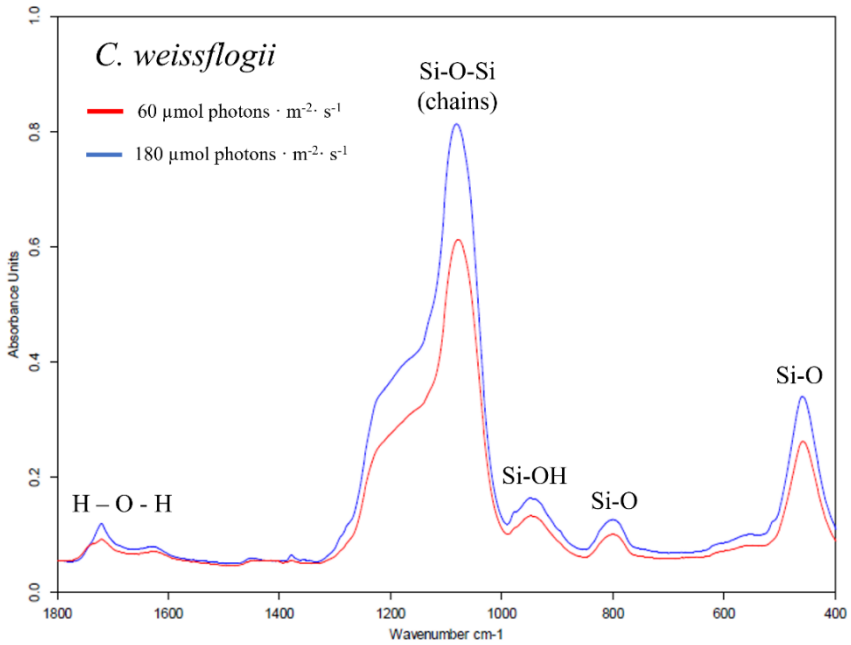

Figure 5.3: FT IR spectra (400 – 1800 nm) of *C. weissflogii* frustules derived from cells acclimated to different light intensities. Spectra are average of three distinct biological replicas.

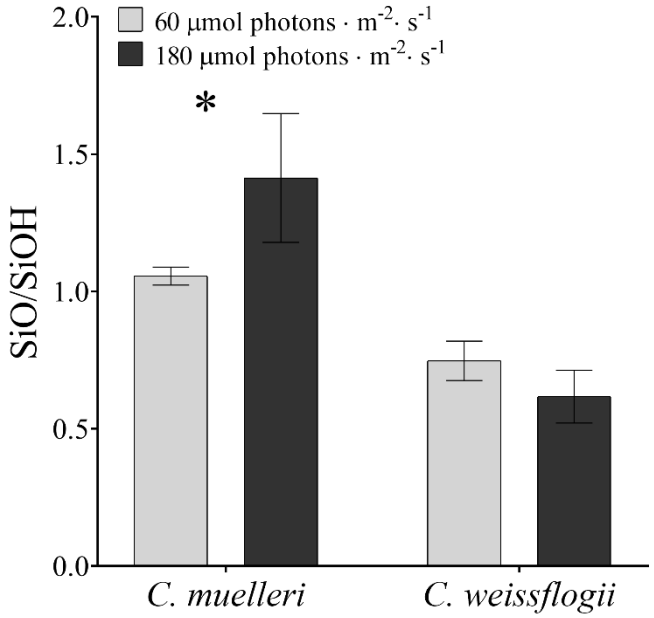

Figure 5.4: Comparison between *C.muelleri* and *C. weissflogii* SiO/SiOH ratio in frustules derived from cells acclimated to different light intensities. Data are means of three biological replicas ± SD. Letters indicate significant difference between the two species.

5.1.3.3 UV absorption

The relation between frustules and UV radiation is pictured in **Figure 5.5**. In general, frustules derived from cells acclimated to lower light intensities showed a higher capacity to absorb UV radiation at 275 nm (**Figure 5.5**).

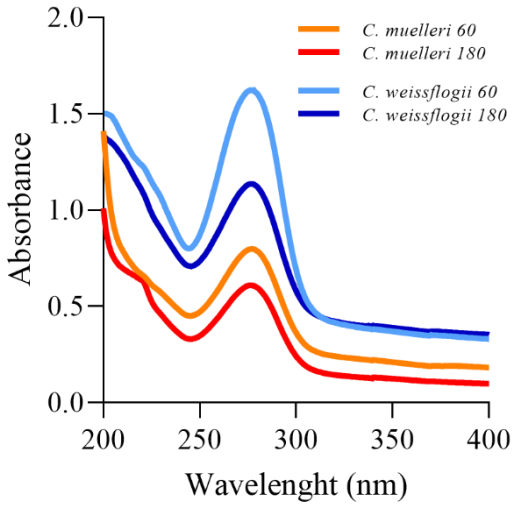

Figure 5.5: Comparison between *C. muelleri* and *C. weissflogii* absorbance in frustules derived from cells acclimated to different light intensities. Data are means of three biological replicas.

5.1.3.4 Assessment of frustules proton buffer capacity

Titration curves on whole cells and cleaned frustules were carried out and presented in **Figure 5.6**; sample were normalized on the Si content. Results showed that buffer capacity of frustules reflected buffer capacity of whole cells: indeed, the highest buffer capacity was observed in frustules and cells of *C. muelleri* acclimated to the lower light intensity. Moreover, while *C. muelleri* modulated its buffer capacity, *C. weissflogii* did not show any change in response to light intensity (**Figure 5.6**).

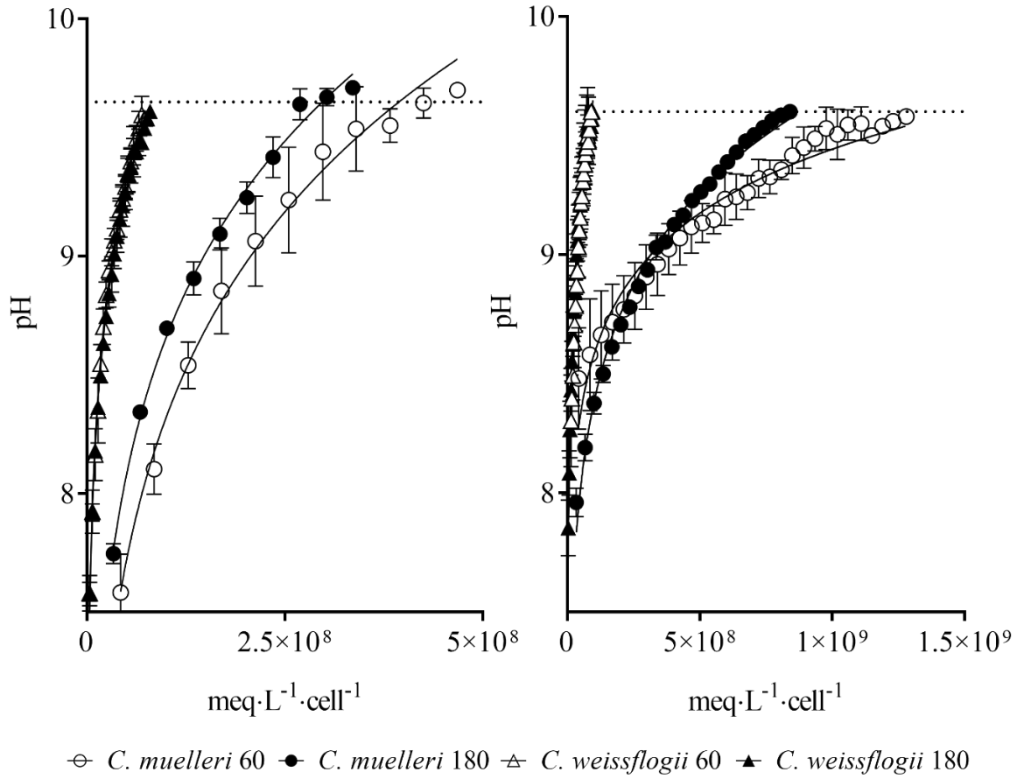

Figure 5.6: Comparison between *C.muelleri* and *C. weissflogii* proton buffer capacity in frustules derived from cells acclimated to different light intensities (left graph) and in entire cells acclimated to different light intensities (right graph) . Data are means of three biological replicas ± SD.

5.1.3.5 Surface characterization

BET analysis was carried out on frustules of *C. muelleri* cells acclimated to different light intensities (**Figure 5.7**). Calculated surface area was the same at both the light intensities (about 90 m^2g^{-1}) and was maintained also when the analysis was performed at higher temperature (500°C

instead of 350°C). On the other hand, as shown in the **Figure 5.7**, frustules lost their basic sites already after a thermal treatment at 350°C, resulting in a small CO_2 uptake flux (roughly 200 µl absorbed CO_2 g^{-1} of frustule).

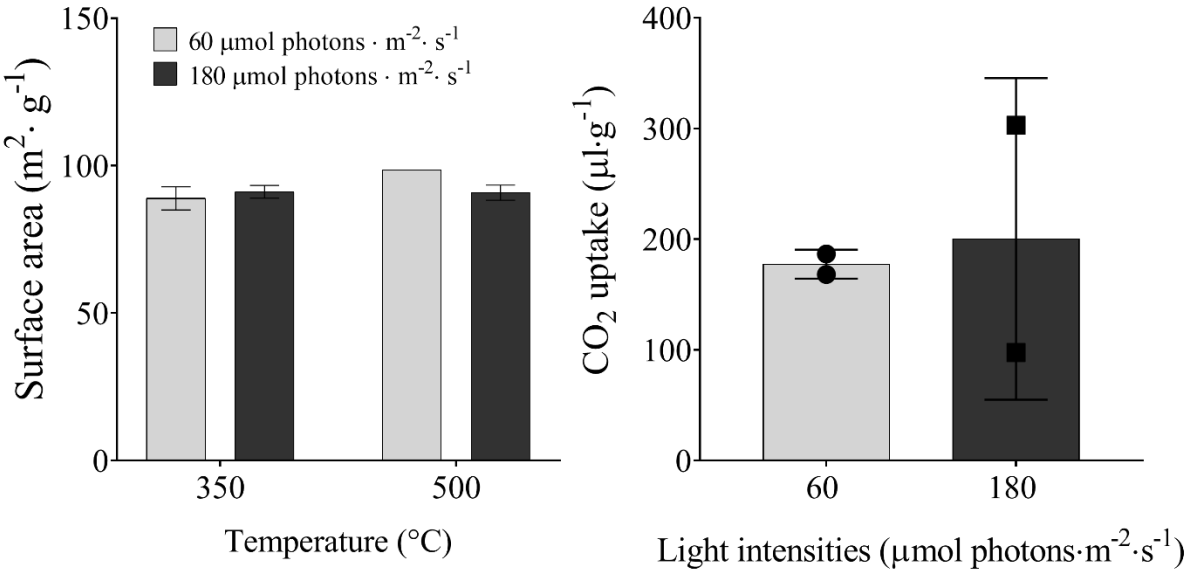

Figure 5.7: Assessment of Surface area at two different temperatures (left graph) and CO_2 uptake at 350°C (right graph) in *C. muelleri* frustules derived from cells acclimated to different light intensities and in entire cells acclimated to different light intensities. Data are means of at least two biological replicas ± SD.

5.1.4 Discussion

The role of frustules in light absorption and waveguide is poorly understood; it has been documented that structure-based optics of centric frustules allow modulation of the *in vivo* incident radiation to support photosynthesis after UV screening (Aguirre et al., 2018, Ellegaard et al., 2018, De Tommasi et al., 2018). Indeed, centric diatoms comprising mainly planktonic forms, live suspended in the water column and are characterized by a noticeable UVR tolerance even though they accumulate low concentration of UV-absorbing compounds (i. e. mycosporyne-like amino acids, carotenoids, De Tommasi et al., 2018, Aguirre et al., 2018, Ellegaard et al., 2018). Frustules are known to screen UV B damaging light, operating through different mechanisms: (1) absorption by amorphous silica, as confirmed by this data, (2) diffraction-based redistribution of transmitted intensity through the ordered pattern of micro- and nano-pores, (3) efficient conversion of UV in PAR radiation by photoluminescence (Quin et al., 2008, Goswami et al., 2011, Artega – Larios et al., 2014, De Tommasi et al., 2018). In this study, both centric species showed an increased UV B absorption when cells were acclimated to lower light intensities (**Figure 5.5**). The modulation of light thanks to the optical properties in centric frustules belonging to low light acclimated cells to support photosynthesis could be an explanation. This effect was already observed in *Coscinodiscus granii* where the photonic structure of the frustule allowed a facilitated light redistribution and efficient photosynthesis in cell regions distant from the directly illuminated area (Goessling et al., 2018).

The ability to screen UV is due to the radiation interacting with electrons of Si-O bonds and with point defects such as -OH groups, Si-Si bonds and strained Si-O-Si bonds of the hydrated, porous, amorphous silica and with the possible presence of impurities (i.e. S compounds involved in silica precipitation, biosilica synthesis and frustule formation) (De Tommasi et al., 2018). Nevertheless, frustules of *C. muelleri* here analysed did not change the amount of S accumulated (**Table 5.1**) but decreased the SiO/SiOH ratio in response to lower light intensity (**Figure 5.4**) indicating an

increased amount of O_2 adsorbed to these frustules and a higher concentration of silanol groups. This change in silanol groups resulted also in a better proton buffer capacity in *C. muelleri* frustules acclimated to lower light intensity (**Figure 5.6**), likely enhancing CCM activity (Milligan and Morel, 2002) without changing diatom surface area (**Figure 5.7**).

C. muelleri also showed a better plasticity in terms of Si deposition in response to light, allowing a decreased Si content in frustules when less energy was available (**Figure 5.1**). On the other hand, bigger frustules of *C. weissflogii* showed a more homeostatic behaviour in terms of Si content (**Figure 5.1**), SiO/SiOH ratio (**Figure 5.4**) and proton buffer capacity (**Figure 5.6**) when cells were acclimated to different light intensities.

Beside the possible evolutionary advantages associated with the plasticity of frustules in response to light observed in *C. muelleri* cells (protecting from UV radiation, enhancing CCMs), this study contributed to unveil an easy way to manipulate frustule biosilica in a view of multiple and novel applications. The common strategy to develop engineering devices with diatoms and the potential to form functionalised bio-materials is based on a chemical modification by targeting free reactive silanol (SiOH) groups, thus improving drug loading/release properties and adding other reactive groups ($-NH_2$, −COOH, −SH, and−CHO), which can be useful for the conjugation of biomolecules (e.g. enzymes, proteins, antibodies, peptides, DNA, aptamers) (Terracciano et al., 2018, Li et al., 2019). A simple change in the growth light of cells could increase the number of silanol groups, improving the potential frustule functionalization, and could increase UV absorption, useful for UV filtering production (i.e. biocompatible sun lotions for skin pro-tection under light exposure) (De Tommasi et al., 2018).

Thus, the structural, chemical, and mechanical characterization of *C. muelleri* and *C. weissflogii* frustules highlighted that the smaller *C. muelleri* cells resulted more suitable for biotechnological application in the microscale.

5.2 Potential scale up of frustule exploitation

5.2.1 Introduction

Beside the key role in ocean ecosystems, diatoms are deeply investigated for several biotechnological applications. Microalgae in general show a great potential for the cheap production of important metabolites exploited as cosmetic ingredients (Mourelle et al., 2017), food or feed supplements (Dineshbabu et al., 2019, Lamminen et al., 2019, Pudney et al., 2019, Cui et al., 2020, Amorim et al., 2021), fertilizers (Li et al., 2018), accumulators for the bioremediation of aquatic environments (Hedayatkhah et al., 2018, Mojiri et al., 2020) and biofuels production (Hildebrand et al., 2012, D'Ippolito et al., 2015). The characteristic that gives diatoms a further quality is their natural reservoir of biosilica, with high surface area that can be exploited as biomaterial for different purposes: (i) biomedical applications, (ii) metal removal from aquatic environments, (iii) catalyst support or (iv) optical devices and other kinds of applications (Terracciano et al., 2018, Sardo et al., 2021). Biosilica obtained from diatoms can be considered a cheaper and more attractive alternative as compared to synthetic materials, because of the reduced requirements for high temperatures and aggressive chemicals to gain a small, hard, elastic, with high degree of complexity material (Maher et al., 2015, De Tommasi et al., 2017). Understood the potentiality of frustules as silica nanomaterials and their possible exploitation, it is crucial to point out (i) which frustule among a huge diversity is more promising in terms of productivity and (ii) which way to obtain frustules is more sustainable and affordable in a view of a larger scale production. As discussed before, the physical and chemical characterization of frustules is limited to few species despite their huge diversity and the better exploitation of fast-growing cells (producing more frustules in less time). Therefore, a comparison between two species for frustule use was carried out to understand which species maximizes frustule production. To obtain biosilica from diatoms it is crucial to totally remove the organic matter adhered on their surface, preserving frustule shape, and avoiding its erosion (Saad et al., 2020, Sardo et al., 2021). Three ways are mainly used to obtain frustules: (i)

oxidative washing protocols using H_2O_2 solutions, the most commonly used, (ii) chemical treatments with acids and (iii) baking frustules at high temperatures, the simplest and least expensive method more aggressive and altering frustule architecture (Umemura et al., 2010, Gulturk and Guden 2011, Arasuna and Okuno, 2018, Sardo et al., 2021 and reference therein,). In a world moving towards sustainability and looking for always more eco-compatible processes, our purpose was to assess which cleaning procedure has less impact on our planet, comparing through Life Cycle Assessment two procedures, one based on oxidative washing and the other on chemical treatment with acids.

5.2.2 Material and Methods

5.2.2.1 Algal growth

Cultures of two centric diatom species, *Chaetoceros muelleri* (CCAP 1010/3, https://www.ccap.ac.uk/) and *Conticribra weissflogii* (DCG 0320, https://bccm.belspo.be/about-us/bccm-dcg) were established in 1L flasks filled with 400 mL of AMCONA medium (Fanesi et al., 2014) and maintained in a culture chamber at 18 °C, illuminated with cool white fluorescent lamps at 60 µmol photons·$m^{-2}s^{-1}$12:12 h light-dark cycles. Cell number and cell volume were measured using a CASY TT cell counter (Innovatis AG, Reutlingen, Germany as described in chapter 1.2.2 All determinations were carried out on samples from four distinct cultures. Specific growth rates, µ (**Eq. 5.1**), were derived from daily counts of exponentially growing cells, carried out on a minimum of four distinct cultures for each treatment.

$$(\mathbf{5.1})\ \mu = \frac{ln(N_t/N_0)}{t}\ \text{(Monod 1949)}$$

After 7 days cells were collected and washed to obtain cleaned frustules using the protocol by Friedrichs et al. (2012) as described in chapter 5.1.2.1. Frustules were then put in pre-weighted tubes and dried at 80°C till obtaining the frustule dry weight.

5.2.2.2 Cleaning procedures and functionality of two cleaning procedures

Chaetoceros muelleri (CCAP 1010/3, https://www.ccap.ac.uk/) cells were washed using two different procedures to obtain cleaned frustules. The first was based on the oxidation of the organic matter using H_2O_2 (modified from BCCM/DCG protocol). The salts of the culture medium were washed out from the cells for 3 times with deionized water (centrifuge set at 3000 rpm for 10 minutes), then 30% H_2O_2 was added to the cell suspension to a final concentration of about 15%. Samples were dried in oven at 60 °for 3 days. Finally, the material was washed 4 times with deionized water to carefully remove H_2O_2. The second methods relied on a chemical treatment with

acids (modified from Friedrichs et al., 2012). Cells were washed in deionized water 3 times (centrifuge set at 3000 rpm for 10 minutes), then the pellet was resuspended in 1.5 mL deionized water, charged with 1.5 mL of a saturated solution of $KMnO_4$ and left at ambient temperature for 24 h. Subsequently, 3mL of HCl (37%) was added and heated in boiling water until the solution became colourless (1 hour approximately). Finally, cleaned frustules were washed 4 times with deionized to carefully remove acids. Drops of cleaned material obtained with the two methods were mounted on stubs and analysed by SEM (High Resolution ZEISS – SUPRA 40) to assess if the cleaning procedures completely remove the organic matter without affecting frustules ultrastructure.

5.2.2.3 Assessment of the Carbon footprint through LCA

The assessment of the carbon footprint quantified the impact of the two processes on the Climate Change category (expressed as kg CO_2-equiv.), allowing to figure out which is the more sustainable option to obtain cleaning frustules from living cells of diatoms. The choice of this impact category was due to its relevance considering the current decarbonisation target worldwide. In **Figure 5.8** the system boundaries selected for the analysis are reported and algal cultivation was excluded since it was common for both the processes. The process considered then include algal collection and washing, the removal of the organic matter through two different scenarios, and the final frustule washing. Scenario 1 considered the oxidation method through H_2O_2 as way to remove organic matter from frustules, while Scenario 2 used an acid treatment procedure (details of the methods are described in 5.2.2.2). The analysis assessed the impact connected to energy and raw material consumed in order to obtain 150 mg of cleaned frustules, chosen as functional unit. In **Table 5.2** the considered input and output flows involved in the two scenarios are resumed. The thinkstep GaBi software and the Database for Life Cycle Engineering (software 9.2.1, Sphera, Chicago, IL, USA) were employed for the production processes of energy and raw materials and the assessment of the carbon footprint related to the two scenarios.

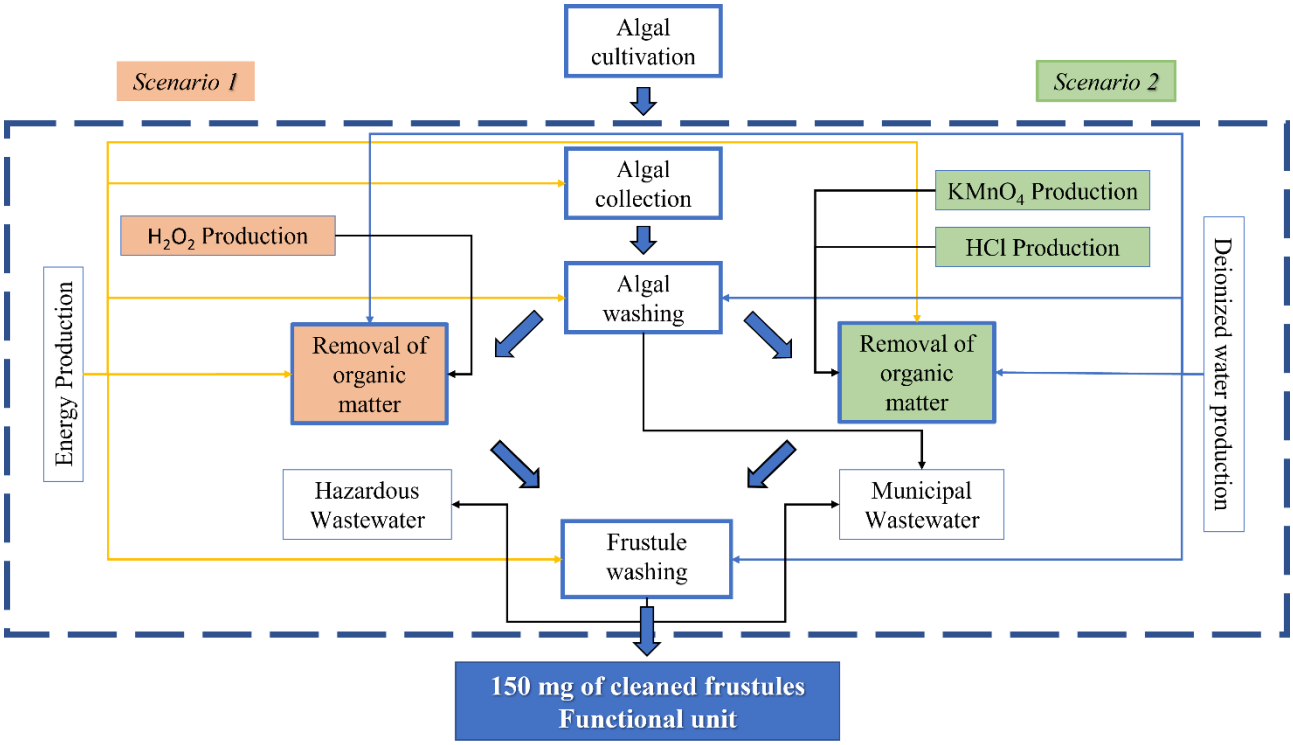

Figure 5.8: System boundaries considered for the carbon footprint assessment.

Table 5.2: Input and output flows considered for the carbon footprint assessment of the 2 scenarios (Functional unit: 150mg of cleaned frustules).

	Input Flow		Output Flow	
Scenario 1	Electricity	33.36 kWh	Municipal wastewater	120Kg
	Deionized Water	116.73 Kg	Hazardous Wastewater	15Kg
	H_2O_2	3.26 Kg		
Scenario 2	Electricity	7.73 kWh	Municipal wastewater	62.7Kg
	Deionized Water	48.90 Kg	Hazardous Wastewater	1.8Kg
	HCl	0.60 Kg		
	$KMnO_4$	0.01 Kg		

5.2.3 Results

5.2.3.1 Comparison between promising species for frustules exploitation

In **Table 5.3** the comparison between two diatoms frustules obtained from *C. muelleri* and *C. weissflogii* is presented. *C. muelleri* cells were 10 times smaller and their growth was two time faster than *C. weissflogii,* leading to a 10-time higher productivity in terms of grams of frustules produced per L of culture per day. Therefore, *C. muelleri* was selected for further studies.

Table 5.3: Mean ± SD of growth rate (d^{-1}), cell volume (μm^3) the corresponding frustules obtained (g) in the two diatoms *C. muelleri* and *C.weissflogii* derived from 0.4 liter of culture. Average ± SD of the calculated productivity as grams of frustules per liter of culture per day (n=4).

	C. muelleri	*C. weissflogii*
Cellular volume (μm^3)	262 ± 11	2383 ± 158
Growth rate (d^{-1})	0.50 ± 0.01	0.21 ± 0.01
Number of cells	5.5 *10^8	1.5*10^8
Volume of culture (L)	0.4	0.4
Frustules weight (g)	0.008 ± 0.001	0.012 ± 0.0006
Productivity Max (g frustules·L^{-1}·d^{-1})	**0.01 ± 0.002**	**0.006 ± 0.0003**

5.2.3.2 Functionality of the two methods

Figure 5.9 presents SEM images of frustules of *C. muelleri* cells obtained with oxidation cleaning procedure using H_2O_2 (**A**, **C**) and through acids treatment (modified from Friedrichs et al., 2012, **B**, **D**). Images highlighted that both the methods lead to the complete removal of the organic matter coating frustule surface (more evident in the detail figures of setae, **C** and **D**) without damaging the ultrastructure of frustules.

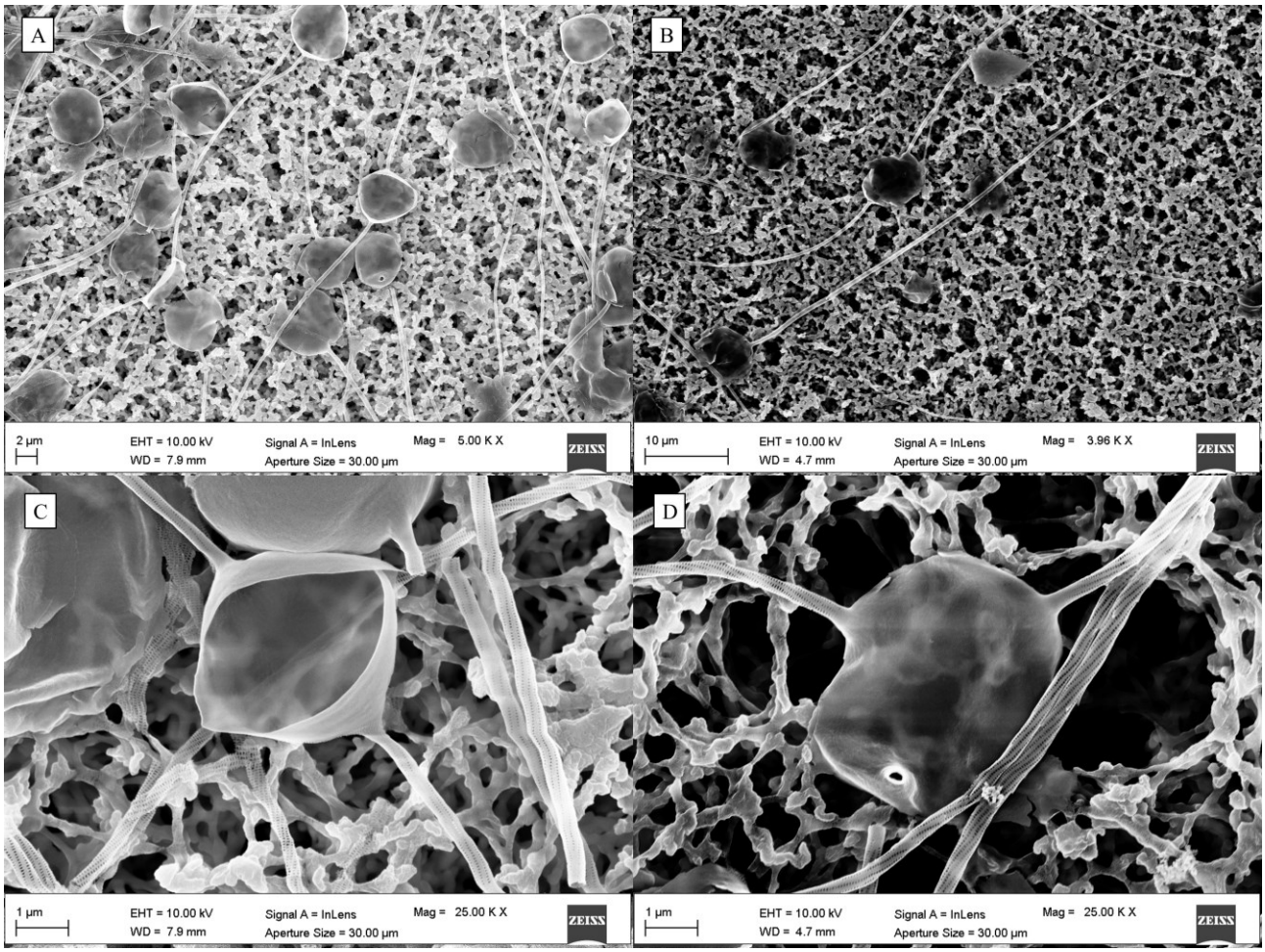

Figure 5.9: SEM images of frustules of the centric diatom *C. muelleri* obtained through oxidation method (**A**, **C**) and acidic treatment (**B**, **D**). Details of *C. muelleri* setae (**C**, **D**) after both cleaning procedures are shown.

5.2.3.3 Assessment of the Carbon footprint through LCA

Results of the carbon footprint assessment showed in **Figure 5.10** highlighted that scenario 1 had a greater impact (20 Kg CO_2 eq.) as compared to the Scenario 2 (5 Kg CO_2 eq.). In detail, in Scenario 2 not only eco-friendlier reagents were used (**Figure 5.10** and **5.11 A**), but water and energy were saved (**Figure 5.11 A, B**) and a lower environmental burden due to hazardous waste was produced (**Figure 5.11 C**). It was clear from the results (**Figure 5.10** and **5.11 A**) that H_2O_2 had a greater impact as compared to HCl and $KMnO_4$ in the removal of organic matter from frustules. The reason is the high impact production process of H_2O_2, known as anthraquinone process. Although, scenario 2 required about 3 times less energy as compared to scenario 1 (**Figure 5.11 B**), energy used for the

thermic treatment (oven in scenario 1 and thermostatic bath in scenario 2) had the highest contribution to the total carbon footprint (**Figure 5.12**).

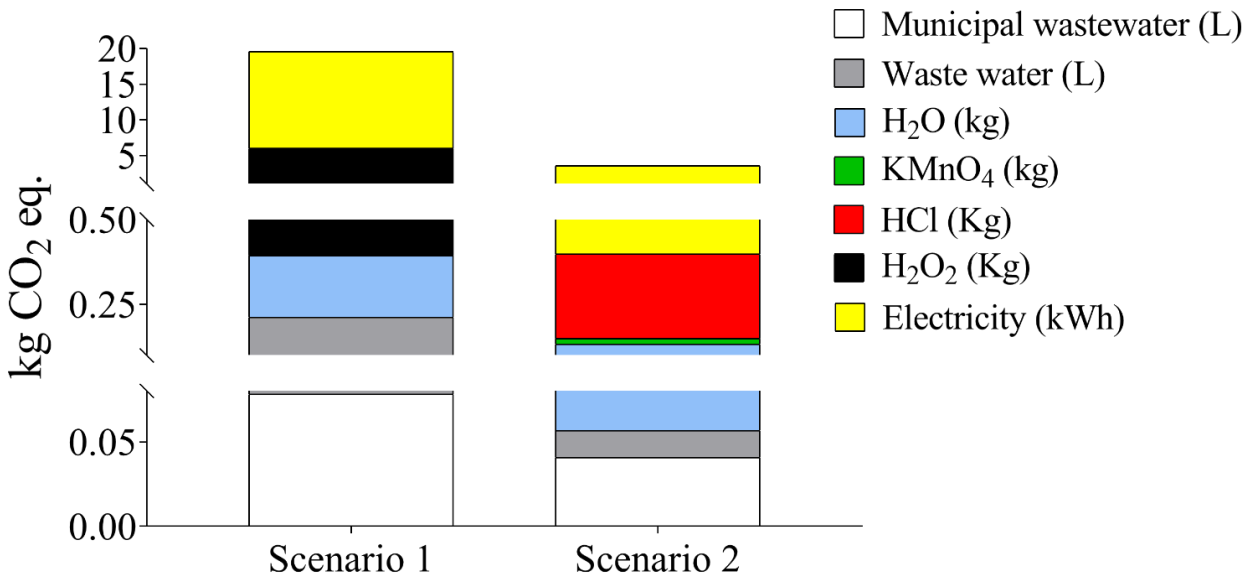

Figure 5.10: Evaluation of the carbon footprint of the 2 considered scenarios: (1) oxidation cleaning procedure through H_2O_2 (2) acid treatment cleaning procedure.

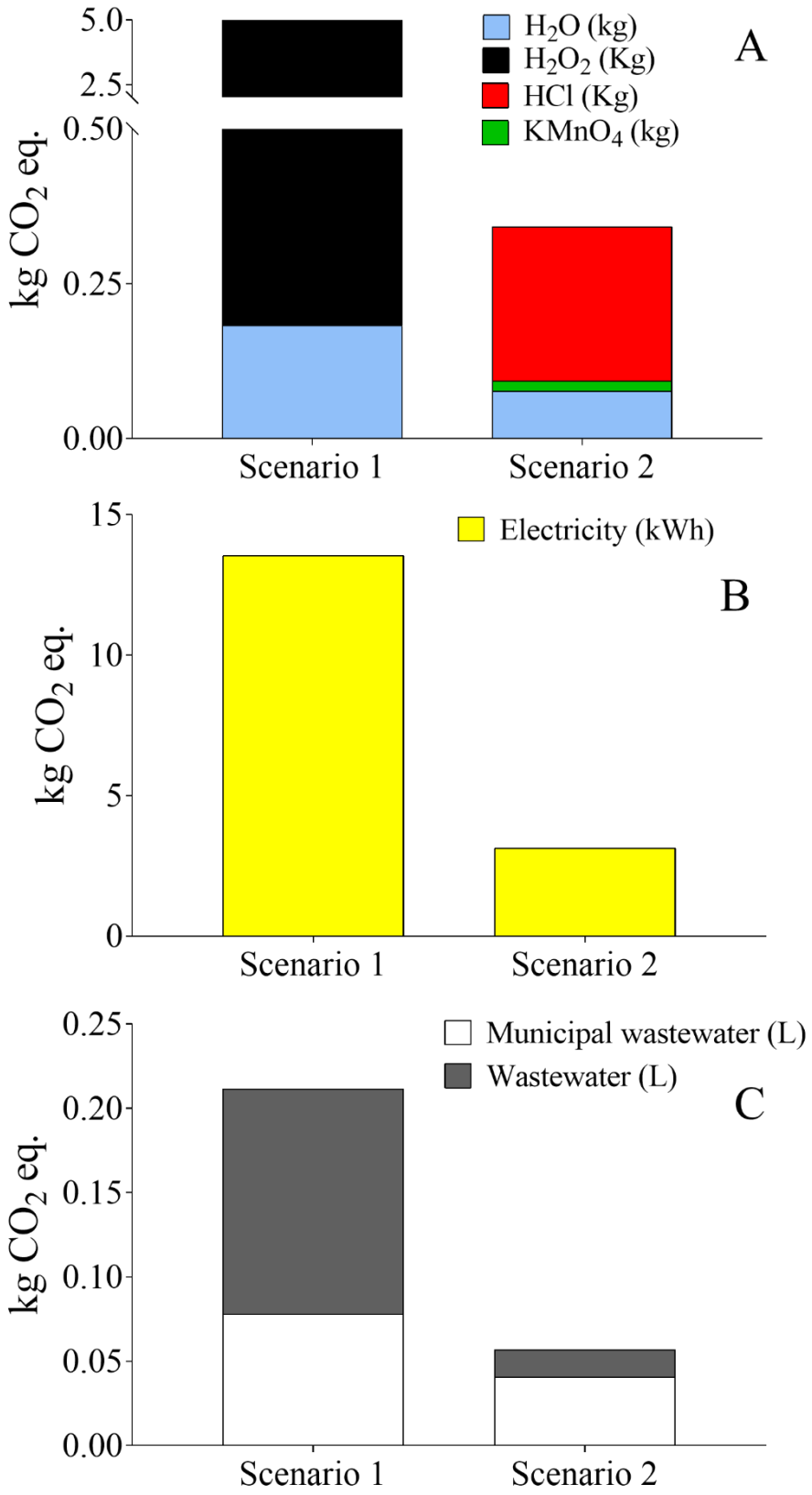

Figure 5.11 Details of the evaluation of the carbon footprint of the 2 considered scenarios. (**A**) impact of the reagents used during cleaning procedures (**B**) impact of energy (**C**) impact of wastes.

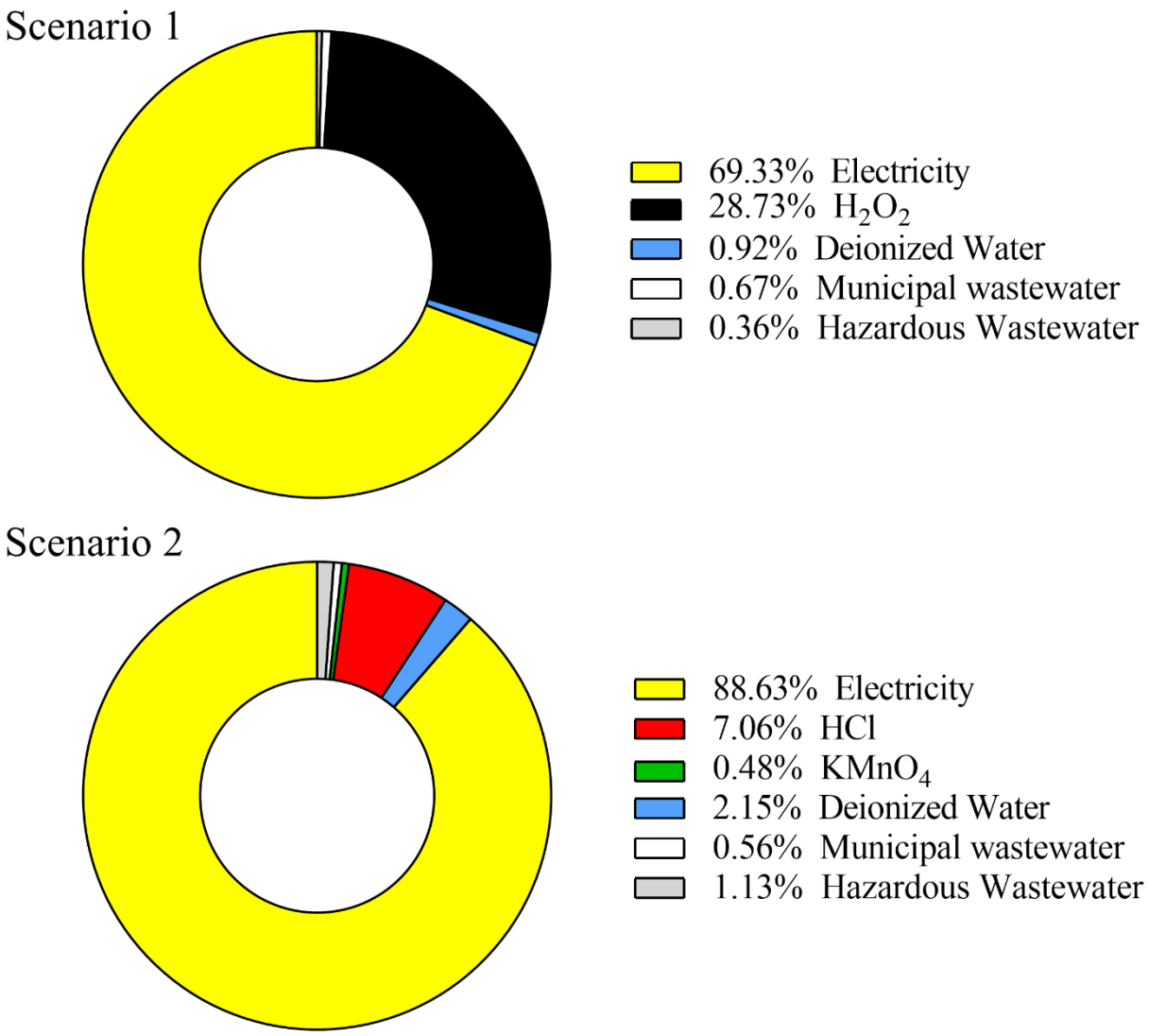

Figure 5.12: Percentage distribution of impacts derived from input and output flows in the 2 considered scenarios.

5.2.4 Discussion

Considering the increasing interest for frustule as biomaterial for biotechnological application, this study demonstrated that *C. muelleri* has the highest potential for future industrial exploitations. Indeed, the small size of this species not only led to a higher surface to volume ratio, allowing a better chemical modification of the frustule and subsequent functionalization (Townley et al., 2008), but also allowed a faster growth as compared to that of *C. weissflogii* (**Table 5.3**). The faster growth rate of *C. muelleri* is indeed crucial for maximizing frustule productivity; in the industrial view of continuous production cultivation and harvesting of diatoms, the quantity of frustules produced by this species per unit of time would be ten time higher than the quantity produced by *C. weissflogii* (**Table 5.3**).

Acidic treatment proved to be a sustainable option to clean frustules of *C. muelleri* in a future perspective of industrial scale up (**Figure 5.10** and **5.11**). Indeed, the robustness of *C. muelleri* frustules allowed the cleaning with less quantity of the more environmentally sustainable reagents (HCl and $KMnO_4$) and for less time. Such treatment did not affect frustule ultrastructure (**Figure 5.9**) while the same treatment is not applicable to frustules of other species (Sardo et al., 2021). The assessment of the carbon footprint highlighted that Friedrichs method using acids is the most sustainable option with an estimated environmental burden of 4kg of equivalent CO_2 compared to 20 kg resulting from the oxidation method; acidic cleaning procedure allows to save electricity, use more sustainable reagents, and produce less wastewater to obtain 150 mg of cleaned *C. muelleri* frustules (**Figures 5.10, 5.11, 5.12**). This treatment is more advantageous due to its lower requirement of energy; indeed, the process is shorter (one hour in boiling water instead of three days in the oven) therefore more suitable for industrial application. The lower requirement of chemical reagent allowed to produce lower wastewater flows with the consequent reduction of impact due to their management. Considering all these aspects, the use of *C. muelleri* frustules washed with acidic treatment was the most sustainable approach applicable at industrial level.

Main conclusions of the thesis

- ✓ The selective pressures, **Si decline through geologic eras** and **interaction of diatoms with competitors and predators,** have driven the evolution of different frustule morphologies. Diatoms with elongated shapes were favoured as compared to centric species since they acclimated to different Si regimes modulating Si use efficiency and escaped from predators also when facing competition for resources. Evolution led to a more competitive morphology.
- ✓ Regarding the adaptative roles of frustules, **defence against predators**, **competition for resource uptake** and **sinking** were related to frustule shape, size and silicification in a role specific manner. In particular, sinking was related to frustule density through its silicification even though neither silicification nor cellular shape and size were involved in buoyancy control at cellular level.
- ✓ In the view of potential frustule exploitation as silica biomaterial, in ***C. muelleri*** silica shell showed interesting properties: its small size, silicification plasticity in response to light intensity, high surface area and relative high presence of basic sites (important for subsequent functionalization). Furthermore, its fast growth rate could be useful for high frustule productivity under an industrial point of view.
- ✓ In the frustule production chain**, acidic removal of the organic matter** to clean biosilica resulted a more environmentally sustainable option releasing 4 kg of equivalent CO_2 compared to 20 kg of equivalent CO_2 released by the oxidation method.

Bibliography

Aguirre, L. E., Ouyang, L., Elfwing, A., Hedblom, M., Wulff, A., and Inganäs, O. (2018). Diatom frustules protect DNA from ultraviolet light. *Sci Rep* 8, 5138. doi:10.1038/s41598-018-21810-2.

Aitken, Z. H., Luo, S., Reynolds, S. N., Thaulow, C., and Greer, J. R. (2016). Microstructure provides insights into evolutionary design and resilience of *Coscinodiscus* sp. frustule. *Proc Natl Acad Sci USA* 113, 2017–2022. doi:10.1073/pnas.1519790113.

Allen, A. E., Dupont, C. L., Oborník, M., Horák, A., Nunes-Nesi, A., McCrow, J. P., et al. (2011). Evolution and metabolic significance of the urea cycle in photosynthetic diatoms. *Nature* 473, 203–207. doi:10.1038/nature10074.

Alvarez, B., Frings, P. J., Clymans, W., Fontorbe, G., and Conley, D. J. (2017). Assessing the potential of sponges (porifera) as indicators of ocean dissolved si concentrations. *Front. Mar. Sci.* 4, 373. doi:10.3389/fmars.2017.00373.

Amato, A., Sabatino, V., Nylund, G. M., Bergkvist, J., Basu, S., Andersson, M. X., et al. (2018). Grazer-induced transcriptomic and metabolomic response of the chain-forming diatom Skeletonema marinoi. *ISME J* 12, 1594–1604. doi:10.1038/s41396-018-0094-0.

Amorim, M. L., Soares, J., Coimbra, J. S. dos R., Leite, M. de O., Albino, L. F. T., and Martins, M. A. (2021). Microalgae proteins: production, separation, isolation, quantification, and application in food and feed. *Critical Reviews in Food Science and Nutrition* 61, 1976–2002. doi:10.1080/10408398.2020.1768046.

Anderson, L. W. J., and Sweeney, B. M. (1977). Diel changes in sedimentation characteristics of *Ditylum brightwelli*: Changes in cellular lipid and effects of respiratory inhibitors and ion-transport modifiers1. *Limnol. Oceanogr.* 22, 539–552. doi:10.4319/lo.1977.22.3.0539.

Anderson, L. W. J., and Sweeney, B. M. (1978). Role of inorganic ions in controlling sedimentation rate of a marine centric diatom *Ditylum brightwelli*. *Journal of Phycology* 14, 204–214. doi:10.1111/j.1529-8817.1978.tb02450.x.

Arasuna, A., and Okuno, M. (2018). Structural change of the frustule of diatom by thermal treatment. *Geosci. Lett.* 5, 1. doi:10.1186/s40562-018-0101-3.

Armbrust, E. V. (2009). The life of diatoms in the world's oceans. *Nature* 459, 185–192. doi:10.1038/nature08057.

Armbrust, E. V., Berges, J. A., Bowler, C., Green, B. R., Martinez, D., Putnam, N. H., et al. (2004). The genome of the diatom *Thalassiosira pseudonana* : ecology, evolution, and metabolism. *Science* 306, 79–86. doi:10.1126/science.1101156.

Artega-Larios, N. V., Nahmad, Y., Navarro-Contreras, H. R., Encinas, A., and García-Meza, J. V. (2014). Photoluminescence shift in frustules of two pennate diatoms and nanostructural changes to their pores. *Luminescence* 29, 969-976. doi:10.1002/bio.2646.

Bannon, C. C., and Campbell, D. A. (2017). Sinking towards destiny: High throughput measurement of phytoplankton sinking rates through time-resolved fluorescence plate

spectroscopy. *PLoS ONE* 12, e0185166. doi:10.1371/journal.pone.0185166.

Barreiro, A., Carotenuto, Y., Lamari, N., Esposito, F., D'Ippolito, G., Fontana, A., et al. (2011). Diatom induction of reproductive failure in copepods: The effect of PUAs versus non volatile oxylipins. *Journal of Experimental Marine Biology and Ecology* 401, 13–19. doi:10.1016/j.jembe.2011.03.007.

Behrenfeld, M. J., Halsey, K. H., Boss, E., Karp-Boss, L., Milligan, A. J., and Peers, G. (2021). Thoughts on the evolution and ecological niche of diatoms. *Ecol Monogr* 91. doi:10.1002/ecm.1457.

Benoiston, A.S., Ibarbalz, F. M., Bittner, L., Guidi, L., Jahn, O., Dutkiewicz, S., et al. (2017). The evolution of diatoms and their biogeochemical functions. *Phil. Trans. R. Soc. B* 372, 20160397. doi:10.1098/rstb.2016.0397.

Bienfang, P. K. (1981). Sinking rate dynamics of *Crzcosphaera carterae* braarud. I. Effects of growth rate, limiting substrate, and diurnal variation in steady-state populations. J. exp. Mar. Biol. Ecol. 49, 217-233.

Bienfang, P., Szyper, J., and Laws, E (1983). Sinking rate and pigment responses to light-limitation of a marine diatom - implications to dynamics of chlorophyll maximum layers. *Oceanologica acta*,6(1), 55-62.

Bondoc, K. G. V., Heuschele, J., Gillard, J., Vyverman, W., and Pohnert, G. (2016a). Selective silicate-directed motility in diatoms. *Nat Commun* 7, 10540. doi:10.1038/ncomms10540.

Bondoc, K. G. V., Lembke, C., Vyverman, W., and Pohnert, G. (2016b). Searching for a mate: pheromone-directed movement of the benthic diatom seminavis robusta. *Microb Ecol* 72, 287–294. doi:10.1007/s00248-016-0796-7.

Bondoc, K. G. V., Lembke, C., Lang, S. N., Germerodt, S., Schuster, S., Vyverman, W., et al. (2019a). Decision-making of the benthic diatom *Seminavis robusta* searching for inorganic nutrients and pheromones. *ISME J* 13, 537–546. doi:10.1038/s41396-018-0299-2.

Bondoc, K. G. V., Lembke, C., Vyverman, W., and Pohnert, G. (2019b). Selective chemoattraction of the benthic diatom *Seminavis robusta* to phosphate but not to inorganic nitrogen sources contributes to biofilm structuring. 10.

Boyle, E. (1998). Pumping iron makes thinner diatoms. *Nature* 393, 733–734. doi:10.1038/31585.

Bowler, C., Allen, A. E., Badger, J. H., Grimwood, J., Jabbari, K., Kuo, A., et al. (2008). The *Phaeodactylum* genome reveals the evolutionary history of diatom genomes. *Nature* 456, 239–244. doi:10.1038/nature07410.

Bowler, C., De Martino, A., and Falciatore, A. (2010). Diatom cell division in an environmental context. *Current Opinion in Plant Biology* 13, 623–630. doi:10.1016/j.pbi.2010.09.014.

Brun, P., Vogt, M., Payne, M. R., Gruber, N., O'Brien, C. J., Buitenhuis, E. T., et al. (2015). Ecological niches of open ocean phytoplankton taxa: Niches of open ocean phytoplankton. *Limnol. Oceanogr.* 60, 1020–1038. doi:10.1002/lno.10074.

Brunner, E., Richthammer, P., Hermann, E. Paasch, S., Simon, P., Ueberlein, S., and Van Pée, C. E. (2009). Chitin-based organic networks: A integral part of cell wall biosilica in the diatom

Talassiosira pseudonana. J. German Chem. Soc. 48(51), 9725-9727. doi:10.1002/anie.200905028.

Brzezinski, M., Olson, R., and Chisholm, S. (1990). Silicon availability and cell-cycle progression in marine diatoms. *Mar. Ecol. Prog. Ser.* 67, 83–96. doi:10.3354/meps067083.

Brzezinski, M. A., Krause, J. W., Baines, S. B., Collier, J. L., Ohnemus, D. C., and Twining, B. S. (2017). Patterns and regulation of silicon accumulation in *Synechococcus* spp. *J. Phycol.* 53, 746–761. doi:10.1111/jpy.12545.

Bucciarelli, E., Pondaven, P., and Sarthou, G. (2010). Effects of an iron-light co-limitation on the elemental composition (Si, C, N) of the marine diatoms *Thalassiosira oceanica* and *Ditylum brightwellii*. *Biogeosciences* 7(2), 657-669. doi: 10.5194/bg-7-657-2010

Burson, A., Stomp, M., Greenwell, E., Grosse, J., and Huisman, J. (2018). Competition for nutrients and light: testing advances in resource competition with a natural phytoplankton community. *Ecology* 99, 1108–1118. doi:10.1002/ecy.2187.

Boyd, C. M., and Gradmann, D. (2002). Impact of osmolytes on buoyancy of marine phytoplankton. *Marine Biology* 141, 605–618. doi:10.1007/s00227-002-0872-z.

Cermeño, P., Falkowski, P. G., Romero, O. E., Schaller, M. F., and Vallina, S. M. (2015). Continental erosion and the Cenozoic rise of marine diatoms. *Proc Natl Acad Sci USA* 112, 4239–4244. doi:10.1073/pnas.1412883112.

Claquin, P., Martin-Jezequel, V., Kromkamp, J. C., Veldhuis, M. J. W., and Kraay, G. W. (2002). Uncoupling of silicon compared with carbon and nitrogen metabolisms and the role of the cell cycle in continuous cultures of *Thalassiosira pseudonana* (bacillariophyceae) under light, nitrogen, and phosphorus control 1. *J Phycol* 38, 922–930. doi:10.1046/j.1529-8817.2002.t01-1-01220.x.

Cohen, N. R., Ellis, K. A., Lampe, R. H., McNair, H., Twining, B. S., Maldonado, M. T., et al. (2017). Diatom transcriptional and physiological responses to changes in iron bioavailability across ocean provinces. *Front. Mar. Sci.* 4, 360. doi:10.3389/fmars.2017.00360.

Cohn, S. A., and Disparti, N. C. (1994). Environmental factors influencing diatom cell motility. *J. Phycology* 30, 818-828. doi:10.1111/j.0022-3646.1994.00818.x.

Cohn, S. A., Halpin, D., Hawley, N., Ismail, A., Kaplan, Z., Kordes, T., et al. (2015). Comparative analysis of light-stimulated motility responses in three diatom species. *Diatom Research* 30, 213–225. doi:10.1080/0269249X.2015.1058295.

Conley, D. J., and Carey, J. C. (2015). Silica cycling over geologic time. *Nature Geosci* 8, 431–432. doi:10.1038/ngeo2454.

Conley, D. J., Frings, P. J., Fontorbe, G., Clymans, W., Stadmark, J., Hendry, K. R., et al. (2017). Biosilicification drives a decline of dissolved si in the oceans through geologic time. *Front. Mar. Sci.* 4, 397. doi:10.3389/fmars.2017.00397.

Conn, S. A., Bahena, M., Davis, J. T., Ragland, R. L., Rauschenberg, C. D., and Smith, B. J. (2004). Characterisation of the diatom photophobic response to high irradiance. *Diatom Research* 19, 167–179. doi:10.1080/0269249X.2004.9705869.

Conway, H. L., Harrison, P. J., and Davis, C. O. (1976). Marine diatoms grown in chemostats under silicate or ammonium limitation. II. Transient response of *Skeletonema costatum* to a single addition of the limiting nutrient. *Marine Biology* 35, 187–199. doi:10.1007/BF00390940.

Conway, H. L., and Harrison, P. J. (1977). Marine diatoms grown in chemostats under silicate or ammonium limitation. IV. Transient response of *Chaetoceros debilis*, *Skeletonema costatum*, and *Thalassiosira gravida* to a single addition of the limiting nutrient. *Marine Biology* 43, 33-43. doi:10.1007/BF00392569.

Cooksey, B., and Cooksey, K. E. (1988). Chemical signal-response in diatoms of the genus *Amphora*. J. cell Science 91(4), 523-529. doi:10.1242/jcs.91.4.523.

Cornelis, J.-T., Delvaux, B., Cardinal, D., André, L., Ranger, J., and Opfergelt, S. (2010). Tracing mechanisms controlling the release of dissolved silicon in forest soil solutions using Si isotopes and Ge/Si ratios. *Geochimica et Cosmochimica Acta* 74, 3913–3924. doi:10.1016/j.gca.2010.04.056.

Cui, Z., Cheng, F., Jarvis, J. M., Brewer, C. E., and Jena, U. (2020). Roles of Co-solvents in hydrothermal liquefaction of low-lipid, high-protein algae. *Bioresource Technology* 310, 123454. doi:10.1016/j.biortech.2020.123454.

D'Ippolito, G., Sardo, A., Paris, D., Vella, F. M., Adelfi, M. G., Botte, P., et al. (2015). Potential of lipid metabolism in marine diatoms for biofuel production. *Biotechnol Biofuels* 8, 28. doi:10.1186/s13068-015-0212-4.

De La Rocha, C., Hutchins, D., Brzezinski, M., and Zhang, Y. (2000). Effects of iron and zinc deficiency on elemental composition and silica production by diatoms. *Mar. Ecol. Prog. Ser.* 195, 71–79. doi:10.3354/meps195071.

De Stefano, L., Rea, I., Rendina, I., De Stefano, M., and Moretti, L. (2007). Lensless light focusing with the centric marine diatom *Coscinodiscus walesii*. *Opt. Express* 15, 18082. doi:10.1364/OE.15.018082.

De Tommasi, E. (2016). Light manipulation by single cells: the case of diatoms. *Journal of Spectroscopy* 2016, 1–13. doi:10.1155/2016/2490128.

De Tommasi, E., Congestri, R., Dardano, P., De Luca, A. C., Managò, S., Rea, I., et al. (2018). UV-shielding and wavelength conversion by centric diatom nanopatterned frustules. *Sci Rep* 8, 16285. doi:10.1038/s41598-018-34651-w.

De Tommasi, E., Gielis, J., and Rogato, A. (2017). Diatom frustule morphogenesis and function: a multidisciplinary survey. *Marine Genomics* 35, 1–18. doi:10.1016/j.margen.2017.07.001.

Desikachary, T. V., and Dweltz, N. E. (1961). The chemical composition of the diatom frustule. *Proceedings of the Indian Academy of Sciences - Section B* 53, 157–165. doi:10.1007/BF03051518.

Dineshbabu, G., Goswami, G., Kumar, R., Sinha, A., and Das, D. (2019). Microalgae–nutritious, sustainable aqua- and animal feed source. *Journal of Functional Foods* 62, 103545. doi:10.1016/j.jff.2019.103545.

Domenighini, A., and Giordano, M. (2009). Fourier transform infrared spectroscopy of microalgae as a novel tool for biodiversity studies, species identification, and the assessment of water

quality 1. *Journal of phycology* 45(2), 522-531. doi:10.1111/j.1529-8817.2009.00662.x

Du Clos, K. T., Karp-Boss, L., Villareal, T. A., and Gemmell, B. J. (2019). *Coscinodiscus wailesii* mutes unsteady sinking in dark conditions. *Biol. Lett.* 15, 20180816. doi:10.1098/rsbl.2018.0816.

Du Clos, K. T., Karp-Boss, L., and Gemmell, B. J. (2021). Diatoms rapidly alter sinking behavior in response to changing nutrient concentrations. *Limnol Oceanogr* 66, 892–900. doi:10.1002/lno.11649.

Durante, G., Basset, A., Stanca, E., and Roselli, L. (2019). Allometric scaling and morphological variation in sinking rate of phytoplankton. *J. Phycol.* 55, 1386–1393. doi:10.1111/jpy.12916.

Durbin, E. G. (1977). Studies on the autecology of the marine diatom *Thalassiosira nordenskioeldii.* II. The influence of cell size on growth rate, and carbon, nitrogen, chlorophyll *a* and silica content. *J. Phycol.* 13(2), 150-155. doi:10.1111/j.1529-8817.1977.tb02904.x.

Durkin, C. A., Koester, J. A., Bender, S. J., and Armbrust, E. V. (2016). The evolution of silicon transporters in diatoms. *J. Phycol.* 52, 716–731. doi:10.1111/jpy.12441.

Egan, K. E., Rickaby, R. E. M., Hendry, K. R., and Halliday, A. N. (2013). Opening the gateways for diatoms primes Earth for Antarctic glaciation. *Earth and Planetary Science Letters* 375, 34–43. doi:10.1016/j.epsl.2013.04.030.

Ellegaard, M., Lenau, T., Lundholm, N., Maibohm, C., Friis, S. M. M., Rottwitt, K., et al. (2016). The fascinating diatom frustule—can it play a role for attenuation of UV radiation? *J Appl Phycol* 28, 3295–3306. doi:10.1007/s10811-016-0893-5.

Exley, C. (2015). A possible mechanism of biological silicification in plants. *Front. Plant Sci.* 6. doi:10.3389/fpls.2015.00853.

Falkowski, P. G., Katz, M. E., Knoll, A. H., Quigg, A., Raven, J. A., Schofield, O., et al. (2004). The evolution of modern eukaryotic phytoplankton. *Science* 305, 354–360. doi:10.1126/science.1095964.

Fanesi, A., Raven, J. A., and Giordano, M. (2014). Growth rate affects the responses in the green alga *Tretaselmis suecica* to the external perturbation. *Plant, Cell and Environment* 37(2), 512-519. doi:10.1111/pce.12176.

Farooq, M. A., and Dietz, K.-J. (2015). Silicon as versatile player in plant and human biology: overlooked and poorly understood. *Front. Plant Sci.* 6. doi:10.3389/fpls.2015.00994.

Ferrara, M. A., Dardano, P., De Stefano, L., Rea, I., Coppola, G., Rendina, I., et al. (2014). Optical properties of diatom nanostructured biosilica in arachnoidiscus sp: micro-optics from mother nature. *PLoS ONE* 9, e103750. doi:10.1371/journal.pone.0103750.

Field, C. B., Behrenfeld, M. J., Randerson, J. T., and Falkowski, P. (1998). Primary production of the biosphere: integrating terrestrial and oceanic components. *Science* 281, 237–240. doi:10.1126/science.281.5374.237.

Finkel, Z. V., Katz, M. E., Wright, J. D., Schofield, O. M. E., and Falkowski, P. G. (2005).

Climatically driven macroevolutionary patterns in the size of marine diatoms over the Cenozoic. *Proceedings of the National Academy of Sciences* 102, 8927–8932. doi:10.1073/pnas.0409907102.

Finkel, Z. V., and Kotrc, B. (2010). Silica use through time: macroevolutionary change in the morphology of the diatom fustule. *Geomicrobiology Journal* 27, 596–608. doi:10.1080/01490451003702941.

Finkel, Z. V., Matheson, K. A., Regan, K. S., and Irwin, A. J. (2010). Genotypic and phenotypic variation in diatom silicification under paleo-oceanographic conditions: Diatom silicification. *Geobiology* 8, 433–445. doi:10.1111/j.1472-4669.2010.00250.x.

Flynn, K. J., and Martin-Jezequel, V. (2000). Modelling Si-N-limited growth of diatoms. *Journal of Plankton Research* 22, 447–472. doi:10.1093/plankt/22.3.447.

Fontorbe, G. (2016). *Marine silicon cycle through the Cenozoic*. Lund: Lund University, Faculty of Science, Department of Geology, Quaternary Sciences.

Fontorbe, G., Frings, P. J., De La Rocha, C. L., Hendry, K. R., Carstensen, J., and Conley, D. J. (2017). Enrichment of dissolved silica in the deep equatorial Pacific during the Eocene-Oligocene: Equatorial Pacific DSi Enrichment. *Paleoceanography* 32, 848–863. doi:10.1002/2017PA003090.

Friedrichs, L., Maier, M, and Hamm, C. (2012). A new method for exact three-dimensional reconstruction of diatom frustules. J. Microscopy 248(2), 208-217. doi:10.1111/j.1365-2818.2012.03664.x.

Friedrichs, L., Hörnig, M., Schulze, L., Bertram, A., Jansen, S., and Hamm, C. (2013). Size and biomechanic properties of diatom frustules influence food uptake by copepods. *Mar. Ecol. Prog. Ser.* 481, 41–51. doi:10.3354/meps10227.

Frings, P. J., Clymans, W., Fontorbe, G., De La Rocha, C. L., and Conley, D. J. (2016). The continental Si cycle and its impact on the ocean Si isotope budget. *Chemical Geology* 425, 12–36. doi:10.1016/j.chemgeo.2016.01.020.

Gemmell, B. J., Oh, G., Buskey, E. J., and Villareal, T. A. (2016). Dynamic sinking behaviour in marine phytoplankton: rapid changes in buoyancy may aid in nutrient uptake. *Proc. R. Soc. B.* 283, 20161126. doi:10.1098/rspb.2016.1126.

Gentil, J., Hempel, F., Moog, D., Zauner, S., and Maier, U. G. (2017). Review: origin of complex algae by secondary endosymbiosis: a journey through time. J. Soil Sci. Plant Nutr. 254, 1835-1843. doi:10.1007/s00709-017-1098-8.

Gerotto, C., Norici, A., and Giordano, M. (2020). Toward Enhanced Fixation of CO2 in Aquatic Biomass: Focus on Microalgae. Front. Energy Res. 8:213. doi: 10.3389/fenrg.2020.00213

Giordano, M. (2013). Homeostasis: An underestimated focal point of ecology and evolution. *Plant Science* 211, 92–101. doi:10.1016/j.plantsci.2013.07.008.

Giordano, M., Beardall, J., and Raven, J. A. (2005). CO_2 concentrating mechanisms in algae: mechanisms, environmental modulation, and evolution. *Annu. Rev. Plant Biol.* 56, 99–131. doi:10.1146/annurev.arplant.56.032604.144052.

Giordano, M., Kansiz, M., Heraud, P., Beardall, J., Wood, B. and McNaughton, D. (2001). Fourier transform infrared spectroscopy as a novel tool to investigate changes in intracellular macromolecular pools in the marine microalga Chaetoceros muellerii (bacillariophyceae). Journal of Phycology, 37: 271-279. doi:10.1046/j.1529-8817.2001.037002271.x

Giordano, M., Norici, A., and Beardall, J. (2017). Impact of inhibitors of amino acid, protein, and RNA synthesis on C allocation in the diatom *Chaetoceros muellerii*: a FTIR approach. *ALGAE* 32, 161–170. doi:10.4490/algae.2017.32.6.6.

Giordano, M., Olivieri, C., Ratti, S., Norici, A., Raven, J. A., and Knoll, A. H. (2018). A tale of two eras: Phytoplankton composition influenced by oceanic paleochemistry. *Geobiology* 16, 498–506. doi:10.1111/gbi.12290.

Girard, V., Saint Martin, S., Buffetaut, E., Saint Martin, J.P., Néraudeau, D., Peyrot, D., Roghi, G., Ragazzi, E., Suteethorn, V. (2020). Thai amber: insights into early diatom history?. *Bulletin de la Société Géologique de France* 2020; 191 (1): 23. doi:10.1051/bsgf/2020028.

Goessling, J. W., Su, Y., Cartaxana, P., Maibohm, C., Rickelt, L. F., Trampe, E. C. L., et al. (2018). Structure-based optics of centric diatom frustules: modulation of the *in vivo* light field for efficient diatom photosynthesis. *New Phytol* 219, 122–134. doi:10.1111/nph.15149.

Gordon, J. M., and Polle, J. E. W. (2007). Ultrahigh bioproductivity from algae. *Appl Microbiol Biotechnol* 76, 969–975. doi:10.1007/s00253-007-1102-x.

Görlich, S., Pawolski, D., Zlotnikov, I., and Kröger, N. (2019). Control of biosilica morphology and mechanical performance by the conserved diatom gene Silicanin-1. *Commun Biol* 2, 245. doi:10.1038/s42003-019-0436-0.

Goswami, B., Choudhury, A., and Buragohain, A. K. (2012). Luminescence properties of a nanoporous freshwater diatom: Luminescence properties of a nanoporous freshwater diatom. *Luminescence* 27, 16–19. doi:10.1002/bio.1315.

Grønning, J., and Kiørboe, T. (2020). Diatom defence: Grazer induction and cost of shell-thickening. *Funct Ecol* 34, 1790–1801. doi:10.1111/1365-2435.13635.

Grotzinger, J., Jordan, T. H. (2014). Understanding earth. New York Freeman & Co. 7th Edition.

Gulturk, E., and Guden, M. (2011). Thermal and acid treatment of diatom frustules. *Journal of Achievements in Materials and Manufacturing Engineering* 46, 8.

Hale, M., and Mitchell, J. (2001). Functional morphology of diatom frustule microstructures: hydrodynamic control of Brownian particle diffusion and advection. *Aquat. Microb. Ecol.* 24, 287–295. doi:10.3354/ame024287.

Hale, M. S., and Mitchell, J. G. (2002). Effects of particle size, flow velocity, and cell surface microtopography on the motion of submicrometer particles over diatoms. *Nano Lett.* 2, 657–663. doi:10.1021/nl025557m.

Hamano, R., Shoumura, S., Takeda, Y., Yamazaki, T., Hirayama, K., Hanada, Y., et al. (2021). Sinking of four species of living diatom cells directly observed by a “tumbled” optical microscope. *Microsc Microanal* 27, 1154–1160. doi:10.1017/S1431927621012150.

Hamm, C. E., Merkel, R., Springer, O., Jurkojc, P., Maier, C., Prechtel, K., et al. (2003).

Architecture and material properties of diatom shells provide effective mechanical protection. *Nature* 421, 841–843. doi:10.1038/nature01416.

Hamm, C., and Smetacek, V. (2007). "Armor: Why, When, and How," in *Evolution of Primary Producers in the Sea* (Elsevier), 311–332. doi:10.1016/B978-012370518-1/50015-1.

Hammer, Ø., Harper, D. A. T., and Ryan, P. D. (2009). PAST: Paleontological statistics software package for education and data analysis. Palaeontologia Electronica 4(1).

Hansen, A. N., and Visser, A. W. (2019). The seasonal succession of optimal diatom traits. *Limnol Oceanogr* 64, 1442–1457. doi:10.1002/lno.11126.

Harper, H. E., and Knoll, A. H. (1975). Silica, diatoms, and Cenozoic radiolarian evolution. *Geol* 3, 175. doi:10.1130/0091-7613(1975)3<175:SDACRE>2.0.CO;2.

Hedayatkhah, A., Cretoiu, M. S., Emtiazi, G., Stal, L. J., and Bolhuis, H. (2018). Bioremediation of chromium contaminated water by diatoms with concomitant lipid accumulation for biofuel production. *Journal of Environmental Management* 227, 313–320. doi:10.1016/j.jenvman.2018.09.011.

Henstock, J. R., Canham, L. T., and Anderson, S. I. (2015). Silicon: The evolution of its use in biomaterials. *Acta Biomaterialia* 11, 17–26. doi:10.1016/j.actbio.2014.09.025.

Hervé, V., Derr, J., Douady, S., Quinet, M., Moisan, L., and Lopez, P. J. (2012). Multiparametric analyses reveal the ph-dependence of silicon biomineralization in diatoms. *PLoS ONE* 7, e46722. doi:10.1371/journal.pone.0046722.

Hendry, K. R., Marron, A. O., Vincent, F., Conley, D. J., Gehlen, M., Ibarbalz, F. M., et al. (2018). Competition between silicifiers and non-silicifiers in the past and present ocean and its evolutionary impacts. *Front. Mar. Sci.* 5, 22. doi:10.3389/fmars.2018.00022.

Hildebrand, M. Dahlin, K., and Volcani, B. E. (1998). Characterization of a silicon transporter gene family in *Cylindrotheca fusiformis*: sequences, expression analysis, and identification of homologs in other diatoms. *Mol. Gen. Gene*t. 260, 480-486. doi:10.1007/s004380050920

Hildebrand, M. (2003). Biological processes of nanostructured silica in diatoms. *Progress Organic Coatings* 47(3-4), 256-266. doi:10.1016/s0300-9440(03)00142-5.

Hildebrand, M., Davis, A. K., Smith, S. R., Traller, J. C., and Abbriano, R. (2012). The place of diatoms in the biofuels industry. *Biofuels* 3, 221–240. doi:10.4155/bfs.11.157.

Hildebrand, M., and Lerch, S. J. L. (2015). Diatom silica biomineralization: Parallel development of approaches and understanding. *Seminars in Cell & Developmental Biology* 46, 27–35. doi:10.1016/j.semcdb.2015.06.007.

Hildebrand, M., Lerch, S. J. L., and Shrestha, R. P. (2018). Understanding diatom cell wall silicification-moving forward. *Front. Mar. Sci.* 5, 125. doi:10.3389/fmars.2018.00125.

Hillebrand, H., Dürselen, C.-D., Kirschtel, D., Pollingher, U., and Zohary, T. (1999). Biovolume calculation for pelagic and benthic microalgae. *Journal of Phycology* 35, 403–424. doi:10.1046/j.1529-8817.1999.3520403.x.

Hockin, N. L., Mock, T., Mulholland, F., Kopriva, S., and Malin, G. (2012). The response of

diatom central carbon metabolism to nitrogen starvation is different from that of green algae and higher plants. *Plant Physiology* 158, 299–312. doi:10.1104/pp.111.184333.

Hutchins, D. A., and Bruland, K. W. (1998). Iron-limited diatom growth and Si:N uptake ratios in a coastal upwelling regime. *Nature* 393, 561–564. doi:10.1038/31203.

Ianora, A., and Miralto, A. (2010). Toxigenic effects of diatoms on grazers, phytoplankton and other microbes: a review. *Ecotoxicology* 19, 493–511. doi:10.1007/s10646-009-0434-y.

Ianora, A., Miralto, A., Poulet, S. A., Carotenuto, Y., Buttino, I., Romano, G., et al. (2004). Aldehyde suppression of copepod recruitment in blooms of a ubiquitous planktonic diatom. *Nature* 429, 403–407. doi:10.1038/nature02526.

Ikeda, T. (2021). Bacterial biosilicification: a new insight into the global silicon cycle. *Bioscience, Biotechnology, and Biochemistry* 85, 1324–1331. doi:10.1093/bbb/zbab069.

Iler, K. R. (1979). The chemistry of silica. *Solubility, polymerization, colloid and surface properties and biochemistry of silica*.

Jansen, S. (2008). Copepods grazing on *Coscinodiscus wailesii*: a question of size? *Helgol Mar Res* 62, 251–255. doi:10.1007/s10152-008-0113-z.

Javaheri, N., Dries, R., and Kaandorp, J. (2014). Understanding the sub-cellular dynamics of silicon transportation and synthesis in diatoms using population-level data and computational optimization. *PLoS Comput Biol* 10, e1003687. doi:10.1371/journal.pcbi.1003687.

Jin, X., Gruber, N., Dunne, J. P., Sarmiento, J. L., and Armstrong, R. A. (2006). Diagnosing the contribution of phytoplankton functional groups to the production and export of particulate organic carbon, $CaCO_3$, and opal from global nutrient and alkalinity distributions: diagnosing phytoplankton functional groups. *Global Biogeochem. Cycles* 20, n/a-n/a. doi:10.1029/2005GB002532.

Jugdaohsingh, R. (2009). Silicon and bone health. *J. Nutr. Health Aging*. 11(2), 99-110.

Kammer, M., Hedrich, R., Ehrlich, H., Popp, J., Brunner, E., and Krafft, C. (2010). Spatially resolved determination of the structure and composition of diatom cell walls by Raman and FTIR imaging. *Anal Bioanal Chem* 398, 509–517. doi:10.1007/s00216-010-3924-0.

Keller, K., and Morel, F. (1999). A model of carbon isotopic fractionation and active carbon uptake in phytoplankton. *Mar. Ecol. Prog. Ser.* 182, 295–298. doi:10.3354/meps182295.

Kemp, A. E. S., and Villareal, T. A. (2018). The case of the diatoms and the muddled mandalas: Time to recognize diatom adaptations to stratified waters. *Progress in Oceanography* 167, 138–149. doi:10.1016/j.pocean.2018.08.002.

Key, T., McCarthy, A., Campbell, D. A., Six, C., Roy, S., and Finkel, Z. V. (2010). Cell size trade-offs govern light exploitation strategies in marine phytoplankton. *Environmental Microbiology* 12, 95–104. doi:10.1111/j.1462-2920.2009.02046.x.

Kidder, D. L., and Tomescu, I. (2016). Biogenic chert and the Ordovician silica cycle. *Palaeogeography, Palaeoclimatology, Palaeoecology* 458, 29–38. doi:10.1016/j.palaeo.2015.10.013.

Knight, M. J., Senior, L., Nancolas, B., Ratcliffe, S., and Curnow, P. (2016). Direct evidence of the molecular basis for biological silicon transport. *Nat Commun* 7, 11926. doi:10.1038/ncomms11926.

Knoll, A. H., and Follows, M. J. (2016). A bottom-up perspective on ecosystem changes in Mesozoic oceans. *Proc. R. Soc. B.* 283, 20161755. doi:10.1098/rspb.2016.1755.

Korb, R., Raven, J., Johnston, A., and Leftley, J. (1996). Effects of cell size and specific growth rate on stable carbon isotope discrimination by two species of marine diatom. *Mar. Ecol. Prog. Ser.* 143, 283–288. doi:10.3354/meps143283.

Kotrc, B., and Knoll, A. H. (2015). A morphospace of planktonic marine diatoms. I. Two views of disparity through time. *Paleobiology* 41, 45–67. doi:10.1017/pab.2014.4.

Kotzsch, A., Gröger, P., Pawolski, D., Bomans, P. H. H., Sommerdijk, N. A. J. M., Schlierf, M., et al. (2017). Silicanin-1 is a conserved diatom membrane protein involved in silica biomineralization. *BMC Biol* 15, 65. doi:10.1186/s12915-017-0400-8.

Kröger, N., Deutzmann, R., and Sumper, M. (1999). Polycationic peptides from diatom biosilica that direct silica nanosphere formation. *Science* 286, 1129–1132. doi:10.1126/science.286.5442.1129.

Kröger, N., Lorenz, S., Brunner, E., and Sumper, M. (2002). Self-assembly of highly phosphorylated silaffins and their function in biosilica morphogenesis. *Science* 298, 584–586. doi:10.1126/science.1076221.

Kumar, S., Rechav, K., Kaplan-Ashiri, I., and Gal, A. (2020). Imaging and quantifying homeostatic levels of intracellular silicon in diatoms. *Sci. Adv.* 6, eaaz7554. doi:10.1126/sciadv.aaz7554.

Kumar, S., Soukup, M., and Elbaum, R. (2017). Silicification in grasses: variation between different cell types. *Front. Plant Sci.* 8. doi:10.3389/fpls.2017.00438.

Kumar, S., Natalio, F., and Elbaum, R. (2021). Protein-driven biomineralization: Comparing silica formation in grass silica cells to other biomineralization processes. *Journal of Structural Biology* 213, 107665. doi:10.1016/j.jsb.2020.107665.

Lamminen, M., Halmemies-Beauchet-Filleau, A., Kokkonen, T., Jaakkola, S., and Vanhatalo, A. (2019). Different microalgae species as a substitutive protein feed for soya bean meal in grass silage based dairy cow diets. *Animal Feed Science and Technology* 247, 112–126. doi:10.1016/j.anifeedsci.2018.11.005.

Laruelle, G. G., Roubeix, V., Sferratore, A., Brodherr, B., Ciuffa, D., Conley, D. J., et al. (2009). Anthropogenic perturbations of the silicon cycle at the global scale: Key role of the land-ocean transition: Global Si Cycle. *Global Biogeochem. Cycles* 23, n/a-n/a. doi:10.1029/2008GB003267.

Lavoie, M., and Raven, J. A. (2020). How can large-celled diatoms rapidly modulate sinking rates episodically? *Journal of Experimental Botany* 71, 3386–3389. doi:10.1093/jxb/eraa129.

Lavoie, M., Raven, J. A., and Levasseur, M. (2016). Energy cost and putative benefits of cellular mechanisms modulating buoyancy in a flagellate marine phytoplankton. *J. Phycol.* 52, 239–251. doi:10.1111/jpy.12390.

Lazarus, D. B., Kotrc, B., Wulf, G., and Schmidt, D. N. (2009). Radiolarians decreased silicification as an evolutionary response to reduced Cenozoic Ocean silica availability. *Proceedings of the National Academy of Sciences* 106, 9333–9338. doi:10.1073/pnas.0812979106.

Lazarus, D., Barron, J., Renaudie, J., Diver, P., and Türke, A. (2014). Cenozoic planktonic marine diatom diversity and correlation to climate change. *PLoS ONE* 9, e84857. doi:10.1371/journal.pone.0084857.

Leblanc, K., Quéguiner, B., Diaz, F., Cornet, V., Michel-Rodriguez, M., Durrieu de Madron, X., et al. (2018). Nanoplanktonic diatoms are globally overlooked but play a role in spring blooms and carbon export. *Nat Commun* 9, 953. doi:10.1038/s41467-018-03376-9.

Leflaive, J., and Ten-Hage, L. (2009). Chemical interactions in diatoms: role of polyunsaturated aldehydes and precursors. *New Phytologist* 184, 794–805. doi:10.1111/j.1469-8137.2009.03033.x.

Legendre, L., and Le Fevre, J. (1989). Hydrodynamic singularities as controls of recycled versus export production in oceans. In Berger. W.H., Smetacek. V.S., and Wefer. G. (eds), Productivity of the oceans: present and Past. Dahlem Konferenzen, Wiley, Chichest..

Li, A., Zhao, X., Duan, G., Anderson, S., and Zhang, X. (2019). Diatom frustule-inspired metamaterial absorbers: the effect of hierarchical pattern arrays. *Adv. Funct. Mater.* 29, 1809029. doi:10.1002/adfm.201809029.

Li, Y., Tarpeh, W. A., Nelson, K. L., and Strathmann, T. J. (2018). Quantitative evaluation of an integrated system for valorization of wastewater algae as bio-oil, fuel gas, and fertilizer products. *Environ. Sci. Technol.* 52, 12717–12727. doi:10.1021/acs.est.8b04035.

Lind, J. L., Heimann, K., Miller, E. A., van Vliet, C., Hoogenraad, N. J., and Wetherbee, R. (1997). Substratum adhesion and gliding in a diatom are mediated by extracellular proteoglycans. *Planta* 203, 213–221. doi:10.1007/s004250050184.

Liu, H., Chen, M., Zhu, F., and Harrison, P. J. (2016). Effect of diatom silica content on copepod grazing, growth and reproduction. *Front. Mar. Sci.* 3. doi:10.3389/fmars.2016.00089.

Lohman, K. E. (1960). The ubiquitous diatom–a brief survey of the present state of knowledge. *American Jouranal od Science.* 258, 180-191. doi:10.3389/fmars.2016.00089.

Lopez, P. J., Desclés, J., Allen, A. E., and Bowler, C. (2005). Prospects in diatom research. *Current Opinion in Biotechnology* 16, 180–186. doi:10.1016/j.copbio.2005.02.002.

Loucaides, S., Van Cappellen, P., Roubeix, V., Moriceau, B., and Ragueneau, O. (2012). Controls on the recycling and preservation of biogenic silica from biomineralization to burial. *Silicon* 4, 7–22. doi:10.1007/s12633-011-9092-9.

Lu, J., Sun, C., and Wang, Q. J. (2015). Mechanical simulation of a diatom frustule structure. *J Bionic Eng* 12, 98–108. doi:10.1016/S1672-6529(14)60104-9.

Lürling, M. (2021). Grazing resistance in phytoplankton. *Hydrobiologia* 848, 237–249. doi:10.1007/s10750-020-04370-3.

Ma, J. F., Tamai, K., Yamaji, N., Mitani, N., Konishi, S., Katsuhara, M., et al. (2006). A silicon transporter in rice. *Nature* 440, 688–691. doi:10.1038/nature04590.

Maher, S., Kumeria, T., Aw, M. S., and Losic, D. (2018). Diatom silica for biomedical applications: recent progress and advances. *Adv. Healthcare Mater.* 7, 1800552. doi:10.1002/adhm.201800552.

Maldonado, M., Carmona, M. C., Uriz, M. J., and Cruzado, A. (1999). Decline in Mesozoic reef-building sponges explained by silicon limitation. *Nature* 401, 785–788. doi:10.1038/44560.

Maliva, R. G., Knoll, A. H., and Siever, R. (1989). Secular change in chert distribution: a reflection of evolving biological participation in the silica cycle. *PALAIOS* 4, 519. doi:10.2307/3514743.

Malviya, S., Scalco, E., Audic, S., Vincent, F., Veluchamy, A., Poulain, J., et al. (2016). Insights into global diatom distribution and diversity in the world's ocean. *Proc Natl Acad Sci USA* 113, E1516–E1525. doi:10.1073/pnas.1509523113.

Margaref, R. (1978). Primary partitioning and storage of photosynthate in sucrose and starch in leaves of C4 plants. *Oceanologica Acta* 1(4), 493-509. doi:10.1007/BF00202661.

Marron, A. O., Ratcliffe, S., Wheeler, G. L., Goldstein, R. E., King, N., Not, F., et al. (2016). The evolution of silicon transport in eukaryotes. *Mol Biol Evol* 33, 3226–3248. doi:10.1093/molbev/msw209.

Martin-Jezequel, V., Hildebrand, M., and Brzezinski, M. A. (2000). Silicon metabolism in diatoms: implications for growth. *J Phycol* 36, 821–840. doi:10.1046/j.1529-8817.2000.00019.x.

Mayers, K. M. J., Poulton, A. J., Bidle, K., Thamatrakoln, K., Schieler, B., Giering, S. L. C., et al. (2020). The possession of coccoliths fails to deter microzooplankton grazers. *Front. Mar. Sci.* 7, 569896. doi:10.3389/fmars.2020.569896.

Mayzel, B., Aram, L., Varsano, N., Wolf, S. G., and Gal, A. (2021). Structural evidence for extracellular silica formation by diatoms. *Nat Commun* 12, 4639. doi:10.1038/s41467-021-24944-6.

Medarevic, D., Losic, D., and Ibric, S. (2016). Diatoms-nature materials with great potential for bio-applications. *Hem Ind* 70, 613–627. doi:10.2298/HEMIND150708069M.

Medlin, L. K. (2015). A timescale for diatom evolution based on four molecular markers: reassessment of ghost lineages and major steps defining diatom evolution. *Vie Milieu*, 20.

Meyerink, S., Ellwood, M. J., Maher, W. A., and Strzepek, R. (2017). Iron availability influences silicon isotope fractionation in two Southern Ocean diatoms (*Proboscia inermis* and *Eucampia antarctica*) and a Coastal Diatom (*Thalassiosira pseudonana*). *Front. Mar. Sci.* 4, 217. doi:10.3389/fmars.2017.00217.

Miklasz, K. A., and Denny, M. W. (2010). Diatom sinkings speeds: Improved predictions and insight from a modified Stokes' law. *Limnol. Oceanogr.* 55, 2513–2525. doi:10.4319/lo.2010.55.6.2513.

Miller, C. B., Nelson, D. M., Weiss, C., and Soeldner, A. H. (1990). Morphogenesis of opal teeth in calanoid copepods. *Mar. Biol.* 106, 91–101. doi:10.1007/BF02114678.

Milligan, A. J., and Morel, F. M. M. (2002). A proton buffering role for silica in diatoms. *Science* 297, 1848–1850. doi:10.1126/science.1074958.

Milligan, A. J., Varela, D. E., Brzezinski, M. A., and Morel, F. M. M. (2004). Dynamics of silicon metabolism and silicon isotopic discrimination in a marine diatomas a function of pCO $_2$. *Limnol. Oceanogr.* 49, 322–329. doi:10.4319/lo.2004.49.2.0322.

Misra, A. N., Misra, M., Singh, R., (2012). Chlorophyll Fluorescence in Plant Biology. Biophysics. 49, 322–329. doi:10.4319/lo.2004.49.2.0322.

Mojiri, A., Baharlooeian, M., Kazeroon, R. A., Farraji, H., and Lou, Z. (2020). Removal of pharmaceutical micropollutants with integrated biochar and marine microalgae. *Microorganisms* 9, 4. doi:10.3390/microorganisms9010004.

Moller, E. F., Nielsen, T. G. (2001). Production of bacterial substrate by marine copepods: effect of phytoplankton biomass and cell size. *Journal of Plankton Research* 23, 527–536. doi:10.1093/plankt/23.5.527.

Moller, E. F. (2004). Sloppy feeding in marine copepods: prey-size-dependent production of dissolved organic carbon. *Journal of Plankton Research* 27, 27–35. doi:10.1093/plankt/fbh147.

Monod, J. (1949) The growth of bacterial cultures. Annu. Rev. Microbiol. 3: 371-394

Montsant, A., Jabbari, K., Maheswari, U., and Bowler, C. (2005). Comparative genomics of the pennate diatom *Phaeodactylum tricornutum*. *Plant Physiology* 137, 500–513. doi:10.1104/pp.104.052829.

Moreno, M. D., Ma, K., Schoenung, J., and Dávila, L. P. (2015). An integrated approach for probing the structure and mechanical properties of diatoms: Toward engineered nanotemplates. *Acta Biomaterialia* 25, 313–324. doi:10.1016/j.actbio.2015.07.028.

Moriceau, B., Garvey, M., Ragueneau, O., and Passow, U. (2007). Evidence for reduced biogenic silica dissolution rates in diatom aggregates. *Mar. Ecol. Prog. Ser.* 333, 129–142. doi:10.3354/meps333129.

Morozov, A. A., Galachyants, Y. P. (2019). Diatom genes originating from red and green algae: implications for the secondary endosymbiosis models. *Marine genomics* 45, 72-78. doi:10.1016/j.margen.2019.02.003.

Mourelle, M., Gómez, C., and Legido, J. (2017). The potential use of marine microalgae and cyanobacteria in cosmetics and thalassotherapy. *Cosmetics* 4, 46. doi:10.3390/cosmetics4040046.

Mosseri, J., Quéguiner, B., Armand, L., and Cornet-Barthaux, V. (2008). Impact of iron on silicon utilization by diatoms in the Southern Ocean: A case study of Si/N cycle decoupling in a naturally iron-enriched area. *Deep Sea Research Part II: Topical Studies in Oceanography* 55, 801–819. doi:10.1016/j.dsr2.2007.12.003.

Naselli-Flores, L., and Barone, R. (2011). Fight on plankton! or, Phytoplankton shape and size as adaptive tools to get ahead in the struggle for life. *Cryptogamie, Algologie* 32, 157–204. doi:10.7872/crya.v32.iss2.2011.157.

Naselli-Flores, L., Zohary, T., and Padisák, J. (2021). Life in suspension and its impact on phytoplankton morphology: an homage to Colin S. Reynolds. *Hydrobiologia* 848, 7–30. doi:10.1007/s10750-020-04217-x.

Noyes, J., Sumper, M., and Vukusic, P. (2008). Light manipulation in a marine diatom. *J. Mater. Res.* 23, 3229–3235. doi:10.1557/JMR.2008.0381.

Olsen, S., and Paasche, E. (1986). Variable kinetics of silicon-limited growth in *Thalassiosira pseudonana* (Bacillariophyceae) in response to changed chemical composition of the growth medium. *British Phycological Journal* 21, 183–190. doi:10.1080/00071618600650211.

Opfergelt, S., Cardinal, D., Henriet, C., Draye, X., André, L., and Delvaux, B. (2006). Silicon isotopic fractionation by banana (*Musa* spp.) grown in a continuous nutrient flow device. *Plant Soil* 285, 333–345. doi:10.1007/s11104-006-9019-1.

Pahlow, M., Riebesell, U., and Wolf-Gladrow, D. A. (1997). Impact of cell shape and chain formation on nutrient acquisition by marine diatoms. *Limnol. Oceanogr.* 42, 1660–1672. doi:10.4319/lo.1997.42.8.1660.

Palmucci, M., Ratti, S., and Giordano, M. (2011). Ecological and evolutionary implications of carbon allocation in marine phytoplankton as a function of nitrogen availability: a fourier transform infrared spectroscopy approach1: c allocation as a function of n availability. *Journal of Phycology* 47, 313–323. doi:10.1111/j.1529-8817.2011.00963.x.

Panagiotopoulos, C., Goutx, M., Suroy, M., and Moriceau, B. (2020). Phosphorus limitation affects the molecular composition of *Thalassiosira weissflogii* leading to increased biogenic silica dissolution and high degradation rates of cellular carbohydrates. *Organic Geochemistry* 148, 104068. doi:10.1016/j.orggeochem.2020.104068.

Pančić, M., and Kiørboe, T. (2018). Phytoplankton defence mechanisms: traits and trade-offs: Defensive traits and trade-offs. *Biol Rev* 93, 1269–1303. doi:10.1111/brv.12395.

Pančić, M., Torres, R. R., Almeda, R., and Kiørboe, T. (2019). Silicified cell walls as a defensive trait in diatoms. *Proc. R. Soc. B.* 286, 20190184. doi:10.1098/rspb.2019.0184.

Passow, U., and Carlson, C. (2012). The biological pump in a high CO_2 world. *Mar. Ecol. Prog. Ser.* 470, 249–271. doi:10.3354/meps09985.

Pinkerton, M. H., Boyd, P. W., Deppeler, S., Hayward, A., Höfer, J., and Moreau, S. (2021). Evidence for the impact of climate change on primary producers in the Southern Ocean. *Front. Ecol. Evol.* 9, 592027. doi:10.3389/fevo.2021.592027.

Petrucciani, A., Chaerle, P., and Norici, A. (2022). Diatoms versus copepods: could frustule traits have a role in avoiding predation? *Front. Mar. Sci.* 8, 804960. doi:10.3389/fmars.2021.804960.

Peterson, G. L. (1977). A simplification of the protein assay method of Lowry et al. which is more generally applicable. Analytical Biochemistry 83, 2, 346-356. doi:10.1016/0003-2697(77)90043-4.

Pondaven, P., Gallinari, M., Chollet, S., Bucciarelli, E., Sarthou, G., Schultes, S., et al. (2007). Grazing-induced changes in cell wall silicification in a marine diatom. *Protist* 158, 21–28. doi:10.1016/j.protis.2006.09.002.

Pudney, A., Gandini, C., Economou, C. K., Smith, R., Goddard, P., Napier, J. A., et al. (2019). Multifunctionalizing the marine diatom *Phaeodactylum tricornutum* for sustainable co-production of omega-3 long chain polyunsaturated fatty acids and recombinant phytase. *Sci*

Rep 9, 11444. doi:10.1038/s41598-019-47875-1.

Qin, T., Gutu, T., Jiao, J., Chang, C.-H., and Rorrer, G. L. (2008). Photoluminescence of silica nanostructures from bioreactor culture of marine diatom *Nitzschia frustulum*. *J. nanosci. Nanotechnol.* 8, 2392–2398. doi:10.1166/jnn.2008.241.

Rabosky, D. L., and Sorhannus, U. (2009). Diversity dynamics of marine planktonic diatoms across the Cenozoic. *Nature* 457, 183–186. doi:10.1038/nature07435.

Racki, G.; Cordey, F. (2000). Radiolarian palaeoecology and radiolarites: is the present the key to the past? *Earth-Science Reviews* 52, 83–120. doi:10.1016/S0012-8252(00)00024-6.

Ragueneau, O., Schultes, S., Bidle, K., Claquin, P., and Moriceau, B. (2006). Si and C interactions in the world ocean: Importance of ecological processes and implications for the role of diatoms in the biological pump: Si and C interactions in the ocean. *Global Biogeochem. Cycles* 20, n/a-n/a. doi:10.1029/2006GB002688.

Ratti, S., Knoll, A. H., and Giordano, M. (2011). Did sulfate availability facilitate the evolutionary expansion of chlorophyll a+c phytoplankton in the oceans? Sulfate and evolution of chlorophyll a+c phytoplankton. *Geobiology* 9, 301–312. doi:10.1111/j.1472-4669.2011.00284.x.

Ratti, S., Knoll, A. H., and Giordano, M. (2013). Grazers and phytoplankton growth in the oceans: an experimental and evolutionary perspective. *PLoS ONE* 8, e77349. doi:10.1371/journal.pone.0077349.

Raven, J. A., and Doblin, M. A. (2014). Active water transport in unicellular algae: where, why, and how. *Journal of Experimental Botany* 65, 6279–6292. doi:10.1093/jxb/eru360.

Raven, J. A., and Waite, A. M. (2004). The evolution of silicification in diatoms: inescapable sinking and sinking as escape? *New Phytologist* 162, 45–61. doi:10.1111/j.1469-8137.2004.01022.x.

Reid, A., Buchanan, F., Julius, M., and Walsh, P. J. (2021). A review on diatom biosilicification and their adaptive ability to uptake other metals into their frustules for potential application in bone repair. *J. Mater. Chem. B* 9, 6728–6737. doi:10.1039/D1TB00322D.

Reinke, D. C. (1984). Ultrastructure of *Chaetoceros muelleri* (bacillariophyceae): auxospore, resting spore and vegetative cell morphology. *J.Phycology 20*, 153-155. doi:10.1111/j.0022-3646.1984.00153.x.

Reimann, B.E.F., Lewin, J.C., and Volcani, B.E. (1965). Studies on the biochemistry and fine structure of silica shell formation in diatoms: I. The structure of the cell wall of *Cylindrotheca fusiformis*. *The Journal of Cell Biology 24, 39-55*. doi: 10.1083/jcb.24.1.39

Renaudie, J. (2016) Quantifying the Cenozoic marine diatom deposition history: links to the C and Si cycles. Biogeosciences 13, 6003–6014, doi:10.5194/bg-13-6003

Reynolds, C. S. (2006). The ecology of phytoplankton. Cambridge University Press. doi:10.1017/CBO9780511542145.

Riebesell, U., Burkhardt, S., Dauelsberg, A., and Kroon, B. (2000). Carbon isotope fractionation by a marine diatom: dependence on the growth-rate-limiting resource. *Mar. Ecol. Prog. Ser.*

193, 295–303. doi:10.3354/meps193295.

Ritchie, R. J. (2006). Consistent sets of spectrophotometric chlorophyll equation for acetone, methanol, and ethanol solvents. *Photosynthesis Research* 89, 27-41 doi:10.1007/s11100-006-9065-9.

Rogato, A., and De Tommasi, E. (2020). Physical, chemical, and genetic techniques for diatom frustule modification: applications in nanotechnology. *Applied Sciences* 10, 8738. doi:10.3390/app10238738.

Romann, J., Valmalette, J.-C., Chauton, M. S., Tranell, G., Einarsrud, M.-A., and Vadstein, O. (2015). Wavelength and orientation dependent capture of light by diatom frustule nanostructures. *Sci Rep* 5, 17403. doi:10.1038/srep17403.

Round, F. E., Crawford, R. M., and Mann, D. G., (1990). The diatoms. Biology and morphology of the genera. Cambridge University Press.

Roy, S., Harris, R., and Poulet, S. (1989). Inefficient feeding by *Calanus helgolandicus* and *Temora longicornis* on *Coscinodiscus wailesii*: quantitative estimation using chlorophyll-type pigments and effects on dissolved free amino acids. *Mar. Ecol. Prog. Ser.* 52, 145–153. doi:10.3354/meps052145.

Roubeix, V., Becquevort, S., and Lancelot, C. (2008). Influence of bacteria and salinity on diatom biogenic silica dissolution in estuarine systems. *Biogeochemistry* 88, 47–62. doi:10.1007/s10533-008-9193-8.

Ryabov, A., Kerimoglu, O., Litchman, E., Olenina, I., Roselli, L., Basset, A., et al. (2021). Shape matters: the relationship between cell geometry and diversity in phytoplankton. *Ecology Letters* 24, 847–861. doi:10.1111/ele.13680.

Ryderheim, F., Grønning, J., and Kiørboe, T. (2022). Thicker shells reduce copepod grazing on diatoms. *Limnol Oceanogr Letters*, lol2.10243. doi:10.1002/lol2.10243.

Saad, E. M., Pickering, R. A., Shoji, K., Hossain, M. I., Glover, T. G., Krause, J. W., et al. (2020). Effect of cleaning methods on the dissolution of diatom frustules. *Marine Chemistry* 224, 103826. doi:10.1016/j.marchem.2020.103826.

Sardo, A., Orefice, I., Balzano, S., Barra, L., and Romano, G. (2021). Potential of diatom-derived silica for biomedical applications. *Applied Sciences* 11, 4533. doi:10.3390/app11104533.

Siever, R. (1992). The silica cycle in the Precambrian. *Geochimica et Cosmochimica Acta* 56, 3265–3272. doi:10.1016/0016-7037(92)90303-Z.

Sengupta, A., Carrara, F., and Stocker, R. (2017). Phytoplankton can actively diversify their migration strategy in response to turbulent cues. *Nature* 543, 555–558. doi:10.1038/nature21415.

Shaw, B. A., Andersen, R. J., and Harrison, P. J. (1995). Feeding deterrence properties of apo-fucoxanthinoids from marine diatoms. I. Chemical structures of apo-fucoxanthinoids produced by *Phaeodactylum tricornutum*. *Marine Biology* 124, 467–472. doi:10.1007/BF00363921.

Shaw, B. A., Andersen, R. J., and Harrison, P. J. (1997). Feeding deterrent and toxicity effects of

apo-fucoxanthinoids and phycotoxins on a marine copepod (*Tigriopus californicus*). *Marine Biology* 128, 273–280. doi:10.1007/s002270050092.

Shaw, B. A., Harrison, P. J., and Andersen, R. J. (1994). Evaluation of the copepod *Tigriopus californicus* as a bioassay organism for the detection of chemical feeding deterrents produced by marine phytoplankton. *Marine Biology* 121, 89–95. doi:10.1007/BF00349477.

Shaw, B. A., Harrison, P. J., and Andersen, R. J. (1995). Feeding deterrence properties of apo-fucoxanthinoidsfrom marine diatoms. II. Physiology of production of apo-fucoxanthinoids by the marine diatoms *Phaeodactylum tricornutum* and *Thalassiosira pseudonana*, and their feeding deterrent effects on the copepod *Tigriopus californicus*. *Marine Biology* 124, 473-481.

Shrestha, R. P., and Hildebrand, M. (2015). Evidence for a regulatory role of diatom silicon transporters in cellular silicon responses. *Eukaryot Cell* 14, 29–40. doi:10.1128/EC.00209-14.

Shrestha, R. P., Tesson, B., Norden-Krichmar, T., Federowicz, S., Hildebrand, M., and Allen, A. E. (2012). Whole transcriptome analysis of the silicon response of the diatom *Thalassiosira pseudonana*. *BMC Genomics* 13, 499. doi:10.1186/1471-2164-13-499.

Smayda, T. Y. (1970). The suspension and sinking of phytoplankton in the sea. *Oceanogr. Mar. Biol. Ann. Rev.* 8, 353-414.

Smetacek, V. (2001). A watery arms race. *Nature* 411, 745. doi:10.1038/35081210.

Su, Y., Lundolm, M., and Legaard, M. (2018). The effect of different light regimes on diatom frustule silicon concentration. *Algal Research* 29, 36-40. doi:10.1016/j.algal.2017.11.014.

Suroy, M., Panagiotopoulos, C., Boutorh, J., Goutx, M., Moriceau, B. (2015). Degradation of diatom carbohydrates: A case study with N- and Si-stressed Thalassiosira weissflogii, Journal of Experimental Marine Biology and Ecology 470, 1-11.doi:10.1016/j.jembe.2015.04.018.

Sutton, J. N., André, L., Cardinal, D., Conley, D. J., de Souza, G. F., Dean, J., et al. (2018). A review of the stable isotope bio-geochemistry of the global silicon cycle and its associated trace elements. *Front. Earth Sci.* 5, 112. doi:10.3389/feart.2017.00112.

Svetličić, V., Žutić, V., Pletikapić, G., and Radić, T. (2013). Marine polysaccharide networks and diatoms at the nanometric scale. *IJMS* 14, 20064–20078. doi:10.3390/ijms141020064.

Takeda, S. (1998). Influence of iron availability on nutrient consumption ratio of diatoms in oceanic waters. *Nature* 393, 774–777. doi:10.1038/31674.

Tamburini, C., Garcin, J., Grégori, G., Leblanc, K., Rimmelin, P., and Kirchman, D. (2006). Pressure effects on surface Mediterranean prokaryotes and biogenic silica dissolution during a diatom sinking experiment. *Aquat. Microb. Ecol.* 43, 267–276. doi:10.3354/ame043267.

Tammilehto, A., Nielsen, T. G., Krock, B., Møller, E. F., and Lundholm, N. (2014). Induction of domoic acid production in the toxic diatom *Pseudo-nitzschia* seriata by calanoid copepods. *Aquatic Toxicology* 159, 52–61. doi:10.1016/j.aquatox.2014.11.026.

Terracciano, M., De Stefano, L., and Rea, I. (2018). Diatoms green nanotechnology for biosilica-

based drug delivery systems. *Pharmaceutics* 10, 242. doi:10.3390/pharmaceutics10040242.

Tesson, B., Lerch, S. J. L., and Hildebrand, M. (2017). Characterization of a new protein family associated with the silica deposition vesicle membrane enables genetic manipulation of diatom silica. *Sci Rep* 7, 13457. doi:10.1038/s41598-017-13613-8.

Thamatrakoln, K. (2021). Diatom ecophysiology: crossing signals on the road to recovery from nutrient deprivation. *Current Biology* 31, R253–R254. doi:10.1016/j.cub.2021.01.016.

Thamatrakoln, K., Alverson, A. J., and Hildebrand, M. (2006). Comparative sequence analysis of diatom silicon transporters: toward a mechanistic model of silicon transport. *Journal of Phycology* 42, 822–834. doi:10.1111/j.1529-8817.2006.00233.x.

Thamatrakoln, K., and Hildebrand, M. (2008). Silicon uptake in diatoms revisited: a model for saturable and nonsaturable uptake kinetics and the role of silicon transporters. *Plant Physiol.* 146, 1397–1407. doi:10.1104/pp.107.107094.

Tong, C. Y., and Derek, C. J. C. (2021). The role of substrates towards marine diatom *Cylindrotheca fusiformis* adhesion and biofilm development. *J Appl Phycol* 33, 2845–2862. doi:10.1007/s10811-021-02504-1.

Toster, J., Iyer, K. S., Xiang, W., Rosei, F., Spiccia, L., and Raston, C. L. (2013). Diatom frustules as light traps enhance DSSC efficiency. *Nanoscale* 5, 873–876. doi:10.1039/C2NR32716C.

Tréguer, P., Bowler, C., Moriceau, B., Dutkiewicz, S., Gehlen, M., Aumont, O., et al. (2018). Influence of diatom diversity on the ocean biological carbon pump. *Nature Geosci* 11, 27–37. doi:10.1038/s41561-017-0028-x.

Tréguer, P. J., Sutton, J. N., Brzezinski, M., Charette, M. A., Devries, T., Dutkiewicz, S., et al. (2021). Reviews and syntheses: The biogeochemical cycle of silicon in the modern ocean. *Biogeosciences* 18, 1269–1289. doi:10.5194/bg-18-1269-2021.

Trower, E. J., Strauss, J. V., Sperling, E. A., and Fischer, W. W. (2021). Isotopic analyses of Ordovician–Silurian siliceous skeletons indicate silica-depleted Palaeozoic oceans. *Geobiology* 19, 460–472. doi:10.1111/gbi.12449.

Truesdale, V. W. (2011). Generic issues of batch dissolution exemplified by gypsum rock. Aquatic Geochemistry 17, 21-50. doi:10.1007/s10498-010-9105-0.

Turner, J. T. (2004). The importance of small planktonic copepods and their roles in pelagic marine food webs. *Zoological Studies*, 12.

Umemura, K., Noguchi, Y., Ichinose, T., Hirose, Y., and Mayama, S. (2010). Morphology and physical-chemical properties of baked nanoporous frustules. *J. Nanosci. Nanotech.* 10, 5220–5224. doi:10.1166/jnn.2010.2400.

Vallina, S. M., Follows, M. J., Dutkiewicz, S., Montoya, J. M., Cermeno, P., and Loreau, M. (2014). Global relationship between phytoplankton diversity and productivity in the ocean. *Nat Commun* 5, 4299. doi:10.1038/ncomms5299.

Van Bennekom, A. J., Buma, A. G. J., and Nolting, R. F. (1991). Dissolved aluminium in the Weddell-Scotia Confluence and effect of Al on the dissolution kinetics of biogenic silica. *Marine Chemistry* 35, 423–434. doi:10.1016/S0304-4203(09)90034-2.

Vidussi, F., Claustre, H., Manca, B. B., Luchetta, A., and Marty, J.-C. (2001). Phytoplankton pigment distribution in relation to upper thermocline circulation in the eastern Mediterranean Sea during winter. *J. Geophys. Res.* 106, 19939–19956. doi:10.1029/1999JC000308.

Vincent, F., and Bowler, C. (2020). Diatoms are selective segregators in global ocean planktonic communities. *mSystems* 5. doi:10.1128/mSystems.00444-19.

Vona, D., Ragni, R., Altamura, E., Albanese, P., Giangregorio, M. M., Cicco, S. R., et al. (2021). Light-emitting biosilica by in vivo functionalization of *Phaeodactylum tricornutum* diatom microalgae with organometallic complexes. *Applied Sciences* 11, 3327. doi:10.3390/app11083327.

Vrieling, E. G., Sun, Q., Tian, M., Kooyman, P. J., Gieskes, W. W. C., van Santen, R. A., et al. (2007). Salinity-dependent diatom biosilicification implies an important role of external ionic strength. *Proceedings of the National Academy of Sciences* 104, 10441–10446. doi:10.1073/pnas.0608980104.

Vuorio, K., Meili, M., and Sarvala, J. (2006). Taxon-specific variation in the stable isotopic signatures ($\delta^{13}C$ and $\delta^{15}N$) of lake phytoplankton. *Freshwater Biol* 51, 807–822. doi:10.1111/j.1365-2427.2006.01529.x.

Waite, A. M., Thompson, P. A., and Harrison, P. J. (1992). Does energy control the sinking rates of marine diatoms? *Limnol. Oceanogr.* 37, 468–477. doi:10.4319/lo.1992.37.3.0468.

Waite, A., Fisher, A., Thompson, P., and Harrison, P. (1997). Sinking rate versus cell volume relationships illuminate sinking rate control mechanisms in marine diatoms. *Mar. Ecol. Prog. Ser.* 157, 97–108. doi:10.3354/meps157097.

Walsby, A. E., and Holland, D. P. (2006). Sinking velocities of phytoplankton measured on a stable density gradient by laser scanning. *J. R. Soc. Interface.* 3, 429–439. doi:10.1098/rsif.2005.0106.

Wang, J., Cao, S., Du, C., and Chen, D. (2013). Underwater locomotion strategy by a benthic pennate diatom Navicula sp. *Protoplasma* 250, 1203–1212. doi:10.1007/s00709-013-0502-2.

Westacott, S., Planavsky, N. J., Zhao, M.Y., Hull, P. M. (2021). Revisiting the sedimentary record of the rise of diatoms. PNAS 118 (27) e2103517118. doi:10.1073/pnas.2103517118

Wellburn, A. R. (1994). The Spectral Determination of Chlorophylls a and b, as well as Total Carotenoids, Using Various Solvents with Spectrophotometers of Different Resolution. Journal of Plant Physiology 144, 3, 307-313. doi:10.1016/S0176-1617(11)81192-2.

Wenzl, S., Hett, R., Richthammer, P., and Sumper, M. (2008). Silacidins: highly acidic phosphopeptides from diatom shells assist in silica precipitation in vitro. *Angew. Chem. Int. Ed.* 47, 1729–1732. doi:10.1002/anie.200704994.

Woods, S., and Villareal, T. A. (2008). Intracellular ion concentrations and cell sap density in positively buoyant oceanic phytoplankton. *Nova Hedwigia Beihefte* 133, 131–145. doi:10.1002/anie.200704994.

Worden, A. Z., Follows, M. J., Giovannoni, S. J., Wilken, S., Zimmerman, A. E., and Keeling, P. J.

(2015). Rethinking the marine carbon cycle: Factoring in the multifarious lifestyles of microbes. *Science* 347, 1257594. doi:10.1126/science.1257594.

Xu, H., Shi, Z., Zhang, X., Pang, M., Pan, K., and Liu, H. (2021b). Diatom frustules with different silica contents affect copepod grazing due to differences in the nanoscale mechanical properties. *Limnol Oceanogr* 66, 3408–3420. doi:10.1002/lno.11887.

Zachos, J. C., Dickens, G. R., and Zeebe, R. E. (2008). An early Cenozoic perspective on greenhouse warming and carbon-cycle dynamics. *Nature* 451, 279–283. doi:10.1038/nature06588.

Zhang, S., Liu, H., Ke, Y., and Li, B. (2017). Effect of the silica content of diatoms on protozoan grazing. *Front. Mar. Sci.* 4, 202. doi:10.3389/fmars.2017.00202.

Attached Material

Training Courses

1. Agouron Advanced Geobiology Field School

Caltech Division of Geological and Planetary Sciences
Office of the Chair

John P. Grotzinger
1200 E. California Blvd.
MC 170-25
Pasadena, CA 91125
(626) 395-6108

September 23, 2019

To Whom It May Concern:

I am writing this note on behalf of Ms. Alessandra Petrucciani who was a student in our Advanced Geobiology Field School this summer in Italy. With little background in the field of Geology, Alessandra was excellent at learning, and also engaging. She picked up on important concepts quickly, and was able to work alongside students with far more experience. Alessandra was also excellent at interacting with the other students in the course, and these interactions were important for generating a synthesis of the observations and integration with other working groups.

Alessandra spent 9 days in the field and worked 8 hours each day. The days were long and sometimes hot, but she worked as hard as everyone else in the group. All of the instructors were very impressed with her curiosity, ability, and enthusiasm. I would happily have her attend another of our courses.

Sincerely,

John P. Grotzinger
Ted and Ginger Jenkins Leadership Chair, Division of Geological and Planetary Sciences
Fletcher Jones Professor of Geology

2. 26 – 27 November 2019 –Training of INSPIRE software package (Amnis Corp.) for Imaging Cytofluorimeter FlowSight®

3. Small Private Online Course 'Silica School: from stardust to the living world' (2021) 60 hours of online coursework (held by University of Brest)

CERTIFICATE OF COURSE COMPLETION
Small Private Online Course
Silica School 2021

Ms. **Alessandra Petrucciani**
Institution **Università Politecnica delle Marche**

successfully followed the Small Private Online Course ***'Silica School: from stardust to the living world'*** (2021) and completed a total of **60 hours** of online coursework.

Date and signature of the Silica School coordinator

08-12-2021

Jill Sutton, Associate Professor
Université de Bretagne Occidentale

**This certificate is not a diploma and does not confer credits (ECTS) and does not certify that the participant was registered at the Université de Bretagne Occidentale.*

Involvement in Third Mission actions

Elaboration of the idea of an informative video on risk communication entitled “Dove comincia il mare?”. Progetto Regionale PANDORA “AggregAzione 3a edizione”.

Associazione Culturale
NEXT

Oggetto: *Progetto PANDORA*

Gentile Prof. Paolo Mariani,
L'Università Politecnica della Marche ha preso parte al progetto Regionale PANDORA, finanziato nell'ambito del bando: "AggregAzione 3a edizione"

Hanno partecipato alle riunioni di progetto e hanno elaborato l'idea di un video successivamente realizzata dall'artista Jacopo Sacquegno per una delle postazioni del container itinerante del progetto:

Luca Marisaldi
Deborah D'Angelo
Giulia Merli
Lucia Ventura
Alessandra Petrucciani
Giulia Lucia
Chiara Gregorin
Francesca Caridi
Carola Mazzoli

L'attività si è svolta da marzo a maggio 2021 per un totale complessivo di 20 ore di attività.

Senigallia, 23 settembre 2021

Il presidente
Alessandro Gnucci

Associazione Culturale NEXT - Via Venezia 33a Senigallia (AN)- P.I. e C..F. 02623830425 - info@fosforoscienza.it
www.fosforoscienza.it

Period spent abroad

Assemble Transnational Access at Ghent University and Flanders Marine Institute, Belgium

Project Leader of Grant 730984, Assemble Plus 3rd call

ASSEMBLE

Transnational Access – Confirmation of Access

Ghent University
Krijgslaan 281/S8, 9000 Gent
Flanders Marine Institute –
Marine Station Ostend (VLIZ)
Wandelaarkaai 7, 8400
OOSTENDE

Alessandra Petrucciani
Università Politecnica delle Marche

I, Marleen Roelofs, Andre Cattrijsse herewith confirm that the following Project was carried out at the University /of Gent and Flanders marine institute in the context of ASSEMBLE Plus Transnational Access:

DIGRAE – 730984 ASSEMBLE Plus– 3rd call

Role	Name	Home Institution	Country	Duration of TA (start - end date)
Project Leader	Alessandra Petrucciani	Università Politecnica delle Marche	Italy	31/08/2019 25/09/2019
2nd User	Alessandra Norici	Università Politecnica delle Marche	Italy	08/09/2019 15/09/2019

The amount of Access delivered to the User Group is as follows:

Installation	Unit of access	On-site/ Remote	Unit of access delivered
Diatoms Culture Collection BCCM/DCG	16 days	On - site	16 days
Imaging Flow Cytometer ImageStream^{X} Mark II	11 days	On - site	11 days
Vessel RV Simon Stevin and plankton sampling equipment	3 days	On - site	3 days

Gent, 25/09/2019
Location and date

Alessandra Petrucciani

Name and signature of Project Leader

Gent, 29/09/2019
Location and date

Marleen Roelofs and Andre Cattrijsse

Name and signature of the Person in charge or Liaison Officer at the Access Provider

[1]The document should be named "<User Project number>_Confirmation_of_Access.pdf" and must be sent with the document name in the subject to the Access Office (assembleplus_ta@embrc.eu) by the Person in Charge or Liaison Officer at the end of the TA and no later than 30 days after the TA Period.

This project has received funding from the European Union's Horizon 2020 research and innovation programme under grant agreement No 730984. This output reflects the views only of the author(s), and the European Union cannot be held responsible for any use which may be made of the information contained therein.

Contributions to conferences

1. 12 November 2021 – Catania - Riunione Scientifica annuale del Gruppo di lavoro per l'Algologia della società botanica italiana

Oral presentation entitled "Luce e Silicizzazione: la luce è coinvolta nella deposizione di Si nel frustulo e nella capacità di affondamento di diatomee con diversa morfologia?"

2. 12 – 15 October 2021 – SILICAMICS 3 – Biogeochemistry and genomics of silicifications and silicifiers

Oral presentation entitled:" Light and Silicification: is light affecting Si deposition and sinking capacity in morphologically different diatoms?"

Contribution to the oral presentation entitled "The potential role of Si decline in diatoms radiation: physiological response of morphologically different diatoms to reconstructed paleoenvironments"

Brest, December, 17th, 2021

Professor emeritus Paul Tréguer

To : Alessandra Petrucciani
Università Politecnica delle Marche - UnivPM

***Subject** : Silicamics 3 conference: participation*

Dear Alessandra Petrucciani,

I duely certify your participation in the on-line Silicamics 3 conference titled "Biogeochemistry and genomics of silicification and silicifiers " which was held from 12 to 15 October 2021.

Sicerely yours,

Professor emeritus professor Paul Tréguer

Paul Tréguer is doctor es sciences (oceanography) of the Université de Bretagne Occidentale (1976). He is a marine biogeochemist, whose major contributions to marine sciences deal with the circulation of nutrients in the world ocean, with a focus on the polar and coastal oceans. Founder of the European Institute for Marine Studies and of the Europole Mer, he directed the European Network of Excellence on the impacts of global change on marine ecosystems and on marine biogeochemistry. He has published > 100 manuscripts in peer-reviewed journals. Recipient of the Georges Millot (2013) medal of the French Academy of Sciences, he is fellow and member of the Presidium of the European Academy of Sciences, fellow of the American Geophysical Union, fellow of the Association for Sciences Oceanography and Limnology, and Officer of the Legion of Honour. He presently is distinguished ocean star scholar at the Second Institute of Oceanography, Hongzhou (China).

INSTITUT UNIVERSITAIRE EUROPEEN DE LA MER
Rue Dumont D'Urville – Technopôle Brest-Iroise ☎ 33 (0)2 98 49 86 00
29280 PLOUZANE – FRANCE Internet http://www-iuem.univ-brest.fr/

3. 12 – 14 July 2021 – Molecular life of diatoms

E-poster entitled: “The evolution of morphology in diatoms: assessment of grazing pressure in long-term speciation”

4. 29 – 30 April 2021 – XVII PhD day of CIRCC (interuniversity consortium of chemical reactivity and catalysis)

Oral presentation entitled: “Biosilica from diatoms: factors influencing Si deposition in frustules”

XVII PhD Day

Venezia, 29-30 Aprile 2021

WEBINAR

ATTESTATO DI PARTECIPAZIONE

Si attesta che la **Dott.ssa Alessandra Petrucciani** ha partecipato al XVII PhD Day del giorno 29-30 Aprile 2021 ed ha presentato la relazione dal titolo “*Biosilica from diatoms: factors influencing Si deposition in frustules*”.

Bari, 30 Aprile 2021

Il Direttore
Prof.ssa Angela Dibenedetto

SEGRETERIA AMMINISTRATIVA E SEDE LEGALE:
via Celso Ulpiani, 27 - 70126 Bari
Tel. 0805442430 - fax 0805442429 e-mail: circc@uniba.it
Sito Internet: www.circc.it

5. 22 – 26 March 2021 – International Phycological Congress

Oral presentation entitled: “The evolution of morphology in diatoms: assessment of selective pressure that have shaped their long-term speciation”.

12th INTERNATIONAL PHYCOLOGICAL CONGRESS
22-26 March 2021, Chile

IPS

We hereby certify that

ALESSANDRA PETRUCCIANI

Participated in the 12th International Phycological Congress, IPC2021, with the Oral Presentation entitled
THE EVOLUTION OF MORPHOLOGY IN DIATOMS: ASSESSMENT OF SELECTIVE PRESSURES THAT HAVE SHAPED THEIR LONG-TERM SPECIATION
The 12th IPC2021 was held as a fully virtual Congress on 22 – 26 March, 2021.
www.ipc2021.com

Dr. Alejandro Buschmann
Convener
Local Organizing Committee
12th IPC2021

Chile – March 2021

Dr. Olivier De Clerck
Chairman
Scientific Committee
12th IPC2021

Conferences attended

ASSEMBLE

ASSOCIATION OF EUROPEAN MARINE BIOLOGICAL LABORATORIES EXPANDED

ASSEMBLE 2021: Online Conference

Marine biological research at the frontier

18TH - 29TH JANUARY 2021

CERTIFICATE OF ATTENDANCE

We hereby certify that

ALESSANDRA PETRUCCIANI

attended the online conference **Assemble 2021: Marine biological research at the frontier**, that took place between 18th and 29th of January 2021, organized by EMBRC.EU and Centre of Marine Sciences of Algarve (CCMAR Algarve).

Adelino Vicente Mendonça Canário
Scientific Local Organizer
Assemble 2021 Conference

EMBRC

CCMAR Algarve

UAlg

Publications on international journals

1. **Petrucciani A.**, Chaerle P., Norici A. (2022) " Diatoms versus copepods: could frustule traits have a role in avoiding predation?" *Frontiers in Marine Science* (doi.org/10.3389/fmars.2021.804960)

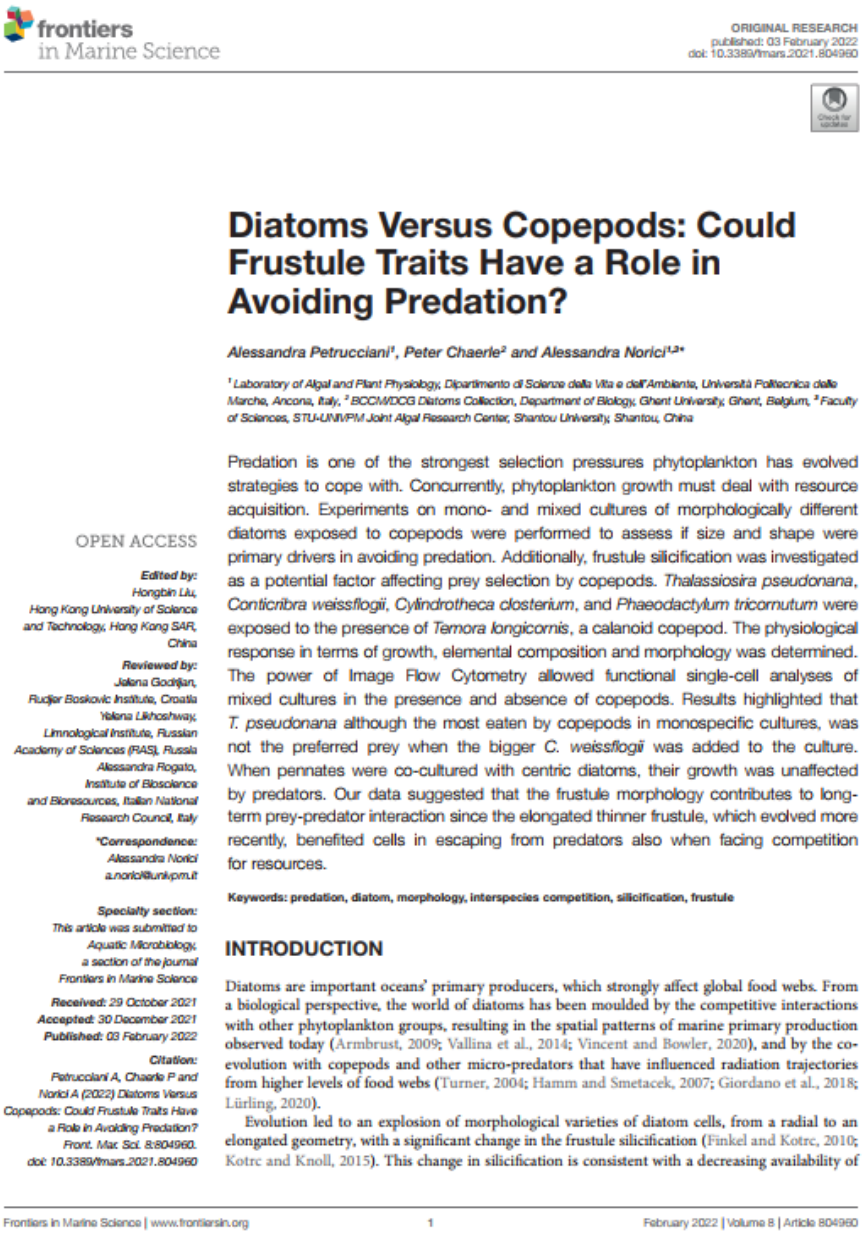

frontiers in Marine Science

ORIGINAL RESEARCH
published: 03 February 2022
doi: 10.3389/fmars.2021.804960

Diatoms Versus Copepods: Could Frustule Traits Have a Role in Avoiding Predation?

*Alessandra Petrucciani[1], Peter Chaerle[2] and Alessandra Norici[1,3]**

[1] Laboratory of Algal and Plant Physiology, Dipartimento di Scienze della Vita e dell'Ambiente, Università Politecnica delle Marche, Ancona, Italy, [2] BCCM/DCG Diatoms Collection, Department of Biology, Ghent University, Ghent, Belgium, [3] Faculty of Sciences, STU-UNIVPM Joint Algal Research Center, Shantou University, Shantou, China

Predation is one of the strongest selection pressures phytoplankton has evolved strategies to cope with. Concurrently, phytoplankton growth must deal with resource acquisition. Experiments on mono- and mixed cultures of morphologically different diatoms exposed to copepods were performed to assess if size and shape were primary drivers in avoiding predation. Additionally, frustule silicification was investigated as a potential factor affecting prey selection by copepods. *Thalassiosira pseudonana*, *Conticribra weissflogii*, *Cylindrotheca closterium*, and *Phaeodactylum tricornutum* were exposed to the presence of *Temora longicornis*, a calanoid copepod. The physiological response in terms of growth, elemental composition and morphology was determined. The power of Image Flow Cytometry allowed functional single-cell analyses of mixed cultures in the presence and absence of copepods. Results highlighted that *T. pseudonana* although the most eaten by copepods in monospecific cultures, was not the preferred prey when the bigger *C. weissflogii* was added to the culture. When pennates were co-cultured with centric diatoms, their growth was unaffected by predators. Our data suggested that the frustule morphology contributes to long-term prey-predator interaction since the elongated thinner frustule, which evolved more recently, benefited cells in escaping from predators also when facing competition for resources.

Keywords: predation, diatom, morphology, interspecies competition, silicification, frustule

OPEN ACCESS

Edited by:
Hongbin Liu,
Hong Kong University of Science and Technology, Hong Kong SAR, China

Reviewed by:
Jelena Godrijan,
Ruđer Bošković Institute, Croatia
Yelena Likhoshway,
Limnological Institute, Russian Academy of Sciences (RAS), Russia
Alessandra Rogato,
Institute of Bioscience and Bioresources, Italian National Research Council, Italy

**Correspondence:*
Alessandra Norici
a.norici@univpm.it

Specialty section:
This article was submitted to Aquatic Microbiology, a section of the journal Frontiers in Marine Science

Received: 29 October 2021
Accepted: 30 December 2021
Published: 03 February 2022

Citation:
Petrucciani A, Chaerle P and Norici A (2022) Diatoms Versus Copepods: Could Frustule Traits Have a Role in Avoiding Predation? Front. Mar. Sci. 8:804960. doi: 10.3389/fmars.2021.804960

INTRODUCTION

Diatoms are important oceans' primary producers, which strongly affect global food webs. From a biological perspective, the world of diatoms has been moulded by the competitive interactions with other phytoplankton groups, resulting in the spatial patterns of marine primary production observed today (Armbrust, 2009; Vallina et al., 2014; Vincent and Bowler, 2020), and by the co-evolution with copepods and other micro-predators that have influenced radiation trajectories from higher levels of food webs (Turner, 2004; Hamm and Smetacek, 2007; Giordano et al., 2018; Lürling, 2020).

Evolution led to an explosion of morphological varieties of diatom cells, from a radial to an elongated geometry, with a significant change in the frustule silicification (Finkel and Kotrc, 2010; Kotrc and Knoll, 2015). This change in silicification is consistent with a decreasing availability of

2. **Petrucciani A.**, Knoll A. H., Norici A. (in revision) " Si decline and diatom evolution: insights from physiological experiments", Invited contribution to Biogeochemistry and Genomics of Silicification and Silicifiers, Frontiers in Marine Science, Marine Biogeochemistry.

Teaching

1. 2018 – 2021: Tutor in Plant Physiology (Bachelor course) and Algal Ecophysiology (Master course

Università Politecnica delle Marche - Dipartimento di Scienze della Vita e dell'Ambiente, Ancona (Italy)

2. 2020 – 2021: Co-supervisor of Master Student thesis in Marine Biology

Università Politecnica delle Marche - Dipartimento di Scienze della Vita e dell'Ambiente, Ancona (Italy). Thesis entitled “Microalgal Communication”

UNIVERSITÀ POLITECNICA DELLE MARCHE

DIPARTIMENTO SCIENZE DELLA VITA E DELL'AMBIENTE

Corso di Laurea Magistrale

Biologia Marina

La comunicazione nelle Microalghe

Candidato
Stefano Maso

Relatore
Alessandra Norici
Correlatore
Alessandra Petrucciani

Anno Accademico 2020/2021